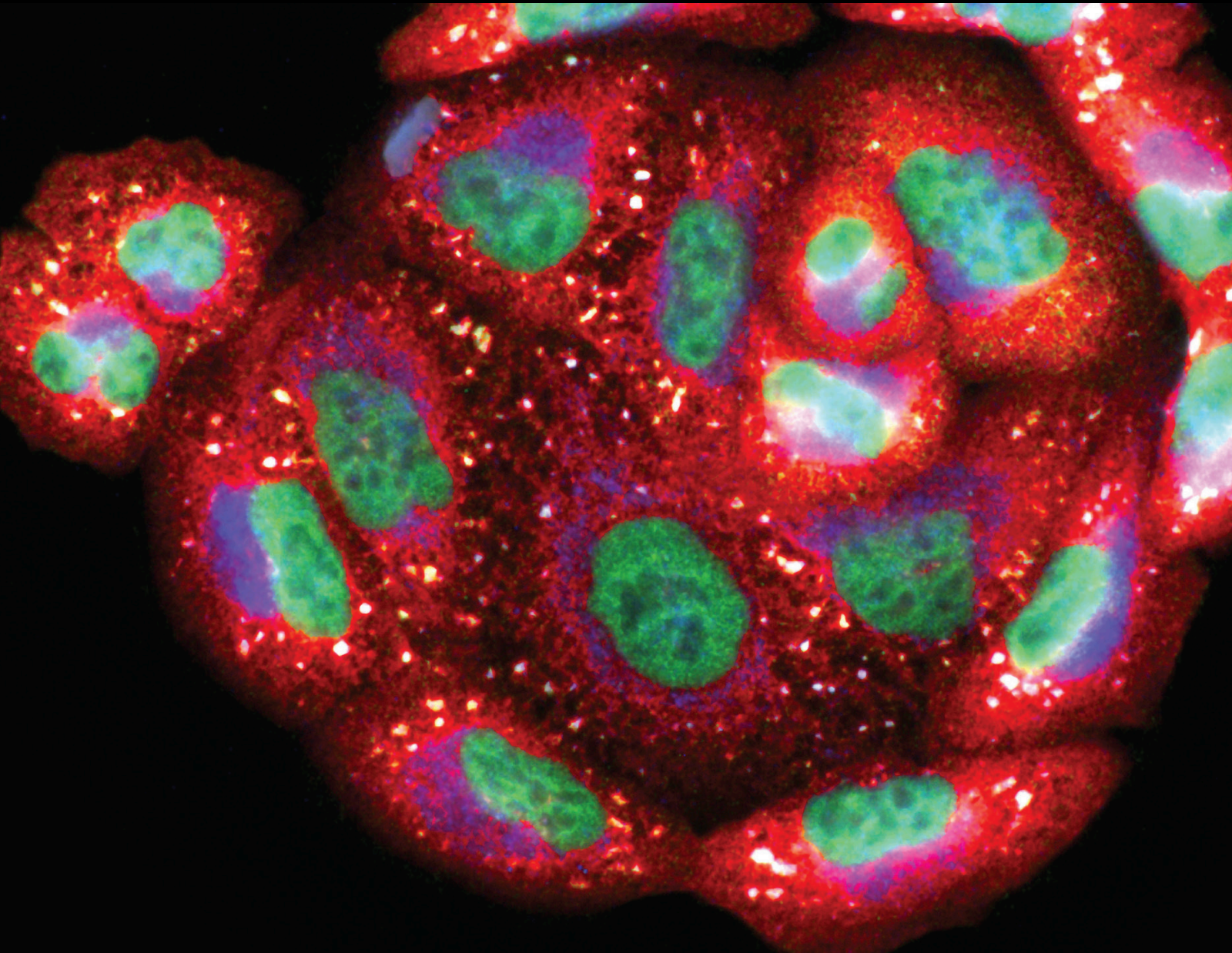


# Gut Microbiota, Diet, and Chronic Diseases: The Role Played by Oxidative Stress

Lead Guest Editor: Elisardo C. Vasquez

Guest Editors: Thiago M. C. Pereira, Manuel Campos-Toimil, Marcelo P. Baldo, and Veronica A. Peotta





---

# **Gut Microbiota, Diet, and Chronic Diseases: The Role Played by Oxidative Stress**

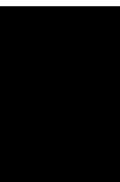
Oxidative Medicine and Cellular Longevity

---

**Gut Microbiota, Diet, and Chronic Diseases:  
The Role Played by Oxidative Stress**

Lead Guest Editor: Elisardo C. Vasquez

Guest Editors: Thiago M. C. Pereira, Manuel Campos-Toimil,  
Marcelo P. Baldo, and Veronica A. Peotta



---

Copyright © 2019 Hindawi Limited. All rights reserved.

This is a special issue published in "Oxidative Medicine and Cellular Longevity" All articles are open access articles distributed under the Creative Commons Attribution License, which permits unrestricted use, distribution, and reproduction in any medium, provided the original work is properly cited.

# Chief Editor

Jeannette Vasquez-Vivar, USA

## Editorial Board

Ivanov Alexander, Russia  
Fabio Altieri, Italy  
Fernanda Amicarelli, Italy  
José P. Andrade, Portugal  
Cristina Angeloni, Italy  
Antonio Ayala, Spain  
Elena Azzini, Italy  
Peter Backx, Canada  
Damian Bailey, United Kingdom  
Sander Bekeschus, Germany  
Ji C. Bihl, USA  
Consuelo Borrás, Spain  
Nady Braidy, Australia  
Ralf Braun, Austria  
Laura Bravo, Spain  
Amadou Camara, USA  
Gianluca Carnevale, Italy  
Roberto Carnevale, Italy  
Angel Catalá, Argentina  
Giulio Ceolotto, Italy  
Shao-Yu Chen, USA  
Ferdinando Chiaradonna, Italy  
Zhao Zhong Chong, USA  
Alin Ciobica, Romania  
Ana Cipak Gasparovic, Croatia  
Giuseppe Cirillo, Italy  
Maria R. Ciriolo, Italy  
Massimo Collino, Italy  
Graziamaria Corbi, Italy  
Manuela Corte-Real, Portugal  
Mark Crabtree, United Kingdom  
Manuela Curcio, Italy  
Andreas Daiber, Germany  
Felipe Dal Pizzol, Brazil  
Francesca Danesi, Italy  
Domenico D'Arca, Italy  
Sergio Davinelli, USA  
Claudio De Lucia, Italy  
Yolanda de Pablo, Sweden  
Sonia de Pascual-Teresa, Spain  
Cinzia Domenicotti, Italy  
Joël R. Drevet, France  
Grégory Durand, France  
Javier Egea, Spain

Ersin Fadillioglu, Turkey  
Ioannis G. Fatouros, Greece  
Qingping Feng, Canada  
Gianna Ferretti, Italy  
Giuseppe Filomeni, Italy  
Swaran J. S. Flora, India  
Teresa I. Fortoul, Mexico  
Rodrigo Franco, USA  
Joaquin Gadea, Spain  
Juan Gambini, Spain  
José Luís García-Giménez, Spain  
Gerardo García-Rivas, Mexico  
Janusz Gebicki, Australia  
Alexandros Georgakilas, Greece  
Husam Ghanim, USA  
Rajeshwary Ghosh, USA  
Eloisa Gitto, Italy  
Daniela Giustarini, Italy  
Saeid Golbidi, Canada  
Aldrin V. Gomes, USA  
Tilman Grune, Germany  
Nicoletta Guaragnella, Italy  
Solomon Habtemariam, United Kingdom  
Eva-Maria Hanschmann, Germany  
Tim Hofer, Norway  
John D. Horowitz, Australia  
Silvana Hrelia, Italy  
Stephan Immenschuh, Germany  
Maria Isagulians, Latvia  
Luigi Iuliano, Italy  
FRANCO J. L, Brazil  
Vladimir Jakovljevic, Serbia  
Marianna Jung, USA  
Peeter Karihtala, Finland  
Eric E. Kelley, USA  
Kum Kum Khanna, Australia  
Neelam Khaper, Canada  
Thomas Kietzmann, Finland  
Demetrios Kouretas, Greece  
Andrey V. Kozlov, Austria  
Jean-Claude Lavoie, Canada  
Simon Lees, Canada  
Christopher Horst Lillig, Germany  
Paloma B. Liton, USA

Ana Lloret, Spain  
Lorenzo Loffredo, Italy  
Daniel Lopez-Malo, Spain  
Antonello Lorenzini, Italy  
Nageswara Madamanchi, USA  
Kenneth Maiese, USA  
Marco Malaguti, Italy  
Tullia Maraldi, Italy  
Reiko Matsui, USA  
Juan C. Mayo, Spain  
Steven McAnulty, USA  
Antonio Desmond McCarthy, Argentina  
Bruno Meloni, Australia  
Pedro Mena, Italy  
Victor M. Mendoza-Núñez, Mexico  
Maria U. Moreno, Spain  
Trevor A. Mori, Australia  
Ryuichi Morishita, Japan  
Fabiana Morroni, Italy  
Luciana Mosca, Italy  
Ange Mouithys-Mickalad, Belgium  
Iordanis Mourouzis, Greece  
Danina Muntean, Romania  
Colin Murdoch, United Kingdom  
Pablo Muriel, Mexico  
Ryoji Nagai, Japan  
David Nieman, USA  
Hassan Obied, Australia  
Julio J. Ochoa, Spain  
Pál Pacher, USA  
Pasquale Pagliaro, Italy  
Valentina Pallottini, Italy  
Rosalba Parenti, Italy  
Vassilis Paschalis, Greece  
Visweswara Rao Pasupuleti, Malaysia  
Daniela Pellegrino, Italy  
Ilaria Peluso, Italy  
Claudia Penna, Italy  
Serafina Perrone, Italy  
Tiziana Persichini, Italy  
Shazib Pervaiz, Singapore  
Vincent Pialoux, France  
Ada Popolo, Italy  
José L. Quiles, Spain  
Walid Rachidi, France  
Zsolt Radak, Hungary  
Namakkal Soorappan Rajasekaran, USA

Sid D. Ray, USA  
Hamid Reza Rezvani, France  
Alessandra Ricelli, Italy  
Paola Rizzo, Italy  
Francisco J. Romero, Spain  
Joan Roselló-Catafau, Spain  
H. P. Vasantha Rupasinghe, Canada  
Gabriele Saretzki, United Kingdom  
Luciano Saso, Italy  
Nadja Schroder, Brazil  
Sebastiano Sciarretta, Italy  
Ratanesh K. Seth, USA  
Honglian Shi, USA  
Cinzia Signorini, Italy  
Mithun Sinha, USA  
Carla Tatone, Italy  
Frank Thévenod, Germany  
Shane Thomas, Australia  
Carlo G. Tocchetti, Italy  
Angela Trovato Salinaro, Italy  
Paolo Tucci, Italy  
Rosa Tundis, Italy  
Giuseppe Valacchi, Italy  
Daniele Vergara, Italy  
Victor M. Victor, Spain  
László Virág, Hungary  
Natalie Ward, Australia  
Philip Wenzel, Germany  
Georg T. Wondrak, USA  
Michal Wozniak, Poland  
Sho-ichi Yamagishi, Japan  
Liang-Jun Yan, USA  
Guillermo Zalba, Spain  
Mario Zoratti, Italy






## Contents

### **Gut Microbiota, Diet, and Chronic Diseases: The Role Played by Oxidative Stress**

Elisardo C. Vasquez , Thiago M. C. Pereira , Manuel Campos-Toimil , Marcelo P. Baldo, and Veronica A. Peotta 



Editorial (3 pages), Article ID 7092032, Volume 2019 (2019)

### **Kalanchoe brasiliensis Cambess., a Promising Natural Source of Antioxidant and Antibiotic Agents against Multidrug-Resistant Pathogens for the Treatment of Salmonella Gastroenteritis**

Oscar Alejandro Santos Mayorga, Ygor Ferreira Garcia da Costa , Jucélia Barbosa da Silva , Elita Scio , Adriana Lúcia Pires Ferreira, Orlando Vieira de Sousa , and Maria Silvana Alves 




Research Article (15 pages), Article ID 9245951, Volume 2019 (2019)

### **Niacin Protects against Butyrate-Induced Apoptosis in Rumen Epithelial Cells**

Dan Luo , Zhipeng Peng, Le Yang, Mingren Qu, Xiaowen Xiong, Lanjiao Xu, Xianghui Zhao, Ke Pan, and Kehui Ouyang 





Research Article (8 pages), Article ID 2179738, Volume 2019 (2019)

### **Proximal Tubular Development Is Impaired with Downregulation of MAPK/ERK Signaling, HIF-1 $\alpha$ , and Catalase by Hyperoxia Exposure in Neonatal Rats**

Xuwen Xu , Kai You , and Renge Bu 


Research Article (16 pages), Article ID 9219847, Volume 2019 (2019)

### **Worsening of Oxidative Stress, DNA Damage, and Atherosclerotic Lesions in Aged LDLr $^{-/-}$ Mice after Consumption of Guarana Soft Drinks**

Layla Aparecida Chisté, Beatriz Peters Pereira, Marcella Leite Porto, Jairo Pinto de Oliveira, Arícia Leone Evangelista Monteiro de Assis, Breno Valentim Nogueira, Silvana Santos Meyrelles , Tadeu Uggere de Andrade, Manuel Campos-Toimil , Elisardo Corral Vasquez, Bianca Prandi Campagnaro , and Thiago Melo Costa Pereira 

Research Article (13 pages), Article ID 9042526, Volume 2019 (2019)

### **Probiotics as Beneficial Dietary Supplements to Prevent and Treat Cardiovascular Diseases: Uncovering Their Impact on Oxidative Stress**

Elisardo C. Vasquez , Thiago M. C. Pereira , Veronica A. Peotta , Marcelo P. Baldo, and Manuel Campos-Toimil 

Review Article (11 pages), Article ID 3086270, Volume 2019 (2019)

### **Protective Effect of Methane-Rich Saline on Acetic Acid-Induced Ulcerative Colitis via Blocking the TLR4/NF- $\kappa$ B/MAPK Pathway and Promoting IL-10/JAK1/STAT3-Mediated Anti-inflammatory Response**

Guanghai Wang, Bing Xu, Feiyu Shi, Mengfan Du, Yaguang Li, Tianyu Yu, and Lihong Chen 

Research Article (12 pages), Article ID 7850324, Volume 2019 (2019)

## Editorial

# Gut Microbiota, Diet, and Chronic Diseases: The Role Played by Oxidative Stress

**Elisardo C. Vasquez** <sup>1</sup>, **Thiago M. C. Pereira** <sup>1,2</sup>, **Manuel Campos-Toimil** <sup>3</sup>,  
**Marcelo P. Baldo**,<sup>4,5</sup> and **Veronica A. Peotta** <sup>6</sup>

<sup>1</sup>Pharmaceutical Sciences Graduate Program, Vila Velha University (UVV), Vila Velha, ES, Brazil

<sup>2</sup>Federal Institute of Education, Science and Technology (IFES), Vila Velha, ES, Brazil

<sup>3</sup>Farmacología de las Enfermedades Crónicas (CDPHARMA), Centro de Investigación en Medicina Molecular y Enfermedades Crónicas (CIMUS), Universidade de Santiago de Compostela, Santiago de Compostela, Spain

<sup>4</sup>Department of Pathophysiology, State University of Montes Claros, Montes Claros, MG, Brazil

<sup>5</sup>Department of Medicine, Faculdades Integradas Pitagoras, Montes Claros, MG, Brazil

<sup>6</sup>Steady Family Department of Pediatrics, The University of Iowa, Iowa City, IA, USA

Correspondence should be addressed to Elisardo C. Vasquez; [evasquez@terra.com.br](mailto:evasquez@terra.com.br)

Received 11 October 2019; Accepted 19 October 2019; Published 9 December 2019

Copyright © 2019 Elisardo C. Vasquez et al. This is an open access article distributed under the Creative Commons Attribution License, which permits unrestricted use, distribution, and reproduction in any medium, provided the original work is properly cited.

## 1. Introduction

While infectious diseases constituted the most serious global health issue until the middle of the 20th century [1]; nowadays, the cardiovascular and metabolic diseases are the largest contributors to global morbimortality [2]. Interestingly, if in the past centuries, bacteria were considered a potential threat to health, currently, it is well known that in normal conditions in some body compartments, such as the gut, there is a pool of microbe that is majorly composed of nonpathogenic microorganisms (“nice guys”) that are relevant to oppose the progression of several chronic diseases. Moreover, recent studies have revealed that diseases related with dysbiosis of the gut microbiota are linked with an exacerbated oxidative stress [3]. Recent data have revealed that the healthy bacteria of gut microbiota may promote a physiological cross-talk with other systems such as the brain, cardiovascular organs, and metabolic-related tissues, helping to avoid and fight hypertension and metabolic syndrome progression [3]. In parallel, other studies demonstrated that the disturbance of gut microbiota (triggered and caused by urban diets and sedentary lifestyle) may result in excessive bioavailability of reactive oxygen species (ROS) and contribute to the increase of oxidative stress [4].

Therefore, the three terms used in the title of this special issue: gut microbiota, diet, and chronic diseases, that have sounded so discrepant until the last century begin to have a stronger meaning in the present century, as illustrated in Figure 1. However, a further and wide investigation is still necessary to reach a better understanding about the interactions either through the influence of microbiota and diet or through pharmacological strategies.

The special issue comprises one review article and innovative research papers that provide new insights about the potential benefits and molecular mechanisms of nutraceuticals and their antioxidant actions, as summarized below.

The review provides a state-of-the-art role showing strong evidence of the effects of the probiotic kefir in the prevention and treatment of gut dysbiosis in cardiometabolic disturbances. The authors discuss about the improvement of autonomic control of cardiovascular function and provide beneficial effects of this kind of nutraceutical in patients suffering heart failure. They also provide details and new insights about the molecular mechanisms by which kefir decreases oxidative stress in such conditions. The review contains 5 schematic figures that can be used by the readers as an updated source of knowledge about the mechanisms related with the treatment of chronic diseases by using probiotics [5].



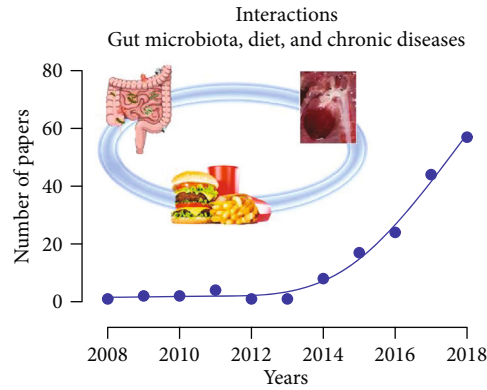


FIGURE 1: Follow-up of a decade of published papers related with the association between the three keywords: gut microbiota, diet, and chronic diseases, based on PubMed indexation. Data source: <https://www.ncbi.nlm.nih.gov/pubmed/>.

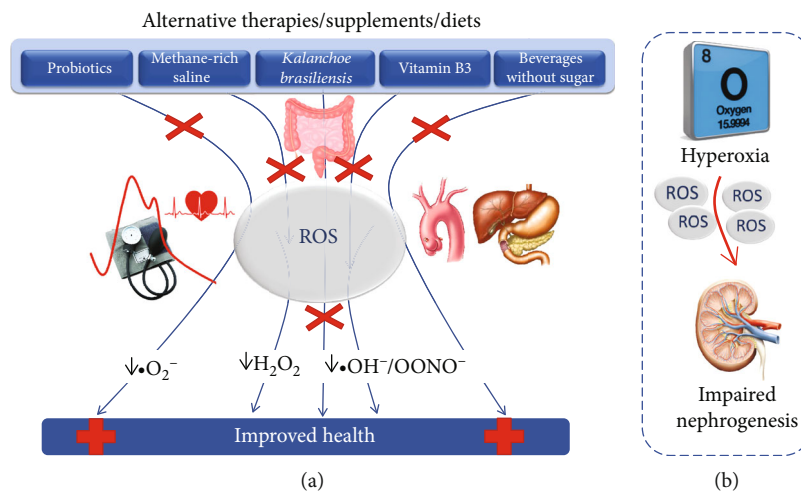


FIGURE 2: (a) Schematic diagram showing alternative therapies proposed in this special issue that exhibit antioxidative properties and become potential promising approaches. (b) illustrates the deleterious actions of hyperoxia exposition that contributes to the worsening of the renal function and that is not yet tested with those therapies.

The translational original paper presented by L. A. Chisté et al. [6] is related with novel insights about the prooxidative and genotoxic effect of sugar-sweetened soft drinks (but not zero soft drinks) and other questions that remain to be addressed concerning the consumption of commercial beverages. This innovative investigation conducted in the laboratory of Pereira and Campagnaro, using a mouse model of dyslipidemia, may effectively provide a basis for further experimental and clinical studies to explore the association between the consumption of soft drinks and metabolic diseases.

Interestingly, Chinese researchers [7] report in this issue data showing that neonatal supplementation of oxygen therapy may compromise the nephrogenesis process. The authors highlight the importance of MAPK/ERK signaling, HIF-1 $\alpha$ , or catalase to protect against hyperoxia-induced oxidative damage in neonatal proximal tubules. Their study may open some news avenues that can provide the understanding of etiology cases of nephrogenesis impairment.

It is known that overproduction/accumulation of butyrate (a short-chain fatty acid of ruminal fermentation)

in the bowel may promote toxic effects in the intestinal mucosa. A second group of Chinese researchers [8] present an interesting data showing that vitamin B3 (niacin) can inhibit butyrate-induced apoptosis of rumen epithelial cells. This protective effect reported by the authors is probably associated with reduced oxidative stress, inhibition of caspase-3 and p53 activation, and DNA-damage repair. The importance of that study is that it expands strategies to mitigate the damage produced by the excessive exposition of short-chain fatty acids. In the same field of research, a second group from China [9] describes the protective effects exhibited by methane-rich saline on acetic acid-induced ulcerative colitis and describes that this approach culminates with antioxidative and anti-inflammatory effects. The authors emphasize that this approach could be anti-inflammatory and antiapoptotic therapeutic alternatives through the inhibition of TLR4/NF- $\kappa$ B/MAPK signaling pathway and promoting IL-10/JAK1/STAT3.

Considering that *Salmonella* infection is frequently observed worldwide and often is resistant to prolonged antibiotic treatment, the search for innovative antibiotics against

these gram-negative bacteria deserves urgent attention. In this regard, the paper published by O. A. S. Mayorga et al. [10] demonstrates that exposition to species rich in flavonoids, the *Kalanchoe brasiliensis*, has beneficial antibacterial effects against *Salmonella* strains, by an interesting mechanism that comprises cell membrane integrity and/or permeability alterations. This discovery published in this special issue by Brazilian researchers deserves special merit because it can provide good candidates to reach the goal of new antibiotics for therapeutic applications against *Salmonella* spp.

In conclusion, the readers will find interesting papers that were accepted and published in this special issue because even if the data are from independent researchers and laboratories, they demonstrate that different alternative therapies/supplements/diets have a molecular mechanism of action converging to anti-ROS action with distinct consequences, as illustrated in a schematic diagram (Figure 2).

### Conflicts of Interest

The editors declare that they have no conflicts of interest regarding the publication of this special issue.

### Acknowledgments

The authors gratefully acknowledge the Espirito Santo Research Foundation (FAPES) (Grant CNPq/FAPES No. 24/2018; Termo Outorga 569/2018) and the Brazilian National Council for Research and Development (CNPq) (CNPq Grant Bolsa Produtividade 2015-2019) for the financial support to our research project.

Elisardo C. Vasquez  
Thiago M. C. Pereira  
Manuel Campos-Toimil  
Marcelo P. Baldo  
Veronica A. Peotta

### References

- [1] G. A. Mensah, G. S. Wei, P. D. Sorlie et al., "Decline in cardiovascular mortality: possible causes and implications," *Circulation Research*, vol. 120, no. 2, pp. 366–380, 2017.
- [2] J. D. Tune, A. G. Goodwill, D. J. Sassoon, and K. J. Mather, "Cardiovascular consequences of metabolic syndrome," *Translational Research*, vol. 183, pp. 57–70, 2017.
- [3] F. S. Pimenta, M. Luaces-Regueira, A. M. Ton et al., "Mechanisms of action of kefir in chronic cardiovascular and metabolic diseases," *Cellular Physiology and Biochemistry*, vol. 48, no. 5, pp. 1901–1914, 2018.
- [4] T. Pereira, F. Pimenta, M. Porto et al., "Coadjuvants in the diabetic complications: nutraceuticals and drugs with pleiotropic effects," *International Journal of Molecular Sciences*, vol. 17, no. 8, article 1273, 2016.
- [5] E. C. Vasquez, T. M. C. Pereira, V. A. Peotta, M. P. Baldo, and M. Campos-Toimil, "Probiotics as beneficial dietary supplements to prevent and treat cardiovascular diseases: uncovering their impact on oxidative stress," *Oxidative Medicine and Cellular Longevity*, vol. 2019, Article ID 3086270, 11 pages, 2019.
- [6] L. A. Chisté, B. P. Pereira, M. L. Porto et al., "Worsening of oxidative stress, DNA damage, and atherosclerotic lesions in aged LDLr<sup>-/-</sup> mice after consumption of guarana soft drinks," *Oxidative Medicine and Cellular Longevity*, vol. 2019, Article ID 9042526, 13 pages, 2019.
- [7] X. Xu, K. You, and R. Bu, "Proximal tubular development is impaired with downregulation of MAPK/ERK signaling, HIF-1 $\alpha$ , and catalase by hyperoxia exposure in neonatal rats," *Oxidative Medicine and Cellular Longevity*, vol. 2019, Article ID 9219847, 16 pages, 2019.
- [8] D. Luo, Z. Peng, L. Yang et al., "Niacin protects against butyrate-induced apoptosis in rumen epithelial cells," *Oxidative Medicine and Cellular Longevity*, vol. 2019, Article ID 2179738, 8 pages, 2019.
- [9] G. Wang, B. Xu, F. Shi et al., "Protective Effect of Methane-Rich Saline on Acetic Acid-Induced Ulcerative Colitis via Blocking the TLR4/NF- $\kappa$ B/MAPK Pathway and Promoting IL-10/JAK1/STAT3-Mediated Anti-inflammatory Response," *Oxidative Medicine and Cellular Longevity*, vol. 2019, Article ID 7850324, 12 pages, 2019.
- [10] O. A. Mayorga, Y. F. G. Costa, J. B. Silva et al., "*Kalanchoe brasiliensis* Cambess., a promising natural source of antioxidant and antibiotic agents against multidrug-resistant pathogens for the treatment of *Salmonella* gastroenteritis," *Oxidative Medicine and Cellular Longevity*, vol. 2019, Article ID 9245951, 15 pages, 2019.

## Research Article

# ***Kalanchoe brasiliensis* Cambess., a Promising Natural Source of Antioxidant and Antibiotic Agents against Multidrug-Resistant Pathogens for the Treatment of *Salmonella* Gastroenteritis**

Oscar Alejandro Santos Mayorga,<sup>1,2</sup> Ygor Ferreira Garcia da Costa <sup>1,2</sup>  
Júcélia Barbosa da Silva <sup>3</sup>, Elita Scio <sup>1,3</sup>, Adriana Lúcia Pires Ferreira,<sup>4</sup>  
Orlando Vieira de Sousa <sup>1,5</sup> and Maria Silvana Alves <sup>1,2</sup>

<sup>1</sup>Programa de Pós-Graduação em Ciências Farmacêuticas, Centro de Pesquisas Farmacêuticas, Faculdade de Farmácia, Universidade Federal de Juiz de Fora, Juiz de Fora, Minas Gerais CEP 36.036-900, Brazil

<sup>2</sup>Laboratório de Bioatividade Celular e Molecular, Centro de Pesquisas Farmacêuticas, Faculdade de Farmácia, Universidade Federal de Juiz de Fora, Juiz de Fora, Minas Gerais CEP 36.036-900, Brazil

<sup>3</sup>Laboratório de Produtos Naturais Bioativos, Departamento de Bioquímica, Instituto de Ciências Biológicas, Universidade Federal de Juiz de Fora, Juiz de Fora, Minas Gerais CEP 36.036-900, Brazil

<sup>4</sup>Hospital Universitário Clementino Fraga Filho, Universidade Federal do Rio de Janeiro, Rio de Janeiro, Rio de Janeiro CEP 21.941-913, Brazil

<sup>5</sup>Laboratório de Química Biomedicinal e Farmacologia Aplicada, Faculdade de Farmácia, Universidade Federal de Juiz de Fora, Juiz de Fora, Minas Gerais CEP 36.036-900, Brazil

Correspondence should be addressed to Orlando Vieira de Sousa; [orlando.sousa@ufjf.edu.br](mailto:orlando.sousa@ufjf.edu.br) and Maria Silvana Alves; [silvana.alves@ufjf.edu.br](mailto:silvana.alves@ufjf.edu.br)

Received 8 May 2019; Accepted 23 August 2019; Published 11 November 2019

Guest Editor: Thiago M. C. Pereira

Copyright © 2019 Oscar Alejandro Santos Mayorga et al. This is an open access article distributed under the Creative Commons Attribution License, which permits unrestricted use, distribution, and reproduction in any medium, provided the original work is properly cited.

*Kalanchoe brasiliensis* Cambess. is a native Brazilian plant popularly known as “saião”, and the juice of its fresh leaves is traditionally used to treat several disorders, including inflammatory and infectious processes such as dysentery. The goals of this study were to characterize the phytochemical composition and investigate the antioxidant activity, the antibiotic effect, and the mode of action against *Salmonella* of the hydroethanolic extracts from *K. brasiliensis* leaves collected in the summer and spring Brazilian seasons. These extracts had their chemical composition established by high-performance liquid chromatography with diode-array detection. Total phenolic and flavonoid contents were spectrophotometrically determined. 2,2-Diphenyl-1-picryl-hydrazyl radical scavenging, phosphomolybdenum reducing power and  $\beta$ -carotene bleaching assays were carried out to evaluate the antioxidant capacity. Antibiotic potential was assessed by minimal inhibitory concentration against 8 bacterial ATCC® and 5 methicillin-resistant *Staphylococcus aureus* and 5 *Salmonella* clinical strains. The mode of action was investigated by time-kill, bacterial cell viability, and leakage of compounds absorbing at 280 nm assays against *Salmonella*. Chromatographic profile and UV spectrum analyses suggested the significant presence of flavonoid type patuletin and eupafolin derivatives, and no difference between both periods of collection was noted. Significant amounts of total phenolic and flavonoid contents and a promising antioxidant capacity were observed. Hydroethanolic extracts (70%, summer and spring) were the most active against the tested Gram-positive and Gram-negative bacterial strains, showing the bacteriostatic action of 5000  $\mu\text{g}/\text{mL}$ . Time-kill data demonstrated that these extracts were able to reduce the *Salmonella* growth rate. Cell number was reduced with release of the bacterial content. Together, these results suggest that *K. brasiliensis* is a natural source of antioxidant and antibacterial agents that can be applied in the research and development of new antibiotics for the treatment of *Salmonella* gastroenteritis because they are able to interfere in the *Salmonella* growth, probably due to cell membrane damage.

## 1. Introduction

Oxidative stress is a well-known event in the cells and tissues related to the action of overproduction of free radicals and reactive metabolites named reactive oxygen species (ROS) and reactive nitrogen species (RNS) and can lead to the damage of cellular molecules such as proteins, lipids, and deoxyribonucleic acid (DNA) [1]. Furthermore, it has been widely documented that increased ROS levels modify cell signaling of host proteins, leading to pathological disorders such as bacterial infections and inflammatory processes [2].

A review of 126 articles focusing on the role of nutrients and phytochemicals in the modulation of antimicrobial resistance (AMR), a serious and alarming public health problem worldwide of the 21<sup>st</sup> century [3], showed that 40 of them involved antioxidants such as n-acetylcysteine, ambroxol, ascorbic acid, glutathione, and vitamin E [4]. Goswami et al. [5] described that commonly used cellular and dietary antioxidants affect the activity of therapeutic antibiotics. These authors demonstrated that the presence of glutathione increased antibacterial activity of  $\beta$ -lactams, revealing that this substance could act as a differential antibiotic susceptibility modulator for bacteria. Moreover, another review reported the use of antioxidants in urinary tract infection and showed that these agents can be effectively used combined with antibiotics to reduce the postpyelonephritic scar formation in correlation to their ability to reduce oxidative stress [6].

In addition, the scenario of AMR and the perspective of new therapeutic approaches to treat multidrug-resistant (MDR) bacterial infections have globally attracted the attention of researchers to the secondary plant metabolites, which may represent an alternative and economically feasible strategy to research, discover, and develop new antibiotics [7]. Among them, the flavonoids, the largest and most important group of phenolic compounds in nature, are considered an essential component in the diversity of medicinal, nutraceutical, pharmaceutical, and cosmetic applications [8]. These compounds are widely found in fruits, vegetables, grains, barks, roots, stems, flowers, and certain beverages like tea and wine [8].

Among the diversity of plant options with expressive flavonoid content, *Kalanchoe* Adans. (Crassulaceae DC.) comprised more than one hundred species and it is widely distributed in tropical areas such as Africa and Brazil [9]. In these places, the fresh leaves juice is traditionally used to treat inflammatory and infectious processes such as dysentery, cholera, gastric ulcers, urinary diseases, and ear and pulmonary infections [9]. *Kalanchoe brasiliensis* Cambess., a native Brazilian plant distributed from Bahia to São Paulo states and often found along the southeast coast, is popularly known as “saião” and traditionally used for its pharmacological properties [10]. The scientific studies reported in the literature described the immunomodulatory [11, 12] and anti-inflammatory activities [10, 12–14], the acetylcholinesterase inhibitory action [15, 16], the antimicrobial effect [17], and the gastroprotective property [18, 19].

Regarding the chemical composition, there were seven glycosylated patuletin-derived flavonoids previously identified from the stems and leaves of this plant species [11], with kalambrosides A, B, and C being firstly described, and patuletin

3-O- $\alpha$ -L-rhamnopyranosyl-7-O- $\alpha$ -L-rhamnopyranoside posteriorly reported as a chemical marker of the hydroethanolic extract from *K. brasiliensis* leaves [20]. Subsequently, flavonoid glycosides derived from eupafolin were additionally detected as well as quercetin-O-hexoside-O-deoxyhexoside [21]. Recently, Araújo et al. [18], using ultra-high-performance liquid chromatography coupled to a mass spectrometer (UHPLC-MS), corroborated the presence of flavonoid glycosides derived from patuletin and eupafolin. The kalanchosine dimalate (kalanchosine (1), 3,6-diamino-4,5-dihydroxyoctanedioic acid, plus malic acid (2)), an anti-inflammatory salt from this plant species, was also reported [10].

Despite the chemical and pharmacological publications presented above, few studies focusing on the possible antioxidant [18] and antimicrobial activities [17] were scientifically cited. Furthermore, the traditional use of *K. brasiliensis* to treat dysentery is noteworthy [9] and the fact that the most severe infectious diarrheas are caused predominantly by bacteria, and among them, nontyphoidal salmonellosis cases are globally widespread [22]. Additionally, according to the global priority pathogens list (global PPL) published by the World Health Organization (WHO) to guide research and development of new antibiotics, the fluoroquinolone-resistant *Salmonella* strains is categorized as a high-priority pathogen, which poses a serious threat to human health [3].

With this context in mind, the present study was aimed at investigating the chemical composition, the *in vitro* antioxidant and antibacterial activities, and the mode of action against *Salmonella* species of the hydroethanolic extracts 30%, 50%, and 70% from *K. brasiliensis* fresh leaves collected in the Brazilian summer and spring seasons looking for new options to treat *Salmonella* gastroenteritis.

## 2. Materials and Methods

**2.1. Chemicals and Reagents.** All chemicals and reagents used (and their sources), including solvents, were of analytical or HPLC grade as follows: acetic acid and pyridine (Vetec Química Farm Ltda, Rio de Janeiro, RJ, Brazil); aluminum chloride (F. Maia, Belo Horizonte, MG, Brazil); chloroform (Labsynth, Diadema, SP, Brazil); ethanol P.A. (99.5%) (Biotec Reagentes Analíticos, Pinhais, PR, Brazil); ampicillin 96.0-100.5% (anhydrous basis), chloramphenicol  $\geq 98\%$  (TLC), 2,2-diphenyl-1-picryl-hydrazyl (DPPH), gallic acid, levofloxacin  $\geq 98\%$  (HPLC), quercetin, rutin, tannic acid, and Tween 40 (Sigma-Aldrich Chemical Co., St. Louis, MI, USA); sodium carbonate (InLab Diadema, SP, Brazil); Müller-Hinton agar and Müller-Hinton Broth (Difco Laboratories®, Detroit, MI, USA); and McFarland scale 0.5 (DME Diagnóstico Microbiológicos Especializados®, São Paulo, SP, Brazil). Purified water was obtained using the Milli-Q Plus® system (Millipore, Milford, MA, USA).

**2.2. Plant Material.** Fresh leaves of *K. brasiliensis* were collected from the medicinal garden of the Faculty of Pharmacy, Universidade Federal de Juiz de Fora, Juiz de Fora city, Minas Gerais state, southeast region of Brazil (21°26'40" S, 43°22'1" W) on January 7 (1<sup>st</sup> collection; Brazilian Summer) and September

22 (2<sup>nd</sup> collection; Brazilian Spring) 2016. The plant species did not show blooming when collected. The botanical identification was performed by Dr. Marcus Alberto Nadruz Coelho, researcher at the Instituto de Pesquisa Jardim Botânico do Rio de Janeiro, Rio de Janeiro city, Rio de Janeiro state, Brazil, and a voucher specimen (CESJ no. 43980) was deposited at the Herbarium Leopoldo Krieger, Universidade Federal de Juiz de Fora. The plant name *Kalanchoe brasiliensis* Cambess. has been checked with <http://www.theplantlist.org>, being a synonym of *Kalanchoe laciniata* (L.) DC. (<http://www.theplantlist.org/tpl1.1/record/tro-8902741>) (accessed 07 May 2019).

**2.3. Preparation of Extracts.** The hydroethanolic extracts 30%, 50%, and 70% [23] of *K. brasiliensis* fresh leaves collected in January (HEJ30, HEJ50, and HEJ70, respectively) and September (HES30, HES50, and HES70, respectively) 2016 were obtained following the method used by Costa et al. [20]. Fresh leaves (300 g) were extracted with ethanol P.A. (99.5%) at a ratio of 30:70 (HEJ30, HES30), 50:50 (HEJ50, HES50), and 70:30 (HEJ70, HES70) ethanol:water (*v/v*) in a plant:solvent proportion of 1:1 (*w/v*) using a mechanical blender. Then, these hydroethanolic extracts were filtered on a standard filter paper and concentrated by rotary evaporator (R-215 Büchi Labortechnik AG, Flawil, Switzerland) at 45°C.

**2.4. Chemical Characterization by High-Performance Liquid Chromatography with Diode-Array Detection (HPLC-DAD).** HEJ30, HEJ50, HEJ70, HES30, HES50, and HES70 were evaluated by HPLC-DAD in a chromatograph Agilent Technologies 1200 series. The analysis was performed in reversed phase using Zorbax SB-C18 column (4.6 mm × 150 mm, 5 μm). The mobile phase was a linear gradient from 0 to 30 min with distilled water and methanol HPLC grade (95:5 to 10:90). The injection volume was 20 μL at the concentration of 1 mg/mL of the extract dissolved in distilled water, and the flow rate remained constant at 0.8 mL/min. Detection was performed by UV-DAD detector set at a wavelength of 254 nm while the UV spectra was acquired by scanning over a range of 190 to 400 nm.

**2.5. Total Phenolic and Flavonoid Determinations.** The total phenolic content was spectrophotometrically determined according to the Folin and Denis [24] protocol using tannic acid as the standard. HEJ30, HEJ50, HEJ70, HES30, HES50, and HES70 were dissolved in distilled water (2 mg/mL), and an aliquot of 300 μL was added to the Folin-Denis reagent (500 μL) and distilled water (500 μL). After 30 min, saturated sodium carbonate (500 μL) was added to neutralize the reaction. The absorbance was recorded at 760 nm in a microplate reader (Thermo Scientific™, Multiskan™ Sky Microplate Spectrophotometer, Waltham, MA, USA) using distilled water as a blank. The analysis was carried out in triplicate, and the results were expressed as milligram of tannic acid equivalent per gram of extract (mgTAE/g).

The spectrophotometric method was applied for total flavonoid determination based on the formation of acid stable complexes with aluminum chloride using rutin as the standard [25]. For this quantification, HEJ30, HEJ50,

HEJ70, HES30, HES50, and HES70 were dissolved in a mixture of ethanol:water (3:7) at different concentrations, added into a tube containing ethanol, acetic acid, pyridine (20% in ethanol, *v/v*), and aluminum chloride hexahydrated (8% in ethanol, *w/v*), and the volume was completed to 5000 μL with distilled water. After 30 min, the absorbance was measured at 412 nm using a spectrophotometer (Shimadzu®, UV-1800, Tokyo, Japan). The analysis was performed in triplicate, and the results were expressed as milligram of rutin equivalent per gram of extract (mgRE/g).

## 2.6. Antioxidant Activity

**2.6.1. DPPH Radical Scavenging Activity.** The free radical scavenging activity of HEJ30, HEJ50, HEJ70, HES30, HES50, and HES70 was determined based on their ability to react with a stable DPPH free radical following the method described by Blois [26]. The hydroethanolic extract solutions (0.49 to 500 μg/mL) were prepared and mixed with an equal volume of methanol solution of DPPH (0.03 mM). After 60 min at room temperature and protected from light, the absorbance was measured in a microplate reader (Thermo Scientific™, Multiskan™ Sky Microplate Spectrophotometer, Waltham, MA, USA) at 517 nm. The experiment was performed in triplicate. Ascorbic acid and quercetin were used as standards. The antioxidant capacity of HEJ30, HEJ50, HEJ70, HES30, HES50, and HES70 was expressed as the 50% effective concentration (EC<sub>50</sub>), which was defined as the concentration (μg/mL) of extract required to reduce 50% of DPPH or to obtain 50% antioxidant effect [27].

**2.6.2. Phosphomolybdenum Reducing Power Assay.** The total antioxidant capacity of HEJ30, HEJ50, HEJ70, HES30, HES50, and HES70 was also evaluated by phosphomolybdenum reducing power assay according to Prieto et al. [28], using ascorbic acid as the standard. This spectrophotometric method is based on the reduction of molybdenum (VI) to molybdenum (V) in the presence of certain substances with antioxidant capacity, with formation of phosphate/molybdenum (V) green complex at acidic pH [28]. The hydroethanolic extract solutions (0.2 mg/mL) were added to 2000 μL of the phosphomolybdenic complex reagent and kept in a water bath at 95°C for 90 min. After cooling, 250 μL was transferred into a 96-well microplate, and absorbance was measured in a microplate reader (Thermo Scientific™, Multiskan™ Sky Microplate Spectrophotometer, Waltham, MA, USA) at 695 nm. The experiment was performed in triplicate. The results were expressed as the relative antioxidant activity of ascorbic acid (%RAA ascorbic acid) ± standard deviation (SD).

**2.6.3. β-Carotene Bleaching Assay.** The antioxidant activity of HEJ30, HEJ50, HEJ70, HES30, HES50, and HES70 was additionally investigated by β-carotene/linoleic acid system method as described by Melo and Mancini-Filho [29], with little adjustments. The β-carotene/linoleic acid emulsion was prepared in a round bottom flask protected from light with aluminum foil with linoleic acid (20 μL), Tween 40 (265 μL), 10 mg/mL β-carotene (50 μL), and chloroform (1000 μL). After mixing, the chloroform was evaporated using a rotary evaporator (TECNAL, Piracicaba, SP, Brazil)

at 40°C, and distilled water previously saturated with oxygen for 30 min was added (20,000  $\mu\text{L}$ ). The emulsion had the absorbance adjusted to 0.6-0.7 at 470 nm. Then, 38.4  $\mu\text{g}/\text{mL}$  HEJ30, HEJ50, HEJ70, HES30, HES50, and HES70 and quercetin (10  $\mu\text{L}$ ) were placed into a 96-well microplate containing 250  $\mu\text{L}$  of the emulsion and maintained at 45°C for 120 min. The reaction was monitored by discoloration of  $\beta$ -carotene by absorbance reduction measurement at 470 nm, with reading at 15 min intervals for a total of 120 min, using a microplate reader (Thermo Scientific™, Multiskan™ Sky Microplate Spectrophotometer, Waltham, MA, USA), in triplicate. The percentage of inhibition (%I) of lipid peroxidation was calculated.

## 2.7. In Vitro Antibacterial Activity

**2.7.1. Bacterial Strains.** *Staphylococcus aureus* subsp. *aureus* (methicillin-sensitive *Staphylococcus aureus* (MSSA)) (ATCC® 6538™ and ATCC® 29213™), *Escherichia coli* (ATCC® 10536™ and ATCC® 25922™), *Salmonella enterica* subsp. *enterica* serovar Choleraesuis (ATCC® 10708™), *Salmonella enterica* subsp. *enterica* serovar Typhimurium (ATCC® 13311™), and *Pseudomonas aeruginosa* (ATCC® 9027™ and ATCC® 27853™) reference strains and methicillin-resistant *Staphylococcus aureus* (MRSA) 1485279, 1605677, 1664534, 1688441, and 1830466; *Salmonella* Enteritidis 1406591, 1418594, and 1628260; and *Salmonella* spp. 1266695 and 1507708 (fluoroquinolone-resistant) clinical strains were selected for the *in vitro* antibacterial activity assessment. The American Type Culture Collection (ATCC®) reference strains were obtained from the Instituto Nacional de Controle de Qualidade em Saúde (INCQS), Fundação Oswaldo Cruz (Fiocruz), Rio de Janeiro, Brazil. The clinical strains were isolated from the blood (MRSA) and the blood or urine (*Salmonella* spp. and *Salmonella* Enteritidis, respectively) of patients who attended at Hospital Universitário Clementino Fraga Filho, Universidade Federal do Rio de Janeiro, Rio de Janeiro city, Rio de Janeiro state, Brazil. These strains were identified by a VITEK® 2 automated system (bioMérieux, Durham, NC, USA). The ATCC® and clinical strains were stored as suspensions in a 10% (*w/v*) skim milk solution containing 10% (*v/v*) glycerol at -20°C. Prior to use in the bioassays, these strains were aerobically grown in Müeller-Hinton agar (MHA) at 35 ± 2°C for 18-24 h. In this article, we used *S. aureus* (ATCC® 6538), *S. aureus* (ATCC® 29213), *E. coli* (ATCC® 10536), *E. coli* (ATCC® 25922), *S. Choleraesuis* (ATCC® 10708), *S. Typhimurium* (ATCC® 13311), *P. aeruginosa* (ATCC® 9027), *P. aeruginosa* (ATCC® 27853), MRSA 1485279, MRSA 1605677, MRSA 1664534, MRSA 1688441, MRSA 1830466, *S. Enteritidis* 1406591, *S. Enteritidis* 1418594, *S. Enteritidis* 1628260, *Salmonella* spp. 1266695, and *Salmonella* spp. 1507708 to simplify the text.

**2.7.2. Determination of Minimal Inhibitory Concentration (MIC) and Minimal Bactericidal Concentration (MBC).** The broth microdilution method following the Clinical and Laboratory Standards Institute (CLSI) guideline M07-A9 [30] with little adjustments was employed to determine MIC values of HEJ30, HEJ50, HEJ70, HES30, HES50, HES70,

ampicillin (AMP), chloramphenicol (CHL), and, when applicable, levofloxacin (LEV), against ATCC® and clinical strains described above. The hydroethanolic extract (12.5 mg/mL (*w/v*)) and antibiotic stock solutions (1.25 mg/mL (*w/v*)) were prepared in sterile distilled water and in solvents and diluents recommended by the M100-S24 document [31], respectively. In a sterile 96-well microplate, twofold serial dilutions of hydroethanolic extracts (quadruplicate) and antibiotics (triplicate) were prepared in Müeller-Hinton broth (MHB) at concentrations ranging from 40 to 5000  $\mu\text{g}/\text{mL}$  and 4 to 500  $\mu\text{g}/\text{mL}$ , in this order. MIC values above 5000  $\mu\text{g}/\text{mL}$  were not determined. Subsequently, 10  $\mu\text{L}$  of standardized bacteria suspension according to the 0.5 McFarland scale were added. After incubation at 35 ± 2°C for 16 to 20 h under aerobic conditions, 20  $\mu\text{L}$  of 1 mg/mL 2,3,5-triphenyl tetrazolium chloride (TTC) solution (*w/v*) was used as an indicator of bacterial growth (any color change from purple to pink was recorded as bacterial growth). Then, the system was incubated for further 30 min, and the MIC was determined. The appropriate controls were performed. After determination of MIC values, MBC was established according to Andrews' method [32] by spreading of 10  $\mu\text{L}$  of suspensions from wells showing no visible bacterial growth on MHA Petri dishes. After incubation at 35 ± 2°C for 16 to 20 h under aerobic conditions, the presence or absence of bacterial growth was analyzed. MBC was determined as the lowest concentration of dilutions that prevented the visible bacterial growth after subculture on MHA Petri dishes. Bacterial growth or no bacterial growth on MHA revealed a bacteriostatic or bactericidal effect, respectively.

**2.7.3. Time-Kill Assay.** The time-kill curves of HEJ70 and HES70 (0.5 × MIC, 1 × MIC, and 1.5 × MIC) and levofloxacin (LEV) (1 × MIC) were carried out for *S. Choleraesuis* (ATCC® 10708), *S. Typhimurium* (ATCC® 13311), and *Salmonella* spp. 1507708 as recommended by da Silva et al. [33]. MHB containing 5 × 10<sup>5</sup> CFU/mL of bacterial cultures and HEJ70 or HES70 or LEV (positive control) were aerobically incubated at 35 ± 2°C. Growth control (GC = MHB + bacterial inoculum) was also prepared and incubated at the same conditions. Optical density (OD) was spectrophotometrically recorded at 640 nm before incubation (*t* = 0) and every 60 min for 12 h, and the final measurement was performed at 24 h. The bacterial growth curve was constructed as a function of the OD<sub>640</sub> variation over time. The experiments were performed in triplicate.

## 2.8. Mode of Action of Hydroethanolic Extracts from *Kalanchoe brasiliensis* Fresh Leaves against *Salmonella* Species

**2.8.1. Bacterial Cell Viability Assay.** Bacterial cell viability in the presence of hydroethanolic extracts and LEV was determined according to da Silva et al. [33]. One mL of the subcultured bacterial cells (OD<sub>610</sub> = 0.7) of *S. Choleraesuis* (ATCC® 10708), *S. Typhimurium* (ATCC® 13311), and *Salmonella* spp. 1507708 resuspended in 0.9% sterile saline solution was added to 19 mL of sterile phosphate buffer pH =

7.1 (50 mM) with HEJ70 or HES70 (0.5 × MIC, 1 × MIC, and 1.5 × MIC) or LEV (1 × MIC). After 1 h at 35 ± 2°C, an aliquot in the order of dilution of 10<sup>5</sup> was inoculated into Petri dishes containing MHA and incubated at 35 ± 2°C, aerobically, for 18 to 20 h. The results were graphically expressed as CFU/mL × 10<sup>5</sup>.

**2.8.2. Leakage of Compounds Absorbing at 280 nm.** Bacterial cell suspensions of *S. Choleraesuis* (ATCC® 10708), *S. Typhimurium* (ATCC® 13311), and *Salmonella* spp. 1507708 were prepared as described above (2.8.1) and used to spectrophotometrically measure the extravasation of compounds absorbing at 280 nm (loss of proteins and intracellular genetic material) in the supernatant as reported by Kim et al. [34]. One mL of the bacterial suspensions treated with HEJ70 or HES70 (0.5 × MIC, 1 × MIC, and 1.5 × MIC) or LEV (1 × MIC) was aerobically incubated for 1 h at 35 ± 2°C. Cell supernatants were obtained by centrifugation (10,000 × g per 10 min) and the absorbance was spectrophotometrically determined at 280 nm. The release of compounds absorbing at 280 nm was graphically expressed as a relative ratio of OD<sub>280</sub> of HEJ70 or HES70 or LEV treated and untreated cells.

**2.9. Statistical Analysis.** Data were expressed as mean ± S.D. or S.E.M. Statistical significance was determined by one-way ANOVA analysis of variance followed by the Tukey test. *p* < 0.05 was considered significant.

### 3. Results and Discussion

The results of weight, yield, and total phenolic and flavonoid contents obtained with HEJ30, HEJ50, HEJ70, HES30, HES50, and HES70 are shown in Table 1. According to this Table, discrete variations in mass and yield values were noted, being the largest results observed when ethanol 50% and 70% were used. Similar results were reported by Seo et al. [23] who investigated the effects of water, ethanol, methanol, and different concentrations of hydroethanolic solvents on total phenolic and flavonoid contents and antioxidant activity of extracts from guava (*Psidium guajava* L.) leaves to establish the best extraction solvent for use with this plant. These authors described that the total phenolic content of hydroethanolic extract 50% of guava leaves was higher than 30%, 70%, and 90%, while the total flavonoid content of hydroethanolic extract 70% was higher than 30%, 50%, and 90%. As displayed in Table 1, the highest values of total phenolic and flavonoid contents were obtained with HEJ70 (30.11 ± 0.27 mgTAE/g and 16.95 ± 0.05 mgRE/g, respectively) and HES70 (27.06 ± 0.10 mgTAE/g and 13.33 ± 0.05 mgRE/g, in this order). Our data were supported by Muzitano et al. [35], who standardized the extract of *Kalanchoe pinnata* leaves, and reported that active flavonoids were significantly more abundant when the leaves were collected in the summer. As can be observed in Table 1, the total flavonoid content of hydroethanolic extracts of *K. brasiliensis* leaves collected in the summer (HEJ30, HEJ50, and HEJ70) increased when compared with those obtained in the spring (HES30, HES50, and HES70).

For better understanding of the phytochemicals of *K. brasiliensis*, the chemical profiles of HEJ30, HEJ50, HEJ70,

HES30, HES50, and HES70 were established by HPLC-DAD, where the chromatograms at 254 nm exhibited six main peaks (1, 2, 3, 4, 5, and 6 or 7), as depicted in Figure 1 (HEJ30, HEJ50, and HEJ70) and Figure 2 (HES30, HES50, and HES70). The data observed by UV-Vis spectrum analysis of these extracts suggested the presence of flavonoids, characterized by two absorbance bands A and B [36]. According to Costa et al. [20], flavonoids could be considered chemical markers of *K. brasiliensis*, and as aforementioned, the majority of these compounds are correlated to glycosylated patuletin derived flavonoids and also derivatives of the flavonoid aglycone eupafolin, with expressive presence of *O*-glycosylated flavonoids [11, 18, 20, 21]. It is noteworthy to reinforce that patuletin 3-*O*- $\alpha$ -L-rhamnopyranosyl-7-*O*- $\alpha$ -L-rhamnopyranoside, the main chemical marker of *K. brasiliensis*, like other patuletin derivatives, are not commercially available [20]. These compounds belong to the subclasses of flavones and flavonols (3-hydroxyflavones (flavonols) or flavonols with substituted 3-hydroxyl groups (methylated or glycosylated)). Additionally, Tsimogiannis et al. [36] wrote that band A is observed at 310-350 nm for flavones, while for flavonols, it is between 350 and 385 nm. Band B found in the 250-290 nm range is much the same in these flavonoid subclasses (Supplementary Materials Figures 1 and 2).

The *in vitro* antioxidant activity of HEJ30, HEJ50, HEJ70, HES30, HES50, and HES70 was evaluated by DPPH radical scavenging, phosphomolybdenum reducing power, and  $\beta$ -carotene bleaching assays. As can be seen in Table 2, in the DPPH assay, among the six hydroethanolic extracts investigated, HEJ50 (EC<sub>50</sub> 54.66 ± 2.64  $\mu$ g/mL) showed the best scavenging activity, followed by HEJ70 (EC<sub>50</sub> 88.68 ± 2.79  $\mu$ g/mL), HEJ30 (EC<sub>50</sub> 99.78 ± 1.67  $\mu$ g/mL), HES50 (EC<sub>50</sub> 102.00 ± 2.23  $\mu$ g/mL), HES70 (EC<sub>50</sub> 113.60 ± 4.34  $\mu$ g/mL), and HES30 (EC<sub>50</sub> 248.40 ± 1.31  $\mu$ g/mL). Seo et al. [23], also using this method among others to investigate the antioxidant ability of hydroethanolic extracts of guava leaves, demonstrated that the activity of 50% hydroethanolic extract was more expressive than 30%, 70%, and 90%. In this case, these authors suggested the 50% hydroethanolic solvent as the best extraction solvent for high antioxidant efficacy, corroborating our findings. As also shown in Table 2, EC<sub>50</sub> values of HEJ50, HEJ70, and HEJ30 were lower than HES50, HES70, and HES30 probably due to the difference of the leaf collection period and consequent total phenolic and flavonoid contents as explained above (Table 1).

The results obtained by phosphomolybdenum reducing power demonstrated that the hydroethanolic extracts presented a weak capacity when compared with ascorbic acid (Table 2). HEJ70 (16.78 ± 0.24% RAA ascorbic acid) and HEJ50 (16.73 ± 0.34% RAA ascorbic acid) were more effective to reduce Mo (VI) to Mo (V) while the lowest effect was shown by HES30 (8.49 ± 0.23% RAA ascorbic acid). Thus, in this method, the *in vitro* antioxidant activity was found in the following order: HEJ70 = HEJ50 > HES70 > HES50 > HEJ30 > HES30, supporting the influence of the percentage of solvent in the efficiency of the antioxidant capability. This data confirmed the DPPH results and showed the ability of the phenolic compounds and flavonoids to reduce both free radicals [37].

TABLE 1: Weight, yield, and total phenolic and flavonoid contents of the hydroethanolic extract 30%, 50%, and 70% of *Kalanchoe brasiliensis* fresh leaves collected in January (HEJ30, HEJ50, and HEJ70) and September (HES30, HES50, and HES70).

Month/year	Extract	Weight (g)	Yield (%)	Total phenolic content (mgTAE/g)	Total flavonoid content (mgRE/g)
January/2016	HEJ30	10.32	3.44	$26.97 \pm 0.27^a$	$16.59 \pm 0.18^a$
	HEJ50	12.43	4.14	$28.16 \pm 0.07^b$	$15.44 \pm 0.19^b$
	HEJ70	12.34	4.11	$30.11 \pm 0.27^c$	$16.95 \pm 0.05^c$
September/2016	HES30	9.11	3.04	$25.47 \pm 0.24^d$	$11.84 \pm 0.00^d$
	HES50	10.21	3.40	$26.17 \pm 0.02^e$	$12.49 \pm 0.10^e$
	HES70	10.81	3.60	$27.06 \pm 0.11^{f,a}$	$13.33 \pm 0.05^f$

The results are expressed as mean  $\pm$  SD. Total phenolic and flavonoid contents were expressed as tannic acid equivalent (mgTAE/g) and rutin equivalent (mgRE/g), respectively. Equal letters in the same column mean no difference ( $p < 0.05$ ) after variance analysis followed by Tukey's test.

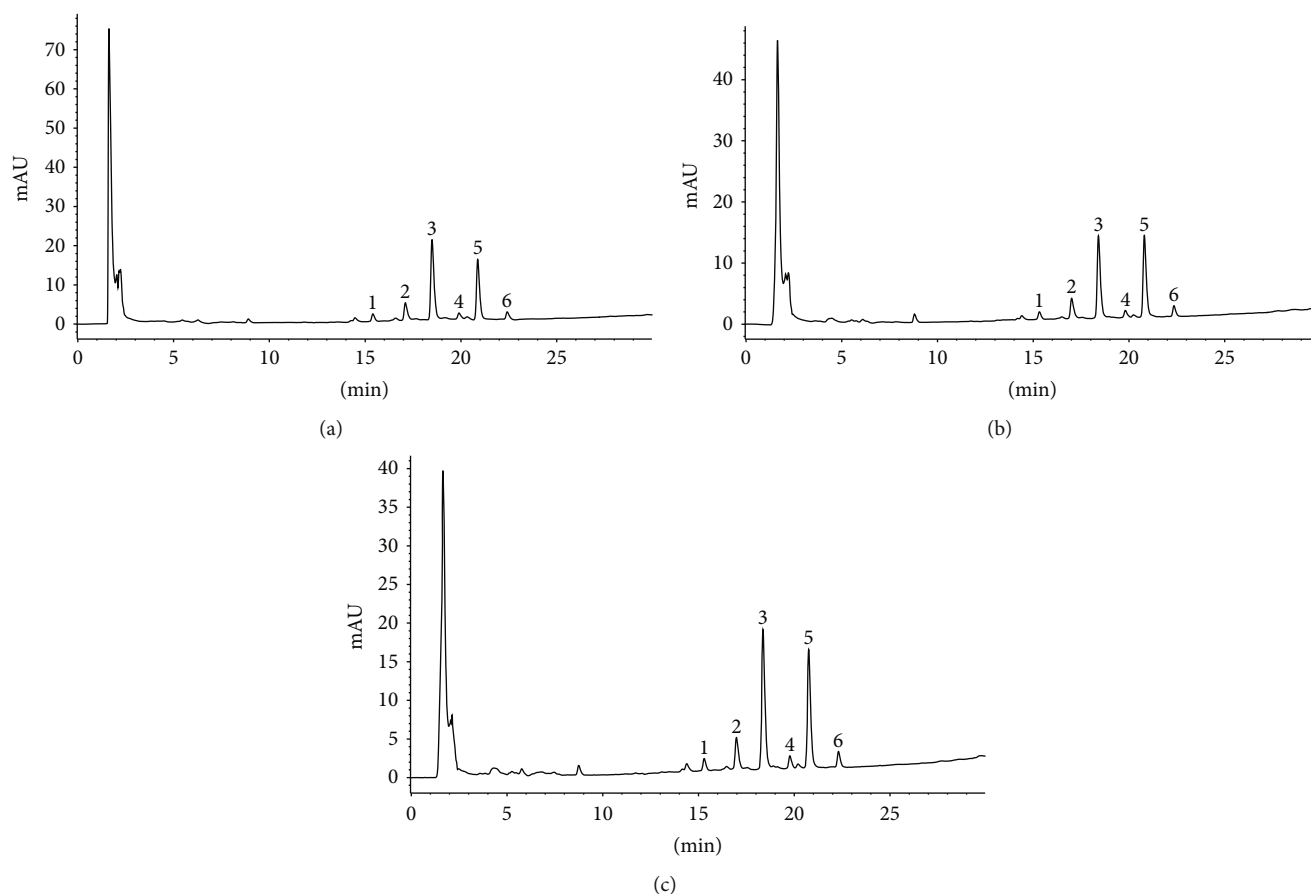


FIGURE 1: Chromatographic profiles of the hydroethanolic extract (a) 30% (HEJ30), (b) 50% (HEJ50), and (c) 70% (HEJ70) from *Kalanchoe brasiliensis* fresh leaves collected in January obtained by HPLC-DAD at 254 nm showing the presence of patuletin and eupafolin derivatives. Peak 1: flavonol indicating a methylated or glycosylated patuletin; peak 2: flavonol indicating a methylated or glycosylated patuletin; peak 3: flavone suggesting eupafolin or derivative or flavonol indicating a methylated or glycosylated patuletin; peak 4: flavone suggesting eupafolin or derivative; peak 5: flavonol indicating a methylated or glycosylated patuletin; and peak 6: flavone suggesting eupafolin or derivative.

The lipid peroxidation method is related to the generation of free radicals in human diseases which play a significant pathological role. For example, peroxidation appears to be important in atherosclerosis and in worsening the initial tissue injury caused by ischemic or traumatic brain damage and neurodegenerative disorders [38]. Additionally, cytoplasmic membrane lipid peroxidation, an autooxidative

process caused by the attack of free radicals, contributes to the progression of various types of regulated cell death [39]. Considering these biological data, our results displayed that HEJ70 and HES70 were more active, since they inhibited the oxidation of linoleic acid and subsequent bleaching of  $\beta$ -carotene, with %I values equal to  $44.46 \pm 0.84$  and  $41.85 \pm 0.39$ , respectively (Table 2). So, these hydroethanolic extracts



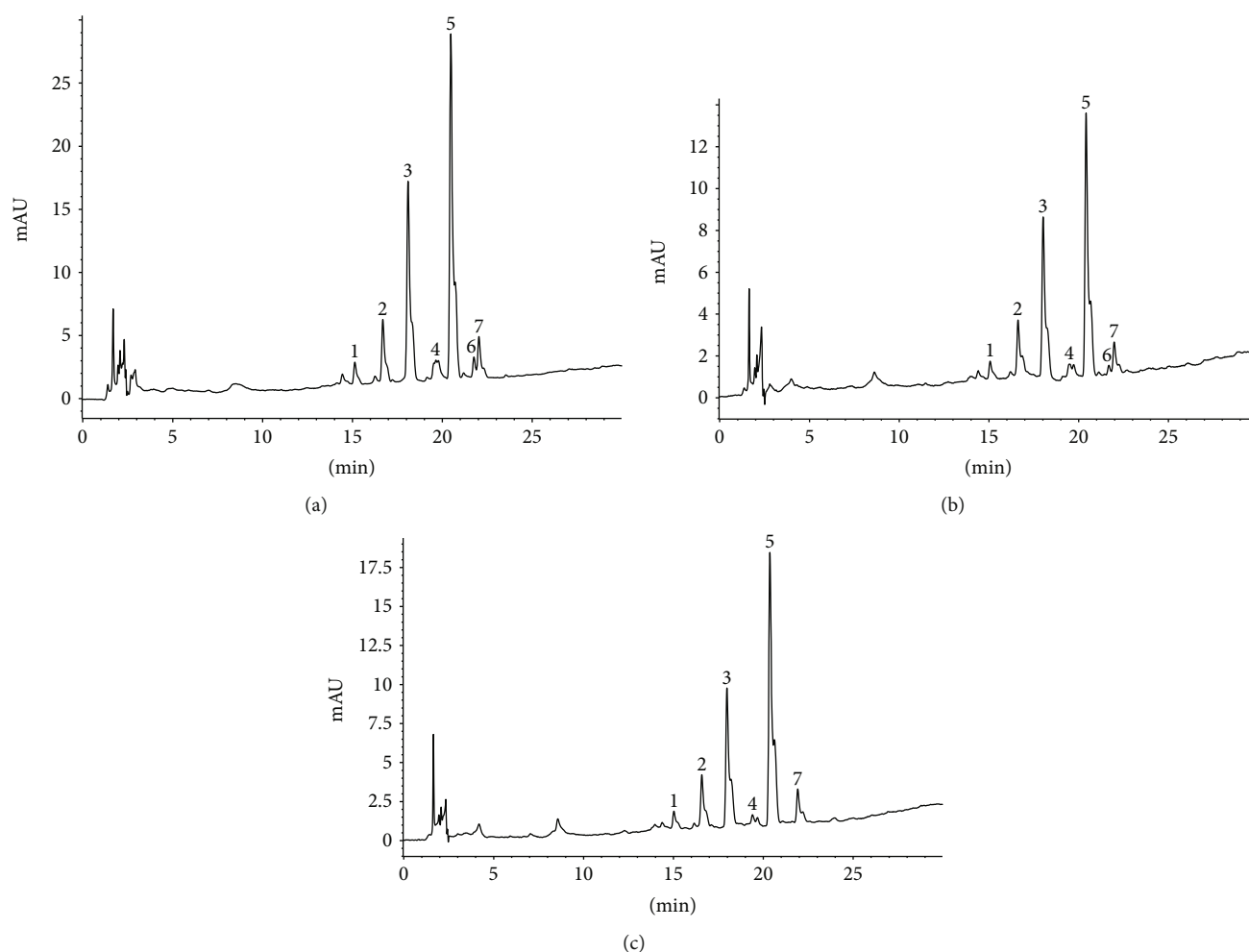


FIGURE 2: Chromatographic profiles of the hydroethanolic extract (a) 30% (HES30), (b) 50% (HES50), and (c) 70% (HES70) from *Kalanchoe brasiliensis* fresh leaves collected in September obtained by HPLC-DAD at 254 nm showing the presence of patuletin and eupafolin derivatives. Peak 1: flavonol indicating a methylated or glycosylated patuletin; peak 2: flavonol indicating a methylated or glycosylated patuletin; peak 3: flavonol indicating a methylated or glycosylated patuletin; peak 4: flavonol indicating a methylated or glycosylated patuletin; peak 5: flavonol indicating a methylated or glycosylated patuletin; peak 6: flavone suggesting eupafolin or derivative or flavonol indicating a methylated or glycosylated patuletin; and peak 7: flavone suggesting eupafolin or derivative.

TABLE 2: *In vitro* antioxidant activity of the hydroethanolic extracts 30%, 50%, and 70% from *Kalanchoe brasiliensis* fresh leaves collected in January (HEJ30, HEJ50, and HEJ70) and September (HES30, HES50, and HES70) by 2,2-diphenyl-1-picryl-hydrazyl (DPPH) radical scavenging, phosphomolybdenum reducing power, and  $\beta$ -carotene bleaching assays.

Extract/standard substance	DPPH radical scavenging EC <sub>50</sub> ( $\mu\text{g}/\text{mL}$ )	Phosphomolybdenum reducing power % RAA ascorbic acid	$\beta$ -Carotene bleaching assay Inhibition of lipid peroxidation (%)
HEJ30	99.78 $\pm$ 1.67 <sup>a</sup>	10.08 $\pm$ 0.23 <sup>a</sup>	40.67 $\pm$ 0.50 <sup>a</sup>
HEJ50	54.66 $\pm$ 2.64 <sup>b</sup>	16.73 $\pm$ 0.34 <sup>b</sup>	39.84 $\pm$ 0.59 <sup>b</sup>
HEJ70	88.68 $\pm$ 2.79 <sup>c</sup>	16.78 $\pm$ 0.24 <sup>c,b</sup>	44.46 $\pm$ 0.84 <sup>c</sup>
HES30	248.40 $\pm$ 1.31 <sup>d</sup>	8.49 $\pm$ 0.23 <sup>d</sup>	41.04 $\pm$ 0.42 <sup>d</sup>
HES50	102.00 $\pm$ 2.23 <sup>e,a</sup>	13.04 $\pm$ 0.36 <sup>e</sup>	37.51 $\pm$ 0.47 <sup>e</sup>
HES70	113.60 $\pm$ 4.34 <sup>f</sup>	14.81 $\pm$ 0.35 <sup>f</sup>	41.85 $\pm$ 0.39 <sup>f</sup>
Ascorbic acid	0.52 $\pm$ 0.04 <sup>g</sup>	Not determined	Not determined
Quercetin	0.40 $\pm$ 0.10 <sup>h</sup>	Not determined	92.33 $\pm$ 0.67 <sup>g</sup>

Values are expressed as mean  $\pm$  SD; the experiment was made in triplicate. Equal letters in the same column mean no difference ( $p < 0.05$ ) after variance analysis followed by Tukey's test.

TABLE 3: Minimal inhibitory concentration values of the hydroethanolic extracts 30%, 50%, and 70% from *Kalanchoe brasiliensis* fresh leaves collected in January (HEJ30, HEJ50, and HEJ70) and September (HES30, HES50, and HES70), ampicillin (AMP), chloramphenicol (CHL), and levofloxacin (LEV) against reference and clinical bacterial strains.

Bacterial strain	Minimal inhibitory concentration (MIC) ( $\mu\text{g/mL}$ )						AMP*	CHL*	LEV*
	HEJ30	HEJ50	HEJ70	HES30	HES50	HES70			
<i>Staphylococcus aureus</i> (ATCC® 6538)	>5000	>5000	5000	>5000	>5000	5000	<4	8	ND
<i>Staphylococcus aureus</i> (ATCC® 29213)	>5000	>5000	>5000	>5000	>5000	>5000	<4	8	ND
<i>Escherichia coli</i> (ATCC® 10536)	>5000	>5000	>5000	>5000	>5000	>5000	<4	<4	ND
<i>Escherichia coli</i> (ATCC® 25922)	5000	5000	5000	>5000	>5000	5000	<4	<4	ND
<i>Salmonella Choleraesuis</i> (ATCC® 10708)	5000	5000	5000	5000	5000	5000	<4	<4	<4
<i>Salmonella Typhimurium</i> (ATCC® 13311)	5000	5000	5000	5000	5000	5000	<4	<4	<4
<i>Pseudomonas aeruginosa</i> (ATCC® 9027)	>5000	>5000	>5000	>5000	>5000	>5000	>500	64	ND
<i>Pseudomonas aeruginosa</i> (ATCC® 27853)	>5000	>5000	>5000	>5000	>5000	>5000	>500	64	ND
Methicillin-resistant <i>Staphylococcus aureus</i> 1485279	5000	5000	5000	>5000	>5000	5000	500	125	ND
Methicillin-resistant <i>Staphylococcus aureus</i> 1605677	5000	5000	5000	5000	>5000	5000	125	8	ND
Methicillin-resistant <i>Staphylococcus aureus</i> 1664534	5000	5000	5000	>5000	>5000	5000	32	8	ND
Methicillin-resistant <i>Staphylococcus aureus</i> 1688441	>5000	>5000	>5000	>5000	>5000	>5000	250	250	ND
Methicillin-resistant <i>Staphylococcus aureus</i> 1830466	5000	5000	5000	5000	>5000	5000	125	<4	ND
<i>Salmonella Enteritidis</i> 1406591	5000	5000	5000	5000	5000	5000	<4	<4	<4
<i>Salmonella Enteritidis</i> 1418594	5000	5000	5000	5000	5000	5000	<4	<4	<4
<i>Salmonella Enteritidis</i> 1628260	5000	5000	5000	5000	5000	5000	<4	<4	<4
<i>Salmonella</i> spp. 1266695	5000	5000	5000	5000	5000	5000	<4	<4	<4
<i>Salmonella</i> spp. 1507708	5000	5000	5000	5000	5000	5000	>500	<4	8

ND: not determined. \*MIC values of AMP, CHL, and LEV were in accordance with the ranges reported by the Clinical and Laboratory Standards Institute, document M100-S24 [31], classifying these bacteria as sensitive, intermediate, and resistant when appropriate. Experiments were carried out in quadruplicate and triplicate for the hydroethanolic extracts and for antibiotics, respectively.

possess compounds able to inhibit the lipid peroxidation, and this capacity can be relevant in the prevention of the oxidative damage.

Some pathologies arising during infection can be attributed to oxidative stress, and generation of ROS in the infectious process can even have fatal consequences [40]. In this sense, antioxidants have the roles to neutralize the excess of free radicals, to protect the cells against their toxic effects, and to contribute to disease prevention [41]. The combination of the antioxidant and antibacterial activities of medicinal plants can be better exploited to manage various disorders, mainly infectious processes. In this way, the results of the *in vitro* antibacterial activity of HEJ30, HEJ50, HEJ70, HES30, HES50, and HES70 by MIC are displayed in Table 3. This Table shows that, among these extracts, HEJ70 and HES70 were the most active, since they were able to inhibit *S. aureus* (ATCC® 6538); *E. coli* (ATCC® 25922); *S. Choleraesuis* (ATCC® 10708); *S. Typhimurium* (ATCC® 13311); MRSA 1605677 and 1830466; *S. Enteritidis* 1406591, 1418594, and 1628260; and *Salmonella* spp. 1266695 and 1507708, with MIC values of 5000  $\mu\text{g/mL}$  and bacteriostatic effect. MBC was not determined because 5000  $\mu\text{g/mL}$  was the highest concentration evaluated. The antibiotic effect was classified based on Kuete's criteria where the antimicrobial activity of plant extracts was categorized as significant (MIC < 100  $\mu\text{g/mL}$ ), moderate (100 < MIC  $\leq$  625  $\mu\text{g/mL}$ ), or weak (MIC > 625  $\mu\text{g/mL}$ ) [42]. However, in an ethnopharmacological survey, Fabry et al. [43] concluded that plants which are used in traditional med-

icine against infections may have some antimicrobial activity with MICs < 8000  $\mu\text{g/mL}$ . So, *K. brasiliensis* possesses a weak antibacterial activity but good enough to explain its use in traditional medicine to treat infectious processes [9] as previously mentioned.

Taking into account that this medicinal plant is widely use in northeastern Brazil for the treatment of wounds, boils, and abscesses [44], and the fact that *S. aureus* is the leading cause of bacterial infections involving skin and soft tissue among other disorders [45], *S. aureus* (ATCC® 6538), *S. aureus* (ATCC® 29213), and five MRSA clinical strains were evaluated as shown in Table 3. These MRSA strains were previously investigated by da Costa et al. [46] focusing on the analysis of the clinical and microbiological characteristics of heteroresistant (hVISA) and vancomycin-intermediate *S. aureus* (VISA) from bloodstream infections (BSI) in a Brazilian teaching hospital. These authors demonstrated the multidrug-resistant (MDR) profile of these strains and corroborated the relevance of the antibiotic effect of the hydroethanolic extracts tested. This antibacterial activity was previously described by Silva et al. [17] that reported the bacteriostatic effect of 4% and 8% essential oils of *K. brasiliensis* leaves against *S. aureus* (ATCC® 6538), *S. aureus* (ATCC® 25923), and ten *S. aureus* clinical strains, including MRSA. With regard to the mechanism of action, Babii et al. [47] evaluated the effect of the synthetic tricyclic flavonoid 1 against *S. aureus* (ATCC® 25923) and described that the mode of action is related to the impairment of the cell

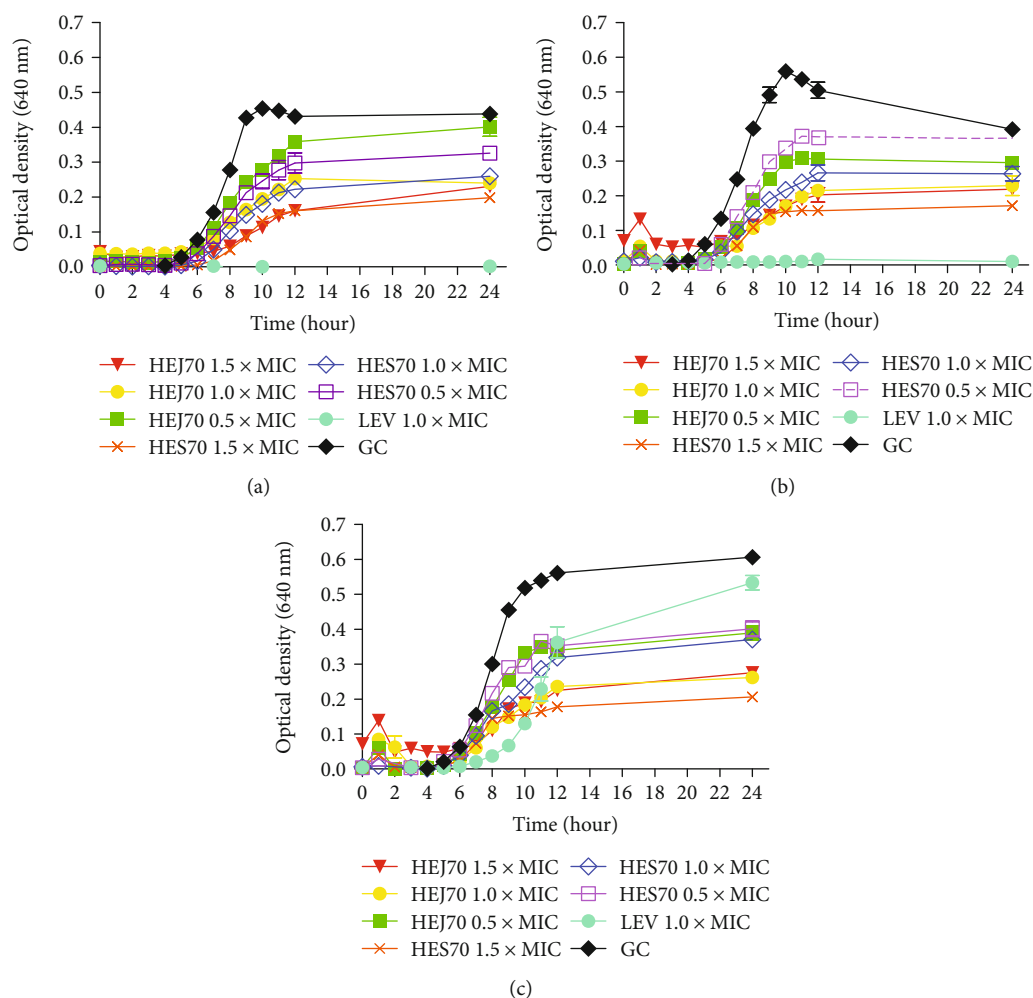


FIGURE 3: Time-kill curves of the hydroethanolic extract 70% from *Kalanchoe brasiliensis* fresh leaves collected in January (HEJ70) and September (HES70) and levofloxacin (LEV) against (a) *Salmonella Choleraesuis* (ATCC® 10708), (b) *Salmonella Typhimurium* (ATCC® 13311), and (c) *Salmonella* spp. 1507708 during 24 h of incubation. Experiments were performed in triplicate.

membrane integrity and to cell agglutination. It is noteworthy that *S. aureus* (ATCC® 25923) is a MSSA and a biofilm forming strain. Furthermore, ultrastructural changes showed that the flavonoid artonin I was able to induce destruction through cell membrane damage and abnormal division pattern alteration on MDR-*S. aureus* strains [48]. Probably, the flavonoids detected in HEJ30, HEJ50, HEJ70, HES30, HES50, and HES70 possess a similar mode of action against *S. aureus* (ATCC® 6538), *S. aureus* (ATCC® 29213), and the five MRSA clinical strains tested.

*K. brasiliensis* is also traditionally used to treat dysentery, an acute diarrheal infection that promotes a loss of water and electrolytes with a clinical scenario of abdominal cramping, fever, and bloody and/or mucoid stools, mainly caused by the *Salmonella* genus [9, 22, 49]. As depicted by Table 3, HEJ30, HEJ50, HEJ70, HES30, HES50, and HES70 were active against all ATCC® and clinical *Salmonella* strains tested. However, Silva et al. [17] described that the hydroethanolic extracts and essential oil of *K. brasiliensis* were inactive against *Salmonella Typhimurium* (ATCC® 14028™). So, to clarify this antibacterial activity and evaluate the mode

of action, time-kill, bacterial cell viability, and leakage of compounds absorbing at 280 nm assays were carried out using HEJ70 and HES70 (0.5x MIC, 1x MIC, and 1.5x MIC), since these extracts were the most active, including against *S. Choleraesuis* (ATCC® 10708), *S. Typhimurium* (ATCC® 13311), and *Salmonella* spp. 1507708 (a fluoroquinolone-resistant *Salmonella* spp. clinical isolate).

According to Figure 3, HEJ70 and HES70 clearly reduced the bacterial multiplication rate in a concentration-dependent manner when compared with the GC, extending the lag phase from 4 to 5 h (*S. Typhimurium* (ATCC® 13311)) and from 4 to 6 h (*S. Choleraesuis* (ATCC® 10708) and *Salmonella* spp. 1507708). The bacteriostatic effect, previously observed by MBC determination, was also preserved during 24 h of incubation for these three *Salmonella* strains. The increased lag period of the growth of these three *Salmonella* strains in the presence of HEJ70 and HES70 seems to be a result of the killing of the majority of the bacteria. HEJ70 and HES70 were more active than LEV against *Salmonella* spp. 1507708, demonstrating its resistance as detected by the VITEK® 2 system and the inability

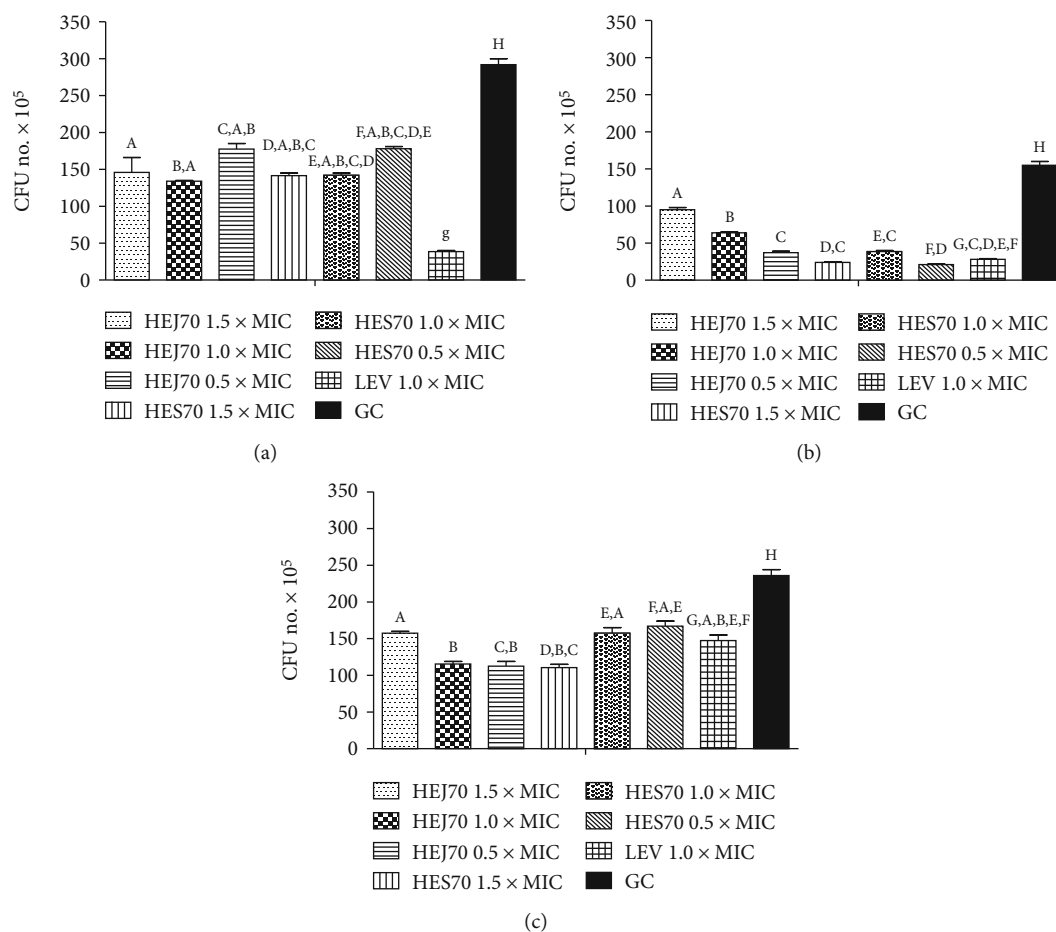


FIGURE 4: Results of the bacterial cell viability assay after exposure to hydroethanolic extract 70% from *Kalanchoe brasiliensis* fresh leaves collected in January (HEJ70) and September (HES70) and levofloxacin (LEV) against (a) *Salmonella Choleraesuis* (ATCC® 10708), (b) *Salmonella Typhimurium* (ATCC® 13311), and (c) *Salmonella* spp. 1507708. CFU: colony forming unit. Results were expressed in mean ± S.E.M. ( $n = 3$ ). Equal letters in the bars mean no difference ( $p < 0.05$ ) after variance analysis followed by Tukey's test.

to express the bactericidal effect, different from that observed with *S. Choleraesuis* (ATCC® 10708) and *S. Typhimurium* (ATCC® 13311). Figure 3 also shows that HES70 (1.5 × MIC) was the most effective extract against the three *Salmonella* strains. These findings are confirmed by Chimnoi et al. [50], who described the antibacterial activity and the mode of action of essential oil from *Ocimum gratissimum* leaves (OGEO) against *S. Typhimurium* TISTR 292 (ATCC® 13311). In addition, the effect of phenolic compounds on the growth of *S. Typhimurium* (ATCC® 14028) was reported by Pacheco-Ordaz et al. [51], which was related to the concentration and bacterial cell structure. These compounds can bind to bacterial cell membranes, and some of them can interact with lipids and proteins, altering membrane permeability, and they can also interfere with bacterial *quorum sensing* [51]. These findings were previously confirmed by Herrerias et al. [52] who described the cytotoxic effect of eupafolin that can partially be explained by alterations promoted on biological membrane properties. These reports support the possible mode of action of the detected phenolic compounds, mainly flavonoids, in HEJ70 and HES70.

The mode of action of HEJ70 and HES70 was initially investigated through the bacterial cell viability assay by the colony forming unit number per mL (CFU/mL) measurement (the CFU number able to survive exposure to the extracts and antibiotic after 1 hour (*lag phase*)). Our results revealed that the three *Salmonella* strains suffered the effect of these extracts which were able to reduce the CFU/mL, but *Salmonella* spp. 1507708 was more sensitive than *S. Choleraesuis* (ATCC® 10708) and *S. Typhimurium* (ATCC® 13311), because HEJ70 and HES70 were more effective when compared with LEV (Figure 4). This reduction can occur by bacterial cell membrane and/or membrane permeability alterations, since Chimnoi et al. [50] reported that 90% of the reduction of green light in *S. Typhimurium* (ATCC® 13311) produced severe damage of the membrane, indicating an alteration of the membrane permeability of this strain. Moreover, Mirzoeva et al. [53] previously described that the flavonoids quercetin and naringenin affected bacterial membrane potential, increasing its permeability. Other flavonoids, such as (-)-epigallocatechin gallate and (-)-epicatechin [54], the synthetic 2,4,2'-trihydroxy-5'-methylchalcone [55] and licochalcones C and D (retrochalcones) [56], and sophoraflavanone

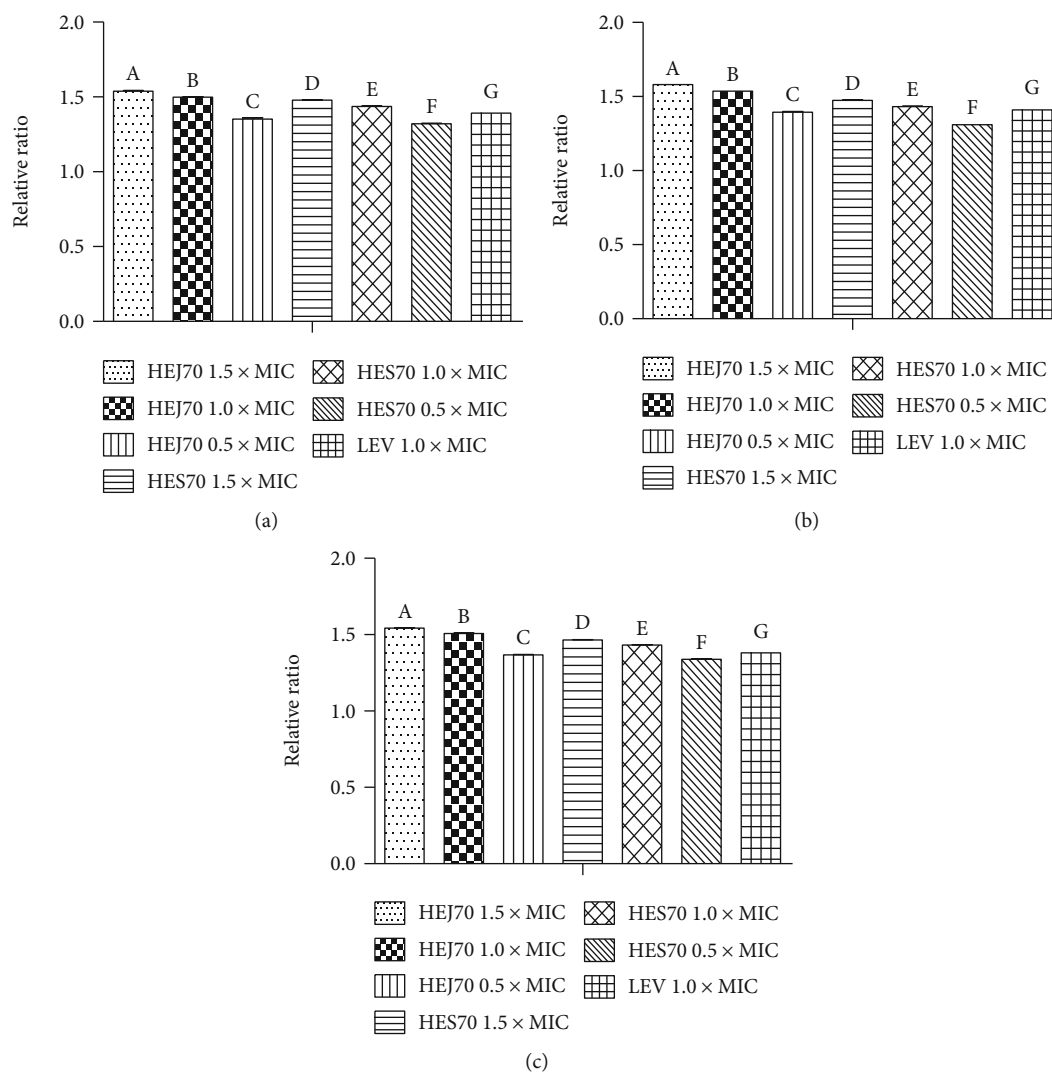


FIGURE 5: Results of the leakage of compounds absorbing at 280 nm assay expressed as a relative ratio of  $OD_{280}$  of the hydroethanolic extract 70% from *Kalanchoe brasiliensis* fresh leaves collected in January (HEJ70) and September (HES70) and treated cells and levofloxacin (LEV) to the one untreated cell of (a) *Salmonella Choleraesuis* (ATCC® 10708), (b) *Salmonella Typhimurium* (ATCC® 13311), and (c) *Salmonella* spp. 1507708. Results were expressed in mean  $\pm$  S.E.M. ( $n = 3$ ). Equal letters in the bars mean no difference ( $p < 0.05$ ) after variance analysis followed by Tukey's test.

G [57], among other subclasses of these compounds, have acted over the bacterial membrane and/or reduced the membrane fluidity. Thus, the flavonoids probably belonging to the subclasses of flavones and flavonols detected in HEJ70 and HES70 may act in the same way, being responsible for the antibiotic effect of these extracts.

The leakage of bacterial cell contents absorbing at 280 nm which indicates cell lysis and nonselective pore formation, demonstrating the membrane damage [58], was also carried out. According to Kim et al. [34], this leakage is mainly related to the loss of cell proteins that are normally retained by the cell membrane. Actually, as described by Bajpai et al. [59], measurement of specific cell leakage markers, including proteins and 260 nm absorbing materials such as nucleic acid, is an indicator of membrane integrity to a specific antibiotic in relationship to

untreated cells. As shown in Figure 5, the results displayed that there was a relevant release of bacterial cell content absorption at 280 nm from *S. Choleraesuis* (ATCC® 10708), *S. Typhimurium* (ATCC® 13311), and *Salmonella* spp. 1507708 when these strains were treated with HEJ70 and HES70 in a concentration-dependent manner. Sadiq et al. [60] demonstrated a rapid loss of proteins and nucleic acids from *S. Typhimurium* human clinical isolates due to irreversible damage to the cytoplasmic membranes in the function of the phenolic content and in the presence of phenolic acids in *Acacia nilotica*. Additionally, Tagousop et al. [61] investigated the mechanism of antibacterial action of flavonoid glycosides from *Graptophyllum grandulosum* and concluded that their mode of antibacterial activity is due to cell lysis and disruption of the cytoplasmic membrane upon membrane permeability. Therefore, the phenolic

compounds, mainly flavonoids, detected in HEJ70 and HES70 could be related to the membrane damage.

#### 4. Conclusions

*K. brasiliensis* is a natural source of flavonols and flavones and showed promising antioxidant and antibacterial agents. The antibacterial action against *Salmonella* strains is related to the cell membrane integrity and/or permeability alterations. Our data are relevant to research and develop possible novel and innovative antibiotics for therapeutic applications and to propose new approaches to manage infectious processes mainly against *Salmonella* spp.

#### Abbreviations

AMP:	Ampicillin
AMR:	Antimicrobial resistance
ATCC:	American Type Culture Collection
BSI:	Blood stream infection
CDC:	Centers for Disease Control and Prevention
CHL:	Chloramphenicol
DPPH:	2,2-Diphenyl-1-picryl-hydrazyl
GC:	Growth control
HEJ30:	Hydroethanolic extract of <i>Kalanchoe brasiliensis</i> leaves at 30% collected in January
HEJ50:	Hydroethanolic extract of <i>Kalanchoe brasiliensis</i> leaves at 50% collected in January
HEJ70:	Hydroethanolic extract of <i>Kalanchoe brasiliensis</i> leaves at 70% collected in January
HES30:	Hydroethanolic extract of <i>Kalanchoe brasiliensis</i> leaves at 30% collected in September
HES50:	Hydroethanolic extract of <i>Kalanchoe brasiliensis</i> leaves at 50% collected in September
HES70:	Hydroethanolic extract of <i>Kalanchoe brasiliensis</i> leaves at 70% collected in September
HPLC-DAD:	High-performance liquid chromatography with diode-array detection
LEV:	Levofloxacin
MDR:	Multidrug-resistant
MHA:	Müeller-Hinton agar
MHB:	Müeller-Hinton broth
MIC:	Minimal inhibitory concentration
MRSA:	Methicillin-resistant <i>Staphylococcus aureus</i>
MSSA:	Methicillin-sensitive <i>Staphylococcus aureus</i>
ROS:	Reactive oxygen species
TTC:	2,3,5-Triphenyl tetrazolium chloride
UHPLC-MS:	Ultra-high-performance liquid chromatography coupled to a mass spectrometer
VISA:	Vancomycin-intermediate <i>Staphylococcus aureus</i>
hVISA:	Heteroresistant vancomycin-intermediate <i>Staphylococcus aureus</i> .

#### Data Availability

The data used to support the findings of this study are included within the article.

#### Additional Points

**Highlights.** The hydroethanolic extracts from *K. brasiliensis* fresh leaves possess flavonoids (flavonols and flavones), mainly patuletin and eupafolin derivatives. HEJ70 and HES70 were the most active against the tested Gram-positive and Gram-negative bacterial strains. HEJ70 and HES70 were able to reduce the *Salmonella* growth rate. The mode of action of HEJ70 and HES70 on *Salmonella* probably involves the cellular membrane damage.

#### Conflicts of Interest

The authors declare that they have no conflict of interest regarding the publication of this research article.

#### Acknowledgments

The current study was financed in part by the Coordenação de Aperfeiçoamento de Pessoal de Nível Superior-Brazil (CAPES) (Finance Code 001). This study was also financially supported by Conselho Nacional de Desenvolvimento Científico e Tecnológico (CNPq), Fundação de Amparo à Pesquisa do Estado de Minas Gerais (FAPEMIG) (Grant no. CDS-APQ-04680-10), and Pró-Reitoria de Pós-Graduação e Pesquisa of the Universidade Federal de Juiz de Fora (including fellowships). The authors are grateful to Dr. Marcus Alberto Nadruz Coelho for the plant identification and to Éder Luis Tostes, Jésus de Paula Sarmento, and Fázia de Oliveira Sales for the technical support.

#### Supplementary Materials

SUPP 1: Figure 1: UV-Vis spectra analysis of the six peaks detected in the chromatographic profiles of the 30%, 50%, and 70% hydroethanolic extracts of *Kalanchoe brasiliensis* fresh leaves collected in January (HEJ30, HEJ50, and HEJ70) by HPLC-DAD at 254 nm. UV spectrum of peaks 1 (A) flavonol indicating a methylated or glycosylated patuletin, 2 (B) flavonol indicating a methylated or glycosylated patuletin, 3 (C) flavone suggesting eupafolin or derivative or flavonol indicating a methylated or glycosylated patuletin, 4 (D) flavone suggesting eupafolin or derivative, 5 (E) flavonol indicating a methylated or glycosylated patuletin, and 6 (F) flavone suggesting eupafolin or derivative; flavonols with a substituted 3-hydroxyl group (methylated or glycosylated) can show band I at 328-357 nm. SUPP 2: Figure 2: UV-Vis spectra analysis of the six peaks detected in the chromatographic profiles of 30%, 50%, and 70% hydroethanolic extracts of *Kalanchoe brasiliensis* fresh leaves collected in September (HES30, HES50, and HES70) by HPLC-DAD at 254 nm. UV spectrum of peaks 1 (A) flavonol indicating a methylated or glycosylated patuletin, 2 (B) flavonol indicating a methylated or glycosylated patuletin, 3 (C) flavonol indicating a methylated or glycosylated patuletin, 4 (D) flavonol indicating a methylated or glycosylated patuletin, 5 (E) flavonol indicating a methylated or glycosylated patuletin, 6 (F) flavone suggesting eupafolin or derivative or flavonol indicating a methylated or glycosylated

patuletin, and 7 (G) flavone suggesting eupafolin or derivative; flavonols with a substituted 3-hydroxyl group (methylated or glycosylated) can show band I at 328–357 nm. (*Supplementary Materials*)

## References

- [1] T. Hussain, B. Tan, Y. Yin, F. Blachier, M. C. B. Tossou, and N. Rahu, "Oxidative stress and inflammation: what polyphenols can do for us?," *Oxidative Medicine and Cellular Longevity*, vol. 2016, Article ID 7432797, 9 pages, 2016.
- [2] J. S. S. de Oliveira, G. da Silva Santos, J. A. Moraes et al., "Reactive oxygen species generation mediated by NADPH oxidase and PI3K/Akt pathways contribute to invasion of *Streptococcus agalactiae* in human endothelial cells," *Memórias do Instituto Oswaldo Cruz*, vol. 113, no. 6, p. e140421, 2018.
- [3] WHO, *Prioritization of Pathogens to Guide Discovery, Research and Development of New Antibiotics for Drug-Resistant Bacterial Infections, including Tuberculosis*, World Health Organization, Geneva, 2017.
- [4] S. Harakeh, I. Khan, S. B. Almasaudi, E. I. Azhar, S. al-Jaouni, and A. Niedzweicki, "Role of nutrients and phyto-compounds in the modulation of antimicrobial resistance," *Current Drug Metabolism*, vol. 18, no. 9, pp. 858–867, 2017.
- [5] M. Goswami, S. H. Mangoli, and N. Jawali, "Antibiotics and antioxidants: friends or foes during the therapy?," *Barc Newsletter*, vol. 323, no. 323, pp. 42–46, 2011.
- [6] Z. Allameh and J. Salamzadeh, "Use of antioxidants in urinary tract infection," *Journal of Research in Pharmacy Practice*, vol. 5, no. 2, pp. 79–85, 2016.
- [7] S. S. Chatterjee, "From covalent bonds to eco-physiological pharmacology of secondary plant metabolites," *Biochemical Pharmacology*, vol. 98, no. 2, pp. 269–277, 2015.
- [8] A. N. Panche, A. D. Diwan, and S. R. Chandra, "Flavonoids: an overview," *Journal of Nutritional Science*, vol. 5, 2016.
- [9] R. Milad, S. El-Ahmady, and A. N. Singab, "Genus *Kalanchoe* (Crassulaceae): a review of its ethnomedicinal, botanical, chemical and pharmacological properties," *European Journal of Medicinal Plants*, vol. 4, no. 1, pp. 86–104, 2014.
- [10] R. H. V. Mourão, F. O. Santos, E. M. Franzotti, M. P. N. Moreno, and A. R. Antonioli, "Anti-inflammatory activity and acute toxicity (LD<sub>50</sub>) of the juice of *Kalanchoe brasiliensis* (Comb.) leaves picked before and during blooming," *Phytotherapy Research*, vol. 13, no. 4, pp. 352–354, 1999.
- [11] S. S. Costa, A. Jossang, B. Bodo, M. L. M. Souza, and V. L. G. Moraes, "Patuletin acetylramnosides from *Kalanchoe brasiliensis* as inhibitors of human lymphocyte proliferative activity," *Journal of Natural Products*, vol. 57, no. 11, pp. 1503–1510, 1994.
- [12] T. Ibrahim, J. M. T. Cunha, K. Madi, L. M. B. da Fonseca, S. S. Costa, and V. L. Gonçalves Koatz, "Immunomodulatory and anti-inflammatory effects of *Kalanchoe brasiliensis*," *International Immunopharmacology*, vol. 2, no. 7, pp. 875–883, 2002.
- [13] S. S. Costa, M. L. M. Souza, T. Ibrahim et al., "Kalanchosine dimalate, an anti-inflammatory salt from *Kalanchoe brasiliensis*," *Journal of Natural Products*, vol. 69, no. 5, pp. 815–818, 2006.
- [14] F. V. Fonseca, M. M. Melo, J. Silva, G. P. Pereira, and A. M. Dantas-Barros, "Extratos de *Curcuma longa* L. e *Kalanchoe brasiliensis* Camb. no tratamento local do envenenamento por *Bothrops alternatus*," *Revista Brasileira de Farmacognosia*, vol. 14, no. 01, pp. 26–29, 2004.
- [15] C. M. Feitosa, R. M. Freitas, N. N. N. Luz, M. Z. B. Bezerra, and M. T. S. Trevisan, "Acetylcholinesterase inhibition by some promising Brazilian medicinal plants," *Brazilian Journal of Biology*, vol. 71, no. 3, pp. 783–789, 2011.
- [16] M. T. S. Trevisan, M. Z. B. Bezerra, G. M. P. Santiago, C. M. Feitosa, R. Verpoorte, and R. Braz Filho, "Atividades larvicida e anticolinesterásica de plantas do gênero *Kalanchoe*," *Química Nova*, vol. 29, no. 3, pp. 415–418, 2006.
- [17] J. G. da Silva, M. d. S. V. Pereira, A. P. D. Gurgel, J. P. de Siqueira-Júnior, and I. A. de Souza, "Atividade inibitória das folhas e caule de *Kalanchoe brasiliensis* Cambess frente a microrganismos com diferentes perfis de resistência a antibióticos," *Revista Brasileira de Farmacognosia*, vol. 19, no. 3, pp. 790–794, 2009.
- [18] E. de Araújo, G. Guerra, D. Araújo et al., "Gastroprotective and antioxidant activity of *Kalanchoe brasiliensis* and *Kalanchoe pinnata* leaf juices against indomethacin and ethanol-induced gastric lesions in rats," *International Journal of Molecular Sciences*, vol. 19, no. 5, p. 1265, 2018.
- [19] G. C. R. Medeiros and A. G. Wanderley, *Validação farmacológica da atividade antiúlcera do extrato seco de *Kalanchoe brasiliensis* Camb. (Crassulaceae)*, XVII Congresso de Iniciação Científica, I Congresso de Iniciação em Desenvolvimento Tecnológico e Inovação, Recife, Pernambuco, 2009.
- [20] A. C. de Oliveira Costa, J. M. Fernandes, T. da Silva Negreiros Neto et al., "Quantification of chemical marker of *Kalanchoe brasiliensis* (Crassulaceae) leaves by HPLC-DAD," *Journal of Liquid Chromatography & Related Technologies*, vol. 38, no. 7, pp. 795–800, 2015.
- [21] J. M. Fernandes, J. Félix-Silva, L. M. da Cunha et al., "Inhibitory effects of hydroethanolic leaf extracts of *Kalanchoe brasiliensis* and *Kalanchoe pinnata* (Crassulaceae) against local effects induced by *Bothrops jararaca* snake venom," *PLoS One*, vol. 11, no. 12, p. e0168658, 2016.
- [22] M. M. Petrov, A. Petrova, I. Stanimirova et al., "Evaluation of antimicrobial resistance among *Salmonella* and *Shigella* isolates in the University Hospital "St. George", Plovdiv, Bulgaria," *Folia Microbiologica*, vol. 62, no. 2, pp. 117–125, 2017.
- [23] J. Seo, S. Lee, M. L. Elam, S. A. Johnson, J. Kang, and B. H. Arjmandi, "Study to find the best extraction solvent for use with guava leaves (*Psidium guajava* L.) for high antioxidant efficacy," *Food Science & Nutrition*, vol. 2, no. 2, pp. 174–180, 2014.
- [24] O. Folin and W. Denis, "On phosphotungstic-phosphomolybdic compounds as color reagents," *Journal of Biological Chemistry*, vol. 12, no. 2, pp. 239–243, 1912.
- [25] T. J. da Silva Peixoto Sobrinho, C. H. T. P. da Silva, J. E. do Nascimento, J. M. Monteiro, U. P. de Albuquerque, and E. L. C. de Amorim, "Validação de metodologia espectrofotométrica para quantificação dos flavonóides de *Bauhinia cheilantha* (Bongard) Steudel," *Revista Brasileira de Ciências Farmacêuticas*, vol. 44, no. 4, pp. 683–689, 2008.
- [26] M. S. Blois, "Antioxidant Determinations by the Use of a Stable Free Radical," *Nature*, vol. 181, no. 4617, pp. 1199–1200, 1958.
- [27] Z. Chen, R. Bertin, and G. Frolidi, "EC<sub>50</sub> estimation of antioxidant activity in DPPH<sup>•</sup> assay using several statistical programs," *Food Chemistry*, vol. 138, no. 1, pp. 414–420, 2013.
- [28] P. Prieto, M. Pineda, and M. Aguilar, "Spectrophotometric quantitation of antioxidant capacity through the formation

- of a phosphomolybdenum complex: specific application to the determination of vitamin E,” *Analytical Biochemistry*, vol. 269, no. 2, pp. 337–341, 1999.
- [29] M. S. O. M. Melo and J. Mancini-Filho, “Antioxidantes naturais do fruto do dendezeiro (*Elaeis guineensis*, Jacq),” *Revista de Farmácia e Bioquímica da Universidade de São Paulo*, vol. 25, no. 2, pp. 147–157, 1989.
- [30] CLSI, *Methods for Dilution Antimicrobial Susceptibility Tests for Bacteria That Grow Aerobically. Approved Standard. CLSI Document M07-A9*, Clinical and Laboratory Standards Institute, Wayne, PA, USA, 9th edition, 2012.
- [31] CLSI, *Performance Standards for Antimicrobial Susceptibility Testing. Approved Standard. CLSI Document M100-S24*, Clinical and Laboratory Standards Institute, Wayne, PA, USA, 24rd Informational Supplement, 2014.
- [32] J. M. Andrews, “Determination of minimum inhibitory concentrations,” *Journal of Antimicrobial Chemotherapy*, vol. 48, suppl\_1, pp. 5–16, 2001.
- [33] J. B. da Silva, M. E. de Bessa, O. A. Santos Mayorga et al., “A promising antibiotic, synergistic and antibiofilm effects of *Vernonia condensata* Baker (Asteraceae) on *Staphylococcus aureus*,” *Microbial Pathogenesis*, vol. 123, pp. 385–392, 2018.
- [34] S. Kim, H. Lee, S. Lee, Y. Yoon, and K. H. Choi, “Antimicrobial action of oleanolic acid on *Listeria monocytogenes*, *Enterococcus faecium*, and *Enterococcus faecalis*,” *PLoS One*, vol. 10, no. 3, p. e0118800, 2015.
- [35] M. F. Muzitano, M. C. Bergonzi, G. O. de Melo et al., “Influence of cultivation conditions, season of collection and extraction method on the content of antileishmanial flavonoids from *Kalanchoe pinnata*,” *Journal of Ethnopharmacology*, vol. 133, no. 1, pp. 132–137, 2011.
- [36] D. Tsimogiannis, M. Samiotaki, G. Panayotou, and V. Oreopoulou, “Characterization of flavonoid subgroups and hydroxy substitution by HPLC-MS/MS,” *Molecules*, vol. 12, no. 3, pp. 593–606, 2007.
- [37] J. A. M. Pérez and T. A. F. Aguilar, “Chapter 3, chemistry of natural antioxidants and studies performed with different plants collected in Mexico,” in *Oxidative Stress and Chronic Degenerative Diseases - A Role for Antioxidants*, J. A. Morales-González, Ed., InTech, Rijeka, 2013.
- [38] J. I. Sbodio, S. H. Snyder, and B. D. Paul, “Redox mechanisms in neurodegeneration: from disease outcomes to therapeutic opportunities,” *Antioxidants & Redox Signaling*, vol. 30, no. 11, pp. 1450–1499, 2019.
- [39] M. M. Gaschler and B. R. Stockwell, “Lipid peroxidation in cell death,” *Biochemical and Biophysical Research Communications*, vol. 482, no. 3, pp. 419–425, 2017.
- [40] M. Pohanka, “Role of oxidative stress in infectious diseases. A review,” *Folia Microbiologica*, vol. 58, no. 6, pp. 503–513, 2013.
- [41] L. A. Pham-Huy, H. He, and C. Pham-Huy, “Free radicals, antioxidants in disease and health,” *International Journal of Biomedical Sciences*, vol. 4, no. 2, pp. 89–96, 2008.
- [42] V. Kuete, “Potential of Cameroonian plants and derived products against microbial infections: a review,” *Planta Medica*, vol. 76, no. 14, pp. 1479–1491, 2010.
- [43] W. Fabry, P. O. Okemo, and R. Ansorg, “Antibacterial activity of East African medicinal plants,” *Journal of Ethnopharmacology*, vol. 60, no. 1, pp. 79–84, 1998.
- [44] G. M. A. Cunha, A. A. B. Maia, E. D. R. Neri, N. A. P. Nogueira, and F. J. A. Matos, “Atividade antimicrobiana de plantas popularmente usadas no Ceará,” *Revista Brasileira de Farmácia*, vol. 76, pp. 5–6, 1995.
- [45] P. N. Reddy, K. Srirama, and V. R. Dirisala, “An update on clinical burden, diagnostic tools, and therapeutic options of *Staphylococcus aureus*,” *Infectious Diseases*, vol. 10, p. 117991611770399, 2017.
- [46] T. M. da Costa, P. G. M. Morgado, F. S. Cavalcante, A. P. Damasco, S. A. Nouér, and K. R. N. dos Santos, “Clinical and microbiological characteristics of heteroresistant and vancomycin-intermediate *Staphylococcus aureus* from blood-stream infections in a Brazilian teaching hospital,” *PLoS One*, vol. 11, no. 8, p. e0160506, 2016.
- [47] C. Babii, L. G. Bahrin, A. N. Neagu et al., “Antibacterial activity and proposed action mechanism of a new class of synthetic tricyclic flavonoids,” *Journal of Applied Microbiology*, vol. 120, no. 3, pp. 630–637, 2016.
- [48] S. Farooq, A. T. Wahab, C. D. A. Fozing, A. U. Rahman, and M. I. Choudhary, “Artonin I inhibits multidrug resistance in *Staphylococcus aureus* and potentiates the action of inactive antibiotics *in vitro*,” *Journal of Applied Microbiology*, vol. 117, no. 4, pp. 996–1011, 2014.
- [49] C. N. Fhogartaigh and D. A. B. Dance, “Bacterial gastroenteritis,” *Medicine*, vol. 41, no. 12, pp. 693–699, 2013.
- [50] N. Chimnoi, N. Reuk-ngam, P. Chuysinuan et al., “Characterization of essential oil from *Ocimum gratissimum* leaves: antibacterial and mode of action against selected gastroenteritis pathogens,” *Microbial Pathogenesis*, vol. 118, pp. 290–300, 2018.
- [51] R. Pacheco-Ordaz, A. Wall-Medrano, M. G. Goñi, G. Ramos-Clamont-Montfort, J. F. Ayala-Zavala, and G. A. González-Aguilar, “Effect of phenolic compounds on the growth of selected probiotic and pathogenic bacteria,” *Letters in Applied Microbiology*, vol. 66, no. 1, pp. 25–31, 2018.
- [52] T. Herrerias, A. A. Oliveira, M. L. Belem et al., “Effects of natural flavones on membrane properties and cytotoxicity of HeLa cells,” *Revista Brasileira de Farmacognosia*, vol. 20, no. 3, pp. 403–408, 2010.
- [53] O. K. Mirzoeva, R. N. Grishanin, and P. C. Calder, “Antimicrobial action of propolis and some of its components: the effects on growth, membrane potential and motility of bacteria,” *Microbiological Research*, vol. 152, no. 3, pp. 239–246, 1997.
- [54] H. Ikigai, T. Nakae, Y. Hara, and T. Shimamura, “Bactericidal catechins damage the lipid bilayer,” *Biochimica et Biophysica Acta*, vol. 1147, no. 1, pp. 132–136, 1993.
- [55] M. Sato, H. Tsuchiya, M. Akagiri, N. Takagi, and M. Iinuma, “Growth inhibition of oral bacteria related to denture stomatitis by anticandidal chalcones,” *Australian Dental Journal*, vol. 42, no. 5, pp. 343–346, 1997.
- [56] H. Haraguchi, K. Tanimoto, Y. Tamura, K. Mizutani, and T. Kinoshita, “Mode of antibacterial action of retrochalcones from *Glycyrrhiza inflata*,” *Phytochemistry*, vol. 48, no. 1, pp. 125–129, 1998.
- [57] H. Tsuchiya and M. Iinuma, “Reduction of membrane fluidity by antibacterial sophoraflavanone G isolated from *Sophora exigua*,” *Phytomedicine*, vol. 7, no. 2, pp. 161–165, 2000.
- [58] K. Zhou, W. Zhou, P. Li, G. Liu, J. Zhang, and Y. Dai, “Mode of action of pentocin 31-1: an antilisteria bacteriocin produced by *Lactobacillus pentosus* from Chinese traditional ham,” *Food Control*, vol. 19, no. 8, pp. 817–822, 2008.
- [59] V. K. Bajpai, A. Sharma, and K.-H. Baek, “Antibacterial mode of action of *Cudrania tricuspidata* fruit essential oil, affecting



membrane permeability and surface characteristics of food-borne pathogens,” *Food Control*, vol. 32, no. 2, pp. 582–590, 2013.

- [60] M. Sadiq, J. Tarning, T. Aye Cho, and A. Anal, “Antibacterial activities and possible modes of action of *Acacia nilotica* (L.) Del. against multidrug-resistant *Escherichia coli* and *Salmonella*,” *Molecules*, vol. 22, no. 1, p. 47, 2017.
- [61] C. N. Tagousop, J. D. Tamokou, S. E. Ekom, D. Ngnokam, and L. Voutquenne-Nazabadioko, “Antimicrobial activities of flavonoid glycosides from *Graptophyllum grandulosum* and their mechanism of antibacterial action,” *BMC Complementary and Alternative Medicine*, vol. 18, no. 1, p. 252, 2018.

## Research Article

# Niacin Protects against Butyrate-Induced Apoptosis in Rumen Epithelial Cells

Dan Luo <sup>1</sup>, Zhipeng Peng,<sup>2</sup> Le Yang,<sup>3</sup> Mingren Qu,<sup>1</sup> Xiaowen Xiong,<sup>1</sup> Lanjiao Xu,<sup>1</sup> Xianghui Zhao,<sup>1</sup> Ke Pan,<sup>1</sup> and Kehui Ouyang <sup>1</sup>

<sup>1</sup>Jiangxi Provincial Key Laboratory of Animal Nutrition, Jiangxi Agricultural University, Nanchang 330045, China

<sup>2</sup>Menon Animal Nutrition Technology Co. Ltd., Shanghai 201800, China

<sup>3</sup>Kaihua County Animal Husbandry and Veterinary Bureau, Quzhou 324000, China

Correspondence should be addressed to Kehui Ouyang; [ouyangkehui@sina.com](mailto:ouyangkehui@sina.com)

Received 6 May 2019; Revised 4 August 2019; Accepted 10 September 2019; Published 13 October 2019

Guest Editor: Manuel Campos-Toimil

Copyright © 2019 Dan Luo et al. This is an open access article distributed under the Creative Commons Attribution License, which permits unrestricted use, distribution, and reproduction in any medium, provided the original work is properly cited.

The effects and underlying mechanisms of butyrate and butyrate+niacin on apoptosis in sheep rumen epithelial cells were investigated. Cells were exposed to butyrate (0–140 mM) for 6 h. A low concentration (20 mM) of butyrate increased cell viability and promoted growth whereas high concentrations (40–140 mM) inhibited proliferation. Cells were then cocultured with 120 mM butyrate and niacin (0–100 mM) for 6 h. Niacin addition attenuated butyrate-induced cellular damage and promoted proliferation at 20–80 mM; 40 mM presented the optimal effect. Higher concentrations (100 mM) of niacin resulted in low cell viability. Subsequent experiments confirmed that 120 mM butyrate increased intracellular reactive oxygen species (ROS) production and reduced the intracellular total antioxidant capacity (T-AOC) versus the untreated control. Compared with 120 mM butyrate, cotreatment with 40 mM niacin significantly reduced the intracellular ROS content and increased the intracellular T-AOC. Flow cytometry analysis revealed that 120 mM butyrate increased the proportion of apoptotic cells by 17.8% versus the untreated control, and 120 mM butyrate+40 mM niacin treatment reduced the proportion of apoptotic cells by 28.6% and 39.4% versus the untreated control and butyrate treatment, respectively. Treatment with 120 mM butyrate increased caspase-9 and p53 mRNA levels and decreased the expression of Bcl-2 and Bax, and the Bcl-2/Bax ratio versus the untreated control. Treatment with 120 mM butyrate+40 mM niacin downregulated the expression of caspase-3 and p53 and increased the expression of Bcl-2 and Bax versus butyrate treatment alone but had no effect on the Bcl-2/Bax ratio. Thus, high concentrations of butyrate may induce rumen epithelial cell apoptosis by increasing oxidative stress and inducing caspase-9 and p53 expression. Cotreatment with niacin regulates apoptosis-related gene expression by reducing intracellular ROS production and DNA damage and downregulating caspase-3 and p53 expressions to protect rumen epithelial cells against butyrate-induced apoptosis.

## 1. Introduction

Butyrate, a short-chain fatty acid (SCFA), serves as an important energy source for ruminants [1], which promotes the growth and fission of rumen epithelial cells, and increases the size and number of rumen papillae in calves. (daily intraruminal infusions of 500 g n-butyrate) [2]. However, increased butyrate concentrations in the rumen may decrease ruminal pH, putting cattle at a high risk of ruminal acidosis [3, 4], which causes exfoliation of ruminal epithelium cuticles and erosion of the rumen. Kristensen and Harmon [5] found that when butyrate absorption in the rumen exceeds the meta-

bolic capacity of the ruminal epithelium, apoptosis of rumen epithelial cells was enhanced. Butyrate has been shown to induce apoptosis in some human cells, including tumor cells [6] and cancer cells [7]. Accumulating evidence suggests that butyrate can increase oxidative stress [8], including the overproduction of highly reactive oxygen species (ROS) [9] owing to the disturbed prooxidant/antioxidant balance. ROS should regulate the binding of p53 to DNA, thus promoting the transcriptional activity of p53 [10]. Stabilization of p53 activity leads to their increased intracellular levels and subsequently promotes apoptosis by enhancing the expression of proapoptotic proteins such as Bax and Noxa [11]. However, it is

unclear whether butyrate can induce apoptosis of rumen epithelial cells in this way.

Niacin is a precursor of the coenzymes nicotinamide adenine dinucleotide (NAD) and nicotinamide adenine dinucleotide-phosphate (NADP), which play important roles in mitochondrial respiration and have redox functions during cellular metabolism. It is reported that the supplement ruminant diets with niacin were unnecessary, because niacin from feed and ruminal microbes synthetic may be sufficient to meet their production requirements [12]. But recent studies have indicated that for high-producing cattle, supplementation of high concentrated diets with 800 mg/kg niacin can reduce the risk of ruminal acidosis, enhance the production of ruminal microbial proteins, increase nutrient ruminal degradation, and improve the growth performance of cattle *in vivo* [13]. In addition, some researches have shown that niacin can prevent excessive apoptosis [14–16] and cell membrane damage. Li et al. [17] found that NAD<sup>+</sup> can reduce intracellular phosphatidylserine (PS) ectropion and DNA damage. However, it remains unknown whether niacin can inhibit the apoptosis of rumen epithelial cells and help to alleviate the symptoms of rumen sedimentation caused by ruminal acidosis. Therefore, the objectives of this study were to investigate the effects and underlying mechanism of butyrate-induced rumen epithelial cell apoptosis and to explore the protective effects of niacin on rumen epithelial cells.

## 2. Materials and Methods

**2.1. Reagents.** Butyrate and niacin were obtained from Sigma, and Dulbecco's modified Eagle's medium (DMEM) was from Wisent. Phosphate-buffered saline (PBS), MTT, dimethyl sulfoxide (DMSO), amphotericin B, penicillin and streptomycin, 0.25% trypsin +0.02% EDTA, and 0.1% collagenase I were purchased from Solarbio. Epidermal growth factor (EGF) was obtained from Corning. ITS was purchased from ScienCell. Fetal bovine serum (FBS) was from BI, and ROS, T-AOC, and Annexin V-FITC/PI kits were obtained from Jiancheng.

**2.2. Isolation and Culture of Rumen Epithelial Cells.** This study was approved by the Animal Care and Use Committee of the College of Animal Science and Technology of Jiangxi Agricultural University.

Rumen epithelial cells were isolated from the rumen epithelial tissues of Hu sheep (aged 3–5 days, breastfeeding, both sexes). Immediately after death, the epithelium of sheep was quickly excised and the tissues were placed in ice-cold PBS. The tissues were repeatedly rinsed until the PBS remained clear. The rumen epithelial tissues were transported immediately to the laboratory. The following steps were performed in biohazard safety equipment. Briefly, the rumen epithelial tissues were washed five times with ice-cold PBS with 0.5 mg/mL amphotericin B and 100 µg/mL gentamicin. The tissues were separated from the muscle layers, cut into small pieces (about 1 cm<sup>3</sup>), and washed twice with D-Hank's buffer. Subsequently, the rumen epithelial cells were isolated from the mucosae using 0.25%

trypsin-0.02% EDTA and 0.1% collagenase I. Then, the rumen epithelial cells were seeded sequentially at a density of 1 × 10<sup>6</sup> cell/mL and cultured in DMEM supplemented with 10% (v/v) FBS, 0.5% mEGF, 0.1% ITS, and 1% (v/v) streptomycin/amphotericin B in 25 cm<sup>2</sup> plastic cell culture flasks at 37°C and 5% CO<sub>2</sub> in an incubator (Thermo Fisher Scientific, Rockford, USA). The medium was replaced every 24 h, and the pH was maintained at 7.4.

To passage, rumen epithelial cells were detached using 0.25% trypsin-0.02% EDTA in PBS and then seeded at 3 × 10<sup>5</sup> cells/25 cm<sup>2</sup> in culture flasks at 37°C with 5% CO<sub>2</sub>. In the present study, we used rumen epithelial cells at passages 1–3; no immortal rumen epithelial cell line is available.

**2.3. Cell Treatment.** Rumen epithelial cells were seeded in 96- and 6-well plates in the appropriate medium. Experiments were performed when cells reached 80%. Cell culture media were maintained at pH 7.4. First, cells were exposed to different concentrations (0–140 mM) of butyrate for 6 h in 96-well plates with six repetitions per group, to determine the effect of butyrate on cell viability. Then, the cells were cocultured with an appropriate concentration (obtained from the first test) of butyrate and different concentrations (0–100 mM) of niacin for 6 h in 96-well plates with six repetitions per group, to determine the effect of niacin on cell viability. After that, the cells were cocultured with butyrate and niacin (optimum dose determined from the above tests) for 6 h in 6-well plates with three repetitions per group, to determine the ROS, total antioxidant capacity (T-AOC), cell apoptosis index, and the relative expression of apoptosis-related genes.

**2.4. Cell Viability Assay.** Cell viability was measured by MTT assay as previously described [18]. In brief, rumen epithelial cells were seeded in 96-well plates at a density of 5 × 10<sup>3</sup>/well and treated with butyrate and/or niacin at 37°C. After 6 h, 5 mg/mL MTT was added, and after 4 h further, MTT was replaced with 150 µL DMSO/well. The cells were lysed by placing the plates on a shaker for 10 min to solubilize the formazan crystals within the cells. Absorbance at 490 nm was measured with a microplate spectrophotometer (Thermo Fisher Scientific, Rockford, USA). All independent experiments were performed in triplicate. Change in relative cell viability was presented as a response ratio (RR), which was calculated by the following formula:

$$RR = \ln \left( \frac{OD_{\text{treated}}}{OD_{\text{untreated}}} \right), \quad (1)$$

where RR represents the response ratio, OD<sub>treated</sub> indicates the OD value of treated cells, OD<sub>untreated</sub> is the OD value of untreated cells, RR > 0 is an increase in viability in treated cells compared with untreated cells, and RR < 0 is a decrease in the viability of treated cells compared with untreated cells.

**2.5. Determination of Intracellular ROS Level.** Intracellular ROS levels were measured using 2',7'-dichlorodihydro-fluorescein diacetate (DCFH-DA) following the manufacturer's protocol. Rumen epithelial cells were collected and washed twice with PBS. After centrifugation, cells were incubated with

TABLE 1: PCR amplification primer design.

Genes	Primer sequence	Origin	Size (bp)	Annealing temperature (°C)
GADPH	F: 5'-AGGTTGTCTCCTGCGACTTCA-3' R: 5'-CCCTGTTGCTGTAGCCGAAT-3'	NM001190390.1	132	84.59
Fas	F: 5'-CTCTGAGGGGCTGAGATTGA-3' R: 5'-GTTTGCCAGGAGGACAAGG-3'	NM001123003.1	107	82.44
Bcl-2	F: 5'-TGTTTGATTTCTCCTGGCTGT-3' R: 5'-ACTGCTTTCACGAACCTTTTG-3'	XM012103831	145	86.69
Bax	F: 5'-TTCCGACGGCAACTTCAAC-3' R: 5'-GAGCACTCCAGCCACAAAGA-3'	XM015100639.1	244	88.29
Caspase-3	F: 5'-GCAGCAAACCTCAGGGAAA-3' R: 5'-CATGGCTTAGAAGCACGCA-3'	XM15104559.1	154	80.98
Caspase-9	F: 5'-TGTTGCCGTTTCCTTCTCC-3' R: 5'-CTAGCACTTCGCTTTCTGGTG-3'	XM015099300.1	111	84.35
Caspase-8	F: 5'-AAAATGCCCTTCCCTTGTG-3' R: 5'-CTTCCCTCTGTCTGAGTCGGT-3'	XM012142500.2	110	80.95
PARP-1	F: 5'-CTCCAATCGCTTCTACACC-3' R: 5'-AACCACCCCTGAGTAGACTGTAG-3'	XM_012118480.2	49	86.07
P53	F: 5'-CAGGAGACATTTTCCGACTTG-3' R: 5'-TCATCCAGCCAGGTGACAA-3'	NM001009403.1	122	83.89

10  $\mu$ M DCFH-DA for 30 min at 37°C in the dark. Subsequently, cells were washed twice and then resuspended in PBS. Fluorescence was measured using a plate reader (Thermo Fisher Scientific, Rockford, USA) with an excitation wavelength of 485 nm and an emission wavelength of 530 nm. The results were expressed as the fluorescence value.

**2.6. Determination of Intracellular T-AOC.** Intracellular T-AOC was estimated using a commercial kit according to the manufacturer's protocol. Cells were collected, centrifuged for 5 min at 1200 rpm, and resuspended in PBS. After cell disruption, homogeneous protein and T-AOC were measured at 595 and 520 nm, respectively, with a spectrophotometer (Thermo Fisher Scientific, Rockford, USA). T-AOC levels were expressed per mg of protein (U/mg prot).

**2.7. Annexin V-FITC/PI Apoptotic Assay.** Annexin V and propidium iodide (PI) staining were used to quantify the number of apoptotic cells. Rumen epithelial cells were collected and washed twice with PBS. After centrifuging, cells were resuspended in 500  $\mu$ L of binding buffer in a flow cytometric tube, to which 5  $\mu$ L of Annexin V-FITC and 5  $\mu$ L of PI were added and mixed well. After incubating for 10 min at room temperature in the dark, the stained cells were analyzed by flow cytometry (Becton Dickinson, San Jose, USA).

**2.8. Real-Time Polymerase Chain Reaction.** Total RNA was extracted from rumen epithelial cells with an RNA kit (Takara) according to the manufacturer's instructions. The amount and quality of RNA were determined using a spectrophotometer (Bio-Rad Laboratories, Hercules, USA). Total

RNA (2.0  $\mu$ g) was then reverse transcribed to form cDNA using Transcript reverse transcriptase (Bio-Rad Laboratories, Hercules, USA) for quantitative real-time PCR, according to the manufacturer's instructions. Every reaction consisted of 2  $\mu$ L cDNA, 1  $\mu$ L of each primer (100 pmol), 1  $\mu$ L of dNTP Mix (0.5 mmol/L final concentration), and 9.5  $\mu$ L RNase-free ddH<sub>2</sub>O (total reaction volume 14.5  $\mu$ L). Selected genes were quantified by RT-PCR using Primer 5.0 software according to the gene sequence provided by GenBank in NCBI. Primer sequences are shown in Table 1. RT-PCR cycles consisted of 95°C for 3 min, followed by 45 cycles of 95°C for 7 s, 57°C for 10 s, and 72°C for 15 s (Roche, Applied Science, Mannheim, Germany). Fold change in target gene expression was normalized by that of GAPDH using the  $2^{-\Delta\Delta C_t}$  method.

**2.9. Statistical Analysis.** All results are presented as the mean  $\pm$  standard deviation (SD). GraphPad Prism 5.01 software and Statistical Package for the Social Sciences (SPSS 17.0) packages were used for statistical analyses. Differences among groups were tested using a one-way analysis of variance (ANOVA). Duncan's multiple comparison test was used to compare statistical differences between treatments. A value of  $P < 0.05$  was considered to indicate a significant difference.

### 3. Results

**3.1. Effects of Butyrate on the Relative Viability of Rumen Epithelial Cells.** First, we examined whether butyrate affects the relative viability of rumen epithelial cells. Data are

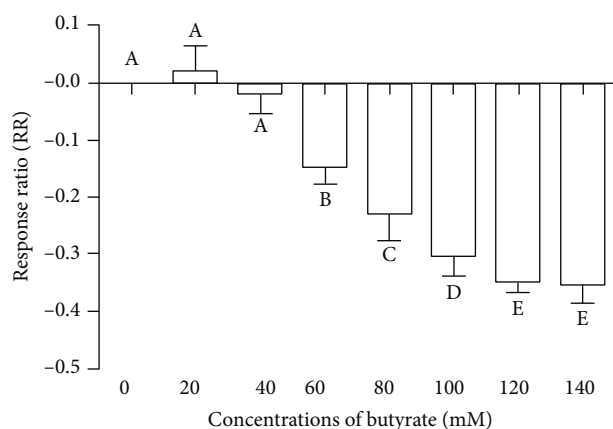


FIGURE 1: Effects of different concentrations of butyrate on the response ratio (RR) of relative cell viability. Rumen epithelial cells were treated with various concentrations of butyrate for 6 h, and cell viability was determined by MTT assay. Data are presented as the RR.  $RR = \ln(OD_{\text{treated}}/OD_{\text{untreated}})$ , where RR is the response ratio,  $OD_{\text{treated}}$  refers to the OD value of treated cells,  $OD_{\text{untreated}}$  is the OD value of untreated cells,  $RR > 0$  indicates an increase in relative viability in treated cells compared with untreated cells, and  $RR < 0$  indicates a decrease in the relative viability of treated cells compared with untreated cells. Values with different letters indicate significant differences ( $P < 0.05$ ).

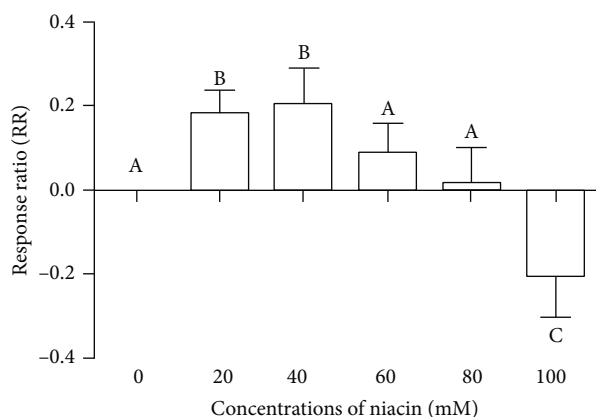


FIGURE 2: Effects of different concentrations of niacin on the response ratio (RR) of relative cell viability. Rumen epithelial cells were cotreated with 120 mM butyrate and various concentrations niacin for 6 h, and cell viability was determined by MTT assay. Data are presented as the RR.  $RR = \ln(OD_{\text{(butyrate+niacin)-treated}}/OD_{\text{butyrate-treated}})$ , where RR is the response ratio,  $OD_{\text{butyrate-treated}}$  is the OD value of butyrate-treated cells,  $OD_{\text{(butyrate+niacin)-treated}}$  is the OD value of cells cotreated with butyrate and niacin,  $RR > 0$  indicates an increase in the relative viability of cells cotreated with butyrate and niacin compared with butyrate-treated cells, and  $RR < 0$  indicates a decrease in the relative viability of cells cotreated with butyrate and niacin compared with butyrate-treated cells. Values with different letters indicate significant differences ( $P < 0.05$ ).

presented as the RR as shown in Figure 1. The results showed that the relative viability was higher in cells treated with 20 mM butyrate compared with untreated cells, although this was not statistically significant ( $P > 0.05$ ). However, cell growth was significantly inhibited following exposure to

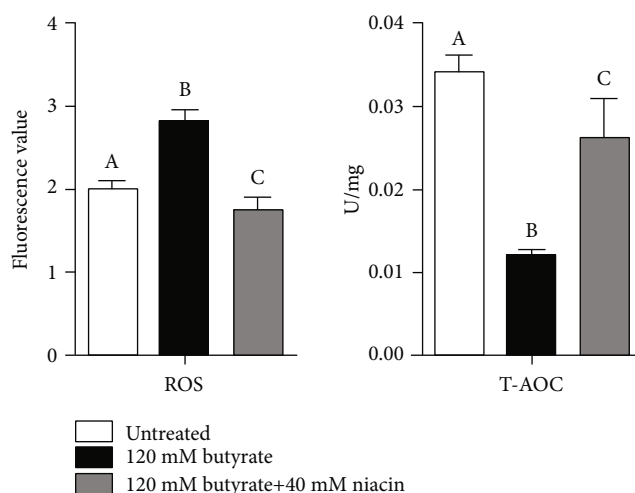


FIGURE 3: Effects of butyrate and niacin on the intracellular reactive oxygen species (ROS) and the intracellular total antioxidant capacity (T-AOC) of rumen epithelial cells. Rumen epithelial cells were exposed to 120 mM butyrate with or without 40 mM niacin for 6 h. Intracellular ROS levels were measured using 2',7'-dichlorodihydro-fluorescein-diacetate (DCFH-DA). Intracellular T-AOC was estimated using a commercial kit according to the manufacturer's protocol. Data are presented as the mean  $\pm$  standard deviation (SD). Values with different letters indicate significant differences ( $P < 0.05$ ).

butyrate at 60–120 mM ( $P < 0.05$ ), and the differences in relative cell viability were not significant following treatment with butyrate 120–140 mM ( $P > 0.05$ ). Therefore, 120 mM butyrate was confirmed as the optimum dose for use in subsequent experiments.

**3.2. Effects of Niacin on the Relative Viability of Rumen Epithelial Cells Cocultured with Butyrate.** We further investigated the effect of niacin on butyrate-induced damage in rumen epithelial cells. The results are presented as the RR as shown in Figure 2. The results showed that, compared with butyrate treatment alone, 20 and 40 mM niacin significantly increased relative cell viability ( $P < 0.05$ ), which peaked with 40 mM niacin. Niacin at 60 and 80 mM had no effect on relative cell viability ( $P > 0.05$ ), while 100 mM significantly decreased relative cell viability ( $P < 0.05$ ) and was found to be cytotoxic.

**3.3. Effects of Butyrate and Niacin on Intracellular ROS Levels and T-AOC in Rumen Epithelial Cells.** 120 mM butyrate and 120 mM butyrate+40 mM niacin were used in subsequent experiments. As shown in Figure 3, intracellular ROS levels were significantly increased and intracellular T-AOC was significantly decreased in cells treated with butyrate alone ( $P < 0.05$ ) compared with untreated cells. Cotreatment with niacin significantly attenuated the excess generation of intracellular ROS and enhanced the intracellular T-AOC in butyrate-stimulated cells ( $P < 0.05$ ). Furthermore, it significantly decreased the intracellular ROS levels in untreated cells ( $P < 0.05$ ). The intracellular T-AOC in untreated cells

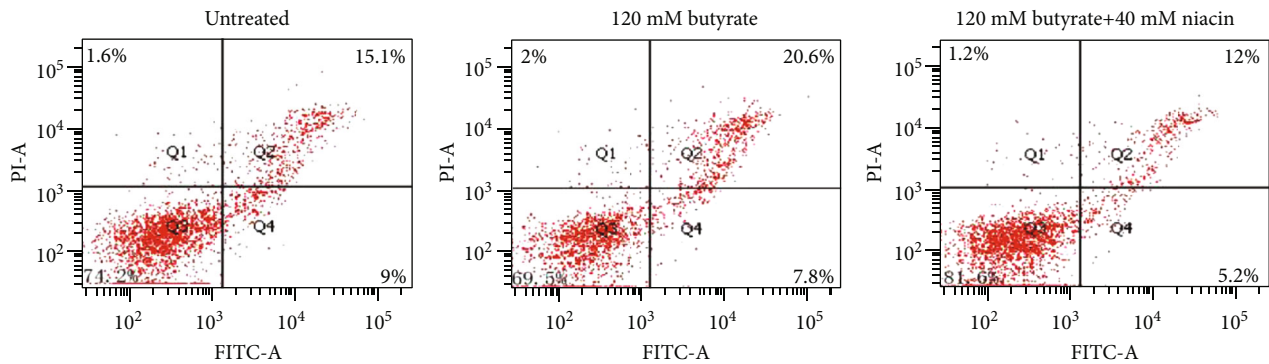


FIGURE 4: Apoptosis in rumen epithelial cell apoptosis determined by flow cytometry.

TABLE 2: Effects of butyrate and niacin on rumen epithelial cell apoptosis (%).

	Normal cells	Necrotic cells	Early apoptotic cells	Late apoptotic cells	Apoptosis index
Untreated	74.3 ± 1.3 <sup>a</sup>	1.6 ± 0.1 <sup>ab</sup>	9.0 ± 1.1 <sup>a</sup>	15.1 ± 1.6 <sup>a</sup>	24.1 ± 1.3 <sup>a</sup>
120 mM butyrate	69.6 ± 1.8 <sup>b</sup>	2.0 ± 0.5 <sup>a</sup>	7.8 ± 1.2 <sup>ab</sup>	20.6 ± 1.8 <sup>b</sup>	28.4 ± 2.3 <sup>b</sup>
120 mM butyrate+40 mM niacin	81.6 ± 0.7 <sup>c</sup>	1.2 ± 0.1 <sup>b</sup>	5.2 ± 0.3 <sup>b</sup>	12.0 ± 0.6 <sup>c</sup>	17.2 ± 0.7 <sup>c</sup>

was not improved by the addition niacin and was lower than that observed in untreated cells ( $P < 0.05$ ).

**3.4. Effects of Butyrate and Niacin on the Apoptosis of Rumen Epithelial Cells.** To determine whether cellular viability is affected by butyrate treatment, cells were analyzed by flow cytometry following Annexin-V FITC/PI double staining. As shown in Figure 4 and Table 2, butyrate treatment significantly decreased the proportion of normal cells and increased the proportion of late-apoptotic cells compared with the untreated control ( $P < 0.05$ ). The rate of apoptosis with butyrate significantly increased by 17.8% compared with the untreated control ( $P < 0.05$ ). Cotreatment with niacin markedly increased the proportion of normal cells and decreased the proportion of necrotic and late-apoptotic cells compared with butyrate treatment alone ( $P < 0.05$ ). The rate of apoptosis following butyrate+niacin treatment was significantly decreased by 28.6% ( $P < 0.05$ ) compared with the untreated control and was significantly decreased by 39.4% ( $P < 0.05$ ) compared with butyrate treatment alone.

Rumen epithelial cells were exposed to 120 mM butyrate with or without 40 mM niacin for 6 h. Apoptosis was examined by Annexin V-FITC/PI double staining and analyzed by flow cytometry. Data are presented as the mean ± standard deviation (SD). Values with different letters indicate significant differences ( $P < 0.05$ ).

**3.5. Effects of Butyrate and Niacin on the Relative Expression of Apoptosis-Related Factors in Rumen Epithelial Cells.** As shown in Figure 5, compared with the untreated control, caspase-3 expression was not affected following butyrate treatment ( $P > 0.05$ ); however, caspase-3 expression was significantly decreased in cells treated with butyrate+niacin ( $P < 0.05$ ). Caspase-3 expression was lower with butyrate+niacin treatment than with butyrate treatment alone ( $P < 0.05$ ). The expression of caspase-9 was significantly increased ( $P < 0.05$ ) with butyrate treatment and butyrate+

niacin treatment ( $P < 0.05$ ) compared with the untreated control, but there were no significant differences between butyrate treatment and butyrate+niacin treatment ( $P > 0.05$ ). P53 mRNA levels with butyrate treatment were higher than in the untreated cells and with butyrate+niacin treatment ( $P < 0.05$ ); however, there were no significant differences between the untreated control and with butyrate+niacin treatment ( $P > 0.05$ ). Butyrate treatment alone significantly decreased the expression of Bcl-2 and Bax and the ratio of Bcl-2/Bax compared with the untreated control ( $P < 0.05$ ). Cotreatment with niacin markedly increased the expression of Bcl-2 and Bax ( $P < 0.05$ ); however, there was no difference in the ratio of Bcl-2/Bax in butyrate-stimulated cells ( $P > 0.05$ ). Butyrate exposure, with and without niacin, had no effect on caspase-8, Fas, and poly-ADP-ribose polymerase-1 (PARP-1) mRNA levels in rumen epithelial cells ( $P > 0.05$ ).

## 4. Discussion

**4.1. Effects of Butyrate and Niacin on the Growth of Rumen Epithelial Cells.** Butyrate, a product of ruminal fermentation, is also an energy source for rumen epithelial cells [1]. The results of a previous study suggested that butyrate promotes cell proliferation by accelerating cell division [19] and inhibiting apoptosis [20]. In addition, butyrate can inhibit cell proliferation by stimulating apoptosis and promoting differentiation. The effects of butyrate on cell growth are cell- and concentration-dependent. Ruemmele et al. [21] found no differences in the viability of Caco-2 cells following treatment with 0.1–2 mmol/L butyrate for 48 h, whereas growth was inhibited with 100 mmol/L butyrate. Siavoshian et al. [22] reported that 1 mmol/L butyrate can hinder the growth of intestinal epithelial cells, while 8 mmol/L butyrate completely inhibited cell growth. In the current study, we found that a low concentration (20 mM) of butyrate promoted the growth of rumen epithelial cells, whereas high

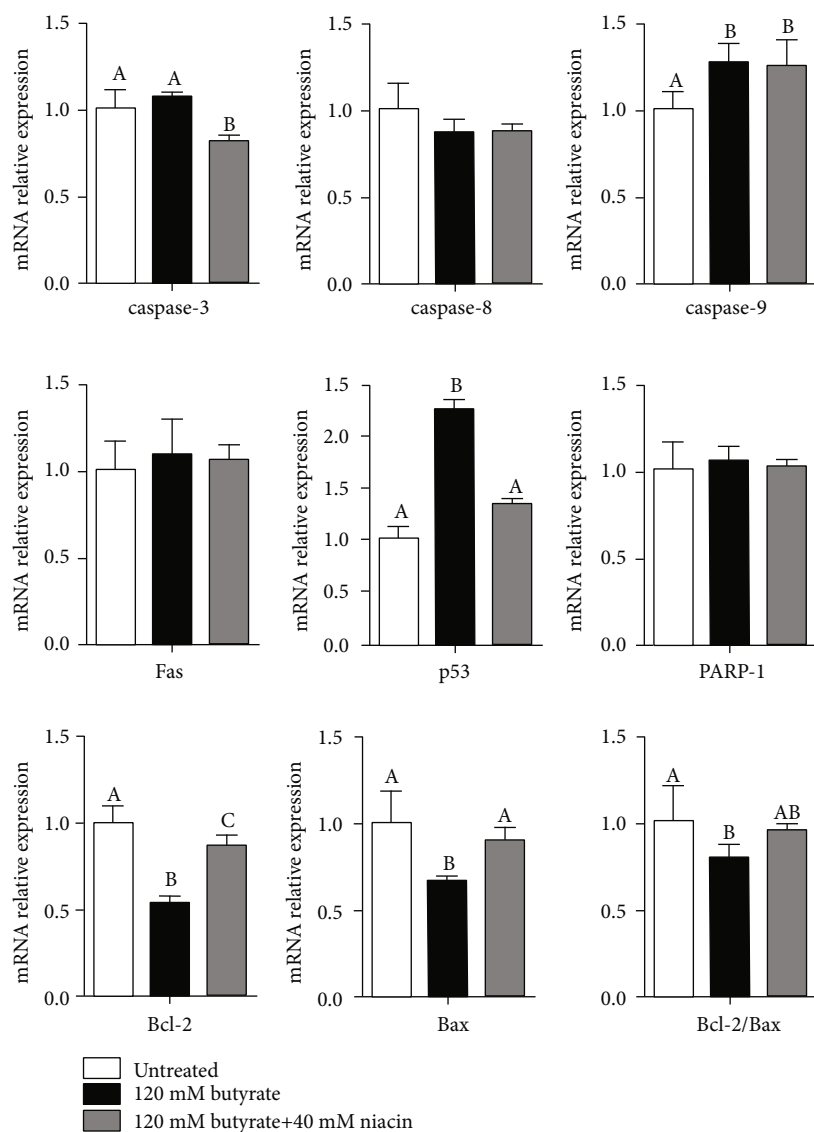


FIGURE 5: Effects of butyrate and niacin on the relative mRNA expression of apoptosis-related genes in rumen epithelial cells. Rumen epithelial cells were exposed to 120 mM butyrate with or without 40 mM niacin for 6 h. The expressions of caspase-3, caspase-8, caspase-9, Fas, p53, PARP-1, Bcl-2, and Bax mRNA were determined by RT-PCR analysis, and the ratio of Bcl-2/Bax was determined. Data are presented as the mean  $\pm$  standard deviation (SD). Values with different letters indicate significant differences ( $P < 0.05$ ).

concentrations (40–140 mM) of butyrate inhibited cell proliferation. These results suggest that rumen epithelial cells may have tolerance to butyrate.

Niacin, also known as vitamin B<sub>3</sub>, is the dietary precursor for NAD(H) and NADP(H) synthesis. NAD participates in cellular metabolism and plays an important role in cellular proliferation and the repair of damaged cells [23]. Lin et al. [14] reported significant improvements in cell viability with a graded increase in niacin concentrations from 5 to 20  $\mu$ M, while 40  $\mu$ M niacin decreased viability of spontaneously immortalized human keratinocytes treated with ultraviolet irradiation. Liu et al. [24] showed that 200 mg/kg nicotinic acid or nicotinamide effectively increased the level of NAD<sup>+</sup> and protected the functional cells in damaged brain tissue. The results of the present study indicated that low concentrations (20–80 mM) of niacin had a positive effect on the

reduced cell viability induced by butyrate, similar to the results of previous studies. However, high concentrations (100 mM) of niacin decreased cell viability and presented toxic effects, whereby the observed proportion of dead cells may have been due to the duration of niacin exposure.

**4.2. Effects of Butyrate and Niacin on the Redox State of Rumen Epithelial Cells.** Overproduction of intracellular ROS can induce DNA and protein damage, which may contribute to cell death [9]. In this study, butyrate increased intracellular ROS production, decreased intracellular T-AOC, led to imbalanced redox levels in rumen epithelial cells, and increased cellular oxidative stress [25], which may be related to DNA double-strand DNA damage [26]. Niacin is an important antioxidant, which reduces oxidative damage through the conversion of NAD<sup>+</sup> to NADP<sup>+</sup> (the precursor

for reductive NADPH formation) by NADK [27], the direct antioxidation effects of NADH [28], and reduced intracellular ROS production [29]. Here, we found that butyrate increased intracellular oxidative stress, which may induce apoptosis, as reported by Pant et al. [30] and Salimi et al. [31], and niacin can reduce butyrate-induced oxidative damage in cells; thus, these results may be related to the antioxidant function of niacin [32].

**4.3. Effects of Butyrate and Niacin on the Apoptosis of Rumen Epithelial Cells.** Our data indicate that high concentrations of butyrate inhibited the proliferation of rumen epithelial cells. Our results showed that the cytotoxic effect of butyrate was related to the induction of apoptosis. Sodium butyrate can also sensitize human pancreatic cancer cell lines via both the intrinsic and extrinsic apoptotic pathways, as reported by Natoni et al. [33]. In the present study, we demonstrated a significant accumulation of apoptotic cells during butyrate treatment. Meanwhile, cotreatment with niacin can prevent butyrate-induced apoptosis in rumen epithelial cells and decrease the proportion of apoptotic cells, as shown in a previous study [34]. This may be explained by the ability of NAD<sup>+</sup> to reduce the ectopion of PS during prophase in apoptosis, DNA damage during anaphase in apoptosis [17], and promote ATP generation. In addition, Mateuszuk et al. [35] found that nicotinamide can deacetylate p53 proteins, directly inhibit p53 transcription and activation through sirt, and prevent growth arrest and inhibit apoptosis, thereby prolonging the life of cells *in vivo*. To further validate these findings, we determined the mRNA expression of genes associated with apoptosis. When cells are subjected to stress, apoptotic initiators, such as Fas, caspase-8, caspase-9, and Bax, are activated, followed by the executor caspase, caspase-3. Activated caspase-3 increases expression of PARP, which acts as a “DNA nick sensor” and plays an important role in the response to intracellular DNA damage [23]. P53 is an important transcription factor, which can participate in cell cycle progression and apoptosis by regulating the transcriptional activity of many genes [33]. In the present study, we found that compared with the untreated control, butyrate increased the expression of caspase-9 and p53 and decreased the expression of Bcl-2 and Bax and the ratio of Bcl-2/Bax. Therefore, we suggest that butyrate may induce apoptosis in rumen epithelial cells by increasing intracellular oxidative stress and inducing the expression of caspase-9 and p53. Meanwhile, compared with butyrate treatment alone, cotreatment with butyrate and niacin can decrease oxidative damage and the expression of caspase-3 and p53 and increase the expression of Bcl-2 and Bax. These results suggested that the inhibitory effect of niacin on butyrate-induced apoptosis in rumen epithelial cells may be related to improvement cell antioxidant capacity, promotion DNA repair, and the inhibition of downstream caspase-3 and p53 activation. However, expression of Fas, caspase-8, and PARP-1 was unchanged in rumen epithelial cells exposed to butyrate, regardless of the presence of niacin, indicating that butyrate-induced rumen epithelial cell apoptosis is independent of the extrinsic pathway, and the protective effect of niacin on butyrate-induced apoptosis does not occur through this pathway.

## 5. Conclusions

In summary, low concentrations of butyrate promoted the growth of rumen epithelial cells, whereas high concentrations induced apoptosis. The underlying mechanism may be related to butyrate increasing intracellular ROS levels and inducing the expression of caspase-9 and p53. Adding an appropriate concentration (40 mM) of niacin can inhibit butyrate-induced apoptosis of rumen epithelial cells, which may be associated with reduced intracellular oxidative stress, inhibition of caspase-3 and p53 activation, and DNA damage repair.

## Data Availability

The data used to support the findings of this study are available from the corresponding author upon request.

## Conflicts of Interest

The authors declare that there is no conflict of interest regarding the publication of this paper.

## Acknowledgments

The authors gratefully acknowledge the National Natural Science Foundation of China (31560648, 31260561), Jiangxi Provincial Cattle and Sheep Industry Technology & System (JXARS-13), National Beef Cattle Industry Technology & System (CARS-38), and Jiangxi Modern Agricultural Scientific and Technology Cooperative Innovation Project (JXXTCX201702).

## References

- [1] M. Bugaut, “Occurrence, absorption and metabolism of short chain fatty acids in the digestive tract of mammals,” *Comparative Biochemistry and Physiology Part B: Comparative Biochemistry*, vol. 86, no. 3, pp. 439–472, 1987.
- [2] Z. Shen, S. Kuhla, R. Zitnan et al., “Intraruminal infusion of n-butyric acid induces an increase of ruminal papillae size independent of IGF-1 system in castrated bulls,” *Archives of Animal Nutrition*, vol. 59, no. 4, pp. 213–225, 2005.
- [3] A. M. Danscher, S. C. Li, P. H. Andersen, E. Khafipour, N. B. Kristensen, and J. C. Plaizier, “Indicators of induced subacute ruminal acidosis (SARA) in Danish Holstein cows,” *Acta Veterinaria Scandinavica*, vol. 57, no. 1, p. 39, 2015.
- [4] N. Schlau, L. L. Guan, and M. Oba, “The relationship between rumen acidosis resistance and expression of genes involved in regulation of intracellular pH and butyrate metabolism of ruminal epithelial cells in steers,” *Journal of Dairy Science*, vol. 95, no. 10, pp. 5866–5875, 2012.
- [5] N. B. Kristensen and D. L. Harmon, “Effect of increasing ruminal butyrate absorption on splanchnic metabolism of volatile fatty acids absorbed from the washed reticulorumen of steers,” *Journal of Animal Science*, vol. 82, no. 7, pp. 2033–2042, 2004.
- [6] J. S. Chen, D. V. Faller, and R. A. Spanjaard, “Short-chain fatty acid inhibitors of histone deacetylases: promising anticancer therapeutics,” *Current Cancer Drug Targets*, vol. 3, no. 3, pp. 219–236, 2003.



- [7] P. Rouet-Benzineb, T. Aparicio, S. Guilmeau et al., "Leptin counteracts sodium butyrate-induced apoptosis in human colon cancer ht-29 cells via NF- $\kappa$ B signaling," *Journal of Biological Chemistry*, vol. 279, no. 16, pp. 16495–16502, 2004.
- [8] M. C. Chang, Y. L. Tsai, Y. W. Chen et al., "Butyrate induces reactive oxygen species production and affects cell cycle progression in human gingival fibroblasts," *Journal of Periodontal Research*, vol. 48, no. 1, pp. 66–73, 2013.
- [9] A. J. McGowan, A. G. Bowie, L. A. J. O'Neill, and T. G. Cotter, "The production of a reactive oxygen intermediate during the induction of apoptosis by cytotoxic insult," *Experimental Cell Research*, vol. 238, no. 1, pp. 248–256, 1998.
- [10] C. Méplan, M. J. Richard, and P. Hainaut, "Redox signalling and transition metals in the control of the p53 pathway," *Biochemical Pharmacology*, vol. 59, no. 1, pp. 25–33, 2000.
- [11] M. Schuler and D. R. Green, "Mechanisms of p53-dependent apoptosis," *Biochemical Society Transactions*, vol. 29, no. 6, pp. 684–688, 2001.
- [12] G. Flachowsky, "Niacin in dairy and beef cattle nutrition," *Archives of Animal Nutrition*, vol. 43, no. 3, pp. 195–213, 1993.
- [13] K. H. Ouyang, Q. Zhang, Y. Y. Lu, M. R. Qu, X. W. Xiong, and K. Pan, "Effects of nicotinic acid supplementation in high concentrate diet on dynamic changes of culture solution pH and fermentation parameters of *in vitro* rumen fermentation," *China Journal of Animal Nutrition*, vol. 26, no. 1, pp. 115–124, 2014, in Chinese.
- [14] F. Lin, W. Xu, C. Guan et al., "Niacin protects against uvb radiation-induced apoptosis in cultured human skin keratinocytes," *International Journal of Molecular Medicine*, vol. 29, no. 4, pp. 593–600, 2012.
- [15] G. Su, G. L. Sun, H. Liu et al., "Niacin suppresses progression of atherosclerosis by inhibiting vascular inflammation and apoptosis of vascular smooth muscle cells," *Medical Science Monitor*, vol. 21, pp. 4081–4089, 2015.
- [16] H. Huang, P. Koelle, M. Fendler et al., "Niacin reverses migratory macrophage foam cell arrest mediated by oxLDL *in vitro*," *PLoS One*, vol. 9, no. 12, pp. 1–18, 2014.
- [17] F. Li, Z. C. Zhao, and K. Maiese, "Cell life versus cell longevity: the mysteries surrounding the NAD<sup>+</sup> precursor nicotinamide," *Current Medicinal Chemistry*, vol. 13, no. 8, pp. 883–895, 2005.
- [18] T. Mosmann, "Rapid colorimetric assay for cellular growth and survival: application to proliferation and cytotoxicity assays," *Journal of Immunological Methods*, vol. 65, no. 1–2, pp. 55–63, 1983.
- [19] T. Sakata and H. Tamate, "Rumen epithelial cell proliferation accelerated by rapid increase in intraruminal butyrate," *Journal of Dairy Science*, vol. 61, no. 8, pp. 1109–1113, 1978.
- [20] J. Mentschel, R. Leiser, C. Mülling, C. Pfarrer, and R. Claus, "Butyric acid stimulates rumen mucosa development in the calf mainly by a reduction of apoptosis," *Archiv Für Tierernährung*, vol. 55, no. 2, pp. 85–102, 2001.
- [21] F. M. Ruumemele, S. Schwartz, E. G. Seidman, S. Dionne, E. Levy, and M. J. Lentze, "Butyrate induced Caco-2 cell apoptosis is mediated via the mitochondrial pathway," *Gut*, vol. 52, no. 1, pp. 94–100, 2003.
- [22] S. Siavoshian, J. P. Segain, M. Kornprobst et al., "Butyrate and trichostatin A effects on the proliferation/differentiation of human intestinal epithelial cells: induction of cyclin D3 and p21 expression," *Gut*, vol. 46, no. 4, pp. 507–514, 2000.
- [23] K. Oumouna-Benachour, C. P. Hans, and Y. Suzuki, "Poly(ADP-ribose) polymerase inhibition reduces atherosclerotic plaque size and promotes factors of plaque stability in apolipoprotein E-deficient mice: effects on macrophage recruitment, NF- $\kappa$ B nuclear translocation, and foam cell death," *Circulation*, vol. 115, no. 18, pp. 2442–2450, 2007.
- [24] D. Liu, R. Gharavi, M. Pitta, M. Gleichmann, and M. P. Mattson, "Nicotinamide prevents NAD<sup>+</sup> depletion and protects neurons against excitotoxicity and cerebral ischemia: NAD<sup>+</sup> consumption by sirt1 may endanger energetically compromised neurons," *Neuromolecular Medicine*, vol. 11, no. 1, pp. 28–42, 2009.
- [25] M. Louis, R. R. Rosato, L. Brault et al., "The histone deacetylase inhibitor sodium butyrate induces breast cancer cell apoptosis through diverse cytotoxic actions including glutathione depletion and oxidative stress," *International Journal of Oncology*, vol. 25, no. 6, pp. 1701–1711, 2004.
- [26] L. Li, Y. Sun, J. Liu et al., "Histone deacetylase inhibitor sodium butyrate suppresses DNA double strand break repair induced by etoposide more effectively in MCF-7 cells than in HEK293 cells," *BMC Biochemistry*, vol. 16, no. 1, p. 2, 2015.
- [27] E. T. McGuinness and J. R. Butler, "NAD<sup>+</sup> kinase-A review," *International Journal of Biochemistry*, vol. 17, no. 1, pp. 1–11, 1985.
- [28] R. A. Olek, W. Ziolkowski, J. J. Kaczor, L. Greci, J. Popinigis, and J. Antosiewicz, "Antioxidant activity of NADH and its analogue—an *in vitro* study," *Journal of Biochemistry and Molecular Biology*, vol. 37, no. 4, pp. 416–421, 2004.
- [29] S. H. Ganji, M. L. Kashyap, and V. S. Kamanna, "Niacin inhibits fat accumulation, oxidative stress, and inflammatory cytokine IL-8 in cultured hepatocytes: impact on non-alcoholic fatty liver disease," *Metabolism-Clinical and Experimental*, vol. 64, no. 9, pp. 982–990, 2015.
- [30] K. Pant, A. K. Yadav, P. Gupta, R. Islam, A. Saraya, and S. K. Venugopal, "Butyrate induces ROS-mediated apoptosis by modulating mir-22/sirt-1 pathway in hepatic cancer cells," *Redox Biology*, vol. 12, no. C, pp. 340–349, 2017.
- [31] V. Salimi, Z. Shahsavari, B. Safizadeh, A. Hosseini, N. Khademian, and M. Tavakoli-Yaraki, "Sodium butyrate promotes apoptosis in breast cancer cells through reactive oxygen species (ROS) formation and mitochondrial impairment," *Lipids in Health and Disease*, vol. 16, no. 1, pp. 208–219, 2017.
- [32] C. X. Zhuo and B. L. Yun, "Chemical induction of cellular antioxidants affords marked protection against oxidative injury in vascular smooth muscle cells," *Biochemical and Biophysical Research Communications*, vol. 292, no. 1, pp. 50–57, 2002.
- [33] F. Natoni, L. Diolordi, C. Santoni, and M. S. G. Montani, "Sodium butyrate sensitises human pancreatic cancer cells to both the intrinsic and the extrinsic apoptotic pathways," *Biochimica et Biophysica Acta*, vol. 1745, no. 3, pp. 318–329, 2005.
- [34] B. Zhang and H. B. Liu, "Study on inhibition of niacin on apoptosis of human endothelial cells induced by angiotensin II," *Journal of Clinical and Experimental Medicine*, vol. 11, no. 10, pp. 731–733, 2012, in Chinese.
- [35] Ł. Mateuszuk, T. I. Khomich, E. Słomińska et al., "Activation of nicotinamide n-methyltransferase and increased formation of 1-methylnicotinamide (MNA) in atherosclerosis," *Pharmacological Reports*, vol. 61, no. 1, pp. 76–85, 2009.

## Research Article

# Proximal Tubular Development Is Impaired with Downregulation of MAPK/ERK Signaling, HIF-1 $\alpha$ , and Catalase by Hyperoxia Exposure in Neonatal Rats

Xuwen Xu <sup>1</sup>, Kai You <sup>2</sup>, and Renge Bu <sup>1</sup>

<sup>1</sup>Department of Urology, Shengjing Hospital of China Medical University, Shenyang 110004, China

<sup>2</sup>Department of Neonatology, Shengjing Hospital of China Medical University, Shenyang 110004, China

Correspondence should be addressed to Renge Bu; [burg@sj-hospital.org](mailto:burg@sj-hospital.org)

Received 28 January 2019; Accepted 4 June 2019; Published 28 August 2019

Guest Editor: Veronica A. Peotta

Copyright © 2019 Xuwen Xu et al. This is an open access article distributed under the Creative Commons Attribution License, which permits unrestricted use, distribution, and reproduction in any medium, provided the original work is properly cited.

Supplemental oxygen therapy (hyperoxia) is a widely used treatment for alveolar hypoxia in preterm infants. Despite being closely monitored, hyperoxia exposure is believed to undermine neonatal nephrogenesis and renal function caused by elevated oxidative stress. Previous studies have mostly focused on the hyperoxia-induced impairment of glomerular development, while the long-term impact of neonatal hyperoxia on tubular development and the regulatory component involved in this process remain to be clarified. Here, we examined tubular histology and apoptosis, along with the expression profile of mitogen-activated protein kinase (MAPK)/extracellular signal-regulated kinase (ERK) signaling, hypoxia-inducible factor 1 $\alpha$  (HIF-1 $\alpha$ ), and catalase, following hyperoxia exposure in neonatal rats. Hematoxylin and eosin (H&E) staining revealed the early disappearance of the nephrogenic zone, as well as dilated lumens and reduced epithelial cells, of mature proximal tubules following neonatal hyperoxia. A robust increase in tubular cell apoptosis caused by neonatal hyperoxia was found using a TUNEL assay. Moreover, neonatal hyperoxia altered renal MAPK/ERK signaling activity and downregulated the expression of HIF-1 $\alpha$  and catalase in the proximal tubules throughout nephrogenesis from S-shaped bodies to mature proximal tubules. Cell apoptosis in the proximal tubules was positively correlated with HIF-1 $\alpha$  expression on the 14th postnatal day. Our data indicates that proximal tubular development is impaired by neonatal hyperoxia, which is accompanied by altered MAPK/ERK signaling as well as downregulated HIF-1 $\alpha$  and catalase. Therapeutic management that targets MAPK/ERK signaling, HIF-1 $\alpha$ , or catalase may serve as a protective agent against hyperoxia-induced oxidative damage to neonatal proximal tubules.

## 1. Introduction

The structural and functional development of the neonatal kidney is responsible for postnatal adaptation to extrauterine life [1]. Developmental changes of the kidney after birth involve the further maturation and hypertrophy of nephrons, which continue until adult morphology and size are reached from 3 to 5 years of age. The glomerular filtration rate (GFR) increases with the progression of neonatal renal function, reaching adult levels by 2 years of age [2]. The postnatal maturation of renal tubules follows this rapid maturation and is characterized by a 10-fold increase in proximal tubular length and diameter within the weaning period. The diluting capacity of urine in newborn infants is similar to that of

adults. Functional maturity and full urinary concentrating ability are reached at approximately 18 months of age [1]. Low oxygen concentrations (1–3%) are optimal for renal vascular and tubular development in newborn rats [3]. Moreover, an appropriate oxygen tension is critically required in the final papillary development [4].

Since alveolar hypoxia can lead to inadequate tissue oxygenation, pulmonary vasoconstriction, and pulmonary artery hypertension, supplemental oxygen therapy (hyperoxia) is widely used in neonatology and plays a vital role in the management of preterm infants [5]. Despite close monitoring, mounting evidence from various clinical and experimental observations suggests that neonatal hyperoxia causes systemic injury to several organs. Hyperoxia is a key contributor

to neonatal and pediatric lung diseases, including airway disease (wheezing and asthma) and bronchopulmonary dysplasia [6]. Chronic exposure to hyperoxia causes oxidative stress and contributes to the pathogenesis of injury in the preterm as well as full-term brain, with a dramatic deterioration of brain function in later life [7]. Neonatal hyperoxia causes severe vitreoretinal pathologic changes that persist into adulthood [8]. Thus, it is important to clarify the adverse impact of neonatal hyperoxia upon nephrogenesis.

Accumulating evidence suggests that neonatal hyperoxia impairs nephrogenesis. Neonatal mice exposed to hyperoxia had smaller glomeruli in both the short and long term [9, 10]. Crescentic glomeruli, which indicate glomerular injury, were markedly increased in 11-month-old, hyperoxia-exposed rats [11]. Hyperoxia led to increases in renal tubular necrosis, dilation, and interstitial inflammation, with higher tubular injury scores [12, 13]. Capillary density per kidney was decreased by neonatal hyperoxia [14]. Impaired renal development is considered a pathophysiological process in that neonatal hyperoxia-induced oxidative stress may initiate apoptosis of renal cells, causing subclinical acute kidney injury or even kidney fibrosis [10, 13, 15, 16]. The hyperoxia-induced early differentiation of renal epithelial cells is another explanation for impaired nephrogenesis [17]. Renal function can also be impaired; for instance, creatinine clearance at 5 months was significantly reduced following the exposure of neonates to hyperoxia [11]. Previous studies on the hyperoxia-induced impairment of nephrogenesis have mainly focused on glomeruli, while the long-term effect of neonatal hyperoxia to tubular development remains unclear.

Several molecular pathways and genes are involved in regulating the complex process of nephrogenesis, such as transcriptional regulators, growth factors, oncogenes, the extracellular matrix, and vascular factors [1, 15]. As a proliferative and antiapoptotic signaling pathway, MAPK/ERK signaling regulates the maintenance and differentiation of kidney progenitor cells in kidney development [18]. Hypoxia-inducible factor 1 $\alpha$  (HIF-1 $\alpha$ ) is known to be essential for organogenesis by regulating the expression of numerous factors involved in angiogenesis, cellular proliferation, and apoptosis [10]. Catalase plays a critical protective role against oxidative stress in embryogenesis [19]. However, the dynamic expression profile of MAPK/ERK signaling, HIF-1 $\alpha$ , and catalase in response to neonatal hyperoxia remains undefined. Thus, the aim of this study is to investigate the long-term effect of neonatal hyperoxia on tubular development as well as MAPK/ERK signaling activity, HIF-1 $\alpha$ , and catalase expression.

## 2. Materials and Methods

**2.1. Animal Model.** Sprague-Dawley (SD) rats were purchased from the Experimental Animal Center, Shengjing Hospital of China Medical University (Shenyang, China). Pregnant SD rats were housed in transparent cages of our laboratory one week before delivery. Pups were delivered naturally when the gestational age was 21 to 23 days. All pups were separated from mothers within 12 h after delivery

and were randomly divided into normoxia (fraction of inspired air (FiO<sub>2</sub>) = 0.21,  $n = 80$ ) and hyperoxia groups (FiO<sub>2</sub> = 0.85,  $n = 80$ ). The inhaled oxygen concentration was measured and recorded continuously with an analyzer equipped with a strip-chart recorder (model 572; Servomex, Norwood, MA, USA). Other environmental conditions of the hyperoxia group were the same as those of the normoxia group except for inhaling room air. Using alkaline lime to absorb CO<sub>2</sub>, the CO<sub>2</sub> concentration was maintained to less than 0.5%. Room temperature (25~27°C), humidity (60%~70%), and daily light and dark circulation were monitored and regulated automatically. Rats in the hyperoxia group were transited and cross-fostered by mother rats in a normoxia environment every 24 h to avoid the toxicity of hyperoxia and to equalize their nutritional condition. The dams, food, and drinking water were renewed every 24 h. Rats were scheduled for euthanasia in CO<sub>2</sub> on postnatal days 1, 3, 5, 7, 10, 14, 30 (exposed to normoxia or hyperoxia in the first 14 days), and 60 (exposed to normoxia or hyperoxia in the first 14 days), respectively. The carcasses were dissected and bilateral kidneys were obtained immediately after euthanasia. The left kidney was fixed in 4% paraformaldehyde (PFA) for hematoxylin and eosin (H&E) staining, Periodic Acid-Schiff (PAS) staining, terminal deoxynucleotidyl transferase dUTP nick end labelling (TUNEL) assay, and immunohistochemical staining, while the right kidney was kept at -80°C for western blotting.

**2.2. Kidney Histology.** After fixation in PFA for 24 h, kidney samples were dehydrated in gradient ethanol, then embedded in paraffin and sectioned (5  $\mu$ m) for H&E and PAS staining, which was performed as described by Chen et al. [20]. Ten fields of view were randomly chosen and observed at an original magnification of  $\times 400$ . The significance of tubular injury was determined via evaluating tubular dilation, casts, vacuolization, degeneration of tubule epithelial cells, and the disappearance of the brush border [21, 22]. Histological evaluations were conducted blindly by two pathologists. The width of the nephrogenic zone was determined by averaging the width of the renal cortex containing immature glomeruli in five separate areas per kidney [23]. To identify tubular dilation, bright-field images of H&E-stained slides were analyzed and the diameter of tubular lumen was measured using ImageJ 1.51 (National Institutes of Health, Bethesda, MD, USA). Briefly, a grid of dots, 13  $\mu$ m apart, was superimposed on images. No dilation was defined as no dots within lumens, and tubular dilation was defined as more than one dot within each tubular lumen [24]. Tubular cell number was counted automatically using ImageJ 1.51 as per the protocol described by Parlee et al. [25].

**2.3. Apoptosis Assay.** Cell apoptosis was evaluated by TUNEL assay using an ApopTag Plus peroxidase *in situ* apoptosis detection kit (Intergen, Norcross, GA, USA). After fixation in PFA for 24 h, kidney samples were dehydrated in gradient ethanol, then embedded in paraffin and sectioned (5  $\mu$ m). Sections were deparaffinized in xylene and rehydrated by incubation in graded ethanols and then immersed in phosphate-buffered saline (PBS). For permeabilization,

50  $\mu\text{L}$  of 0.1% Triton X-100 (prepared with 0.1% sodium citrate) was added and incubated at room temperature for 8 min. Fifty microliters of a TUNEL reaction solution (prepared with enzyme and label Solutions at a ratio of 1:9) was added and incubated at 37°C for 30 min. Fifty microliters of converter-POD (peroxidase) was added and incubated for 30 min. Fifty microliters of 3,3'-diaminobenzidine (DAB) substrate was added for color development, and slides were washed with PBS three times. Hematoxylin was added to counterstain slides for 3 min. For derivatization, slides were immersed in 1% hydrogen chloride-ethanol solution for 3 s and then rinsed in running water for 20 min. Slides were dehydrated in gradient ethanols, immersed in xylene, then mounted with neutral balsam. TUNEL positive cells were defined as cells with darkly stained nuclei or pyknotic nuclei with apoptotic bodies. Ten fields of view from the renal cortex and medulla were randomly chosen and observed at an original magnification of  $\times 400$ . TUNEL positive cell numbers from the proximal tubules and collecting ducts were counted automatically using ImageJ 1.51 as per the protocol described by Parlee et al. [25].

**2.4. Immunohistochemical Staining.** Rat kidney tissues were fixed in formalin, embedded in paraffin, sectioned at a thickness of 5  $\mu\text{m}$ , dewaxed, rehydrated, placed in sodium citrate, and microwaved for antigen retrieval. A nonspecific stain blocking agent was added to slides, which were then incubated for 30 min at room temperature. Anti-rat HIF-1 $\alpha$  primary antibody (Thermo Fisher, Shanghai, China; dilution 1:200) or anti-rat catalase primary antibody (Thermo Fisher; dilution 1:100) was added and slides incubated overnight at 4°C. After washing in PBS, the slides were incubated with secondary antibody (Gene Tech, Shanghai, China; dilution 1:100) for 30 min at room temperature. Excess secondary antibody was washed off. Slides were incubated with streptavidin-avidin-biotin complex, developed with 3,3'-diaminobenzidine, washed with running water, counterstained with hematoxylin, dehydrated with gradient alcohol, dried, and mounted with neutral balsam. Tissue morphology was observed and photographed under the microscope and compared with known positive staining slides. The results were interpreted blindly by two pathologists. Ten high-power fields of view (original magnification  $\times 400$ ) were randomly selected from each slide and images obtained with a light microscope, with 200 cells observed in each field of view. Cells with cytoplasm or nucleus stained yellow or dark brown were defined as positive cells. Semi-quantitative results were obtained by determining the intensity of cell staining using image-analyzing software, ImageJ 1.51. Images in 8-bit format were used and adjusted with the Image/Adjust/Brightness/Contrast command. The threshold was then adjusted with the Image/Adjust/Threshold command. The Analyze/Measure command was then required. ImageJ 1.51 will automatically display the percentage of total area that positive cells occupy [26].

**2.5. Western Blotting.** An appropriate volume of RIPA buffer was added to tissue samples to make cell lysates. After centrifugation, the protein concentration of each sample superna-

tant was determined using a bicinchoninic acid protein concentration assay kit (Beyotime, Shanghai, China). A 5 $\times$  Loading Buffer was used to dilute the protein samples, which were boiled in a water bath for 5 min. Proteins were separated by SDS-polyacrylamide gel electrophoresis and subsequently transferred to a polyvinylidene difluoride membrane (Millipore, Burlington, MA, USA). After incubation with primary (1:1000) and secondary antibodies (1:5000), respectively, an electrochemical luminescence solution (Sigma, St. Louis, MO, USA) was added for substrate luminescence. All bands were scanned with Chemi Imager 5500 V2.03 software (Alpha InnCh, Miami, FL, USA), and integrated density values were calculated by computerized image analysis system (Fluor Chen 2.0) and normalized to that of  $\beta$ -actin or GAPDH.

**2.6. Statistical Analysis.** GraphPad Prism 7 software (GraphPad Software, San Diego, CA, USA) was used for statistical analyses and plotting scattered dot as well as box and whisker graphs. The results of each assay were obtained after three repeated independent experiments and expressed as mean  $\pm$  standard deviation (SD). The two groups of numerical data were compared by Student's *t*-test. One-way analysis of variance (ANOVA) and post hoc comparisons (Bonferroni test) were used to determine significant differences among multiple groups. Simple regression was used to correlate immunostaining intensity as an independent variable, with the TUNEL positive cell count as a dependent variable. A *P* value of less than 0.05 was considered to be statistically significant.

**2.7. Research Approval.** The study was approved by the Ethics Committee of the Shengjing Hospital, China Medical University (Shenyang, China).

### 3. Results

**3.1. Neonatal Hyperoxia Dilates the Lumen and Decreases the Cell Density of Mature Proximal Tubules.** Neonatal hyperoxia can cause bronchopulmonary dysplasia [27]. To test the hypothesis that neonatal hyperoxia may disrupt kidney development, a histologic examination was undertaken of kidney samples from the normoxia and hyperoxia groups. Morphological differences of the proximal tubules and collecting ducts from adult rats (30th and 60th postnatal days) between the normoxia and hyperoxia groups were compared by H&E staining, and tubular dilation was observed in the hyperoxia group on the 60th postnatal day (Figure 1(a)). Besides tubular dilation, intratubular debris, thinner tubules, and vacuolation in the proximal tubules were also observed in the hyperoxia group on the 60th postnatal day (Figure 1(b)). In order to facilitate the evaluation of tubular dilation, the image type was changed to an HSB stack using ImageJ 1.51 software (Supplementary figure 1a). The diameter of the proximal tubular lumen was significantly increased in the hyperoxia group ( $8.72 \pm 2.46 \mu\text{m}$ ) over that of the normoxia group ( $1.51 \pm 0.54 \mu\text{m}$ ) as detected on the 60th postnatal day ( $P < 0.001$ ), while the difference in lumen diameter between the normoxia and hyperoxia

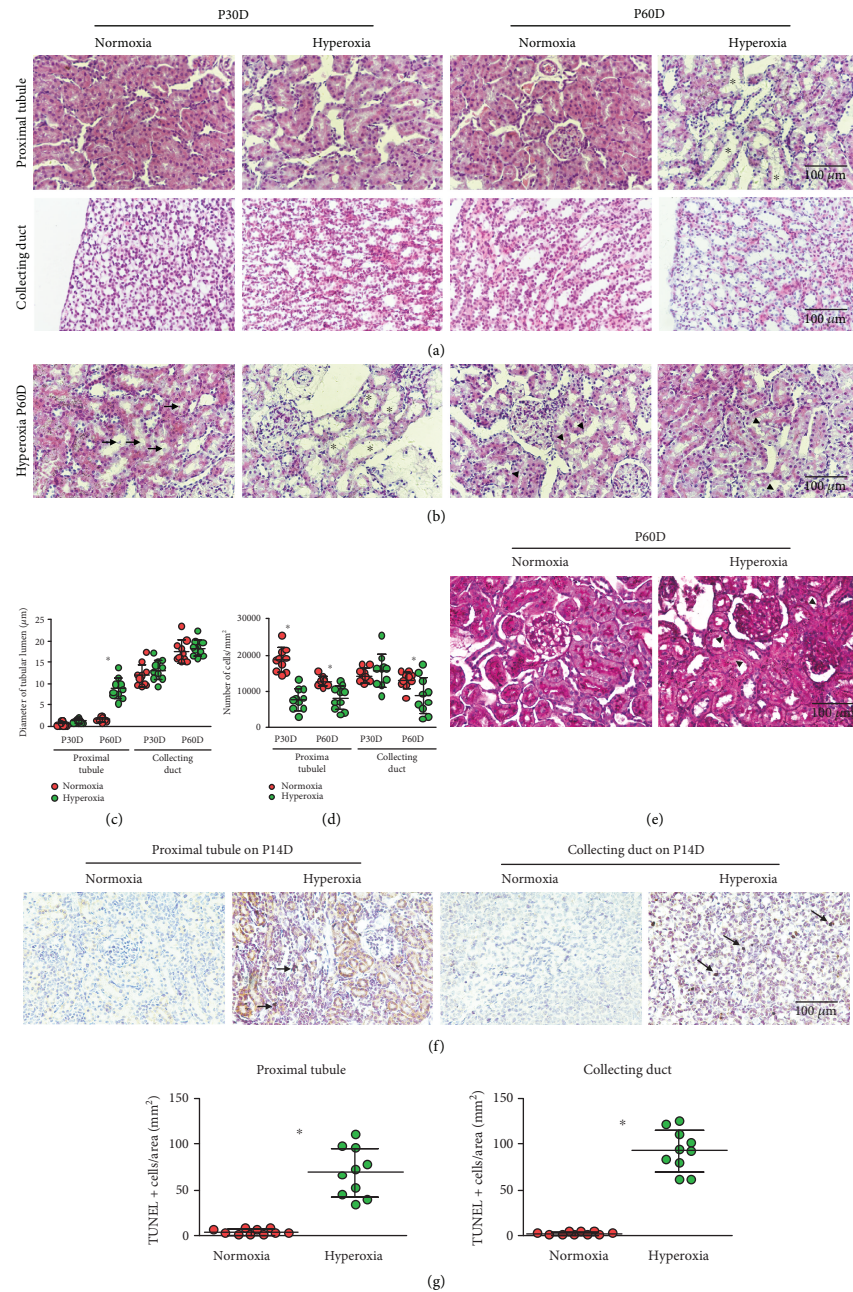


FIGURE 1: Neonatal hyperoxia dilates the lumen and decreases the cell density of mature proximal tubules. (a) The proximal tubules and collecting ducts of adult rats, including those from the 30th (P30D) and 60th postnatal days (P60D), exposed to neonatal normoxia or hyperoxia were detected by hematoxylin & eosin (H&E) staining (original magnification  $\times 400$ ; scale bar,  $100\ \mu\text{m}$ ). Asterisks show tubular dilation. (b) The proximal tubules from the hyperoxia group on P60D showing intratubular debris (arrows), thinner tubules (asterisks), and vacuolation (arrowheads) were detected by H&E staining (original magnification  $\times 400$ ; scale bar,  $100\ \mu\text{m}$ ). (c) The lumen diameters of the proximal tubules and collecting ducts from adult rats exposed to neonatal normoxia or hyperoxia are shown (mean  $\pm$  standard deviation (SD)) by scatter dot plots. The error bars represent the SD of measurements for 10 rats with the mean value of 10 separate fields of view ( $n = 10$ ).  $*P < 0.001$ , one-way ANOVA, Bonferroni post hoc test. (d) The cell densities of the proximal tubules and collecting ducts from adult rats exposed to neonatal normoxia or hyperoxia (mean  $\pm$  SD) are shown by scatter dot plots. The error bars represent the SD of measurements for 10 rats with the mean value of 10 separate fields of view ( $n = 10$ ).  $*P < 0.05$ , one-way ANOVA, Bonferroni post hoc test. (e) The proximal tubules from the hyperoxia group on P60D showing discontinuous brush border (arrowheads) were detected by Periodic Acid-Schiff (PAS) staining (original magnification  $\times 400$ ; scale bar,  $100\ \mu\text{m}$ ). (f) Apoptosis in the proximal tubules and collecting ducts from newborn rats exposed to normoxia or hyperoxia and harvested on the 14th postnatal day (P14D) was detected by terminal deoxynucleotidyl transferase dUTP nick end labeling (TUNEL) assay (original magnification  $\times 400$ ; scale bar,  $100\ \mu\text{m}$ ). Arrows indicate apoptotic bodies. (g) TUNEL positive cell numbers in  $\text{mm}^2$  of the proximal tubules and collecting ducts from newborn rats exposed to normoxia or hyperoxia and harvested on the 14th postnatal day are shown (mean  $\pm$  SD) by scatter dot plots. The error bars represent the SD of measurements for 10 rats with the mean value of 10 separate fields of view ( $n = 10$ ).  $*P < 0.001$ , Student's *t*-test.

groups was not significant in the collecting ducts ( $P > 0.05$ ; Figure 1(c)). In order to quantify the number of tubular cells on the slides of H&E stains, the image type was changed to an RGB stack and the threshold adjusted using ImageJ 1.51 software according to Papadopoulos et al. (Supplementary figure 1b) [28]. The number of proximal tubular cells was significantly decreased in the hyperoxia group compared to that of the normoxia group as detected on both 30th ( $7776 \pm 3014$  vs.  $18605 \pm 3326/\text{mm}^2$ ,  $P < 0.01$ ) and 60th postnatal days ( $8064 \pm 3213$  vs.  $12730 \pm 1343/\text{mm}^2$ ,  $P < 0.001$ ). The difference was also significant for collecting tubular cells on the 60th postnatal day ( $8755 \pm 5012$  vs.  $13075 \pm 2240/\text{mm}^2$ ,  $P < 0.05$ ) but was not significant for the collecting ducts on the 30th postnatal day ( $P > 0.05$ ; Figure 1(d)). In order to examine the damage of brush border, PAS was performed using sections of the proximal tubules from adult rats on the 30th and 60th postnatal days. Discontinuous brush border in the proximal tubules was observed in the hyperoxia group on the 60th postnatal day (Figure 1(e)). Since apoptosis is a critical risk for decreased cell density in the proximal tubules during nephrogenesis [29], apoptosis in tubular cells was evaluated via TUNEL on the 14th postnatal day (Figure 1(f)). The number of TUNEL positive cells per  $\text{mm}^2$  was significantly higher in the hyperoxia group compared to that in the normoxia group (proximal tubule:  $69.20 \pm 26.11/\text{mm}^2$  vs.  $4.80 \pm 2.97/\text{mm}^2$ ; collecting duct:  $92.8 \pm 22.40/\text{mm}^2$  vs.  $3.20 \pm 1.81/\text{mm}^2$ ,  $P < 0.001$  for both; Figure 1(g)). These findings demonstrated that neonatal hyperoxia impaired proximal tubular development.

**3.2. Hyperoxia Accelerates Attenuation of the Nephrogenic Zone in Newborn Rat Kidney.** The activity of the nephrogenic zone is critical for nephrogenesis [30]. Since neonatal hyperoxia disrupted tubular development as observed above, it is important to evaluate the effect of hyperoxia on the nephrogenic zone. The width of the nephrogenic zone in neonatal rats (3rd, 5th, 7th, and 10th postnatal days) was evaluated by H&E staining. The nephrogenic zone completely vanished on the 10th postnatal day in both the normoxia and hyperoxia groups (Figure 2(a)). In order to facilitate measuring the width of the nephrogenic zone, the image contrast was enhanced to 80% saturated pixels using ImageJ 1.51 software (Supplementary figure 1c). It was found that the width of the nephrogenic zone was significantly decreased in the hyperoxia group ( $14.35 \pm 20.81 \mu\text{m}$ ) compared to that in the normoxia group ( $155.74 \pm 21.86 \mu\text{m}$ ) on the 7th postnatal day ( $P < 0.001$ ; Figure 2(b)). This demonstrated that hyperoxia accelerated attenuation of the nephrogenic zone in the newborn rat kidney.

**3.3. MAPK/ERK Signaling Activity Is Altered in the Kidney of Newborn Rats following Hyperoxia.** MAPK/ERK signaling is an essential pathway activated during kidney development [18]. To evaluate MAPK/ERK signaling activity following hyperoxia, the expression of phospho-ERK (p-ERK), ERK, phospho-ERK (p-MEK), and MEK in the kidneys of newborn rats was detected by western blotting (Figure 3(a)). In the normoxia group, MAPK/ERK signaling activity reached

its peak on the 5th postnatal day (Figure 3(a)). In the hyperoxia group, MAPK/ERK signaling activity was mainly downregulated on the 1st and 3rd postnatal days, while it was significantly upregulated after the 5th postnatal day ( $P < 0.05$ ; Figure 3(a)). HIF-1 $\alpha$  and catalase are important downstream proteins of MAPK/ERK signaling [31–33]. Therefore, the expression of HIF-1 $\alpha$  and catalase in the kidneys of newborn rats following hyperoxia was measured by western blotting (Figure 3(b)). The expression of HIF-1 $\alpha$  was significantly decreased following hyperoxia on the 1st postnatal day (normoxia group  $1.0 \pm 0.22$  vs. hyperoxia group  $0.77 \pm 0.18$ ;  $P < 0.05$ ; Figure 3(b)). With regard to catalase, its expression was significantly increased on the 3rd postnatal day following hyperoxia (normoxia group  $0.78 \pm 0.19$  vs. hyperoxia group  $1.01 \pm 0.17$ ;  $P < 0.05$ ), while it was decreased on the 14th postnatal day (normoxia group  $1.37 \pm 0.16$  vs. hyperoxia group  $1.03 \pm 0.13$ ;  $P < 0.001$ ; Figure 3(b)). The above observations indicated that MAPK/ERK signaling activity was originally downregulated and then upregulated in the kidney of newborn rats following hyperoxia, which was not compliant with the expression pattern of HIF-1 $\alpha$  or catalase.

**3.4. Peak Expression of HIF-1 $\alpha$  and Catalase Was Reduced by Hyperoxia in Proximal Tubules.** To further investigate the expression of HIF-1 $\alpha$  and catalase in the proximal tubules and collecting ducts following hyperoxia, immunohistochemical staining was performed on kidney tissues from neonatal rats exposed to hyperoxia or normoxia. Cytoplasmic staining of HIF-1 $\alpha$  was observed in the proximal tubules and collecting ducts of neonatal rats (Figure 4(a)). In the normoxia group, HIF-1 $\alpha$  expression in the proximal tubules reached its peak on the 5th postnatal day (Figure 4(b)), which was consistent with observations on MAPK/ERK signaling activity. HIF-1 $\alpha$  expression in the proximal tubules was significantly downregulated following hyperoxia on the 3rd (normoxia group  $1.24 \pm 0.35$  vs. hyperoxia group  $0.44 \pm 0.11$ ,  $P < 0.001$ ), 5th (normoxia group  $1.83 \pm 0.27$  vs. hyperoxia group  $0.32 \pm 0.13$ ;  $P < 0.001$ ), and 7th postnatal days (normoxia group  $1.73 \pm 0.28$  vs. hyperoxia group  $0.06 \pm 0.04$ ;  $P < 0.001$ ), showing that the expression peak of HIF-1 $\alpha$  was decreased by hyperoxia in the proximal tubules. However, HIF-1 $\alpha$  expression in the proximal tubules was significantly upregulated following hyperoxia on the 14th postnatal day (normoxia group  $0.32 \pm 0.22$  vs. hyperoxia group  $0.62 \pm 0.14$ ;  $P < 0.01$ ; Figure 4(b)). A positive TUNEL cell count positively correlated with the immunostaining intensity of HIF-1 $\alpha$  in the proximal tubules detected on the 14th postnatal day ( $r^2 = 0.6203$ ,  $P < 0.001$ ; Figure 4(c)). HIF-1 $\alpha$  expression in the collecting ducts was significantly downregulated following hyperoxia on the 1st (normoxia group  $1.0 \pm 0.13$  vs. hyperoxia group  $0.86 \pm 0.10$ ,  $P < 0.05$ ), 3rd (normoxia group  $1.04 \pm 0.11$  vs. hyperoxia group  $0.86 \pm 0.17$ ,  $P < 0.001$ ), and 14th postnatal days (normoxia group  $1.03 \pm 0.11$  vs. hyperoxia group  $0.62 \pm 0.05$ ,  $P < 0.001$ ), while it was significantly upregulated following hyperoxia on the 5th (normoxia group  $0.85 \pm 0.15$  vs. hyperoxia group  $1.19 \pm 0.09$ ,  $P < 0.001$ ) and 10th postnatal days (normoxia group  $0.12 \pm 0.03$  vs. hyperoxia group  $0.44 \pm 0.10$ ,  $P < 0.001$ ;

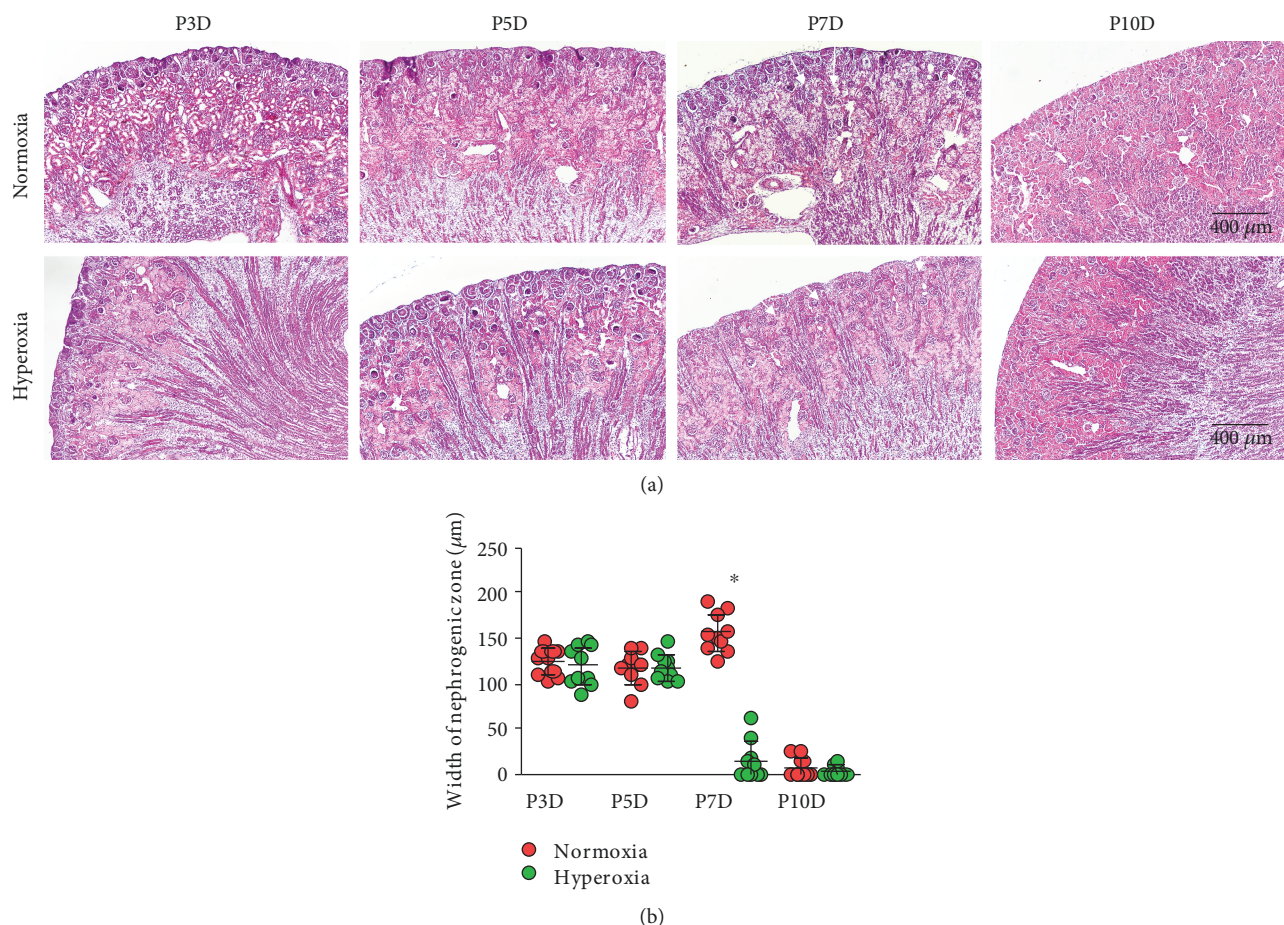


FIGURE 2: Hyperoxia accelerates the disappearance of the nephrogenic zone in newborn rat kidney. (a) The nephrogenic zone in the kidney of newborn rats, including those from the 3rd (P3D), 5th (P5D), 7th (P7D), and 10th (P10D) postnatal days after exposure to normoxia or hyperoxia and visualized by hematoxylin & eosin (H&E) staining (original magnification  $\times 100$ ; scale bar,  $400 \mu\text{m}$ ). Arrows indicate the width of the nephrogenic zone. (b) The width of the neonatal nephrogenic zone, when rats were exposed to normoxia or hyperoxia, is shown (mean  $\pm$  standard deviation (SD)) by scatter dot plots. The error bars represent the SD of measurements for 10 rats with the mean value of 10 separate fields of view ( $n = 10$ ). \* $P < 0.001$ , one-way ANOVA, Bonferroni post hoc test.

Figure 4(d)). No correlation between a positive TUNEL cell count and the immunostaining intensity of HIF-1 $\alpha$  was found in the collecting ducts ( $P > 0.05$ , data not shown).

Cytoplasmic and nucleic staining of catalase was observed in the proximal tubules and collecting ducts of neonatal rats (Figure 5(a)). In the normoxia group, catalase expression in the proximal tubules reached its peak on the 5th postnatal day (Figure 5(b)), which resembled observations on HIF-1 $\alpha$  expression and MAPK/ERK signaling activity. Catalase expression in the proximal tubules was significantly downregulated following hyperoxia on the 1st (normoxia group  $1.0 \pm 0.39$  vs. hyperoxia group  $0.51 \pm 0.28$ ,  $P < 0.01$ ), 3rd (normoxia group  $2.08 \pm 0.53$  vs. hyperoxia group  $0.60 \pm 0.29$ ,  $P < 0.001$ ), 5th (normoxia group  $2.36 \pm 0.38$  vs. hyperoxia group  $0.46 \pm 0.18$ ,  $P < 0.001$ ), and 7th postnatal days (normoxia group  $1.56 \pm 0.40$  vs. hyperoxia group  $0.50 \pm 0.19$ ,  $P < 0.001$ ), showing that peak expression of catalase was attenuated by hyperoxia in the proximal tubules. However, catalase expression in the proximal tubules was significantly upregulated following hyperoxia on the 10th

postnatal day (normoxia group  $0.45 \pm 0.10$  vs. hyperoxia group  $0.84 \pm 0.31$ ;  $P < 0.05$ ; Figure 5(b)). No correlation between a positive TUNEL cell count and the immunostaining intensity of catalase was found in the proximal tubules ( $P > 0.05$ , data not shown). Catalase expression in the collecting ducts was significantly downregulated following hyperoxia on the 7th postnatal day (normoxia group  $1.07 \pm 0.15$  vs. hyperoxia group  $0.44 \pm 0.13$ ,  $P < 0.001$ ), while it was significantly upregulated following hyperoxia on the 5th (normoxia group  $0.91 \pm 0.13$  vs. hyperoxia group  $1.25 \pm 0.14$ ,  $P < 0.001$ ) and 14th postnatal days (normoxia group  $1.05 \pm 0.14$  vs. hyperoxia group  $1.26 \pm 0.11$ ,  $P < 0.01$ ; Figure 5(c)). No correlation between a positive TUNEL cell count and the immunostaining intensity of catalase was found in the collecting ducts ( $P > 0.05$ , data not shown). Therefore, the expression of HIF-1 $\alpha$  and catalase was downregulated by hyperoxia in the proximal tubules.

**3.5. Hyperoxia Downregulated Expression of HIF-1 $\alpha$  and Catalase in S-Shaped Bodies.** The distal portion of an

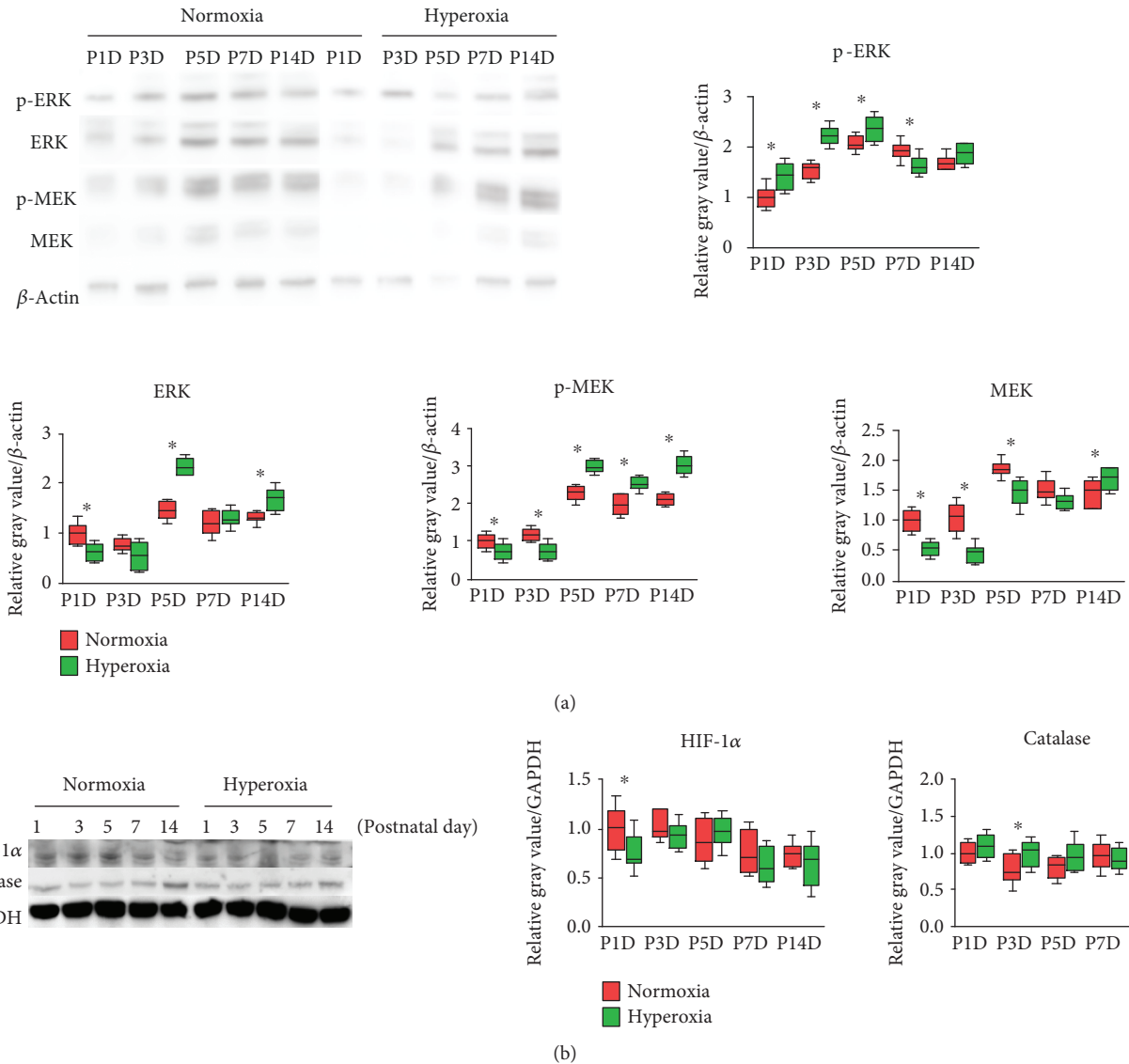
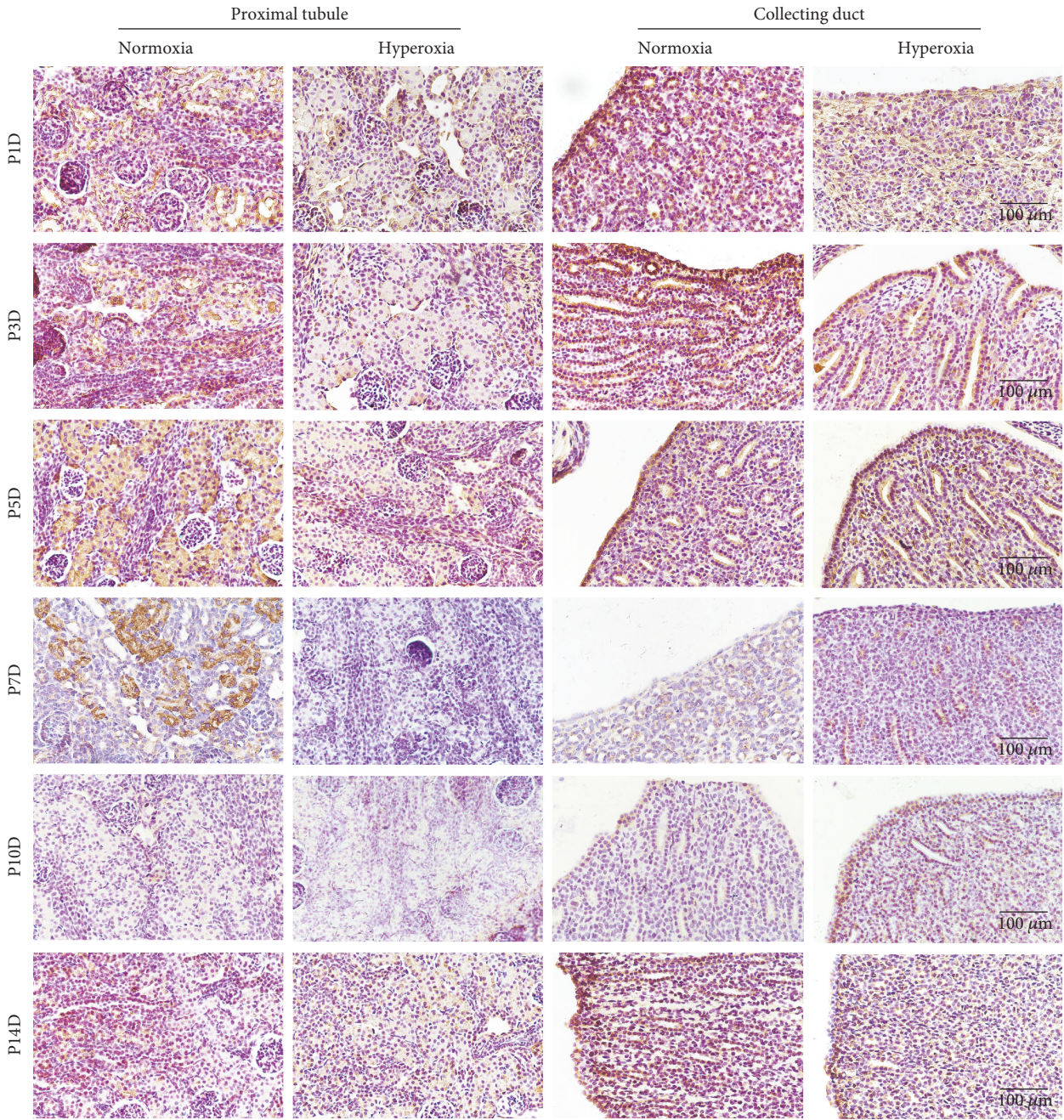


FIGURE 3: ERK/MEK signaling pathway is inactivated and then activated following hyperoxia. (a) Expression bands of phospho-ERK (p-ERK), ERK, phospho-ERK (p-MEK), and MEK in the kidneys of newborn rats exposed to normoxia or hyperoxia as detected by western blotting. Relative expression adjusted to the reference gene  $\beta$ -actin and then standardized to the value of the normoxia group on P1D is shown by box and whisker plots. The whiskers represent the minimal or the maximal gray value, and the boxes span the interquartile range of measurements for 10 rats with the mean value of 3 replicates ( $n = 10$ ).  $*P < 0.05$ , one-way ANOVA, Bonferroni post hoc test. (b) Expression bands of hypoxia-inducible factor 1 $\alpha$  (HIF-1 $\alpha$ ) and catalase in the kidneys of newborn rats exposed to normoxia or hyperoxia and detected by western blotting. Relative expression adjusted to the reference gene GAPDH and then standardized to the value of the normoxia group on P1D is shown by box and whisker plots. The whiskers represent the minimal or the maximal gray value, and the boxes span the interquartile range of measurements for 10 rats with the mean value of 3 replicates ( $n = 10$ ).  $*P < 0.05$ , one-way ANOVA, Bonferroni post hoc test.

S-shaped body develops into a proximal tubule [34]. Since hyperoxia downregulated the expression of HIF-1 $\alpha$  and catalase in the proximal tubules, whether this downregulation started from an S-shaped body stage needed to be clarified. Cytoplasmic and nucleic staining of HIF-1 $\alpha$  and catalase was observed in the S-shaped bodies of neonatal rats by immunohistochemical staining (Figure 6(a)). HIF-1 $\alpha$  expression in S-shaped bodies was significantly downregulated following hyperoxia on the 3rd (normoxia group  $1.04 \pm 0.20$

vs. hyperoxia group  $0.82 \pm 0.18$ ,  $P < 0.05$ ) and 7th postnatal days (normoxia group  $0.51 \pm 0.14$  vs. hyperoxia group  $0.25 \pm 0.10$ ,  $P < 0.01$ ; Figure 6(b)), while catalase expression in S-shaped bodies was significantly downregulated following hyperoxia on the 1st postnatal day (normoxia group  $1.0 \pm 0.19$  vs. hyperoxia group  $0.66 \pm 0.06$ ,  $P < 0.001$ ; Figure 6(c)). The observation above demonstrated that the downregulation of HIF-1 $\alpha$  and catalase following hyperoxia started at an S-shaped body stage.





(a)

FIGURE 4: Continued.

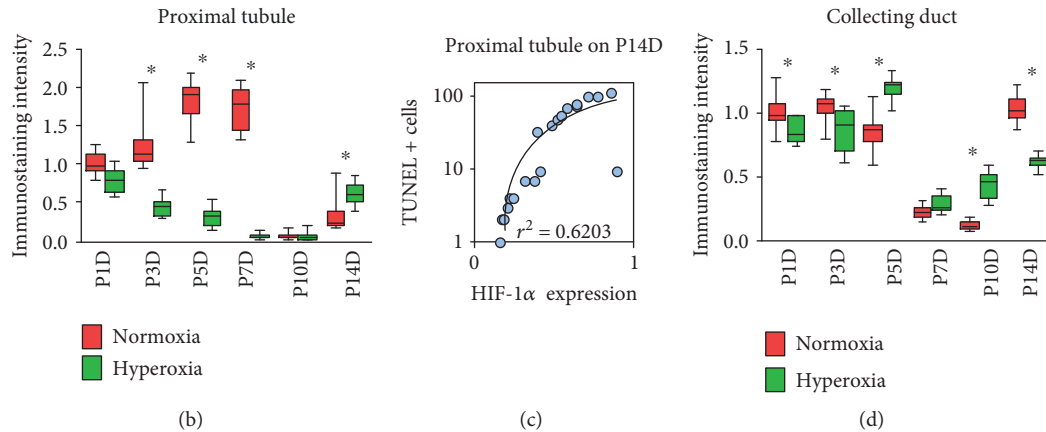


FIGURE 4: Hyperoxia downregulates hypoxia-inducible factor 1 $\alpha$  (HIF-1 $\alpha$ ) expression in the proximal tubules and collecting ducts. (a) HIF-1 $\alpha$  expression in the proximal tubules and collecting ducts of newborn rats exposed to normoxia or hyperoxia was detected by immunohistochemical staining (original magnification  $\times 400$ ; scale bar, 100  $\mu\text{m}$ ). (b) The immunostaining intensity of HIF-1 $\alpha$  expression in the proximal tubules from newborn rats exposed to normoxia or hyperoxia is shown by box and whisker plots. Relative expression is standardized to the value of the normoxia group on P1D. The whiskers represent the minimal intensity or the maximal intensity, and the boxes span the interquartile range of measurements for 10 rats with the mean value of 10 separate fields of view ( $n = 10$ ). \* $P < 0.01$ , one-way ANOVA, Bonferroni post hoc test. (c) Linear correlation between relative immunostaining intensity of HIF-1 $\alpha$  and TUNEL positive cell number per  $\text{mm}^2$  in the proximal tubules from newborn rats exposed to hyperoxia or normoxia and harvested on the 14th postnatal day. The graph was plotted using a log-10 scale for just the Y axis. The correlation coefficient ( $r^2 = 0.6203$ ) was found to be highly significant as shown in the graph ( $n = 20$ ,  $P < 0.001$ ). Simple regression. (d) The immunostaining intensity of HIF-1 $\alpha$  expression in the collecting duct from newborn rats exposed to normoxia or hyperoxia is shown by box and whisker plots. Relative expression is standardized to the value of the normoxia group on P1D. The whiskers represent the minimal intensity or the maximal intensity, and the boxes span the interquartile range of measurements for 10 rats with the mean value of 10 separate fields of view ( $n = 10$ ). \* $P < 0.05$ , one-way ANOVA, Bonferroni post hoc test.

**3.6. Neonatal Hyperoxia Downregulates HIF-1 $\alpha$  and Catalase Expression in Mature Proximal Tubules.** To evaluate the long-term effect of neonatal hyperoxia on the expression of HIF-1 $\alpha$  and catalase in the kidney, western blotting was performed on kidney tissues of adult rats (Figure 7(a)). The expression of HIF-1 $\alpha$  was not significantly altered following neonatal hyperoxia on the 30th and 60th postnatal days ( $P > 0.05$ ; Figure 7(a)). However, the expression of catalase was significantly upregulated following neonatal hyperoxia on the 30th postnatal day (normoxia group  $1.0 \pm 0.20$  vs. hyperoxia group  $1.28 \pm 0.25$ ,  $P < 0.01$ ), while it was downregulated on the 60th postnatal day (normoxia group  $1.38 \pm 0.11$  vs. hyperoxia group  $1.16 \pm 0.23$ ,  $P < 0.05$ ; Figure 7(a)). Moderate cytoplasmic staining of HIF-1 $\alpha$  and catalase was observed in the proximal tubules of adult rats (Figure 7(b)). The expression of HIF-1 $\alpha$  in the proximal tubules was significantly downregulated following neonatal hyperoxia on the 30th postnatal day (normoxia group  $1.0 \pm 0.30$  vs. hyperoxia group  $0.32 \pm 0.09$ ,  $P < 0.001$ ; Figure 7(c)), while the expression of catalase in the proximal tubules was significantly downregulated following neonatal hyperoxia on the 30th (normoxia group  $1.0 \pm 0.25$  vs. hyperoxia group  $0.46 \pm 0.30$ ,  $P < 0.001$ ) and 60th postnatal days (normoxia group  $0.96 \pm 0.33$  vs. hyperoxia group  $0.36 \pm 0.26$ ,  $P < 0.001$ ; Figure 7(d)). The observations above indicate that neonatal hyperoxia downregulates HIF-1 $\alpha$  and catalase expression in the proximal tubule of the adult rat.

## 4. Discussion

Increasing evidence has demonstrated that neonatal hyperoxia undermines renal function [11]; however, hyperoxia-induced long-term injury to the glomeruli seems to be moderate [3, 9]. It is of interest to characterize hyperoxia-induced tubular impairment that may cause a loss of renal function. We found that neonatal hyperoxia induced the early disappearance of the nephrogenic zone in the short term. In the long term, it dilated the lumen of the proximal tubules, reduced the epithelial cell density of the proximal tubules, and induced apoptosis of tubular cells, showing that neonatal hyperoxia impairs the development of the proximal tubules. The MAPK/ERK signaling pathway promotes HIF-1 $\alpha$  expression and plays a vital role in proximal tubular epithelial cell growth and differentiation [18, 35, 36], while catalase as an antioxidant plays a protective role against oxygen toxicity and apoptosis via the activation of MAPK/ERK signaling in renal cells [37, 38]. Thus, it is important to know whether MAPK/ERK signaling as well as HIF-1 $\alpha$  and catalase expression in renal cells is altered by neonatal hyperoxia. Our data shows that neonatal hyperoxia altered renal MAPK/ERK signaling activity and downregulated the expression of HIF-1 $\alpha$  and catalase in renal cells, while HIF-1 $\alpha$  expression in the proximal tubule was positively correlated with cell apoptosis on the 14th postnatal day. This indicates that the developmental impairment induced by neonatal

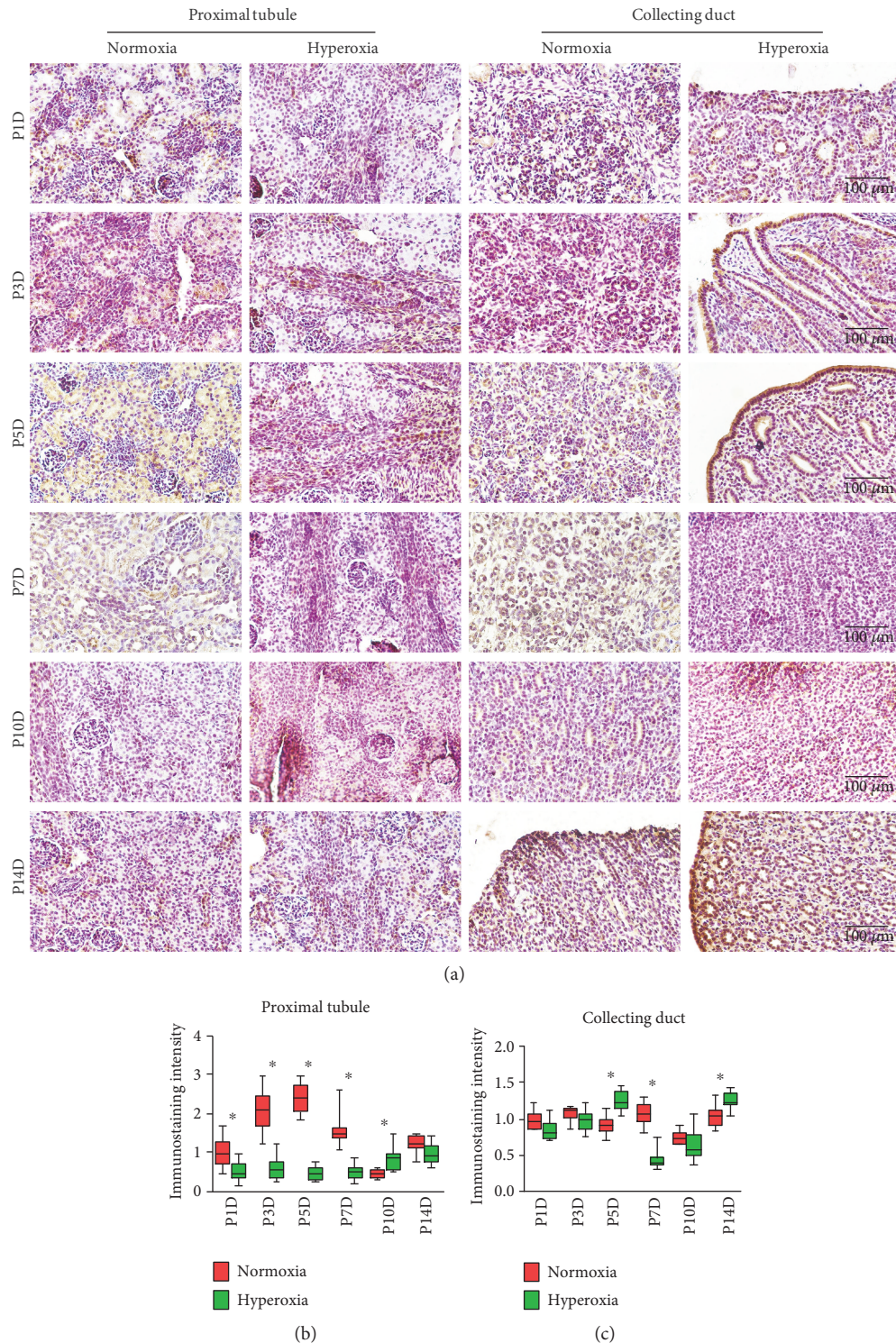
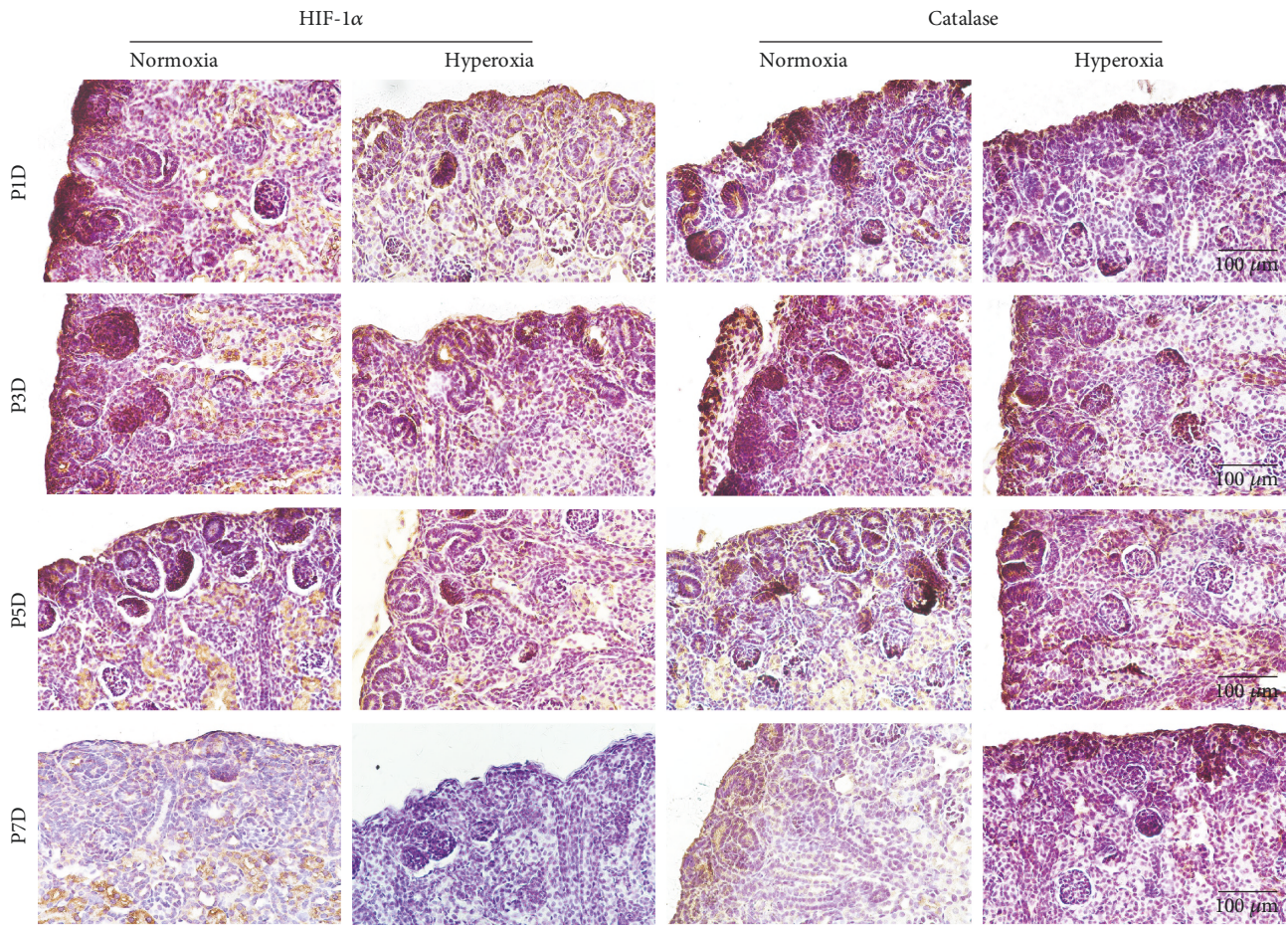
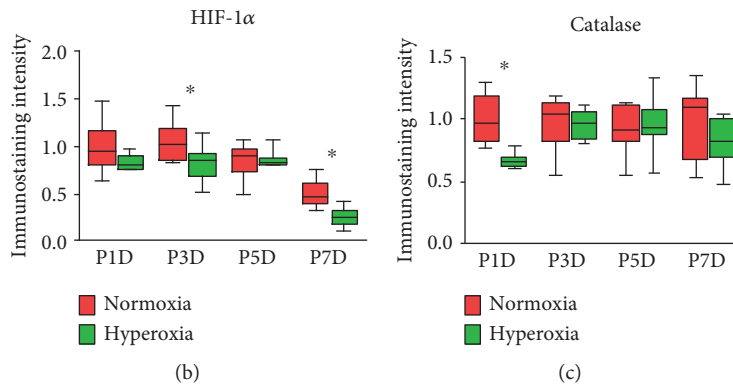


FIGURE 5: Hyperoxia downregulates catalase expression in the proximal tubules and collecting ducts. (a) Catalase expression in the proximal tubules and collecting ducts of newborn rats exposed to normoxia or hyperoxia was detected by immunohistochemical staining (original magnification  $\times 400$ ; scale bar,  $100 \mu\text{m}$ ). (b) The immunostaining intensity of catalase expression in the proximal tubules exposed to normoxia or hyperoxia is shown by box and whisker plots. Relative expression is standardized to the value of the normoxia group on P1D. The whiskers represent the minimal intensity or the maximal intensity, and the boxes span the interquartile range of measurements for 10 rats with the mean value of 10 separate fields of view ( $n = 10$ ).  $*P < 0.05$ , one-way ANOVA, Bonferroni post hoc test. (c) The immunostaining intensity of catalase expression in the collecting ducts exposed to normoxia or hyperoxia is shown by box and whisker plots. Relative expression is standardized to the value of normoxia group on P1D. The whiskers represent the minimal intensity or the maximal intensity, and the boxes span the interquartile range of measurements for 10 rats with the mean value of 10 separate fields of view ( $n = 10$ ).  $*P < 0.01$ , one-way ANOVA, Bonferroni post hoc test.



(a)



(b)

(c)

FIGURE 6: Hyperoxia alters HIF-1 $\alpha$  and catalase expression in S-shaped bodies. (a) Hypoxia-inducible factor 1 $\alpha$  (HIF-1 $\alpha$ ) and catalase expression in S-shaped bodies of newborn rats exposed to normoxia or hyperoxia was detected by immunohistochemical staining (original magnification  $\times 400$ ; scale bar, 100  $\mu\text{m}$ ). (b) The immunostaining intensity of HIF-1 $\alpha$  expression in S-shaped bodies exposed to normoxia or hyperoxia is shown by box and whisker plots. Relative expression is standardized to the value of the normoxia group on P1D. The whiskers represent the minimal intensity or the maximal intensity, and the boxes span the interquartile range of measurements for 10 rats and the mean value of 10 separate fields of view ( $n = 10$ ). \* $P < 0.05$ , one-way ANOVA, Bonferroni post hoc test. (c) The immunostaining intensity of catalase expression in S-shaped bodies exposed to normoxia or hyperoxia is shown by box and whisker plots. Relative expression is standardized to the value of the normoxia group on P1D. The whiskers represent the minimal intensity or the maximal intensity, and the boxes span the interquartile range of measurements for 10 rats and the mean value of 10 separate fields of view ( $n = 10$ ). \* $P < 0.001$ , one-way ANOVA, Bonferroni post hoc test.

hyperoxia in renal cells is accompanied by an alteration of MAPK/ERK signaling and the downregulation of HIF-1 $\alpha$  and catalase.

The nephrogenic zone of a fetal kidney is a narrow band along the entire inner side of the renal capsule that contains a lot of progenitor cells and undergoes continuous attenuation

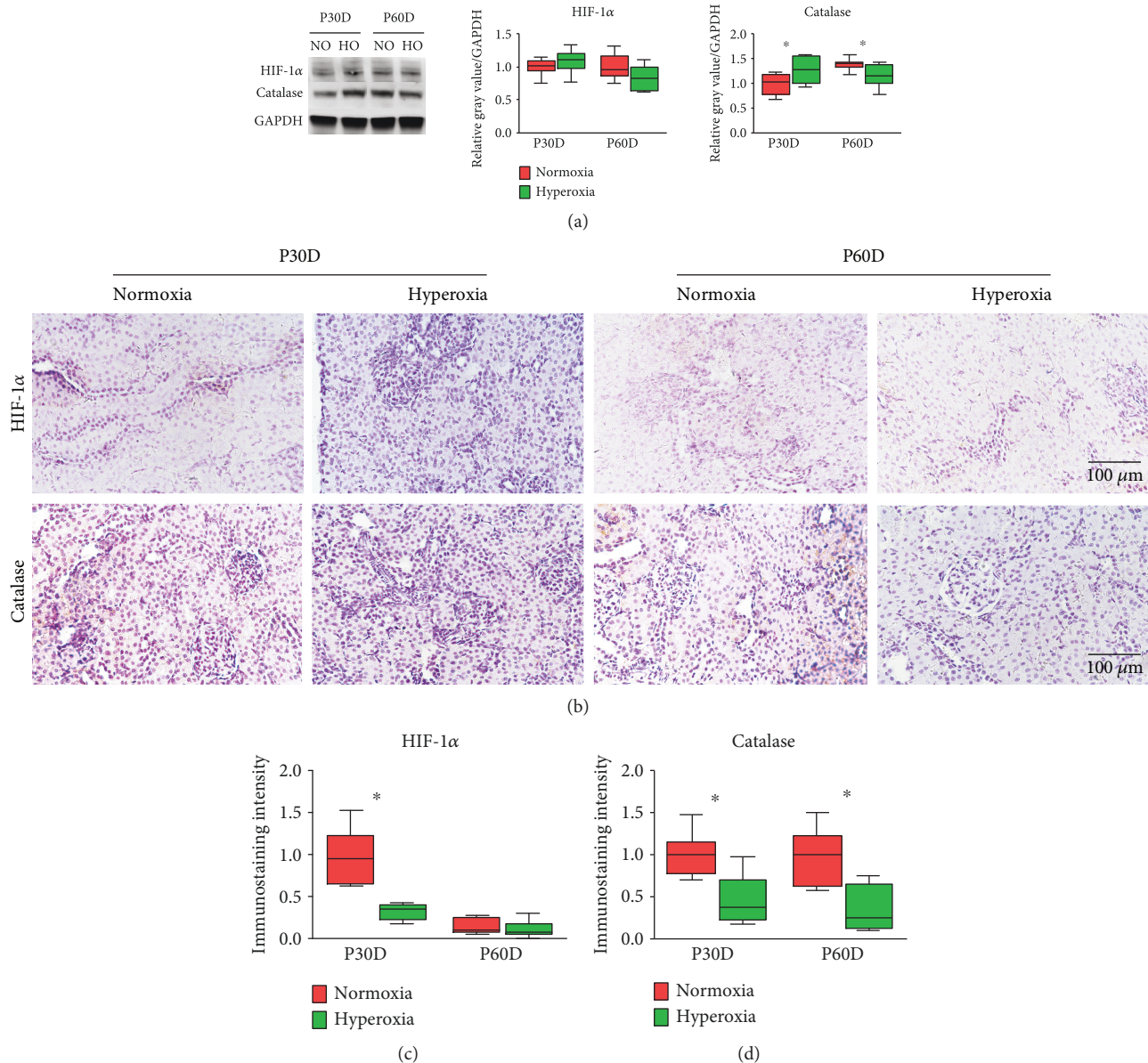


FIGURE 7: Neonatal hyperoxia downregulates hypoxia-inducible factor 1 $\alpha$  (HIF-1 $\alpha$ ) and catalase expression in mature proximal tubules. (a) Expression bands of HIF-1 $\alpha$  and catalase in mature kidneys exposed to neonatal normoxia or hyperoxia as detected by western blotting. Relative expression adjusted to the reference gene GAPDH and then standardized to the value of the normoxia group on P30D is shown by box and whisker plots. The whiskers represent the minimal or the maximal gray value, and the boxes span the interquartile range of measurements for 10 rats with the mean value of 3 replicates ( $n = 10$ ). \* $P < 0.001$ , one-way ANOVA, Bonferroni post hoc test. (b) HIF-1 $\alpha$  and catalase expression in the proximal tubules of adult rats exposed to neonatal normoxia or hyperoxia as detected by immunohistochemical staining (original magnification  $\times 400$ ; scale bar, 100  $\mu$ m). (c) The immunostaining intensity of HIF-1 $\alpha$  expression in the proximal tubules of adult rats exposed to neonatal normoxia or hyperoxia is shown by box and whisker plots. Relative expression is standardized to the value of the normoxia group on P30D. The whiskers represent the minimal intensity or the maximal intensity, and the boxes span the interquartile range of measurements for 10 rats and a mean value of 10 separate fields of view ( $n = 10$ ). \* $P < 0.001$ , one-way ANOVA, Bonferroni post hoc test. (d) The immunostaining intensity of catalase expression in the proximal tubules of adult rats exposed to neonatal normoxia or hyperoxia is shown by box and whisker plots. Relative expression is standardized to the value of the normoxia group on P30D. The whiskers represent the minimal intensity or the maximal intensity, and the boxes span the interquartile range of measurements for 10 rats and a mean value of 10 separate fields of view ( $n = 10$ ). \* $P < 0.001$ , one-way ANOVA, Bonferroni post hoc test.

during kidney development [39]. The width of the nephrogenic zone, which is inversely correlated to gestational age, is considered to indicate the state of ongoing nephrogenesis [40]. By dynamic observation, we found that when exposed

to hyperoxia, the nephrogenic zone vanished on the 7th post-natal day, which significantly preceded the disappearance of the nephrogenic zone exposed to normoxia. The effect of hyperoxia on various types of progenitor cells seems to be

controversial. Hyperoxia stimulated the proliferation and differentiation of dopaminergic progenitors during early and late embryogenesis [41]. However, it reduced the population of progenitor cells in the lung and had no effect on cell growth but increased the differentiation of hepatic progenitor cells [42, 43]. In this regard, hyperoxia causes the early differentiation of renal epithelial cells [17], which may be the reason for an earlier vanishing of the nephrogenic zone observed in the current study.

Proximal tubule dilation is a common pathological abnormality in urinary tract obstruction, acute kidney injury, and renal dysplasia [24, 44, 45]; of these, acute kidney injury is considered a hyperoxia-induced lesion [13]. We found that neonatal hyperoxia contributed to abnormal proximal tubule dilation in adult rats. Thus, we have reason to believe that hyperoxia-induced proximal tubule dilation may represent a subclinical acute kidney injury. The two major causes of acute kidney injury are ischemic and nephrotoxic damages that may induce a loss of renal function and consequent pathological alterations, such as tubular dilatation, loss of renal microvilli, apoptosis, and even necrosis [46]. Cell density in the proximal tubules indicates the developmental status of renal epithelial cells in nephrogenesis [47]. The number of proximal tubular epithelial cells in adult mice was significantly decreased following neonatal hyperoxia in the current study. Considering that hyperoxia induces the apoptosis of alveolar epithelial cells [48], we evaluated apoptosis in tubular cells. We found that hyperoxia consistently induced apoptosis of tubular cells, which may cause acute kidney injury and impaired nephrogenesis.

MAPK/ERK signaling is a critical pathway in regulating cell proliferation and is antiapoptotic [49, 50]. In regard to kidney development, MAPK/ERK signaling initially controls niche organization and nephron progenitor maintenance, after which it is needed for the progression of differentiation in nephron precursors [18]. We observed a peak in MAPK/ERK signaling on the 5th postnatal day, while exposure to hyperoxia overactivated MAPK/ERK signaling on the 1st and 3rd postnatal days and inactivated it after the 5th postnatal day. Since MAPK/ERK signaling plays an important role in the proliferation and differentiation of nephron progenitors, we postulate that the hyperoxia-induced alteration of MAPK/ERK signaling activity may impair neonatal nephrogenesis. HIF-1 $\alpha$  is a basic helix-loop-helix PAS domain-containing protein and is considered as the master transcriptional regulator of the cellular and developmental response to hypoxia [51]. Hyperoxia exposure in the neonatal period results in impaired nephrogenesis via the downregulation of HIF-1 $\alpha$  [10], which is consistent with our observation that neonatal hyperoxia blunted the expression peak of HIF-1 $\alpha$  in the proximal tubules. A blunted expression peak in response to neonatal hyperoxia is also observed in other tissues [52]. HIF-1 $\alpha$  can trigger apoptosis in renal tubular epithelial cells [53], which is consistent with our observation that proximal tubular apoptosis is positively correlated to the expression of HIF-1 $\alpha$  on the 14th postnatal day. Short-term hyperoxia downregulates HIF-1 $\alpha$  via modulating MAPK/ERK signaling to reduce smooth muscle proliferation in a local blood vessel [54]. Similarly, we observed

that neonatal hyperoxia inhibited HIF-1 $\alpha$  expression, which was accompanied by the downregulation of MAPK/ERK signaling after the 5th postnatal day. MAPK/ERK signaling activates catalase under some circumstances [33, 55]. Catalase catalyzes the decomposition of hydrogen peroxide to water and oxygen and is a very important enzyme in protecting the cell from oxidative damage by reactive oxygen species (ROS) [56]. Hyperoxia has a protective effect against kidney damage by activating catalase [57, 58]. Our study found that neonatal hyperoxia blunted the expression peak of catalase during nephrogenesis, which is consistent with observations in lung tissue [59]. In preterm rabbits, the translational/post-translational inhibition of catalase expression is due to an inability to induce a protective increase in hyperoxic catalase activity [60]. Such translational/posttranslational inhibition may also induce the downregulation of catalase following neonatal hyperoxia in the current study. Since catalase enhances cell viability by reducing ROS-induced apoptosis [61], the hyperoxia-induced downregulation of catalase may cause tubular apoptosis, as we observed, and undermine proximal tubular development.

Proximal tubular cells differentiate from the distal domain of S-shaped bodies during nephrogenesis [24]. HIF-1 $\alpha$  and catalase expression in S-shaped bodies was investigated in order to identify the initial response of proximal tubular cells to neonatal hyperoxia. The expression of HIF-1 $\alpha$  and catalase in S-shaped bodies was downregulated instantly following hyperoxia on the 1st postnatal day. Since the expression of HIF-1 $\alpha$  and catalase is vital in nephrogenesis [62, 63], our findings above indicate that the nephrogenic role of HIF-1 $\alpha$  and catalase expression is attenuated early by hyperoxia exposure during the S-shaped body stage. The long-term effect of hyperoxia on the expression of HIF-1 $\alpha$  and catalase in the proximal tubules was also investigated in the current study, which demonstrated that HIF-1 $\alpha$  and catalase expression in mature proximal tubules was downregulated following neonatal hyperoxia. However, neonatal mice exposed to hyperoxia for the first 7 days of life did not show altered catalase mRNA expression in mature lung tissue [64]. Differences in the tissues studied and the duration of exposure to hyperoxia may have resulted in the discrepancy between two studies. A relevant study was not found with regard to long-term HIF-1 $\alpha$  expression following neonatal hyperoxia. Since both HIF-1 $\alpha$  and catalase play a protective role against oxidative stress in the proximal tubules [65, 66], our findings above indicate that the protective role of HIF-1 $\alpha$  and catalase expression against hyperoxia is attenuated continuously up to adulthood.

## 5. Conclusions

In summary, our present investigation shows that neonatal hyperoxia causes an early disappearance of the nephrogenic zone and the impaired development of the proximal tubules, which is accompanied by a significant downregulation of MAPK/ERK signaling activity and the expression of HIF-1 $\alpha$  and catalase throughout nephrogenesis, from S-shaped bodies to mature proximal tubules. Overall, our results indicate that neonatal hyperoxia may impair nephrogenesis

by inhibiting MAPK/ERK signaling as well as HIF-1 $\alpha$  and catalase expression. Therapeutic management targeting MAPK/ERK signaling, HIF-1 $\alpha$ , or catalase may serve to protect against hyperoxia-induced oxidative damage in neonatal proximal tubules.

### Data Availability

The data used to support the findings of this study are available from the corresponding author upon request.

### Conflicts of Interest

The authors declare that there is no conflict of interest regarding the publication of this paper.

### Acknowledgments

The authors would like to thank Mrs. Sun Hanxue of Shengjing Hospital for her excellent technical assistance on histology and also thank Mrs. Gao Linlin of Shengjing Hospital for her kind guidance on animal model preparation. The present study was supported by a National Natural Science Foundation Youth Fund from the National Natural Science Foundation of China (No. 81501292).

### Supplementary Materials

Supplementary figure 1: (a) to facilitate measuring the diameter of the tubular lumen, the image type was changed to a HSB stack (original magnification  $\times 400$ ; scale bar, 100  $\mu\text{m}$ ). Arrows indicate the diameter of the tubular lumen. (b) To facilitate measuring the cell density, the image type was changed to an RGB stack and the threshold was adjusted (original magnification  $\times 400$ ; scale bar, 100  $\mu\text{m}$ ). (c) To facilitate measuring the width of the neonatal nephrogenic zone, the contrast of the image was enhanced to 80% saturated pixels (original magnification  $\times 100$ ; scale bar, 400  $\mu\text{m}$ ). Arrows indicate the width of the nephrogenic zone. (*Supplementary Materials*)

### References

- [1] M. Saint-Faust, F. Boubred, and U. Simeoni, "Renal development and neonatal adaptation," *American Journal of Perinatology*, vol. 31, no. 9, pp. 773–780, 2014.
- [2] C. A. Botwinski and G. A. Falco, "Transition to postnatal renal function," *The Journal of Perinatal & Neonatal Nursing*, vol. 28, no. 2, pp. 150–154, 2014.
- [3] M. R. Sutherland, M. O'Reilly, K. Kenna et al., "Neonatal hyperoxia: effects on nephrogenesis and long-term glomerular structure," *American Journal of Physiology-Renal Physiology*, vol. 304, no. 10, pp. F1308–F1316, 2013.
- [4] Y. L. Phua, T. Gilbert, A. Combes, L. Wilkinson, and M. H. Little, "Neonatal vascularization and oxygen tension regulate appropriate perinatal renal medulla/papilla maturation," *The Journal of Pathology*, vol. 238, no. 5, pp. 665–676, 2016.
- [5] S. Cherian, I. Morris, J. Evans, and S. Kotecha, "Oxygen therapy in preterm infants," *Paediatric Respiratory Reviews*, vol. 15, no. 2, pp. 135–141, 2014.
- [6] C. M. Pabelick, M. A. Thompson, and R. D. Britt Jr., "Effects of hyperoxia on the developing airway and pulmonary vasculature," in *Pulmonary Vasculature Redox Signaling in Health and Disease*, Y. X. Wang, Ed., vol. 967 of *Advances in Experimental Medicine and Biology*, pp. 179–194, Springer, Cham, 2017.
- [7] B. Reich, D. Hoerber, I. Bendix, and U. Felderhoff-Mueser, "Hyperoxia and the immature brain," *Developmental Neuroscience*, vol. 38, no. 5, pp. 311–330, 2016.
- [8] P. G. McMenamin, R. Kenny, S. Tahija et al., "Early postnatal hyperoxia in mice leads to severe persistent vitreoretinopathy," *Investigative Ophthalmology & Visual Science*, vol. 57, no. 15, pp. 6513–6526, 2016.
- [9] V. H. S. Kumar, H. Wang, S. Kishkurno, B. S. Paturi, L. Nielsen, and R. M. Ryan, "Long-term effects of neonatal hyperoxia in adult mice," *The Anatomical Record*, vol. 301, no. 4, pp. 717–726, 2018.
- [10] C. R. Popescu, M. R. Sutherland, A. Cloutier et al., "Hyperoxia exposure impairs nephrogenesis in the neonatal rat: role of HIF-1 $\alpha$ ," *PLoS One*, vol. 8, no. 12, article e82421, 2013.
- [11] M. R. Sutherland, C. Béland, M. A. Lukaszewski, A. Cloutier, M. Bertagnolli, and A. M. Nuyt, "Age- and sex-related changes in rat renal function and pathology following neonatal hyperoxia exposure," *Physiological Reports*, vol. 4, no. 15, article e12887, 2016.
- [12] D. Torbati, G. H. Tan, S. Smith et al., "Multiple-organ effect of normobaric hyperoxia in neonatal rats," *Journal of Critical Care*, vol. 21, no. 1, pp. 85–93, 2006.
- [13] J. S. Jiang, H. C. Chou, T. F. Yeh, and C. M. Chen, "Neonatal hyperoxia exposure induces kidney fibrosis in rats," *Pediatrics and Neonatology*, vol. 56, no. 4, pp. 235–241, 2015.
- [14] C. Zydorczyk, B. Comte, G. Cambonie et al., "Neonatal oxygen exposure in rats leads to cardiovascular and renal alterations in adulthood," *Hypertension*, vol. 52, no. 5, pp. 889–895, 2008.
- [15] M. Nakagawa, N. Nishizaki, A. Endo et al., "Impaired nephrogenesis in neonatal rats with oxygen-induced retinopathy," *Pediatrics International*, vol. 59, no. 6, pp. 704–710, 2017.
- [16] M. Vento, J. Sastre, M. A. Asensi, and J. Vina, "Room-air resuscitation causes less damage to heart and kidney than 100% oxygen," *American Journal of Respiratory and Critical Care Medicine*, vol. 172, no. 11, pp. 1393–1398, 2005.
- [17] D. Dreher and T. Rochat, "Hyperoxia induces alkalization and dome formation in MDCK epithelial cells," *American Journal of Physiology-Cell Physiology*, vol. 262, no. 2, pp. C358–C364, 1992.
- [18] A. Ihermann-Hella, T. Hirashima, J. Kupari et al., "Dynamic MAPK/ERK activity sustains nephron progenitors through niche regulation and primes precursors for differentiation," *Stem Cell Reports*, vol. 11, no. 4, pp. 912–928, 2018.
- [19] L. Miller-Pinsler and P. G. Wells, "Embryonic catalase protects against ethanol embryopathies in acatalasemic mice and transgenic human catalase-expressing mice in embryo culture," *Toxicology and Applied Pharmacology*, vol. 287, no. 3, pp. 232–239, 2015.
- [20] Y. J. Chen, L. Kong, Z. Z. Tang et al., "Hesperetin ameliorates diabetic nephropathy in rats by activating Nrf2/ARE/glyoxalase 1 pathway," *Biomedicine & Pharmacotherapy*, vol. 111, pp. 1166–1175, 2019.
- [21] E. Yuluğ, S. Türedi, Ö. Yıldırım et al., "Biochemical and morphological evaluation of the effects of propolis on cisplatin





- induced kidney damage in rats," *Biotechnic & Histochemistry*, vol. 94, no. 3, pp. 204–213, 2019.
- [22] J. Chen, J. K. Chen, and R. C. Harris, "Deletion of the epidermal growth factor receptor in renal proximal tubule epithelial cells delays recovery from acute kidney injury," *Kidney International*, vol. 82, no. 1, pp. 45–52, 2012.
- [23] D. A. Callaway, L. L. McGill-Vargas, A. Quinn et al., "Prematurity disrupts glomeruli development, whereas prematurity and hyperglycemia lead to altered nephron maturation and increased oxidative stress in newborn baboons," *Pediatric Research*, vol. 83, no. 3, pp. 702–711, 2018.
- [24] O. Akchurin, Z. du, N. Ramkellawan et al., "Partitioning-defective 1a/b depletion impairs glomerular and proximal tubule development," *Journal of the American Society of Nephrology*, vol. 27, no. 12, pp. 3725–3737, 2016.
- [25] S. D. Parlee, S. I. Lentz, H. Mori, and O. A. MacDougald, "Quantifying size and number of adipocytes in adipose tissue," *Methods in Enzymology*, vol. 537, pp. 93–122, 2014.
- [26] K. Young and H. Morrison, "Quantifying microglia morphology from photomicrographs of immunohistochemistry prepared tissue using ImageJ," *Journal of Visualized Experiments*, vol. 5, no. 136, article e57648, 2018.
- [27] A. Porzionato, D. Guidolin, V. Macchi et al., "Fractal analysis of alveolarization in hyperoxia-induced rat models of bronchopulmonary dysplasia," *American Journal of Physiology-Lung Cellular and Molecular Physiology*, vol. 310, no. 7, pp. L680–L688, 2016.
- [28] F. Papadopoulos, M. Spinelli, S. Valente et al., "Common tasks in microscopic and ultrastructural image analysis using ImageJ," *Ultrastructural Pathology*, vol. 31, no. 6, pp. 401–407, 2007.
- [29] C. Y. Lin, T. Y. Lin, M. C. Lee, S. C. Chen, and J. S. Chang, "Hyperglycemia: GDNF-EGR1 pathway target renal epithelial cell migration and apoptosis in diabetic renal embryopathy," *PLoS One*, vol. 8, no. 2, article e56731, 2013.
- [30] W. W. Minuth, "Key features of the nephrogenic zone in the fetal human kidney—hardly known but relevant for the detection of first traces impairing nephrogenesis," *Cell and Tissue Research*, vol. 375, no. 3, pp. 589–603, 2019.
- [31] R. Guan, J. Wang, Z. Li et al., "Sodium tanshinone IIA sulfonate decreases cigarette smoke-induced inflammation and oxidative stress via blocking the activation of MAPK/HIF-1 $\alpha$  signaling pathway," *Frontiers in Pharmacology*, vol. 9, p. 263, 2018.
- [32] K. E. Barrett and D. F. McCole, "Hydrogen peroxide scavenger, catalase, alleviates ion transport dysfunction in murine colitis," *Clinical and Experimental Pharmacology & Physiology*, vol. 43, no. 11, pp. 1097–1106, 2016.
- [33] J. Liu, J. Wang, S. Lee, and R. Wen, "Copper-caused oxidative stress triggers the activation of antioxidant enzymes via ZmMPK3 in maize leaves," *PLoS One*, vol. 13, no. 9, article e0203612, 2018.
- [34] H. T. Cheng, M. Kim, M. T. Valerius et al., "Notch2, but not Notch1, is required for proximal fate acquisition in the mammalian nephron," *Development*, vol. 134, no. 4, pp. 801–811, 2007.
- [35] W. C. Chen, H. H. Lin, and M. J. Tang, "Regulation of proximal tubular cell differentiation and proliferation in primary culture by matrix stiffness and ECM components," *American Journal of Physiology-Renal Physiology*, vol. 307, no. 6, pp. F695–F707, 2014.
- [36] D. Zepeda-Orozco, H. M. Wen, B. A. Hamilton, N. S. Raikwar, and C. P. Thomas, "EGF regulation of proximal tubule cell proliferation and VEGF-A secretion," *Physiological Reports*, vol. 5, no. 18, 2017.
- [37] R. Zhang, R. Liu, and W. Zong, "Bisphenol S interacts with catalase and induces oxidative stress in mouse liver and renal cells," *Journal of Agricultural and Food Chemistry*, vol. 64, no. 34, pp. 6630–6640, 2016.
- [38] S. J. Lin, S. K. Shyue, P. L. Liu et al., "Adenovirus-mediated overexpression of catalase attenuates oxLDL-induced apoptosis in human aortic endothelial cells via AP-1 and C-Jun N-terminal kinase/extracellular signal-regulated kinase mitogen-activated protein kinase pathways," *Journal of Molecular and Cellular Cardiology*, vol. 36, no. 1, pp. 129–139, 2004.
- [39] W. W. Minuth, "Reading first coordinates from the nephrogenic zone in human fetal kidney," *Nephron*, vol. 138, no. 2, pp. 137–146, 2018.
- [40] D. Ryan, M. R. Sutherland, T. J. Flores et al., "Development of the human fetal kidney from mid to late gestation in male and female infants," *eBioMedicine*, vol. 27, pp. 275–283, 2018.
- [41] L. Wagenfuhr, A. K. Meyer, L. Marrone, and A. Storch, "Oxygen tension within the neurogenic niche regulates dopaminergic neurogenesis in the developing midbrain," *Stem Cells and Development*, vol. 25, no. 3, pp. 227–238, 2016.
- [42] V. Balasubramaniam, C. F. Mervis, A. M. Maxey, N. E. Markham, and S. H. Abman, "Hyperoxia reduces bone marrow, circulating, and lung endothelial progenitor cells in the developing lung: implications for the pathogenesis of bronchopulmonary dysplasia," *American Journal of Physiology-Lung Cellular and Molecular Physiology*, vol. 292, no. 5, pp. L1073–L1084, 2007.
- [43] M. van Wenum, A. A. A. Adam, V. A. van der Mark et al., "Oxygen drives hepatocyte differentiation and phenotype stability in liver cell lines," *Journal of Cell Communication and Signaling*, vol. 12, no. 3, pp. 575–588, 2018.
- [44] D.-C. Tarnag, I.-S. Liu, L.-C. Lin, and N.-J. Chen, "Attenuation of tubular injury and renal fibrosis by TI-HU-YIN via reduction in transforming growth factor- $\beta$ 1 expression in unilateral ureteral obstruction mice," *The Chinese Journal of Physiology*, vol. 58, no. 6, pp. 367–376, 2015.
- [45] D. Thomasova, M. Ebrahim, K. Fleckinger et al., "MDM2 prevents spontaneous tubular epithelial cell death and acute kidney injury," *Cell Death & Disease*, vol. 7, no. 11, article e2482, 2016.
- [46] D. P. Basile, M. D. Anderson, and T. A. Sutton, "Pathophysiology of acute kidney injury," *Comprehensive Physiology*, vol. 2, no. 2, pp. 1303–1353, 2012.
- [47] A. J. Sparrow, D. Sweetman, and S. J. M. Welham, "LIM kinase function and renal growth: potential role for LIM kinases in fetal programming of kidney development," *Life Sciences*, vol. 186, pp. 17–24, 2017.
- [48] Y. Jin, L. Q. Peng, and A. L. Zhao, "Hyperoxia induces the apoptosis of alveolar epithelial cells and changes of pulmonary surfactant proteins," *European Review for Medical and Pharmacological Sciences*, vol. 22, no. 2, pp. 492–497, 2018.
- [49] N. An, J. Peng, G. He, X. Fan, F. Li, and H. Chen, "Involvement of activation of mitogen-activated protein kinase (MAPK)/extracellular signal-regulated kinase (ERK) signaling pathway in proliferation of urethral plate fibroblasts in finasteride-induced rat hypospadias," *Medical Science Monitor*, vol. 24, pp. 8984–8992, 2018.



- [50] T. Luo, H. Zhang, Q. Yu et al., "ERK1/2 MAPK promotes autophagy to suppress ER stress-mediated apoptosis induced by cadmium in rat proximal tubular cells," *Toxicology In Vitro*, vol. 52, pp. 60–69, 2018.
- [51] N. V. Iyer, L. E. Kotch, F. Agani et al., "Cellular and developmental control of O<sub>2</sub> homeostasis by hypoxia-inducible factor 1 alpha," *Genes & Development*, vol. 12, no. 2, pp. 149–162, 1998.
- [52] R. T. Menon, A. K. Shrestha, and B. Shivanna, "Hyperoxia exposure disrupts adrenomedullin signaling in newborn mice: implications for lung development in premature infants," *Biochemical and Biophysical Research Communications*, vol. 487, no. 3, pp. 666–671, 2017.
- [53] R. Malhotra, D. W. Tyson, H. M. Rosevear, and F. C. Brosius III, "Hypoxia-inducible factor-1alpha is a critical mediator of hypoxia induced apoptosis in cardiac H9c2 and kidney epithelial HK-2 cells," *BMC Cardiovascular Disorders*, vol. 8, no. 1, p. 9, 2008.
- [54] J. Wan, C. Lata, A. Santilli, D. Green, S. Roy, and S. Santilli, "Supplemental oxygen reverses hypoxia-induced smooth muscle cell proliferation by modulating HIF-alpha and VEGF levels in a rabbit arteriovenous fistula model," *Annals of Vascular Surgery*, vol. 28, no. 3, pp. 725–736, 2014.
- [55] A. Yang, L. Yu, Z. Chen et al., "Label-free quantitative proteomic analysis of chitosan oligosaccharide-treated rice infected with southern rice black-streaked dwarf virus," *Viruses*, vol. 9, no. 5, p. 115, 2017.
- [56] M. Naziroğlu, "Molecular role of catalase on oxidative stress-induced Ca<sup>2+</sup> signaling and TRP cation channel activation in nervous system," *Journal of Receptor and Signal Transduction Research*, vol. 32, no. 3, pp. 134–141, 2012.
- [57] H. Wahhabaghai, R. Heidari, A. Zeinoddini et al., "Hyperoxia-induced preconditioning against renal ischemic injury is mediated by reactive oxygen species but not related to heat shock proteins 70 and 32," *Surgery*, vol. 157, no. 6, pp. 1014–1022, 2015.
- [58] M. Tavafi, H. Ahmadvand, A. Tamjidipour, and B. Rasolian, "Effect of normobaric hyperoxia on gentamicin-induced nephrotoxicity in rats," *Iranian Journal of Basic Medical Sciences*, vol. 17, no. 4, pp. 287–293, 2014.
- [59] R. Ozdemir, G. Demirtas, H. Parlakpınar et al., "Dexpanthenol therapy reduces lung damage in a hyperoxic lung injury in neonatal rats," *The Journal of Maternal-Fetal & Neonatal Medicine*, vol. 29, no. 11, pp. 1801–1807, 2016.
- [60] I. R. S. Sosenko, Y. Chen, L. T. Price, and L. Frank, "Failure of premature rabbits to increase lung antioxidant enzyme activities after hyperoxic exposure: antioxidant enzyme gene expression and pharmacologic intervention with endotoxin and dexamethasone," *Pediatric Research*, vol. 37, no. 4, pp. 469–475, 1995.
- [61] S. Li, X. Yang, Z. Feng, P. Wang, W. Zhu, and S. Cui, "Catalase enhances viability of human chondrocytes in culture by reducing reactive oxygen species and counteracting tumor necrosis factor- $\alpha$ -induced apoptosis," *Cellular Physiology and Biochemistry*, vol. 49, no. 6, pp. 2427–2442, 2018.
- [62] H. Hayashibe, K. Asayama, K. Dobashi, and K. Kato, "Prenatal development of antioxidant enzymes in rat lung, kidney, and heart: marked increase in immunoreactive superoxide dismutases, glutathione peroxidase, and catalase in the kidney," *Pediatric Research*, vol. 27, no. 5, pp. 472–475, 1990.
- [63] Y. Yu, H. Cui, C. Chen et al., "Hypoxia-inducible factor-1 $\alpha$  directs renal regeneration induced by decellularized scaffolds," *Biomaterials*, vol. 165, pp. 48–55, 2018.
- [64] S. Bouch, M. O'Reilly, J. B. de Haan, R. Harding, and F. Sozo, "Does lack of *glutathione peroxidase 1* gene expression exacerbate lung injury induced by neonatal hyperoxia in mice?," *American Journal of Physiology. Lung Cellular and Molecular Physiology*, vol. 313, no. 1, pp. L115–L125, 2017.
- [65] F. Wang, G. Zhang, T. Xing et al., "Renalase contributes to the renal protection of delayed ischaemic preconditioning via the regulation of hypoxia-inducible factor-1 $\alpha$ ," *Journal of Cellular and Molecular Medicine*, vol. 19, no. 6, pp. 1400–1409, 2015.
- [66] C. C. Yang, S.-P. Hsu, K.-H. Chen, and C.-T. Chien, "Effect of adenoviral catalase gene transfer on renal ischemia/reperfusion injury in rats," *The Chinese Journal of Physiology*, vol. 58, no. 6, pp. 420–430, 2015.

## Research Article

# Worsening of Oxidative Stress, DNA Damage, and Atherosclerotic Lesions in Aged LDLr<sup>-/-</sup> Mice after Consumption of Guarana Soft Drinks

Layla Aparecida Chisté,<sup>1</sup> Beatriz Peters Pereira,<sup>1</sup> Marcella Leite Porto,<sup>2</sup>  
Jairo Pinto de Oliveira,<sup>3</sup> Arícia Leone Evangelista Monteiro de Assis,<sup>3</sup>  
Breno Valentim Nogueira,<sup>3</sup> Silvana Santos Meyrelles ,<sup>4</sup> Tadeu Uggere de Andrade,<sup>1</sup>  
Manuel Campos-Toimil ,<sup>5</sup> Elisardo Corral Vasquez,<sup>1,4</sup> Bianca Prandi Campagnaro ,<sup>1</sup>  
and Thiago Melo Costa Pereira <sup>1,2,5</sup>

<sup>1</sup>Pharmaceutical Sciences Graduate Program, Vila Velha University (UVV), Vila Velha, ES, Brazil

<sup>2</sup>Federal Institute of Education, Science, and Technology (IFES), Vila Velha, ES, Brazil

<sup>3</sup>Laboratory of Cellular Ultrastructure Carlos Alberto Redins (LUCCAR), Department of Morphology, Health Sciences Center, Federal University of Espírito Santo (UFES), Vitoria, ES, Brazil

<sup>4</sup>Laboratory of Translational Physiology, Health Sciences Center, Federal University of Espírito Santo, Vitoria, ES, Brazil

<sup>5</sup>Pharmacology of Chronic Diseases (CDPHARMA), Molecular Medicine and Chronic Diseases Research Center (CIMUS), University of Santiago de Compostela, Santiago de Compostela, Spain

Correspondence should be addressed to Thiago Melo Costa Pereira; pereiratmc@gmail.com

Received 8 February 2019; Accepted 12 May 2019; Published 10 June 2019

Academic Editor: Silvana Hrelia

Copyright © 2019 Layla Aparecida Chisté et al. This is an open access article distributed under the Creative Commons Attribution License, which permits unrestricted use, distribution, and reproduction in any medium, provided the original work is properly cited.

**Background.** Excessive consumption of soft drinks (SD) has become a health problem worldwide due to its association with related cardiovascular diseases. We investigated the possible impacts associated with the consumption of Brazilian guarana (normal and zero) SD in dyslipidemic mice, thus mitigating potential clinical confounders such as poor-quality diet, lifestyle, body composition, and/or comorbidities. **Methods.** Sixteen-month-old LDLr<sup>-/-</sup> mice were divided into the following groups: (1) control; (2) GSD: normal guarana SD; and (3) Z-GSD: zero guarana SD. All were fed *ad libitum*, and blood pressure was measured noninvasively. After 8 weeks, aorta, blood, liver, and stomach samples were collected for histological and biochemical analyses. **Results.** Guarana soft drinks increased atherosclerosis (~60%) and were associated with hypercholesterolemia, hypertension, oxidative stress, DNA fragmentation, and apoptosis (~2-fold) of blood cells, besides presenting an increase in liver and gastric damage even in normoglycemia. Interestingly, Z-GSD did not cause the aforementioned changes, except in hemodynamic and renal parameters. **Conclusions.** Chronic administration of GSD is prooxidative, compromising the cardiovascular, gastric, and hepatic systems; the effects are due at least in part to free sugar consumption but not to guarana extract per se.

## 1. Introduction

Excessive consumption of sugar-sweetened soft drinks (SD) has become an alarming public health problem worldwide due to its association with dyslipidemia, weight gain, diabetes type 2, and other related cardiovascular diseases [1, 2]. As an alternative, SD containing artificial sweeteners, considered as “healthier,” have

emerged to try to maintain the profitability of companies [3, 4]. However, the intrinsic toxicity of these carbonated beverages is still controversial, reinforced by scarce experimental data and potential clinical confounders, such as poor-quality diet, lifestyle, body composition, and/or comorbidities [5–7]. Thus, experimental studies are needed to clarify the impact of long-term consumption of SD and its consequences.

Interestingly, only in the last decade have some experimental studies described pathophysiological metabolic alterations after chronic exposure to sugar and artificially sweetened SD, especially colas [2, 8–13]. However, these data may not be extrapolated to all SD, as specific substances are present only in cola beverages (e.g., natural flavorings, colorants, fluid extract of coca, and phosphoric acid), and it is necessary to investigate other SD consumed in the world, such as guarana SD. Guarana SD are made from extracts that have been obtained from the dried seeds of guarana (*Paullinia cupana* H.B.K., Sapindaceae) in the Brazilian Amazonian region since 1921 [14, 15]. In the global market, guarana SD, available in both sugar and artificially sweetened forms, are among the fifteen highest selling SD in the world and the second most consumed in Brazil [16]. Until now, the possible consequences of long-term guarana consumption on cardiovascular-metabolic diseases have not yet been evaluated. Thus, this study reports for the first time the effects of long-term consumption of regular guarana SD (sucrose-sweetened, GSD) and zero guarana SD (aspartame-acesulfame K-sweetened, Z-GSD) in the LDLr<sup>-/-</sup> mouse model.

As rats are commonly resistant to the effects of overabundant nutrients, genetically modified mice have been widely used in studies of cardiovascular-metabolic diseases, thus expanding translational applications [17–21]. Among these, LDLr<sup>-/-</sup> mice show age-dependent susceptibility to concomitant metabolic complications such as dyslipidemia, obesity, and insulin resistance, mimicking humans with metabolic syndrome [21–23].

In this context, the objective of this study was to investigate possible biochemical and/or morphofunctional impacts associated with the consumption of GSD and Z-GSD in aged dyslipidemic mice, mitigating the influence of potential confounders associated with SD consumption in human subjects. These new results may help to fill the data gaps to better inform scientists, patients, clinicians, and governments.

## 2. Methods

**2.1. Animals and Experimental Design.** Under a normal chow diet provided *ad libitum*, female LDLr<sup>-/-</sup> mice, aged ~16 months old, were randomly separated into 3 groups with free access to one of the following drinks: water (control), regular guarana SD (GSD) (sucrose-sweetened carbonated drink, Guaraná Antarctica®, Brazil), or zero guarana SD (Z-GSD) (low-calorie aspartame-acesulfame K-sweetened carbonated drink, Guaraná Antarctica Zero®, Brazil). The CO<sub>2</sub> content was completely removed from both guarana drinks by vigorous shaking using a magnetic bar and a stirring plate in a container filled with the SD, after which the SD was offered to the animals at room temperature. Body weight and food and drink consumption were measured weekly. Cumulative food intake was calculated from the difference in weight before and after feeding. The average caloric food consumption was determined proportionally to food intake under the classic nutritional parameters: carbohydrate (4 kcal/g), protein (4 kcal/g), and fat (9 kcal/g).

Animals were bred and maintained in the animal care facility at the Experimental Monitoring Laboratory of Vila Velha University (UVV) under standard conditions in individual acclimatized plastic cages at ~22°C and 60% humidity under a 12-hour dark-light cycle. After 8 weeks of the diets, all animals were euthanized. All experimental procedures were performed in accordance with the guidelines for the care and handling of laboratory animals as recommended by the National Institutes of Health (NIH), and all protocols were approved by the Institutional Animal Care Committee (Protocol # 375/2016).

**2.2. Blood Pressure Measurements.** Systolic, diastolic, and mean blood pressure (BP) were measured using plethysmography of the tail (CODA Mouse Tail-Cuff Blood Pressure System, Kent Scientific Co., Connecticut, USA). Conscious mice were placed individually in a restraint that allowed free access to the tail and acclimated at 30°C for approximately 15 min to ensure adequate blood flow to the tail. BP measurements were performed in the morning in a quiet laboratory, and the mice were kept calm and handled by the same observer. Thirty-five measurements were recorded over 15 min, and valid readings (at least 10) were averaged to determine the values for BP. All measurements were recorded after a 3-day measurement acclimatization schedule on the first and last day of the diet.

**2.3. Oral Glucose Tolerance Test (OGTT).** On the last day of the diet, basal glycemia was measured after 6 hours of total food and drink deprivation according to Andrikopoulos et al. [24] and Ayala et al. [25]. Fasted mice were orally administered 2 g of glucose/kg body weight, and blood glucose was checked through tail blood extraction at regular intervals (0, 20, 40, 60, and 120 min) as graphically indicated. For this, animals were placed in a restraint, and the last 4 mm of the tail was covered with clean gauze swabbed with lidocaine cream (4%). After 2 min, the anesthetic was removed with ethanol solution (70%), and the last 1 mm of the tip of the tail was then removed using sterilized surgical scissors. Then, the tail was gently massaged to ensure adequate blood flow. The total glucose response vs. time was evaluated by area under the curve (AUC) using Prism software (Prism 6.0, GraphPad Software Inc., San Diego, CA, USA).

**2.4. Clinical Biochemistry Parameters.** The blood was collected from the heart (right ventricle) of mice euthanized with sodium thiopental (100 mg/kg, i.p.). The blood was then centrifuged at 4,000 g for 10 min. Then, the serum was separated and kept at -80°C until analysis. Serum concentrations of glucose, triglycerides, total plasma cholesterol, high-density lipoprotein (HDL), uric acid, urea, creatinine, C-reactive protein (CRP), and homocysteine and the activity of AST and ALT were determined by an automatic biochemical analyzer (AU 680, Olympus/Beckman Coulter, Munich, Germany) according to the manufacturers' instructions. Standard controls were run before each determination. The levels of non-HDL lipoprotein were calculated by subtracting HDL from total serum cholesterol.

For the determination of enzymuria, as described by Fang et al. [26], urine samples were collected before euthanasia for the measurement of glutamyl transpeptidase (GGT) and creatinine. The samples were kept at  $-80^{\circ}\text{C}$  before being assayed. All measurements were performed by standard laboratory methods using the same automatic biochemical analyzer.

**2.5. Morphological Analysis of Aortic Lipid Deposition.** The analysis of aortic lipid deposition was performed as previously described [20, 21, 27]. After euthanasia and venous blood collection, the animals were perfused with PBS-formaldehyde (4%; pH 7.4; 0.1 mol/L) (Merck S.A., São Paulo, Brazil) via the left ventricle, and the thoracic cavity was opened. Briefly, *en face* aortic surfaces were opened, fixed in ethylene vinyl-acetate (EVA), and stained with Oil Red O (Sigma-Aldrich, St. Louis, MO) to identify neutral lipids; images were captured using a digital camera. Then, quantification was performed using imaging software (ImageJ 1.35d, USA, public domain software from National Institutes of Health). Finally, the aortic lesion area was measured by a “blind” investigator.

**2.6. Measurement of Oxidative Stress in the Blood (ROS Production).** ROS were quantified by flow cytometry analysis according to previous protocols [21, 28]. To estimate the bioavailability of intracellular superoxide ( $\bullet\text{O}_2^-$ ) and hydrogen peroxide ( $\text{H}_2\text{O}_2$ ), dihydroethidium (DHE, 160  $\mu\text{M}$ ) and 2',7'-dichlorofluorescein diacetate (DCF, 20 mM) were, respectively, added to a cell suspension ( $10^6$  cells) and incubated for 30 min (at  $37^{\circ}\text{C}$ ) in the dark. In relation to highly reactive oxygen species (hROS), such as peroxynitrite and hydroxyl radicals, they were selectively measured using HPF (2-[6-(4'-hydroxy)phenoxy-3H-xanthen-3-on-9-yl] benzoic acid). After washing the cells and resuspension in PBS, the samples were analyzed using a flow cytometer (FACSCanto II, BD Biosciences, San Jose, CA). All the data were obtained through the FACSDiva software (BD Biosciences, San Jose, CA), and histograms were generated using the FCS Express software (De Novo Software, Thornhill, Ontario). For the measurement of the probes DHE, DCF, and HPF fluorescence, ten thousand events per sample were explored for each analysis in monoplicate with excitation occurring at 488 nm. For  $\bullet\text{O}_2^-$  quantification, DHE fluorescence was measured through a bandpass filter at an excitation/emission wavelength of 585/42 nm, whereas DCF and HPF fluorescence were analyzed through 530/30 nm. Finally, the results were reported as the median fluorescence intensity (MFI).

**2.7. Cell Viability.** This protocol was analyzed through propidium iodide (PI) as previously described [29]. A total of one million cells were exposed to PI (2  $\mu\text{L}$ ) in the medium (5 min at  $25^{\circ}\text{C}$  in the dark).

After the washing step with PBS, the blood cells were submitted to flow cytometry using a FACSCanto II Flow Cytometer (BD Biosciences). For viability analysis, samples were obtained in triplicate. A total of 10,000 events were analyzed for each experiment at 488 nm excitation whereas PI

fluorescence was observed through a bandpass filter at 585/42 nm. All the data are represented as the proportion (%) of unstained/viable cells [29].

Apoptotic blood cells were analyzed according to the protocol of our lab (Porto et al. [28] and Bôa et al. [29]). In brief, cells were washed two times with PBS and adjusted to 0.5 mL with the binding buffer (500,000 cells). After the incubation with annexin V-FITC and PI (at  $25^{\circ}\text{C}$  in the dark for 15 min), the cells were detected using a FACSCanto II (BD Biosciences) flow cytometer. Apoptotic cells were identified by the positive staining for annexin V (Q2 + Q4).

**2.8. Advanced Oxidation Protein Products (AOPP) in Plasma, Liver, and Stomach.** The analyses of AOPP were performed according to Witko-Sarsat et al. [30] and Coutinho et al. [21] using spectrophotometry with a microplate reader (SpectraMax 190, Molecular Devices, Sunnyvale, CA, USA). Forty microliters of plasma, liver, or stomach homogenate (diluted at 1: 10, 1: 30, and 1: 10, respectively) was solubilized 1: 5 in PBS or chloramine-T standard solutions (0 to 100  $\mu\text{mol/L}$ ). Then, the samples were placed in each well of a 96-well microtiter plate (BD Discover Labware, Lincoln Park, NJ, USA), and 10  $\mu\text{L}$  of 1.16 mol/L potassium iodide (KI, Sigma-Aldrich) was added, followed by the addition of 20  $\mu\text{L}$  of acetic acid. The absorbance of the reaction mixture was immediately read at 340 nm in a microplate reader against a blank containing 200  $\mu\text{L}$  of PBS, 10  $\mu\text{L}$  of KI, and 20  $\mu\text{L}$  of acetic acid. Finally, the AOPP was determined when the correlation coefficient was  $>0.95$ . The concentrations were presented in  $\mu\text{mol/mg}$  of total protein as determined by the Bradford method [31] from dilutions of 1: 200 for plasma, 1: 50 for liver, and 1: 4 for stomach for each measurement.

**2.9. Comet Assay.** DNA damage was assessed using an alkaline comet assay (single-cell gel electrophoresis), based on Singh et al. [32] following minor adaptations established from our laboratory [33, 34]. Briefly, histological slides were precoated with 1.5% normal melting point agarose in water in a water bath at  $65^{\circ}\text{C}$ . Subsequently, 10  $\mu\text{L}$  of blood cell suspension was embedded in 110  $\mu\text{L}$  of 1% low melting point agarose in PBS at  $37^{\circ}\text{C}$  and spread on agarose-precoated slides using coverslips. The experiment was conducted in duplicate, i.e., two slides per animal. After gelling at  $4^{\circ}\text{C}$  for 30 min, the coverslips were removed, and the slides were incubated in freshly prepared lysis solution (in mmol/L: 2500 NaCl, 100 EDTA, 10 Tris, and 34 N-lauroylsarcosine sodium, adjusted to pH 10.0-10.5, using freshly added 1% Triton X-100 and 10% DMSO) for 1 hour at  $4^{\circ}\text{C}$ . Then, the slides were placed in an electrophoresis chamber filled with freshly prepared alkaline buffer (in mmol/L: 300 NaOH and 1 EDTA, pH  $>13$ ) for 40 min at  $4^{\circ}\text{C}$  and conducted at 300 mA and 32 V (1 V/cm) for 20 min. Afterwards, the slides were neutralized with a 0.4 mol/L Tris buffer (pH 7.5) for 5 min (3 times) and finally dried with cold pure methanol ( $-20^{\circ}\text{C}$ ) for fixation. Migration of DNA fragments towards the anode creates a comet “tail,” visualized by staining with ethidium bromide (20  $\mu\text{g/mL}$ , Sigma-Aldrich). Immediately afterwards, images were obtained at a magnification of 20x

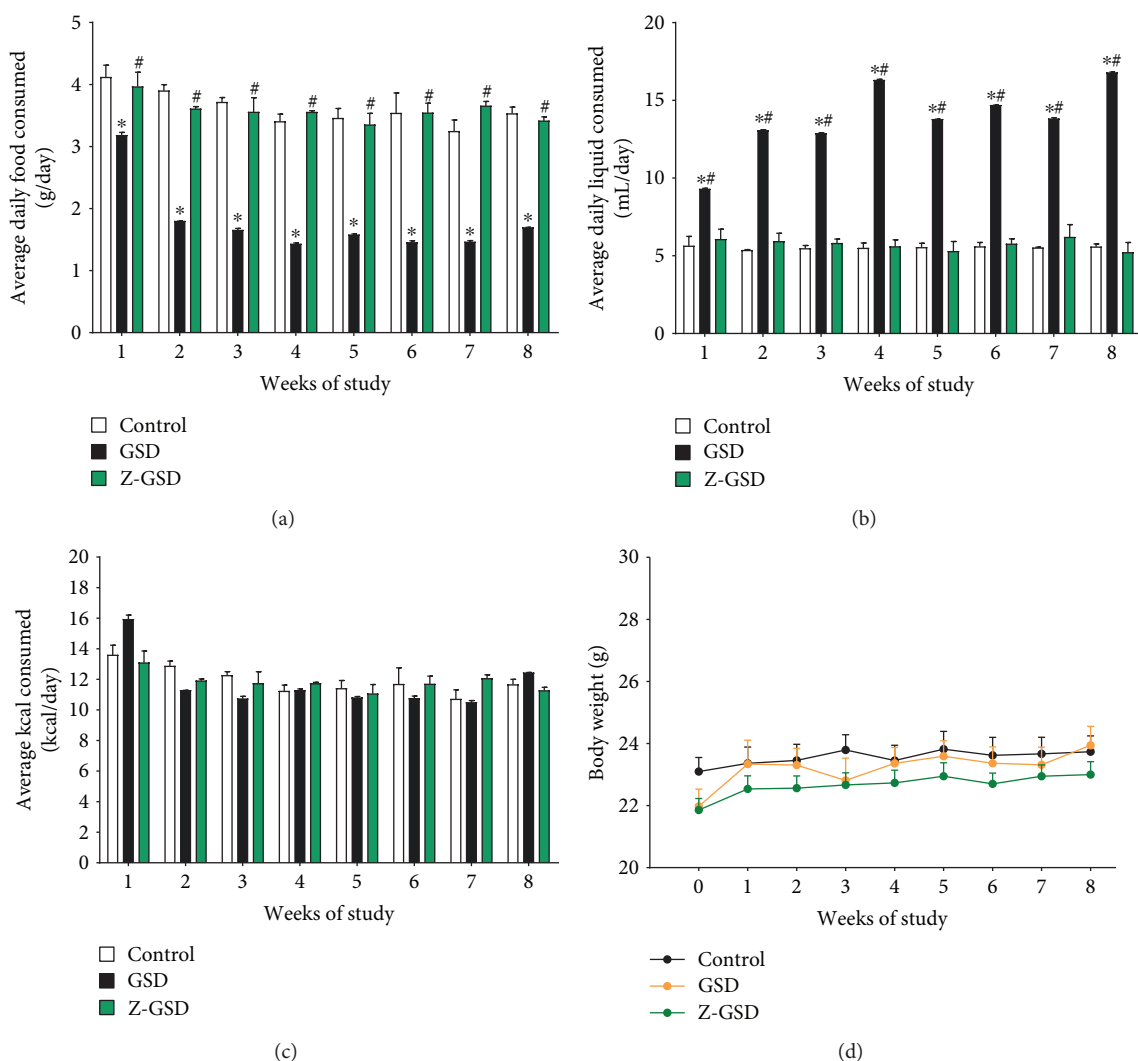


FIGURE 1: Variation in nutrient intake and body weight of  $LDLr^{-/-}$  mice after treatment with guarana soft drinks (normal and zero) for 8 consecutive weeks. (a) GSD mice consumed less food on average daily than control or Z-GSD-fed mice during 8 consecutive weeks ( $*p < 0.05$ ). (b) On the other hand, the GSD group presented polydipsia compared to the control ( $*p < 0.05$ ) and Z-GSD groups ( $^{\#}p < 0.05$ ). (c) There were no differences in caloric intake between groups. (d) During this period, transient changes in body weight in response to GSD or Z-GSD intake were not observed (two-way ANOVA with repeated measures).

using a fluorescence optical microscope (Eclipse TI, Nikon Instruments Inc., Melville, NY, USA) equipped with excitation (420–490 nm) and barrier (520 nm) filters. The coded images were acquired using a CCD camera (Nikon) and were analyzed with the CASP 98beta program (public domain).

Among the several parameters provided by the CASP program, we used the percentage of DNA in the tail and the tail moment for analysis of DNA damage. The images of 50 randomly selected nucleoids from each sample were analyzed for each animal. During the image analysis, nucleoids without clearly identifiable heads, showing overlap, or containing an artifact were excluded as a quality control measure.

**2.10. Liver and Stomach Histology.** For detection of neutral lipids for morphometric analyses, the organs were isolated and fixed in buffered formaldehyde solution (4%) for at least

2 days. The samples were cross-sectioned at  $8 \mu\text{m}$  thicknesses in a  $-25^{\circ}\text{C}$  cryostat (Jung CM1860; Leica, Wetzlar, Germany). Sections were then mounted on gelatin-coated slides and colored with Oil Red O or hematoxylin-eosin (Sigma-Aldrich). Finally, all images were captured using a camera (AxioCam ERc 5 s, Carl Zeiss, Germany) coupled to an optical microscope (AX70, Olympus Corporation, Japan) with a 40x objective and quantified using ImageJ software (NIH, USA). For each analysis, 10 distinct fields per animal were randomly used to calculate the average percentage of the red area. All analyses were performed by a “blind” researcher.

**2.11. Statistical Analysis.** All data are expressed as the mean  $\pm$  SEM (standard error of the mean). For the statistical analysis, two-way ANOVA was performed to analyze differences in biometric parameters and chow, liquid, and caloric intake. For the other analyses, we used one-way ANOVA followed

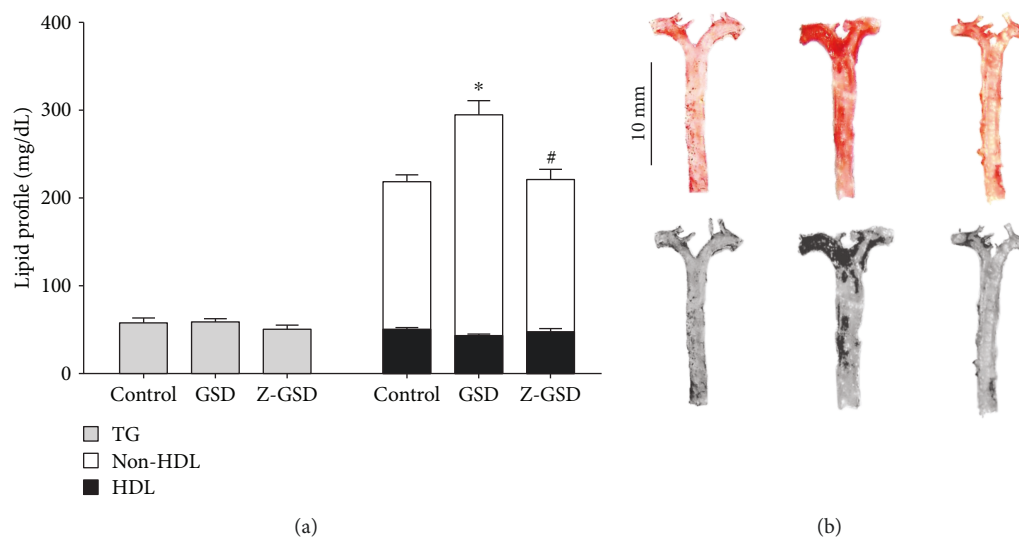


FIGURE 2: Plasma lipoprotein profiles in the three experimental groups of  $LDLr^{-/-}$  mice showing that guarana soft drinks (GSD) increase non-HDL cholesterol (~30%) and vascular lipid deposition (~60%) compared with the control and zero guarana soft drink (Z-GSD) diets. (a) Bar graphs show the lipid profile between groups. (b) Representative aorta *en face* images of Oil Red O staining and their respective densitometry analyses. Bar graph depicting average vascular lipid deposition areas. Values are presented as the mean  $\pm$  SEM for  $n = 6-9$  animals per group. \* $p < 0.05$  vs. the control group and # $p < 0.05$  vs. the GSD group (one-way ANOVA).

TABLE 1: Serum biochemical parameters in experimental groups of  $LDLr^{-/-}$  mice.

Parameters	Control	Groups GSD	Z-GSD	<i>P</i>
Glucose (mg/dL)	206 $\pm$ 12	211 $\pm$ 19	196 $\pm$ 20	0.2856
OGTT (AUC <sub>0-120</sub> )	28476 $\pm$ 2159	20170 $\pm$ 1962*	20830 $\pm$ 1552*	0.0154
Uric acid (mg/dL)	2.8 $\pm$ 0.2	2.9 $\pm$ 0.2	3.0 $\pm$ 0.7	0.9577
Blood urea (mg/dL)	57 $\pm$ 4	57 $\pm$ 4	58 $\pm$ 4	0.9651
Serum creatinine (mg/dL)	0.20 $\pm$ 0.01	0.21 $\pm$ 0.02	0.33 $\pm$ 0.05*#	0.0082
GGT/urinary creatinine (100 U/g)	1.66 $\pm$ 0.34	2.00 $\pm$ 0.46	3.34 $\pm$ 0.46*	0.0323
ALT (U/L)	37 $\pm$ 3	41 $\pm$ 6	39 $\pm$ 8	0.8829
AST (U/L)	168 $\pm$ 29	250 $\pm$ 52	371 $\pm$ 134	0.2626
AST/ALT ratio	3.9 $\pm$ 0.5	4.4 $\pm$ 0.5	4.5 $\pm$ 0.6	0.7576
CRP (mg/L)	0.29 $\pm$ 0.03	0.39 $\pm$ 0.09	0.31 $\pm$ 0.04	0.4656

Note: the values are presented as the mean  $\pm$  SEM for  $n = 7$  to 13 animals per group. \* $p < 0.05$  vs. the control group and # $p < 0.05$  vs. GSD (guarana soft drink group). Z-GSD: zero guarana soft drink.

by post hoc Tukey's test using Prism software (Prism 6.0, GraphPad Software Inc., San Diego, CA, USA). A value of  $p < 0.05$  was considered statistically significant.

### 3. Results

**3.1. Biometric Parameters and Chow, Liquid, and Caloric Intake.** Figure 1 summarizes the general parameters of food and liquid intake, caloric consumption, and body weight during the 8-week follow-up period. The GSD group exhibited hypophagia (~50%,  $p < 0.05$ , Figure 1(a)) and polydipsia (~2.5-fold,  $p < 0.05$ , Figure 1(b)) when compared to the control and Z-GSD groups, without a difference in caloric consumption and body weight between groups.

**3.2. Lipid Profile and En Face Analysis.** Figure 2 represents the serum lipid profile and lipid deposition in the aortas of all groups studied. We observed an augmentation in non-HDL cholesterol in GSD mice (252  $\pm$  16 mg/dL,  $n = 10$ ,  $p < 0.05$ ) compared with the control and Z-GSD groups (168  $\pm$  8,  $n = 9$ , and 174  $\pm$  11 mg/dL,  $n = 10$ , respectively) without a difference in the level of HDL and triglycerides (Figure 2(a)). Figure 2(b) summarizes the results of typical analyses of the aorta, showing that GSD mice had significantly increased lipid deposition, by ~60% ( $p < 0.05$ ), compared with the control group (3.5  $\pm$  0.5%). On the other hand, in the aortas obtained from Z-GSD mice, the lipid deposition was similar to that under control conditions (4.4  $\pm$  0.4%,  $p > 0.05$ ).

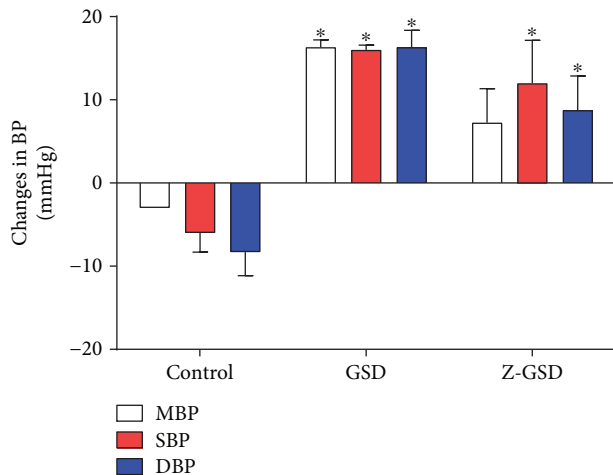


FIGURE 3: Variations in hemodynamic parameters of mean, systolic, and diastolic blood pressure (MBP, SBP, and DBP, respectively) among 3 experimental groups of  $LDLr^{-/-}$  mice. The graph demonstrates that both normal (GSD) and zero (Z-GSD) guarana soft drinks increase the absolute BP over 8 consecutive weeks. Values are presented as the mean  $\pm$  SEM for  $n = 3-5$  animals per group. \* $p < 0.05$  vs. the control group (one-way ANOVA).

**3.3. Other Serum Biochemical Parameters.** Table 1 shows the results of other relevant biochemical analyses of the 3 groups studied after 8 weeks of the diets. Interestingly, we highlighted that the nonfasting glycemic level was not different between the groups. Surprisingly, in the OGTT, the GSD and Z-GSD groups showed augmented sensitivity to insulin ( $\sim 30\%$ ) compared with control mice ( $p < 0.05$ ). In parallel, the renal biomarkers worsened due to Z-GSD supplementation: serum creatinine increased significantly ( $\sim 65\%$ ,  $p < 0.05$ ) in the Z-GSD group compared to the control and GSD groups. Moreover, the GGT/urinary creatinine was also higher in the Z-GSD group than in the control and GSD groups ( $\sim 100$  and  $65\%$ , respectively,  $p < 0.05$ ). No differences were observed between hepatic (ALT and AST) and nonspecific inflammatory (CRP) biomarkers.

**3.4. Blood Pressure Determination.** As shown in Figure 3, the GSD group exhibited significant increases in mean, systolic, and diastolic BP (+19, 22, and 24 mmHg, respectively,  $p < 0.05$ ) compared with the control group. On the other hand, the Z-GSD mice showed increases in only systolic and diastolic BP (18 and 17 mmHg, respectively,  $p < 0.05$ ). No change in heart rate was observed between groups (data not shown).

**3.5. Oxidative Stress Biomarkers in Blood Cells.** Based on previous data showing that high levels of ROS are crucial for atherosclerosis [19, 21, 35–37] and hypertension [38], we evaluated the intracellular ROS levels in white blood cells in all groups studied. As illustrated in Figure 4(a), we showed that GSD supplementation increased  $\cdot O_2^-$  production by  $\sim 50\%$  ( $2,333 \pm 135$  a.u.) compared to that in the control mice ( $\cdot O_2^-$ :  $1,544 \pm 85$  a.u.,  $p < 0.05$ ). Interestingly, Z-GSD prevented the overproduction of ROS ( $\cdot O_2^-$ :  $1,388 \pm 79$ ,

$H_2O_2$ :  $1,038 \pm 48$ ), producing levels similar to that in the control group ( $H_2O_2$ :  $1,140 \pm 41$ ,  $p > 0.05$ ). In relation to hROS, we did not detect differences between groups (control:  $831 \pm 41$ , GSD:  $897 \pm 30$ , Z-GSD:  $792 \pm 29$  a.u.,  $p > 0.05$ ). Concerning other serum biomarkers of oxidative stress, we demonstrated that the GSD group had increased plasma homocysteine ( $\sim 3$ -fold, Figure 4(b)) and AOPP levels ( $\sim 2.5$ -fold, Figure 4(c)) compared to the Z-GSD group ( $p < 0.05$ ).

**3.6. Genotoxic Effect.** The assessment of genotoxic stress by the comet assay indicated greater DNA damage in the GSD group ( $8.9 \pm 0.9\%$ ,  $p < 0.05$ ) than in control mice ( $6.2 \pm 0.5\%$ ), and this damage was significantly reduced in the Z-GSD group ( $4.5 \pm 0.6\%$ ) (Figures 4(d) and 4(e)). Another parameter measured was the comet tail moment, the product of the tail length and the portion of total DNA in the tail [34, 39]. This analysis demonstrated an increase in DNA fragmentation in the GSD group ( $2.6 \pm 0.35$  a.u.,  $p < 0.05$ ) compared with the control and Z-GSD mice ( $1.2 \pm 0.2$  and  $0.6 \pm 0.2$  a.u., respectively) (Figure 4(f)).

**3.7. Cell Viability and Apoptosis in Blood Cells.** Apoptosis was investigated in the same blood cells using PI and annexin V staining and flow cytometry analysis. Figure 5(a) shows typical dot plots for each group. Our results in Figure 5(b) indicate that GSD increased the number of apoptotic cells (Q2 + Q4) by 80% ( $p < 0.05$ ) compared with that of control mice ( $5.1 \pm 0.7$ ). On the other hand, the Z-GSD group showed a profile similar to that of the control mice ( $3.3 \pm 1.2\%$ ,  $p < 0.05$ ). Concerning cell viability (Figure 5(c)), the GSD group showed impaired cell viability ( $86 \pm 1.6\%$ ) compared with that of the other groups (control:  $91 \pm 0.7\%$  and Z-GSD:  $95 \pm 1.8\%$ ,  $p < 0.05$ ).

**3.8. Oxidized Protein and Histological Analysis in Liver and Stomach.** We also investigated the impact of chronic guarana consumption on oxidative damage in the liver and stomach of  $LDLr^{-/-}$  mice. The levels of oxidized proteins were increased in the GSD group compared to control animals, in both the liver (25%,  $p < 0.05$ , Figure 6(a)) and stomach (75%,  $p < 0.05$ , Figure 6(c)). Interestingly, the Z-GSD group and the control mice had similar profiles ( $p > 0.05$ ) in both organs (Figures 6(a) and 6(c)). Moreover, the GSD group showed greater lipid deposition (120%,  $p < 0.05$ ) in liver cells (Figure 6(b)) compared with that of the control group. The Z-GSD group showed no difference compared to the other groups ( $p > 0.05$ ). In regard to stomach damage (Figure 6(d)), we observed that only the GSD group developed atrophy and degeneration in gastric glands.

## 4. Discussion

In the present study, we showed for the first time that long-term consumption of the regular classic guarana beverage (GSD) by adult dyslipidemic mice resulted in an increase in hypercholesterolemia, aortic lipid deposition, BP, oxidative stress, and DNA fragmentation, as well as apoptosis in mononuclear cells, and greater hepatic and gastric injuries (even without weight gain or hyperglycemia). Interestingly,

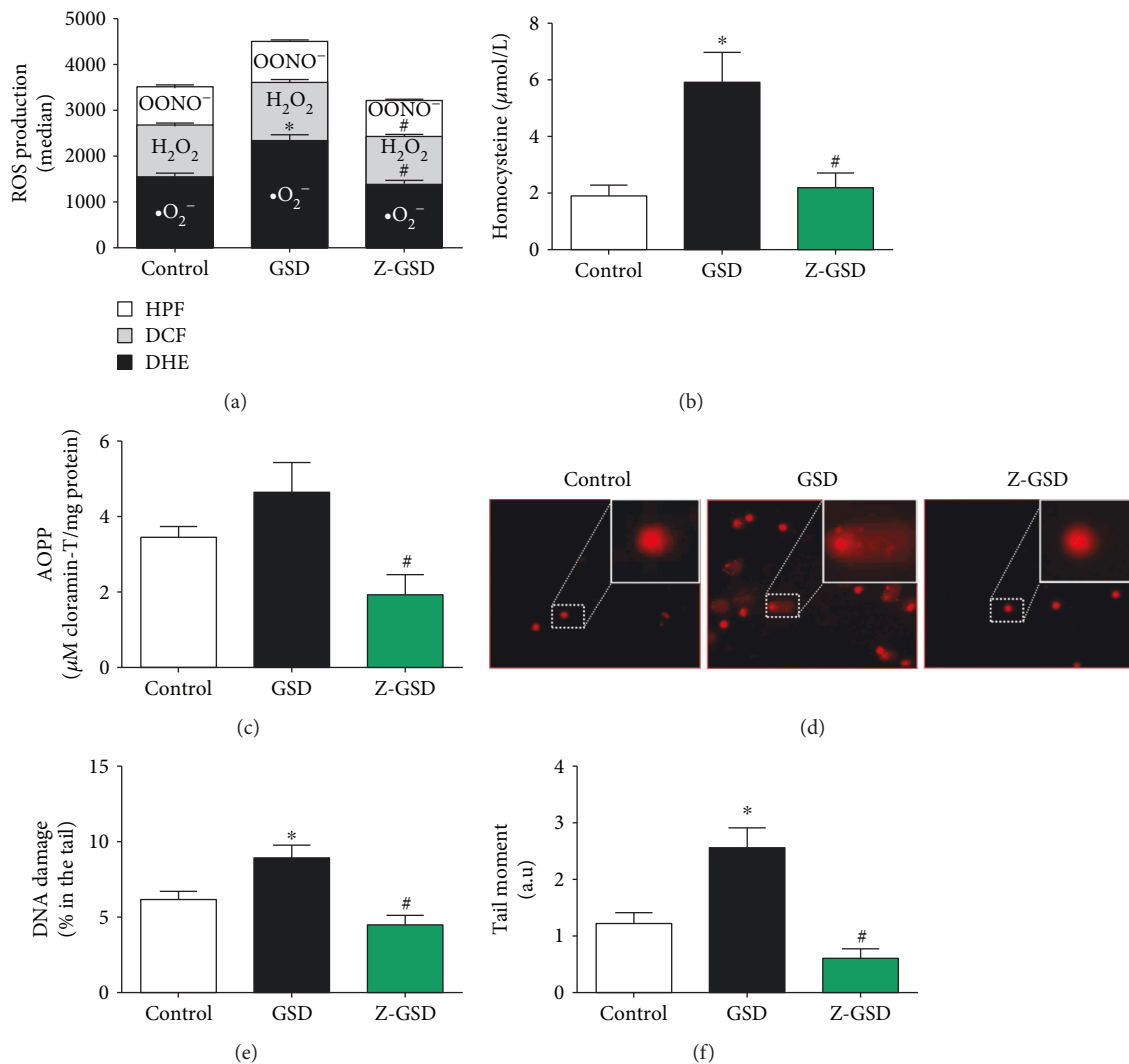


FIGURE 4: ROS overproduction and genotoxic effects are associated with normal guarana soft drink (GSD) but not in zero guarana soft drink (Z-GSD) intake. (a) ROS production was assessed by DHE, DCF, and HPF and measured by flow cytometry. (b) Quantification of homocysteine and (c) protein oxidation (AOPP) in the serum of the 3 groups. (d) Detection of DNA damage in blood is assessed by an alkaline comet assay. Typical comets show greater DNA fragmentation only in the GSD group compared to that in the control group, which contrasts with the Z-GSD group, quantified and represented in the graph in (e). Bar graph in (f) shows the percentage of DNA tail moments (~2-fold higher in the GSD group). Values are presented as the mean  $\pm$  SEM for  $n = 6-7$  animals per group. \* $p < 0.05$  vs. the control group and # $p < 0.05$  vs. the GSD group (one-way ANOVA).

the zero guarana soft drinks (Z-GSD) did not cause most of the described negative effects, except those on hemodynamic and renal parameters.

First, although several clinical studies have indicated a positive association between sugar-sweetened beverage consumption and the risk of obesity [40–42], our results, as well as other related experimental findings [1, 12, 43], have not confirmed the clinical hypothesis that the regular consumption of sugar-sweetened beverages could induce weight gain. It is important to emphasize that, contrary to rational human behavior, the animals exposed to classic guarana halved their consumption of food, thereby normalizing their caloric intake, as previously described by Otero-Losada et al. [12], who investigated cola beverage consumption in the same exposure period. Though some researchers suggest that

consumption of nonnutritive sweeteners may increase appetite [10, 44, 45], our results using zero guarana SD do not show modified food intake or body weight. Therefore, our data reinforce recent experimental findings using diet cola, which had similar results [10–12], and suggest that an increase in food consumption associated with aspartame-sweetened drinks in humans might be related to psychological influences (eating in excess) that apparently did not occur in our experimental animals.

It is well documented that consumption of SD is linked to cardiometabolic risk factors [46–48]. However, the parameters of the traditional serum biochemical profile (e.g., glycemia, triglycerides, and cholesterol) under SD exposure are still conflicting in experimental [1, 10, 12] and clinical studies [45–51]. Our results showed that GSD, but not Z-GSD,



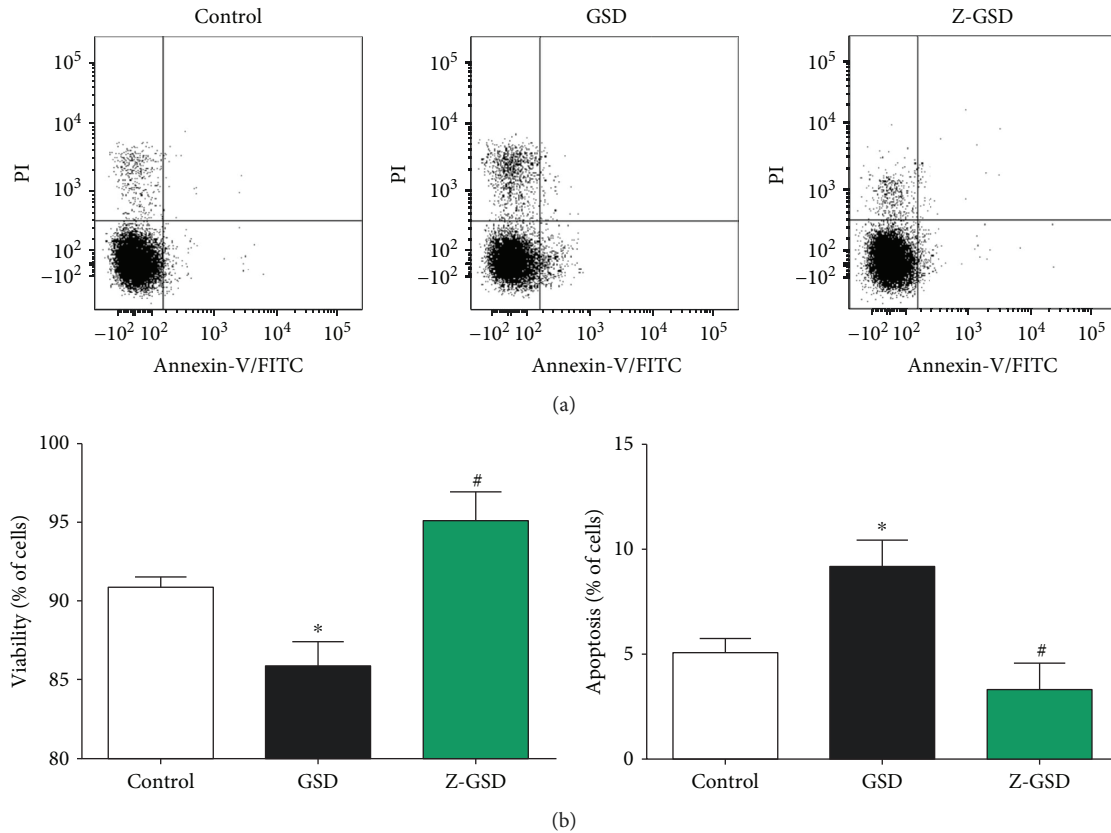


FIGURE 5: Normal (GSD) but not zero (Z-GSD) guarana soft drink intake increases apoptosis and compromises cell viability in blood cells. (a) Dot plots showing the apoptosis ratios from the control, GSD, and Z-GSD groups ( $n = 5$ ). (b) The apoptosis and cell viability ratios were determined using propidium iodide (PI) and FITC-annexin V. The Q2 + Q4 quadrants represent the cells that are in apoptosis. Note the remarkable decrease in the number of apoptotic cells (Q2 + Q4) in the Z-GSD group. Values are presented as the mean  $\pm$  SEM. \* $p < 0.05$  vs. the control group and # $p < 0.05$  vs. the GSD group (one-way ANOVA).

increased only non-HDL cholesterol, maintaining triglyceride and glycemic control. A possible explanation for the euglycemic control is that drinks containing a moderate amount of caffeine [1, 8, 52] and/or acesulfame K [12, 53] might stimulate insulin secretion and/or upregulate glucose transporters, which is partially corroborated by the improvement of the OGTT profile detected in our study. Despite the discrete metabolic impact observed, we demonstrated several consequences of long-term nonzero guarana consumption, described as follows.

The exact influence of chronic SD consumption on atherosclerosis is poorly known. Until now, experimental data have been collected only for cola beverages [12, 54]. Therefore, the proatherogenic effect observed with GSD (but not with Z-GSD) opens new perspectives about this issue, justified by the following points: (1) it is possible to induce significant aortic lipid deposition in aged female  $LDLr^{-/-}$  mice under only sugar-sweetened beverage exposure without a high-fat diet, which opposes the classical methodology [21, 55]; (2) the atherogenesis might be more related to the excessive exposure to free sugars than other substances (nonnutritive sweeteners) in these SD, as observed in a study using cola beverages that detected atherogenesis after exposure to even light cola drinks [54]; and (3) glycemia per se may not be sufficient to evaluate the impact of chronic

exposure to carbohydrate-rich beverages, verified by hemodynamic parameters, redox homeostasis, and cellular/tissue losses, as detected in our study.

Concerning hemodynamic parameters, several reports have shown that hypertension is a major contributor to the development of cardiovascular diseases, which are associated with endothelial dysfunction and altered contractility [27, 56, 57]. For the first time, our study demonstrated an increase in BP due to chronic guarana SD consumption, which could be involved in the development of hypertension. Although we and others have not yet explored the vascular reactivity of animals exposed to classic SD, some studies have previously shown abnormal reactivity in animals fed a high fructose diet [58, 59], justified at least in part by an increase in angiotensin II and downregulation of eNOS [60]. On account of the present data, we suggest that other substances may be involved in the potential development of hypertension because the group treated with an artificially sweetened drink (Z-GSD) also showed a rise in BP. Among them, we cannot discard the role of aspartame (which contains 50% phenylalanine), a relevant precursor of highly vasoactive substances (i.e., dopamine, noradrenaline, and adrenaline) [61], and caffeine, an enhancer of adrenergic activity [10].

It is well established that oxidative stress is a central phenomenon in the progression of cardiovascular [19, 21, 23,

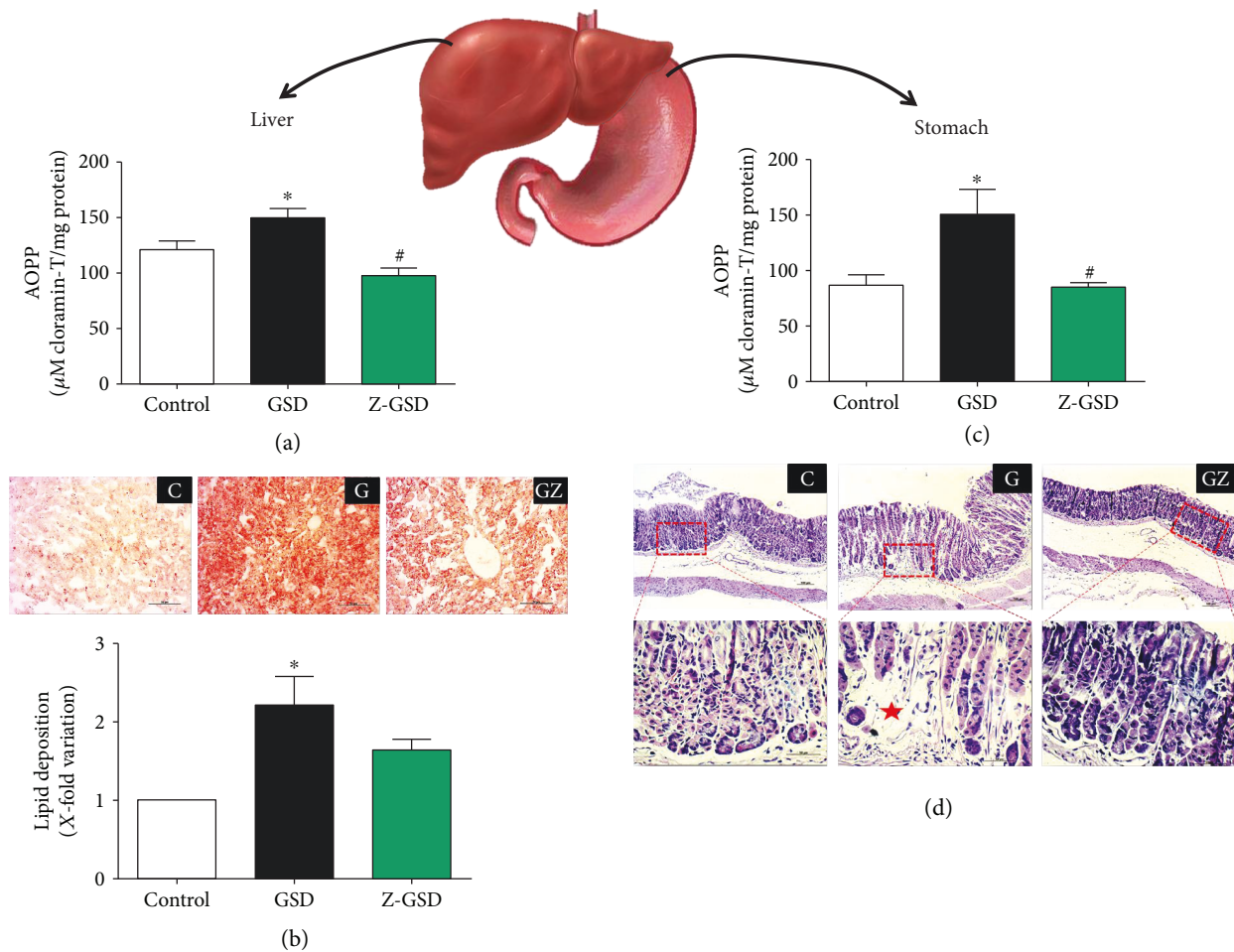


FIGURE 6: Chronic normal (GSD) but not zero (Z-GSD) guarana soft drink intake increases liver and stomach damage. (a) GSD intake augments advanced oxidation protein products (AOPP) and (b) lipid deposition in liver, illustrated through representative images in the top panel. (c) Similarly, GSD increases AOPP formation in the stomach. (d) Only the GSD group developed atrophy and degeneration in gastric glands. The values are presented as the mean  $\pm$  SEM for  $n = 4 - 6$  animals per group. \* $p < 0.05$  vs. the control group and # $p < 0.05$  vs. the GSD group.

27, 35, 62] and other age-related diseases [63, 64]. At the same time, several studies have shown that hyperglycemia increases ROS production mainly via mitochondrial dysfunction and endoplasmic reticulum stress [28, 65–67]. Therefore, we decided to investigate the impact of ROS generation and possible cell/tissue oxidative damage under exposure to guarana drinks. For the first time, we showed that classic guarana soft drinks (GSD) present a prooxidative effect by both direct (flow cytometry) and indirect (homocysteine, AOPP, and DNA fragmentation) detection and that all these factors may influence, at least in part, the increase in BP and the lipid deposition observed in our study [35, 68–70]. Additionally, we previously showed that oxidative damage had major consequences, such as elevation of apoptosis and decrease of blood cell viability, whose mechanisms may be through established pathways (e.g., chromosomal cleavage, telomere shortening, and/or activation of caspases) [71–73]. Moreover, we cannot exclude the possibility that hyperhomocysteinemia observed under exposure to guarana might be another direct contributor to hypertension [64], DNA damage, and apoptosis activation, as observed by others [74, 75].

Until the present study, there was no evidence that guarana SD could contribute to liver or gastric damage. In parallel, only a few studies have demonstrated a potential risk of hepatotoxicity under chronic exposure to aspartame [76, 77] or acesulfame K [12]. Thus, our data clarify this question by demonstrating that the excessive consumption of carbohydrates (but not guarana per se) is the main contributor to steatosis and oxidative stress in the liver. These data are supported by previous research showing that fructose and glucose are important inducers of de novo lipogenesis and ROS production [78, 79]. A similar pattern of impacts was observed for the stomach, revealing that the greatest damage occurs in relation to carbohydrates (fructose, glucose, and sucrose) rather than to artificial sweeteners (acesulfame K or aspartame). It is important to emphasize that all damages previously described were generated in normoglycemic conditions, even in the case of chronic exposure to classic SD (rich in carbohydrates). Thus, it is suggested that before classical metabolic alterations are observed clinically, several types of oxidative damage by SD may occur. This should be considered an alert relevant to public health policies.

Last, but not least, the only organ that showed greater damage from zero guarana SD was the kidney, with possible loss of glomerular filtration and tubular injury, demonstrated by creatininemia and increased enzymuria, respectively, according to previous reports [26, 80]. In this case, we suggest that the renal damage might have been generated by aspartame. Recently, some studies have demonstrated that long-term intake of aspartame may develop oxidative stress in the rat kidney through the dysregulation of glutathione homeostasis [81]. However, future investigations will be necessary to explore the impact of acesulfame K or other substances.

Some limitations of our investigation should be considered. First, the lack of monitoring the estrous cycle in adult female mice does not allow us to speculate about the influence of sex hormones on the present results. Second, since this study with SD was carried out for the first time with LDLr<sup>-/-</sup> mice, the comparison with the ApoE<sup>-/-</sup> mouse model would not be appropriate. Third, we do not yet know if all parameters would be normalized after washout for months, indicating the need for more investigations to confirm or rule out the existence of nonreversible, chronic effects after prolonged consumption of these beverages.

## 5. Conclusions

Our results demonstrate that long-term administration of the classic guarana beverage causes adverse prooxidant outcomes at serum, vascular, hepatic, and gastric levels, at least in part due to free sugar exposure but not to guarana extract per se. This experimental investigation may provide a basis for further experimental and clinical studies to better explore the association between the consumption of soft drinks and metabolic diseases.

## Abbreviations

ALT:	Alanine aminotransferase
ANOVA:	Analysis of variance
AOPP:	Advanced oxidation protein products
AST:	Aspartate aminotransferase
AUC:	Area under the curve
BP:	Blood pressure
FITC:	Fluorescein isothiocyanate
GGT:	Glutamyl transpeptidase
GSD:	Normal/classic guarana soft drink
Z-GSD:	Zero guarana soft drink
HDL:	High-density lipoprotein
i.p.:	Intraperitoneal
kcal:	Kilocalories
LDLr <sup>-/-</sup> :	Low-density lipoprotein receptor knockout mice
MFI:	Median fluorescence intensity
min:	Minutes
NIH:	National Institutes of Health
OGTT:	Oral glucose tolerance test
PBS:	Phosphate-buffered saline
CRP:	C-reactive protein
PI:	Propidium iodide
ROS:	Reactive oxygen species

SD:	Soft drinks
SEM:	Standard error of the mean
UVV:	Vila Velha University.

## Data Availability

All data used to support the findings of this study are included within the article.

## Ethical Approval

All experimental procedures were performed in accordance with the guidelines for the care and handling of laboratory animals as recommended by the National Institutes of Health (NIH), and all protocols were approved by the Institutional Animal Care Committee (Protocol # 375/2016).

## Conflicts of Interest

The authors disclosed no conflict of interest.

## Authors' Contributions

LAC contributed to the design of the study and carried out the experimental analysis, acquisition of data, and interpretation of the data. BPP contributed to the experimental analysis and acquisition of data. MLP and SSM made it possible to perform flow cytometry analysis for the evaluation of ROS and apoptosis/cell viability. TUA participated in the design of the study and supervised the care and treatment of the groups of animals. JPO, ALEMA, and BVN carried out the experimental histological analysis and acquisition of data. MCT participated in the critical revision of the manuscript. ECV made it possible to perform flow cytometry analysis and participated in the critical revision of the manuscript. BPC contributed to the comet assay analysis and critical revision of the manuscript. TMCP was the supervisor of the first author, and he designed the study, carried out the experimental analysis, and drafted and critically reviewed the manuscript. All authors read and approved the final version of the manuscript. All authors consented to the publication of the manuscript.

## Acknowledgments

The authors are grateful to the Tommasi Laboratory for use of their facilities. The authors also acknowledge the support provided by the National Council for Scientific and Technological Development (Grants CNPq-445080/2014-0 and CNPq-445736/2014-3) and the State Agency for the Development of Science and Technology (Grants FAPES-239/2016 and FAPES-0606/2015).

## References

- [1] H. Jürgens, W. Haass, T. R. Castañeda et al., "Consuming fructose-sweetened beverages increases body adiposity in mice," *Obesity Research*, vol. 13, no. 7, pp. 1146–1156, 2005.
- [2] A. Narain, C. S. Kwok, and M. A. Mamas, "Soft drink intake and the risk of metabolic syndrome: a systematic review and

- meta-analysis,” *International Journal of Clinical Practice*, vol. 71, no. 2, 2017.
- [3] M. A. Pereira, “Sugar-sweetened and artificially-sweetened beverages in relation to obesity risk,” *Advances in Nutrition*, vol. 5, no. 6, pp. 797–808, 2014.
  - [4] L. D. Silver, S. W. Ng, S. Ryan-Ibarra et al., “Changes in prices, sales, consumer spending, and beverage consumption one year after a tax on sugar-sweetened beverages in Berkeley, California, US: a before-and-after study,” *PLoS Medicine*, vol. 14, no. 4, article e1002283, 2017.
  - [5] M. Otero-Losada, G. Cao, J. González et al., “Functional and morphological changes in endocrine pancreas following cola drink consumption in rats,” *PLoS One*, vol. 10, no. 3, article e0118700, 2015.
  - [6] L. R. Vartanian, M. B. Schwartz, and K. D. Brownell, “Effects of soft drink consumption on nutrition and health: a systematic review and meta-analysis,” *American Journal of Public Health*, vol. 97, no. 4, pp. 667–675, 2007.
  - [7] E. Mantzari, G. J. Hollands, R. Pechey, S. Jebb, and T. M. Marteau, “Impact of bottle size on in-home consumption of sugar-sweetened beverages: a feasibility and acceptability study,” *BMC Public Health*, vol. 17, no. 1, p. 304, 2017.
  - [8] P. Celec, R. Pálffy, R. Gardlík et al., “Renal and metabolic effects of three months of decarbonated cola beverages in rats,” *Experimental Biology and Medicine*, vol. 235, no. 11, pp. 1321–1327, 2010.
  - [9] J. D. Botzelli, R. A. Dalia, I. M. Reis et al., “Chronic consumption of fructose rich soft drinks alters tissue lipids of rats,” *Diabetology & Metabolic Syndrome*, vol. 2, no. 1, 2010.
  - [10] J. Milei, M. Otero Losada, H. Gómez Llambí et al., “Chronic cola drinking induces metabolic and cardiac alterations in rats,” *World Journal of Cardiology*, vol. 3, no. 4, pp. 111–116, 2011.
  - [11] M. E. Otero-Losada, D. R. Grana, A. Müller, G. Ottaviano, G. Ambrosio, and J. Milei, “Lipid profile and plasma antioxidant status in sweet carbonated beverage-induced metabolic syndrome in rat,” *International Journal of Cardiology*, vol. 146, no. 1, pp. 106–109, 2011.
  - [12] M. E. Otero-Losada, S. Mc Loughlin, G. Rodríguez-Granillo et al., “Metabolic disturbances and worsening of atherosclerotic lesions in ApoE<sup>-/-</sup> mice after cola beverages drinking,” *Cardiovascular Diabetology*, vol. 12, no. 1, 2013.
  - [13] G. Cao, J. González, A. Müller et al., “Beneficial effect of moderate exercise in kidney of rat after chronic consumption of cola drinks,” *PLoS One*, vol. 11, no. 3, p. e0152461, 2016.
  - [14] Brazilian Amazon Consortium for Genomic Research (REALGENE), P. C. S. Ângelo, C. G. Nunes-Silva et al., “Guarana (*Paullinia cupana* var. *sorbilis*), an anciently consumed stimulant from the Amazon rain forest: the seeded-fruit transcriptome,” *Plant Cell Reports*, vol. 27, no. 1, pp. 117–124, 2008.
  - [15] R. d. L. Portella, R. P. Barcelos, E. J. F. da Rosa et al., “Guaraná (*Paullinia cupana* Kunth) effects on LDL oxidation in elderly people: an in vitro and in vivo study,” *Lipids in Health and Disease*, vol. 12, no. 1, p. 12, 2013.
  - [16] Ambev, “Guaraná Antarctica,” February 2018, <http://www.guarana-antarctica.net/product>.
  - [17] V. Poitout, J. Amyot, M. Semache, B. Zarrouki, D. Hagman, and G. Fontés, “Glucolipototoxicity of the pancreatic beta cell,” *Biochimica et Biophysica Acta*, vol. 1801, no. 3, pp. 289–298, 2010.
  - [18] S. S. Meyrelles, V. A. Peotta, T. M. Pereira, and E. C. Vasquez, “Endothelial dysfunction in the apolipoprotein E-deficient mouse: insights into the influence of diet, gender and aging,” *Lipids in Health and Disease*, vol. 10, no. 1, p. 211, 2011.
  - [19] E. C. Vasquez, V. A. Peotta, A. L. Gava, T. M. C. Pereira, and S. S. Meyrelles, “Cardiac and vascular phenotypes in the apolipoprotein E-deficient mouse,” *Journal of Biomedical Science*, vol. 19, no. 1, p. 22, 2012.
  - [20] A. F. Santanna, P. F. Filete, E. M. Lima et al., “Chronic administration of the soluble, nonbacterial fraction of kefir attenuates lipid deposition in LDLr<sup>(-/-)</sup> mice,” *Nutrition*, vol. 35, no. 1, pp. 100–105, 2017.
  - [21] P. N. Coutinho, B. P. Pereira, A. C. Hertel Pereira et al., “Chronic administration of antioxidant resin from *Virola oleifera* attenuates atherogenesis in LDLr<sup>(-/-)</sup> mice,” *Journal of Ethnopharmacology*, vol. 206, no. 1, pp. 65–72, 2017.
  - [22] K. Hartvigsen, C. J. Binder, L. F. Hansen et al., “A diet-induced hypercholesterolemic murine model to study atherosclerosis without obesity and metabolic syndrome,” *Arteriosclerosis, Thrombosis, and Vascular Biology*, vol. 27, no. 4, pp. 878–885, 2007.
  - [23] Y. T. Lee, H. Y. Lin, Y. W. F. Chan et al., “Mouse models of atherosclerosis: a historical perspective and recent advances,” *Lipids in Health and Disease*, vol. 16, no. 1, p. 12, 2017.
  - [24] S. Andrikopoulos, A. R. Blair, N. Deluca, B. C. Fam, and J. Proietto, “Evaluating the glucose tolerance test in mice,” *American Journal of Physiology-Endocrinology and Metabolism*, vol. 295, no. 6, pp. E1323–E1332, 2008.
  - [25] J. E. Ayala, V. T. Samuel, G. J. Morton et al., “Standard operating procedures for describing and performing metabolic tests of glucose homeostasis in mice,” *Disease Models & Mechanisms*, vol. 3, no. 9–10, pp. 525–534, 2010.
  - [26] H. C. Fang, P. T. Lee, P. J. Lu et al., “Mechanisms of star fruit-induced acute renal failure,” *Food and Chemical Toxicology*, vol. 46, no. 5, pp. 1744–1752, 2008.
  - [27] M. Leal, C. Balarini, A. Dias et al., “Mechanisms of enhanced vasoconstriction in the mouse model of atherosclerosis: the beneficial effects of sildenafil,” *Current Pharmaceutical Biotechnology*, vol. 16, no. 6, pp. 517–530, 2015.
  - [28] M. L. Porto, L. M. Lirio, A. T. Dias et al., “Increased oxidative stress and apoptosis in peripheral blood mononuclear cells of fructose-fed rats,” *Toxicology In Vitro*, vol. 29, no. 8, pp. 1977–1981, 2015.
  - [29] I. S. F. Bôa, M. L. Porto, A. C. H. Pereira et al., “Resin from *Virola oleifera* protects against radiocontrast-induced nephropathy in mice,” *PLoS One*, vol. 10, no. 12, p. e0144329, 2015.
  - [30] V. Witko-Sarsat, M. Friedlander, C. Capeillère-Blandin et al., “Advanced oxidation protein products as a novel marker of oxidative stress in uremia,” *Kidney International*, vol. 49, no. 5, pp. 1304–1313, 1996.
  - [31] M. M. Bradford, “A rapid and sensitive method for the quantitation of microgram quantities of protein utilizing the principle of protein-dye binding,” *Analytical Biochemistry*, vol. 72, no. 1–2, pp. 248–254, 1976.
  - [32] N. P. Singh, M. T. McCoy, R. R. Tice, and E. L. Schneider, “A simple technique for quantitation of low levels of DNA damage in individual cells,” *Experimental Cell Research*, vol. 175, no. 1, pp. 184–191, 1988.
  - [33] C. Tonini, B. Campagnaro, L. Louro, T. Pereira, E. Vasquez, and S. Meyrelles, “Effects of aging and hypercholesterolemia on oxidative stress and DNA damage in bone marrow

- mononuclear cells in apolipoprotein E-deficient mice,” *International Journal of Molecular Sciences*, vol. 14, no. 2, pp. 3325–3342, 2013.
- [34] B. P. Rodrigues, B. P. Campagnaro, C. M. Balarini, T. M. C. Pereira, S. S. Meyrelles, and E. C. Vasquez, “Sildenafil ameliorates biomarkers of genotoxicity in an experimental model of spontaneous atherosclerosis,” *Lipids in Health and Disease*, vol. 12, no. 1, p. 128, 2013.
- [35] T. M. Pereira, B. V. Nogueira, L. C. Lima et al., “Cardiac and vascular changes in elderly atherosclerotic mice: the influence of gender,” *Lipids in Health and Disease*, vol. 9, no. 1, p. 87, 2010.
- [36] C. M. Balarini, M. A. Leal, I. B. S. Gomes et al., “Sildenafil restores endothelial function in the apolipoprotein E knockout mouse,” *Journal of Translational Medicine*, vol. 11, no. 1, p. 3, 2013.
- [37] Y. Fu, X. Wang, and W. Kong, “Hyperhomocysteinaemia and vascular injury: advances in mechanisms and drug targets,” *British Journal of Pharmacology*, vol. 175, no. 8, pp. 1173–1189, 2018.
- [38] W. G. McMaster, A. Kirabo, M. S. Madhur, and D. G. Harrison, “Inflammation, immunity, and hypertensive end-organ damage,” *Circulation Research*, vol. 116, no. 6, pp. 1022–1033, 2015.
- [39] Y. L. Lin, S. Sengupta, K. Gurdziel, G. W. Bell, T. Jacks, and E. R. Flores, “p63 and p73 transcriptionally regulate genes involved in DNA repair,” *PLoS Genetics*, vol. 5, no. 10, 2009.
- [40] S. B. D. Torre, A. Keller, J. L. Depeyre, and M. Kruseman, “Sugar-sweetened beverages and obesity risk in children and adolescents: a systematic analysis on how methodological quality may influence conclusions,” *Journal of the Academy of Nutrition and Dietetics*, vol. 116, no. 4, pp. 638–659, 2016.
- [41] V. S. Malik, M. B. Schulze, and F. B. Hu, “Intake of sugar-sweetened beverages and weight gain: a systematic review,” *American Journal of Clinical Nutrition*, vol. 84, no. 2, pp. 274–288, 2006.
- [42] T. A. Marshall, J. M. van Buren, J. J. Warren, J. E. Cavanaugh, and S. M. Levy, “Beverage consumption patterns at age 13 to 17 years are associated with weight, height, and body mass index at age 17 years,” *Journal of the Academy of Nutrition and Dietetics*, vol. 117, no. 5, pp. 698–706, 2017.
- [43] A. M. Meyers, D. Mourra, and J. A. Beeler, “High fructose corn syrup induces metabolic dysregulation and altered dopamine signaling in the absence of obesity,” *PLoS One*, vol. 12, no. 12, article e0190206, 2017.
- [44] R. D. Mattes and B. M. Popkin, “Nonnutritive sweetener consumption in humans: effects on appetite and food intake and their putative mechanisms,” *American Journal of Clinical Nutrition*, vol. 89, no. 1, pp. 1–14, 2009.
- [45] S. E. Swithers, “Artificial sweeteners produce the counterintuitive effect of inducing metabolic derangements,” *Trends in Endocrinology & Metabolism*, vol. 24, no. 9, pp. 431–441, 2013.
- [46] R. Dhingra, L. Sullivan, P. F. Jacques et al., “Soft drink consumption and risk of developing cardiometabolic risk factors and the metabolic syndrome in middle-aged adults in the community,” *Circulation*, vol. 116, no. 5, pp. 480–488, 2007.
- [47] T. T. Fung, V. Malik, K. M. Rexrode, J. A. E. Manson, W. C. Willett, and F. B. Hu, “Sweetened beverage consumption and risk of coronary heart disease in women,” *American Journal of Clinical Nutrition*, vol. 89, no. 4, pp. 1037–1042, 2009.
- [48] M. P. Pase, J. J. Himali, A. S. Beiser et al., “Sugar- and artificially sweetened beverages and the risks of incident stroke and dementia: a prospective cohort study,” *Stroke*, vol. 48, no. 5, pp. 1139–1146, 2017.
- [49] M. I. Van Rompay, N. M. McKeown, E. Goodman et al., “Sugar-sweetened beverage intake is positively associated with baseline triglyceride concentrations, and changes in intake are inversely associated with changes in HDL cholesterol over 12 months in a multi-ethnic sample of children,” *Journal of Nutrition*, vol. 145, no. 10, pp. 2389–2395, 2015.
- [50] J. B. Smith, B. E. Niven, and J. I. Mann, “The effect of reduced extrinsic sucrose intake on plasma triglyceride levels,” *European Journal of Clinical Nutrition*, vol. 50, no. 8, pp. 498–504, 1996.
- [51] R. S. Surwit, M. N. Feinglos, C. C. McCaskill et al., “Metabolic and behavioral effects of a high-sucrose diet during weight loss,” *American Journal of Clinical Nutrition*, vol. 65, no. 4, pp. 908–915, 1997.
- [52] S. Park, J. S. Jang, and S. M. Hong, “Long-term consumption of caffeine improves glucose homeostasis by enhancing insulinotropic action through islet insulin/insulin-like growth factor 1 signaling in diabetic rats,” *Metabolism*, vol. 56, no. 5, pp. 599–607, 2007.
- [53] M. Y. Pepino and C. Bourne, “Non-nutritive sweeteners, energy balance, and glucose homeostasis,” *Current Opinion in Clinical Nutrition and Metabolic Care*, vol. 14, no. 4, pp. 391–395, 2011.
- [54] M. Otero-Losada, G. Cao, S. Mc Loughlin, G. Rodríguez-Granillo, G. Ottaviano, and J. Milei, “Rate of atherosclerosis progression in ApoE<sup>-/-</sup> mice long after discontinuation of cola beverage drinking,” *PLoS One*, vol. 9, no. 3, 2014.
- [55] G. S. Getz and C. A. Reardon, “Animal models of atherosclerosis,” *Arteriosclerosis, Thrombosis, and Vascular Biology*, vol. 32, no. 5, pp. 1104–1115, 2012.
- [56] A. M. Briones and R. M. Touyz, “Oxidative stress and hypertension: current concepts,” *Current Hypertension Reports*, vol. 12, no. 2, pp. 135–142, 2010.
- [57] A. C. Montezano, M. Dulak-Lis, S. Tsiropoulou, A. Harvey, A. M. Briones, and R. M. Touyz, “Oxidative stress and human hypertension: vascular mechanisms, biomarkers, and novel therapies,” *Canadian Journal of Cardiology*, vol. 31, no. 5, pp. 631–641, 2015.
- [58] T. Nakagawa, H. Hu, S. Zharikov et al., “A causal role for uric acid in fructose-induced metabolic syndrome,” *American Journal of Physiology-Renal Physiology*, vol. 290, no. 3, pp. F625–F631, 2006.
- [59] N. Wiernsperger, P. Nivoit, L. G. K. de Aguiar, and E. Bouskela, “Microcirculation and the metabolic syndrome,” *Microcirculation*, vol. 14, no. 4-5, pp. 403–438, 2007.
- [60] L. T. Tran, K. M. MacLeod, and J. H. McNeill, “Chronic etanercept treatment prevents the development of hypertension in fructose-fed rats,” *Molecular and Cellular Biochemistry*, vol. 330, no. 1-2, pp. 219–228, 2009.
- [61] M. L. Porto, B. P. Rodrigues, T. N. Menezes et al., “Reactive oxygen species contribute to dysfunction of bone marrow hematopoietic stem cells in aged C57BL/6J mice,” *Journal of Biomedical Science*, vol. 22, no. 1, 2015.
- [62] P. Libby and G. K. Hansson, “Inflammation and immunity in diseases of the arterial tree: players and layers,” *Circulation Research*, vol. 116, no. 2, pp. 307–311, 2015.

- [63] N. Khansari, Y. Shakiba, and M. Mahmoudi, "Chronic inflammation and oxidative stress as a major cause of age-related diseases and cancer," *Recent Patents on Inflammation & Allergy Drug Discovery*, vol. 3, no. 1, pp. 73–80, 2009.
- [64] G. Guo, W. Sun, G. Liu, H. Zheng, and J. Zhao, "Comparison of oxidative stress biomarkers in hypertensive patients with or without hyperhomocysteinemia," *Clinical and Experimental Hypertension*, vol. 40, no. 3, pp. 262–266, 2018.
- [65] A. Avogaro, M. Albiero, L. Menegazzo, S. de Kreutzenberg, and G. P. Fadini, "Endothelial dysfunction in diabetes: the role of reparatory mechanisms," *Diabetes Care*, vol. 34, Supplement 2, pp. S285–S290, 2011.
- [66] T. Fiorentino, A. Prioretta, P. Zuo, and F. Folli, "Hyperglycemia-induced oxidative stress and its role in diabetes mellitus related cardiovascular diseases," *Current Pharmaceutical Design*, vol. 19, no. 32, pp. 5695–5703, 2013.
- [67] I. B. Gomes, M. L. Porto, M. C. L. F. S. Santos et al., "Renoprotective, anti-oxidative and anti-apoptotic effects of oral low-dose quercetin in the C57BL/6J model of diabetic nephropathy," *Lipids in Health and Disease*, vol. 13, no. 1, p. 184, 2014.
- [68] T. Pereira, F. Pimenta, M. Porto et al., "Coadjuvants in the diabetic complications: nutraceuticals and drugs with pleiotropic effects," *International Journal of Molecular Sciences*, vol. 17, no. 8, p. 1273, 2016.
- [69] M. Qasim, S. A. Bukhari, M. J. Ghani et al., "Relationship of oxidative stress with elevated level of DNA damage and homocysteine in cardiovascular disease patients," *Pakistan Journal of Pharmaceutical Sciences*, vol. 29, 6 Suppl, pp. 2297–2302, 2016, Supplement 6.
- [70] I. Chernyavskiy, S. Veeranki, U. Sen, and S. C. Tyagi, "Atherogenesis: hyperhomocysteinemia interactions with LDL, macrophage function, paraoxonase 1, and exercise," *Annals of the New York Academy of Sciences*, vol. 1363, no. 1, pp. 138–154, 2016.
- [71] K. Kannan and S. K. Jain, "Oxidative stress and apoptosis," *Pathophysiology*, vol. 7, no. 3, pp. 153–163, 2000.
- [72] Z. Ungvari, G. Kaley, R. de Cabo, W. E. Sonntag, and A. Csiszar, "Mechanisms of vascular aging: new perspectives," *The Journals of Gerontology Series A: Biological Sciences and Medical Sciences*, vol. 65A, no. 10, pp. 1028–1041, 2010.
- [73] X. Yang, Y. Li, Y. Li et al., "Oxidative stress-mediated atherosclerosis: mechanisms and therapies," *Frontiers in Physiology*, vol. 8, p. 600, 2017.
- [74] M. Currò, A. Gugliandolo, C. Gangemi, R. Risitano, R. Ientile, and D. Caccamo, "Toxic effects of mildly elevated homocysteine concentrations in neuronal-like cells," *Neurochemical Research*, vol. 39, no. 8, pp. 1485–1495, 2014.
- [75] P. Ganguly and S. F. Alam, "Role of homocysteine in the development of cardiovascular disease," *Nutrition Journal*, vol. 14, no. 1, 2015.
- [76] M. E.-S. Alkafafy, Z. S. Ibrahim, M. M. Ahmed, and S. A. El-Shazly, "Impact of aspartame and saccharin on the rat liver: biochemical, molecular, and histological approach," *International Journal of Immunopathology and Pharmacology*, vol. 28, no. 2, pp. 247–255, 2015.
- [77] I. Finamor, S. Pérez, C. A. Bressan et al., "Chronic aspartame intake causes changes in the *trans*-sulphuration pathway, glutathione depletion and liver damage in mice," *Redox Biology*, vol. 11, pp. 701–707, 2017.
- [78] J. S. Lim, M. Mietus-Snyder, A. Valente, J. M. Schwarz, and R. H. Lustig, "The role of fructose in the pathogenesis of NAFLD and the metabolic syndrome," *Nature Reviews Gastroenterology & Hepatology*, vol. 7, no. 5, pp. 251–264, 2010.
- [79] P. Jegatheesan and J. P. De Bandt, "Fructose and NAFLD: the multifaceted aspects of fructose metabolism," *Nutrients*, vol. 9, no. 3, p. 230, 2017.
- [80] P. H. Whiting and P. A. J. Brown, "The relationship between enzymuria and kidney enzyme activities in experimental gentamicin nephrotoxicity," *Renal Failure*, vol. 18, no. 6, pp. 899–909, 1996.
- [81] I. Finamor, M. A. Pavanato, T. Pês et al., "N-acetylcysteine protects the rat kidney against aspartame-induced oxidative stress," *Free Radical Biology and Medicine*, vol. 75, p. S30, 2014.

## Review Article

# Probiotics as Beneficial Dietary Supplements to Prevent and Treat Cardiovascular Diseases: Uncovering Their Impact on Oxidative Stress

Elisardo C. Vasquez <sup>1</sup>, Thiago M. C. Pereira <sup>1,2</sup>, Veronica A. Peotta <sup>3</sup>,  
Marcelo P. Baldo<sup>4,5</sup> and Manuel Campos-Toimil <sup>6</sup>

<sup>1</sup>Laboratory of Translational Physiology and Pharmacology, Pharmaceutical Sciences Graduate Program, Vila Velha University (UVV), Vila Velha, Brazil

<sup>2</sup>Federal Institute of Education, Science and Technology (IFES), Vila Velha, Brazil

<sup>3</sup>Stead Family Department of Pediatrics, The University of Iowa, Iowa City, IA, USA

<sup>4</sup>Department of Pathophysiology, State University of Montes Claros, Montes Claros, MG, Brazil

<sup>5</sup>Department of Medicine, Faculdades Integradas Pitagoras, Montes Claros, MG, Brazil

<sup>6</sup>Pharmacology of Chronic Diseases (CD Pharma), Center for Research in Molecular Medicine and Chronic Diseases (CIMUS), University of Santiago de Compostela, Santiago de Compostela, Spain

Correspondence should be addressed to Manuel Campos-Toimil; [manuel.campos@usc.es](mailto:manuel.campos@usc.es)

Received 9 January 2019; Revised 1 April 2019; Accepted 14 April 2019; Published 7 May 2019

Academic Editor: Saeid Golbidi

Copyright © 2019 Elisardo C. Vasquez et al. This is an open access article distributed under the Creative Commons Attribution License, which permits unrestricted use, distribution, and reproduction in any medium, provided the original work is properly cited.

The gut microbiota, the ecosystem formed by a wide symbiotic community of nonpathogenic microorganisms that are present in the distal part of the human gut, plays a prominent role in the normal physiology of the organism. The gut microbiota's imbalance, gut dysbiosis, is directly related to the origin of various processes of acute or chronic dysfunction in the host. Therefore, the ability to intervene in the gut microbiota is now emerging as a possible tactic for therapeutic intervention in various diseases. From this perspective, evidence is growing that a functional dietary intervention with probiotics, which maintain or restore beneficial bacteria of the digestive tract, represents a promising therapeutic strategy for interventions in cardiovascular diseases and also reduces the risk of their occurrence. In the present work, we review the importance of maintaining the balance of the intestinal microbiota to prevent or combat such processes as arterial hypertension or endothelial dysfunction, which underlie many cardiovascular disorders. We also review how the consumption of probiotics can improve autonomic control of cardiovascular function and provide beneficial effects in patients with heart failure. Among the known effects of probiotics is their ability to decrease the generation of reactive oxygen species and, therefore, reduce oxidative stress. Therefore, in this review, we specifically focus on this antioxidant capacity and its relationship with the beneficial cardiovascular effects described for probiotics.

## 1. Introduction

Literature searches on “gut microbiota” performed by the guest editors via the PubMed platform revealed extensive publications, consisting of approximately 880 reviews in 2018 (~2/day). Approximately 380 (~1/day) reviews on

“probiotics” were published in 2018. Restricting the search with filters to published reviews using the combination of terms “probiotics and cardiovascular diseases” reduced the number to 15. Interestingly, when the term “oxidative stress” was included in the combination “probiotics and cardiovascular diseases (CVD) and oxidative stress,” no published

reviews were identified. It is known that CVD remains the leading cause of death and disability in developed countries. These two scenarios associated with exciting original articles on probiotics and CVD in the prior 3 years motivated us to promote the publication of this special issue.

The gut microbiota is a broad symbiotic community of nonpathogenic microorganisms composed primarily of anaerobic bacteria (although some gut bacteria preferentially grow under microaerophilic conditions) and fungi [1]. One of its functions is the maintenance of a barrier via enterocytes covered with a brush border of mucus, which is produced by goblet cells and nonpenetrable tight junctions between enterocytes [2, 3], a layer of luminal mucus and tight adherens junctions between enterocytes that allows the control of absorption and metabolism and the maturation and stimulation of the immune system, which are essential functions for an effective mechanism of defense against pathogens in the host [4]. Signals generated in the gut microbiota communicate with distant organs by crossing the intestinal epithelium and triggering diverse signaling processes located at the epithelial cell border, subsequently reaching the systemic circulatory system. Different pathways are responsible for the bidirectional interaction between the gut microbiota and systemic organs in healthy individuals (Figure 1).

Currently, there is a growing body of evidence that an abnormal predominance of pathogenic over commensal (nonpathogenic) microorganisms, a condition termed gut dysbiosis, can initiate or worsen the dysfunction of diverse target systemic organs [5–7]. Gut dysbiosis is also a confirmed cause of increased oxidative stress in the body. In fact, frequent consumption of fats and refined sugars in the Western-type diet produces an increase in reactive oxygen species (ROS) production and inflammatory processes [8, 9]. Additionally, the gut microbiota regulates the production of mitochondrial ROS [10]. In recent years, various studies have revealed that gut dysbiosis may contribute to the development and progression of CVD and other related diseases [11, 12].

On the other hand, several studies have demonstrated that probiotics may be beneficial in reestablishing the microbiota through different mechanisms such as appropriate intestinal homeostasis [13]. The name probiotic is applied to those live microorganisms which, when administered in adequate amounts, confer a health benefit on the host. This definition, established by the joint Food and Agriculture Organization of the United Nations (FAO) and World Health Organization (WHO) Working Group, is the one used today and accepted by the International Scientific Association for Probiotics and Prebiotics (ISAPP) [14].

Therefore, the purpose of this review is to update our knowledge concerning the contribution of the exacerbated production of oxidative stress to the development of cardiac and vascular dysfunctions in the clinic and in experimental models of arterial hypertension, as well as the possible beneficial effects of dietary supplementation with probiotics, in an attempt to prevent or reverse these cardiovascular disturbances.

## 2. Probiotics as Promising Coadjuvants for Prevention/Treatment of Arterial Hypertension

Arterial hypertension constitutes a main risk factor for the development of severe pathologies, such as acute myocardial infarction, heart failure, stroke, and renal failure [15–17], as well as for premature death worldwide [18]. Primary (or essential) hypertension is a multifactorial process that involves genetics, demographics, comorbid disorders, and environmental influences [19]. Approximately 8% of cases exhibit secondary hypertension, which has a known origin, including endocrine diseases, drugs, cancer, or hyperactivation of the renin-angiotensin system, among others [20].

Antihypertensive therapy used in clinical practice has been shown to be effective in maintaining blood pressure (BP) at safer levels, thereby reducing the morbidity and mortality associated with this disease. Several international reports, mainly those prepared by the Eighth Joint National Committee (JNC 8), have established the guidelines for the treatment of hypertensive patients and different reference values for those over 60 years old [21].

In addition to pharmacological treatments, it is necessary to establish a series of nonpharmacological measures for the control of the disease. In this sense, the relevance of a good diet is paramount [22], and the contribution of probiotics can be fundamental. It has been demonstrated that the gut microbiota participates in an important manner in the control of BP by several mechanisms, such as exerting control at the level of the central and autonomic nervous system or protecting endothelial function (see illustration in Figure 1). Additionally, gut dysbiosis has been described in animal models of hypertension and hypertensive patients [23].

In agreement with the above discussion and based on the state-of-the-art role of the gut microbiota and its interaction with different organs, a working group at the National Heart, Lung, and Blood Institute recently discussed the current status and future directions for the treatment and prevention of high BP, considering the use of probiotics [24]. Therefore, functional foods that contribute to the maintenance of the intestinal flora can be very useful when avoiding excessively high BP levels, as previously reviewed in detail by several authors (see [11, 25–28]).

Among the foods that have been shown to provide various cardiovascular benefits, kefir has been reported to effectively lower BP [5, 28]. Chronic consumption of this synbiotic attenuates the abnormal increase in BP in spontaneously hypertensive rats (SHR), which has been the most commonly used genetically hypertensive animal for a better understanding of several cardiovascular abnormalities. Kefir has been tested in the protection of vascular endothelial dysfunction [29] and in the correction of impaired autonomic cardiovascular function [30, 31], including its inhibitory effects on angiotensin-converting enzyme (ACE) [32] (Figure 2). Therefore, there is growing evidence that probiotics could be a promising natural coadjuvant in the prevention/treatment of CVD, including the hypertensive process. In another study using SHR, animals fed with Minas Frescal



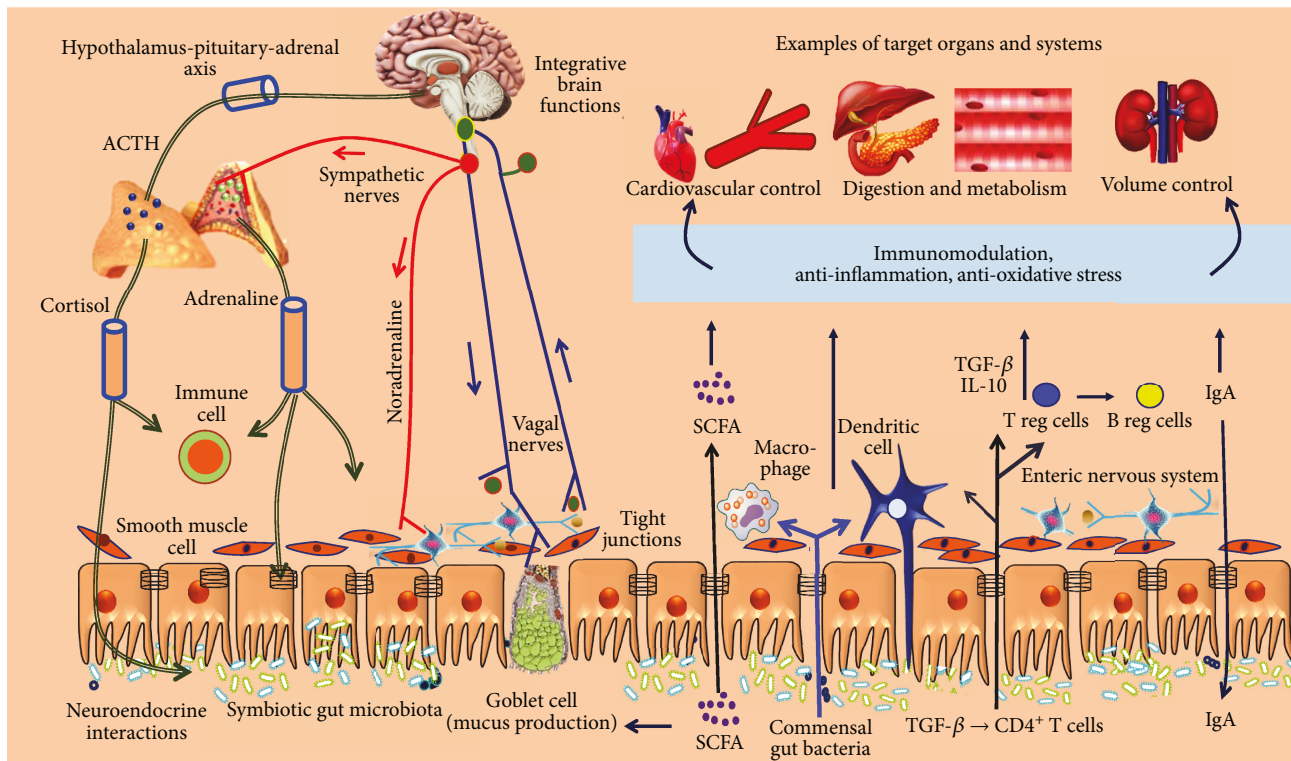


FIGURE 1: Summary of the interaction between the gut microbiota and neuroimmune and neuroendocrine systems and the interaction between the gut microbiota and microbiota target organs of the host. The gut microbiota provides (i) a mucosal barrier through tight and adherens junctions between enterocytes, (ii) immunomodulation and anti-inflammation through recruitment of immune cells, and (iii) energy metabolism via metabolites/short-chain fatty acids (SCFAs), vitamins, and hormones. The brain-intestine axis acts through both an integrative autonomic nervous system, including the sympathetic/parasympathetic (vagal) afferent/efferent nerve pathways, associated with the neural myenteric network, and a neuroendocrine system, including the hypothalamus-adrenocortical gland system.

probiotic cheese showed a significantly lower BP compared with the control group, in addition to an improvement in other indicators of cardiovascular health, such as blood levels of triglycerides and cholesterol [33].

Several clinical studies in humans have also demonstrated the ability of probiotics to reduce abnormally high BP levels. For example, an extract of *Lactobacillus casei*, which has been shown to reduce BP in SHR [34], was able to induce a reduction in systolic/diastolic BP and heart rate in hypertensive patients [35]. In 2002, an interesting study showed that food supplementation with *Lactobacillus plantarum* produced a significant decrease in systolic BP in heavy smokers [36]. A Norwegian study showed, in 2011, that the incidence of preeclampsia, which is associated with hypertension and inflammation, is decreased by chronic intake of probiotics [37]. Additionally, in a randomized double-blind clinical trial with type II diabetes mellitus, probiotic soy milk containing *Lactobacillus plantarum* significantly decreased systolic/diastolic BP [38], and in a study with prediabetic patients, there was a significant tendency to reduce hypertension in those patients receiving a multispecies probiotic [39]. In 2014, a meta-analysis carried out based on the results of nine clinical trials found that consumption of probiotics slightly reduced BP and that this effect was more marked if the basal BP was elevated. The authors also concluded that several species of probiotics used together provided

enhanced effects. Finally, the duration of the intervention must be  $\geq 8$  weeks, and the dose of daily consumption of probiotics should be  $\geq 10^{11}$  colony-forming units [40].

In contrast, several studies have questioned the role of some probiotics in producing low BP. A treatment for 4 weeks by dietary supplementation of *Lactobacillus plantarum* either together with fermented blueberry or with three synthesized phenolic compounds did not lower BP in NG-nitro-L-arginine methyl ester- (L-NAME-) induced hypertensive rats [41]. In a clinical trial, probiotic strains of *Lactobacillus acidophilus* and *Bifidobacterium animalis*, provided in either yogurt or capsule form, did not improve cardiovascular risk factors since they did not modify BP or concentrations of total cholesterol LDL-C, HDL-C, or triglycerides in overweight or obese individuals [42]. Additionally, a study of postmenopausal women with metabolic syndrome showed that administration of milk supplemented with *Lactobacillus plantarum* produced several beneficial effects, but it did not provide a significant decrease in BP [43]. Furthermore, long-term treatment with *Lactobacillus helveticus*-fermented milk containing bioactive peptides reduced arterial stiffness in hypertensive subjects but did not induce statistically significant differences between the effects of the probiotic and placebo treatment on BP [44].

In view of these reports, it will still be necessary to carry out more studies to verify the possible role of probiotic foods

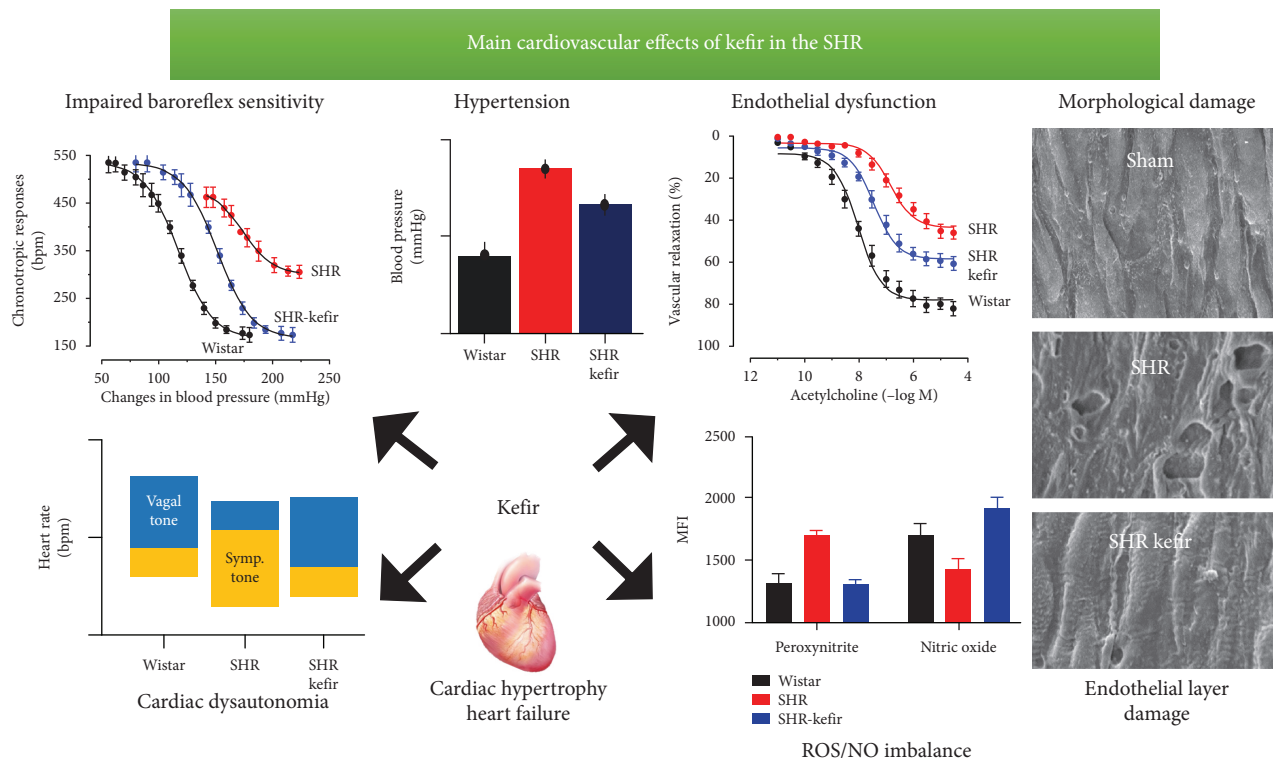


FIGURE 2: Main cardiovascular disturbances observed by our research group in the SHR model and the effectiveness of kefir supplementation to attenuate or revert them. Graphs were constructed based on published data [28–30, 32].

as coadjuvants in the treatment of arterial hypertension. In any case, the results of the different studies suggest that the complicated mechanisms of the development of hypertension, the choice of different bacterial strains, the different types of patients, and the previous state of their microbiome can be decisive in terms of obtaining satisfactory results for the reduction of BP.

### 3. Endothelial Dysfunction: The Role Played by Oxidative Stress

The vascular endothelium is a single layer of smooth, thin cells that constitutes the first barrier between the bloodstream and the vascular muscle. Among its functions is to act as a selective membrane through which fluid and solutes, as well as trafficking of inflammatory cells, interchange between the plasma and tissue spaces [45, 46].

The endothelium also contributes to the regulation of vascular tone by synthesizing and releasing a huge number of vasodilating substances, both vasodilators such as nitric oxide (NO), prostacyclin, and endothelium-derived hyperpolarizing factor (EDHF) and vasoconstrictors such as endothelin (via  $ET_A$ ), angiotensin II (via  $AT_1$  receptors), and ROS. In addition, its action is the key in the control of platelet aggregation and blood hemostasis, regulating the antithrombotic/prothrombotic balance, and it also participates in the inflammatory and immune response (for a detailed review, see [47–49]).

Due to this multifunctional role of the endothelium, it is easy to understand that its alterations may lie at the origin

and/or in the development of various diseases. Therefore, endothelial dysfunction is recognized as a risk factor for the onset of CVD and appears in the early stages and during the development of hypertension, cardiac ischemia, atherosclerosis, stroke, or peripheral vascular disease [48, 50, 51]. Other diseases such as diabetes, kidney failure, infectious diseases, and tumor progression also have a component of endothelial dysfunction [49, 51, 52].

Endothelial dysfunction can be caused by inflammatory processes, leading to a decrease in endothelial NO synthase (eNOS) enzyme activity, thereby decreasing the NO bioavailability and culminating in hypertension [53]. Moreover, oxidative stress also contributes to the development of endothelial dysfunction, reducing the availability of NO [54, 55]. In fact, the generation of ROS caused by hypertension, hypercholesterolemia, diabetes, or other cardiovascular risk factors causes a decrease in the release of endothelial NO [56].

As mentioned above, there is an important relationship between dysbiosis and the development of hypertension (see also [57]), which could involve the impaired endothelial function due to alterations of the gut microbiota during the chronic rise in BP. In fact, fecal microbiota transplantation from SHR to normotensive WKY rats caused a chronic impairment of endothelial function, accompanied by greater vascular oxidative stress and increased systolic BP. In contrast, transplantation of fecal microbiota from WKY to SHR provoked the opposite effects with an improvement of endothelial dysfunction in hypertensive animals [27].

Accordingly, several studies have suggested that probiotics could lead to an improvement in endothelial function. Rashid et al. [58] reported that the endothelial dysfunction of mesenteric artery rings in rats with common bile duct ligation is mediated in part by oxidative stress, possibly due to bacterial translocation inducing a proinflammatory response, and that this effect is improved by the ingestion of a probiotic formulation.

Endothelial dysfunction can be identified physiologically by means of NO-dependent mechanisms (Figure 3). In this situation, blood vessels show a reduced vasodilator response to agents that contribute to the release of NO, such as acetylcholine and, conversely, an exacerbated response to vasoconstrictor agents, such as  $\alpha_1$ -adrenergic agonists or thromboxane A2 analogues. Using this method, chronic probiotic treatment with *Lactobacillus coryniformis* reversed the endothelial dysfunction observed in obese mice and improved the endothelial dysfunction and vascular oxidative stress induced by lipopolysaccharides (LPS) in control mice [59].

In a similar way, our group evaluated the effects of the probiotic kefir on endothelial dysfunction in SHR. Our results suggested that kefir treatment for eight weeks (even at a low dose) could attenuate endothelial dysfunction in the large vessels in hypertensive rats, and the main mechanism for this beneficial effect was exerted through a repair of the vascular endothelial architecture (Figure 2) and a reduction of the oxidative stress, together with an increase in NO bioavailability as well as endothelial progenitor cell recruitment [29]. These beneficial effects of kefir on vascular endothelial function have recently been reviewed [5].

This effect of probiotics was also confirmed in a study in which lactic acid bacteria partially reversed the relaxation deficit of the aorta in SHR. In addition, it also increased the NO level, which is abnormally decreased in SHR serum. Both effects are indicative of a probiotic-induced improvement in endothelial function due to a reduction of vascular oxidative and inflammatory status [60].

In addition, using SHR and WKY rats for comparison, a study by Gomez-Guzman et al. [61] demonstrated that chronic oral administration of the probiotic *Lactobacillus fermentum* or *Lactobacillus coryniformis* plus *Lactobacillus gasseri* restored gut eubiosis and improved endothelial dysfunction as a result of a reduced vascular proinflammatory and prooxidative status.

Some studies in humans or human cells have also shown an improvement in endothelial function due to probiotic treatment. In endothelial cells, soy milk fermented with *Lactobacillus plantarum* or *Streptococcus thermophilus* stimulated NO production and eNOS activity, suggesting their effectiveness for the improvement of endothelial function [62]. A 6-week supplementation with *Lactobacillus plantarum* in men with stable coronary artery disease improved endothelial function for both conduit and resistance vessels through increasing NO bioavailability while concomitantly reducing systemic inflammation, as measured by brachial artery flow-mediated dilation. These results suggest that the intestinal microbiota is mechanistically linked to systemic inflammation and vascular endothelial function [45]. Another clinical trial showed that a multispecies probiotic

supplement improved both functional and biochemical parameters of endothelial dysfunction, including systolic BP, vascular endothelial growth factor, pulse wave velocity (PWV) and its augmentation index, interleukin-6, tumor necrosis factor alpha (TNF $\alpha$ ), and thrombomodulin in obese postmenopausal women [63]. In contrast, in a study of subjects with metabolic syndrome receiving supplementation with the probiotic strain *Lactobacillus casei* Shirota, no significant changes in parameters used to assess low-grade inflammation or endothelial dysfunction were observed [64].

In general, studies both *in vivo* and *in vitro*, as well as clinical studies in humans, suggest that supplementation with several types of probiotics contributes to an improvement in endothelial function through various mechanisms. Although further research is needed, the role of probiotic supplementation in the prevention of CVD by correcting endothelial dysfunction is promising. In addition, the multifunctional role of the endothelium extends this potential use of probiotics to all diseases, not only cardiovascular, in which its pathophysiology may be related to endothelial dysfunction.

#### 4. Evidence of the Beneficial Effects of Probiotics on the Autonomic Control of Cardiovascular Function

Prebiotics, probiotics, and synbiotics are some of the best evidenced ways of manipulating the microbiota, and their potential role in the prevention and treatment of multiple diseases has recently garnered a significant interest. Recent data from experimental time-course studies have shown that long-term treatment with kefir (at least 30 to 60 days), in addition to the antihypertensive effect, attenuated cardiac hypertrophy in SHR [29, 30, 32]. Considering the relationship between the gut microbiota and the target systemic organs, it is important to highlight studies that relate the influence of these microorganisms to cardiovascular function.

Those findings led the authors to investigate whether the benefits of kefir supplementation could also include the autonomic neural control of BP (baroreflex function) and the cardiac pacemakers controlling the chronotropic rhythm under the neural efferent pathways from the brainstem integrative areas. They observed that administration of kefir (for at least 60 days) attenuated and partially reversed the abnormal cardiac sympathetic predominance over the parasympathetic tone in SHR, raising the following question: "by which mechanisms can probiotics and synbiotics affect brain areas?" As illustrated in Figures 1 and 4, there is a consistent and well-recognized neuroendocrine gut-brain axis connection, which includes the hypothalamus-pituitary-suprarenal gland axis and the autonomic sympathetic/parasympathetic afferent/efferent pathways. Others have attempted to address the question by proposing relevant interactions between gut endocrine cells and vagal afferents through gut chemosensing mechanisms [65, 66].

Other exciting findings in recent years has been the demonstration of a marked association between the effects

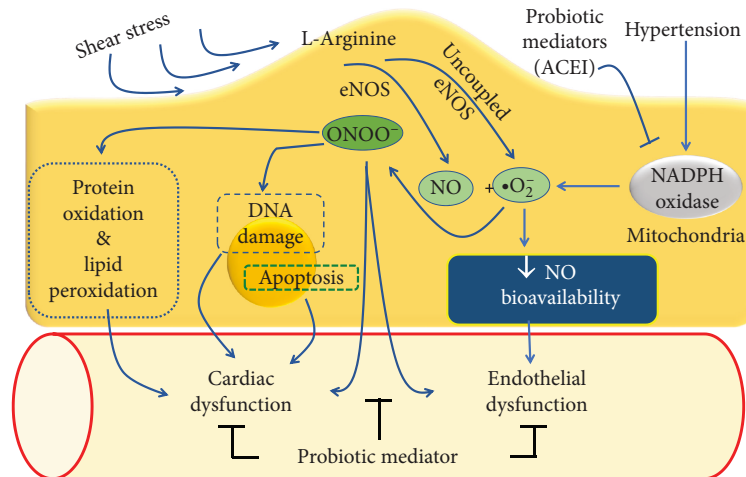


FIGURE 3: Main mechanisms of action of probiotics on the endothelial layer of conductance and resistance vessels showing the deleterious actions of reactive oxygen species and the beneficial actions of probiotics, leading to the attenuation of endothelial dysfunction observed in hypertensive subjects.

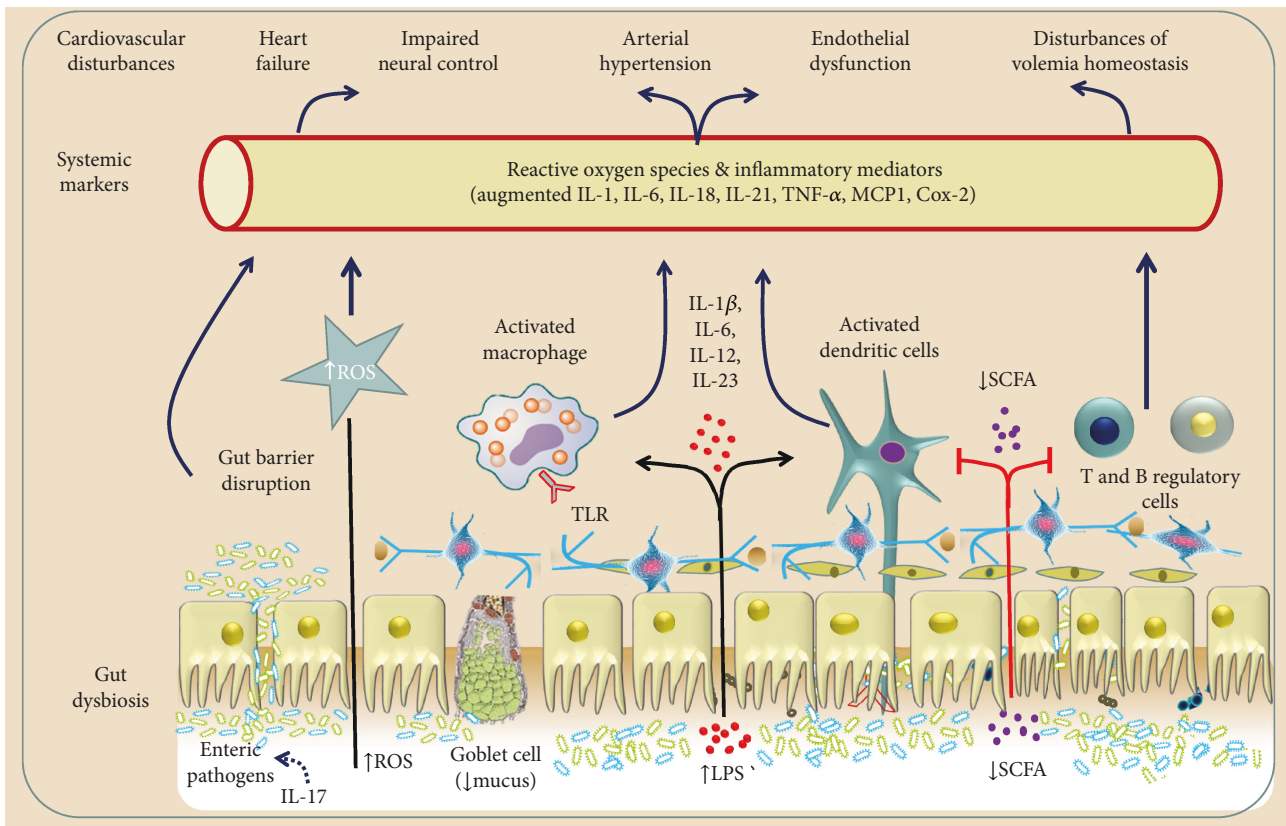


FIGURE 4: Gut microbiota and some relevant molecular pathways linking gut dysbiosis to cardiovascular and cardiometabolic diseases through the bloodstream and via the autonomic nervous system. The main mechanisms of the modulators include the neuroendocrine hypothalamus-pituitary-adrenal axis (ACTH: adrenocorticotrophic hormone), afferent and efferent pathways of the autonomic nervous system (vagal and sympathetic components), reactive oxygen species (ROS), inflammatory markers (interleukins: IL; tumor necrosis factor  $\alpha$ : TNF $\alpha$ ; monocyte chemoattractant protein: MCP1; cyclooxygenase: Cox 2; toll-like receptors: TLR), and dietary metabolic byproducts (short-chain fatty acids: SCFAs; lipopolysaccharides: LPS).

of probiotics and decreased production of intravascular ROS and augmented NO bioavailability. It seems that the mechanisms underlying the beneficial actions of probiotics on

cardiac autonomic control could occur through its capability to decrease the production of cytokines and ROS in the hypothalamic paraventricular nucleus. In turn, it could attenuate

hypertension and end-organ damage by upregulating anti-inflammatory and antioxidant molecules, therefore restoring the normal balance between parasympathetic and sympathetic activity to the heart, as recently observed by our group [30]. In a similar way and as expected, the investigators observed that SHR treated with probiotics presented a partial recovery of the baroreceptor sensitivity, which is characterized in this experimental model by a high variability of the resting BP. The SHR exhibited diminished reflex tachycardia or bradycardia to induce hypotensive or hypertensive changes in the resting BP. Probiotic supplementation was able to partially repair this BP variability and baroreflex sensitivity, and this could occur because kefir repairs the normal gut microbiota and, consequently, restores the production of neuroactive compounds in the intestinal lumen. Therefore, the above findings corroborate the knowledge that probiotics have a modulatory action on the integrative central or peripheral components of the gut-brain axis [65, 67].

Recently, Brasil et al. [32] assessed whether the soluble nonbacterial fraction of kefir (bioactive compounds) and not the probiotic effects would improve cardiovascular hemodynamics, enhancing the baroreflex sensitivity, which could include the ACE inhibitory properties. Therefore, an important mechanism by which probiotics decrease high BP and repair endothelial dysfunction and cardiac autonomic tones could be achieved through probiotic bioactive compounds. In addition, it has been observed that probiotic supplementation caused a decrease in ACE activity measured in the serum of SHR treated with the soluble nonbacterial fraction of kefir, supporting ACE inhibition as a likely mechanism for kefir's beneficial cardiovascular effects during hypertension. These effects indicate that the improvement in baroreflex gain cannot be attributed to the probiotic effect of kefir but rather to other bioactive compounds produced by microbial action. Clearly, how these different fractions (e.g., probiotic bacteria or bioactive compounds) influence the baroreflex and other cardiovascular risk factors are still poorly understood. To our knowledge, very few publications have evaluated the effects of probiotics on baroreflex function and autonomic control of heart rate. These previous studies used the fermented food *kefir* [30] and its bioactive compounds [32].

In conclusion, the benefits of probiotics in the cardiovascular system in models of hypertension include the reversion of cardiac dysautonomia, which is characterized in hypertensive subjects by an inverted predominance of sympathetic over vagal tone, including a significant attenuation of the high variability of BP and heart rate and their effectiveness to partially revert the decreased [68] baroreflex sensitivity. Nonetheless, probiotics attenuate disturbances in the neural control of cardiovascular function in a similar manner to that achieved with physical exercise [68], therapy with flavonoids [69], and pharmacological medication [30]. Therefore, there is clearly a need for more mechanistic studies that would help to identify the missing links to explain the protective effects of fermented foods, such as pre-, pro-, and synbiotics, as well as their bioactive compounds on the neural control of BP. Figure 5 summarizes the possible sites of action of probiotics.

## 5. Heart Failure: A Target for the Benefits of Functional Diets

Heart failure (HF) patients experience some changes in the gut microbiome during disease. Some reports have described increased levels of pathogenic microbes that could have potential deleterious effects on cardiac function [70]. This phenomenon might be explained by the so-called “gut hypothesis,” in which the reduced cardiac pumping function and congestion observed in HF patients would be responsible for an intestinal ischemia [71], favoring bacterial translocation and increases in circulating endotoxins that elicit inflammation [72]. In fact, the intestinal blood flow is reduced in HF patients, contributing to juxtamucosal bacterial growth [73]. Kummen et al. [74] reported that the gut microbiota in HF patients is related to persistent T-cell activation. In fact, the removal of Gram-negative intestinal bacteria by antibiotics reduces the monocyte CD14 expression, along with reduced levels of endotoxins and cytokines, with improved flow-mediated dilation in patients with severe HF [75].

The association between gut dysbiosis and CVD was highlighted when 60 stable HF patients were selected to test whether the characteristics of the gut microbiota would correlate with their cardiovascular functional status. The authors evidenced that HF patients had more colonies of pathogenic bacteria than control participants, along with an increased intestinal permeability that favored bacterial translocation. In addition, severe HF was associated with more pathogenic types of bacteria than mild HF [76]. The contribution of the gut microbiota to the pathogenesis of CVD has been supported by the discovery that some dietary products that are metabolized by gut microbes produce toxic metabolites that could have negative impact on the cardiovascular system. Changes in the gut microbiota can lead to increases in trimethylamine N-oxide (TMAO), which is a major contributor to cardiovascular and renal diseases [77]. TMAO is an endotoxin that is produced via the metabolism of trimethylamine from the carnitine molecule, which is absorbed into the blood and converted into TMAO in the liver by flavin-containing monooxygenases [78]. In fact, intestinal microbes participate in the phosphatidylcholine metabolism and in the increased TMAO levels, which was independently associated with major cardiovascular events [70] and the incidence of chronic kidney diseases [79]. The findings also showed that TMAO could contribute to the risk prediction scores of deaths in acute HF patients, revealing a poor 1-year prognosis [80].

Experimental studies have demonstrated potential therapeutic actions of probiotics in different animal models of HF. Using a rat model of acute myocardial infarction by permanent coronary occlusion, Gan et al. [81] showed improved ventricular function and structure after treatment with the probiotic *Lactobacillus rhamnosus*. The possible mechanism by which probiotics act in the infarcted heart has been described by Lam et al. [82], in which the probiotic *Lactobacillus plantarum* decreased the leptin levels and, thus, reduced the infarct size in rats. Additionally, the antiapoptotic effect of probiotic-fermented purple sweet potato yogurt

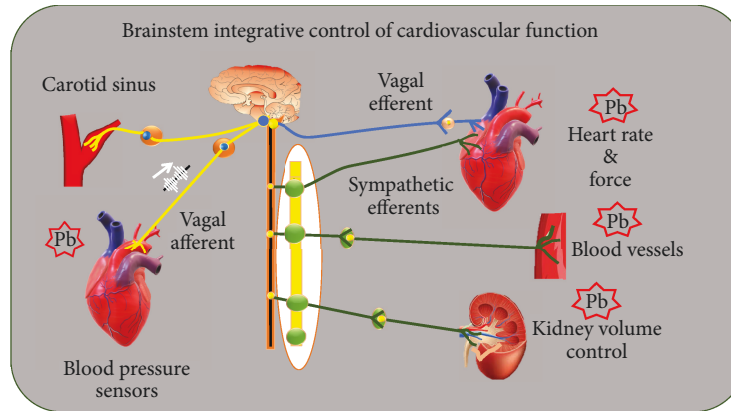


FIGURE 5: Diagram illustrating the pathways of neural control of cardiac and vascular function through the autonomic neural system and possible sites of action of the probiotics (Pb) based on recent evidence. Mechanosensitive baroreceptors are located in the carotid sinus and aortic arch, and they discharge at BP systole-by-systole bursts of action potentials to the brainstem. The autonomic vagal and sympathetic efferents innervate the cardiac pacemakers and the myocardium (sympathetic ends). The resistance and conductance vessels are innervated by sympathetic efferent components. Modified from Vasquez et al. [28], with permission.

was evidenced in a rat model of hypertensive HF [83]. Despite the increasing number of experimental studies on probiotics in HF models, only one study has addressed the prognostic effects of probiotics in HF patients. In this pilot trial, patients with HF class II or III and LVEF <50% were randomized to *Saccharomyces boulardii* or placebo for 3 months in a double-blinded fashion. Patients treated with the probiotic showed a significant reduction in the left atrial diameter, uric acid, CRP, and creatinine levels. An important find of this study was that the treatment was safe and well tolerated, without reports of side effects or adverse events [84].

## 6. Conclusions

Throughout this review, we have presented evidence in the literature indicating that a habitual consumption of probiotics, which restore the balance of the intestinal microbiota, could present cardiovascular benefits based, at least in part, on its ability to reduce oxidative stress. Although many points remain to be clarified and many of the published results are contradictory, it is evident that consumption of probiotics constitutes a promising complement to more conventional cardiovascular therapies, as well as to nonpharmacological measures that are commonly used to counteract the onset and progression of CVD. Further studies are needed to clarify the interaction between the gut microbiota and the neuroimmune system, as well as the endocrine system, to create nutrigenetic profiles that may aid in achieving individual homeostasis. It will also be necessary to improve knowledge concerning the different bacterial strains present in probiotics and how they should be consumed to take full advantage of their potential beneficial effects for each specific situation. Finally, studies of the great variety of enzymes, peptides, and biochemical pathways generated by the intestinal microbiota, which differ from the resources of the host, could constitute an innovative strategy for the design of new drugs for the treatment of CVD.

## Conflicts of Interest

The authors declare that there is no conflict of interests regarding the publication of this paper.

## Authors' Contributions

ECV drafted Section 1, constructed Figures 1–5, and revised the final version. TMCP drafted Sections 3 and 4. VAP drafted Section 4. MPB drafted Section 5. MCT drafted Sections 1, 2, 3, and 6 and revised the final version.

## Acknowledgments

The authors gratefully acknowledge the Espirito Santo Research Foundation (FAPES) and the National Council for Research and Development (CNPq) for the financial support to our research project (Grant CNPq/FAPES No. 24/2018; Termo Outorga 569/2018) and CNPq Grant (Bolsa Produtividade 2015-2019).

## References

- [1] J.-C. Lagier, M. Million, P. Hugon, F. Armougom, and D. Raoult, "Human gut microbiota: repertoire and variations," *Frontiers in Cellular and Infection Microbiology*, vol. 2, p. 136, 2012.
- [2] M. Rescigno, M. Urbano, B. Valzasina et al., "Dendritic cells express tight junction proteins and penetrate gut epithelial monolayers to sample bacteria," *Nature Immunology*, vol. 2, no. 4, pp. 361–367, 2001.
- [3] J. M. Wells, R. J. Brummer, M. Derrien et al., "Homeostasis of the gut barrier and potential biomarkers," *American Journal of Physiology. Gastrointestinal and Liver Physiology*, vol. 312, no. 3, pp. G171–G193, 2017.
- [4] E. C. Martens, M. Neumann, and M. S. Desai, "Interactions of commensal and pathogenic microorganisms with the intestinal mucosal barrier," *Nature Reviews Microbiology*, vol. 16, no. 8, pp. 457–470, 2018.

- [5] F. S. Pimenta, M. Luaces-Regueira, A. M. Ton et al., "Mechanisms of action of kefir in chronic cardiovascular and metabolic diseases," *Cellular Physiology and Biochemistry: International Journal of Experimental Cellular Physiology, Biochemistry, and Pharmacology*, vol. 48, no. 5, pp. 1901–1914, 2018.
- [6] J. Caballero-Villarraso, A. Galvan, B. M. Escribano, and I. Tunez, "Interrelationships among gut microbiota and host: paradigms, role in neurodegenerative diseases and future prospects," *CNS & Neurological Disorders - Drug Targets*, vol. 16, no. 8, pp. 945–964, 2018.
- [7] S. Prakash, L. Rodes, M. Coussa-Charley, and C. Tomaro-Duchesneau, "Gut microbiota: next frontier in understanding human health and development of biotherapeutics," *Biologics: Targets & Therapy*, vol. 5, pp. 71–86, 2011.
- [8] M. Bellavia, G. Tomasello, M. Romeo et al., "Gut microbiota imbalance and chaperoning system malfunction are central to ulcerative colitis pathogenesis and can be counteracted with specifically designed probiotics: a working hypothesis," *Medical Microbiology and Immunology*, vol. 202, no. 6, pp. 393–406, 2013.
- [9] A. Agus, J. Denizot, J. Thévenot et al., "Western diet induces a shift in microbiota composition enhancing susceptibility to adherent-invasive *E. coli* infection and intestinal inflammation," *Scientific Reports*, vol. 6, no. 1, p. 19032, 2016.
- [10] A. Clark and N. Mach, "The crosstalk between the gut microbiota and mitochondria during exercise," *Frontiers in Physiology*, vol. 8, p. 319, 2017.
- [11] Y. Kang and Y. Cai, "Gut microbiota and hypertension: from pathogenesis to new therapeutic strategies," *Clinics and Research in Hepatology and Gastroenterology*, vol. 42, no. 2, pp. 110–117, 2018.
- [12] M. Jin, Z. Qian, J. Yin, W. Xu, and X. Zhou, "The role of intestinal microbiota in cardiovascular disease," *Journal of Cellular and Molecular Medicine*, vol. 23, no. 4, pp. 2343–2350, 2019.
- [13] T. Wilkins and J. Sequoia, "Probiotics for gastrointestinal conditions: a summary of the evidence," *American Family Physician*, vol. 96, no. 3, pp. 170–178, 2017.
- [14] C. Hill, F. Guarner, G. Reid et al., "Expert consensus document. The International Scientific Association for Probiotics and Prebiotics consensus statement on the scope and appropriate use of the term probiotic," *Nature Reviews Gastroenterology & Hepatology*, vol. 11, no. 8, pp. 506–514, 2014.
- [15] M. Santos and A. M. Shah, "Alterations in cardiac structure and function in hypertension," *Current Hypertension Reports*, vol. 16, no. 5, p. 428, 2014.
- [16] B. I. Freedman and A. H. Cohen, "Hypertension-attributed nephropathy: what's in a name?," *Nature Reviews Nephrology*, vol. 12, no. 1, pp. 27–36, 2016.
- [17] T. C. Turin, T. Okamura, A. R. Afzal et al., "Hypertension and lifetime risk of stroke," *Journal of Hypertension*, vol. 34, no. 1, pp. 116–122, 2016.
- [18] M. H. Forouzanfar, P. Liu, G. A. Roth et al., "Global burden of hypertension and systolic blood pressure of at least 110 to 115 mm Hg, 1990–2015," *JAMA*, vol. 317, no. 2, pp. 165–182, 2017.
- [19] M. Singh, A. K. Singh, P. Pandey, S. Chandra, K. A. Singh, and I. S. Gambhir, "Molecular genetics of essential hypertension," *Clinical and Experimental Hypertension*, vol. 38, no. 3, pp. 268–277, 2016.
- [20] S. F. Rimoldi, U. Scherrer, and F. H. Messerli, "Secondary arterial hypertension: when, who, and how to screen?," *European Heart Journal*, vol. 35, no. 19, pp. 1245–1254, 2014.
- [21] P. A. James, et al. S. Oparil, B. L. Carter et al., "2014 evidence-based guideline for the management of high blood pressure in adults: report from the panel members appointed to the Eighth Joint National Committee (JNC 8)," *JAMA*, vol. 311, no. 5, pp. 507–520, 2014.
- [22] J. Rysz, B. Franczyk, M. Banach, and A. Gluba-Brzozka, "Hypertension - current natural strategies to lower blood pressure," *Current Pharmaceutical Design*, vol. 23, no. 17, pp. 2453–2461, 2017.
- [23] B. P. Ganesh, J. W. Nelson, J. R. Eskew et al., "Prebiotics, probiotics, and acetate supplementation prevent hypertension in a model of obstructive sleep apnea," *Hypertension*, vol. 72, no. 5, pp. 1141–1150, 2018.
- [24] M. K. Raizada, B. Joe, N. S. Bryan et al., "Report of the National Heart, Lung, and Blood Institute Working Group on the role of microbiota in blood pressure regulation: current status and future directions," *Hypertension*, vol. 70, no. 3, pp. 479–485, 2017.
- [25] S. K. Yeo, L. G. Ooi, T. J. Lim, and M. T. Liong, "Antihypertensive properties of plant-based prebiotics," *International Journal of Molecular Sciences*, vol. 10, no. 8, pp. 3517–3530, 2009.
- [26] E. B.-M. Daliri, B. H. Lee, and D. H. Oh, "Current perspectives on antihypertensive probiotics," *Probiotics and Antimicrobial Proteins*, vol. 9, no. 2, pp. 91–101, 2017.
- [27] I. Robles-Vera, M. Toral, M. Romero et al., "Antihypertensive effects of probiotics," *Current Hypertension Reports*, vol. 19, no. 4, p. 26, 2017.
- [28] E. C. Vasquez, S. S. Meyrelles, A. L. Gava et al., "Beneficial effects of the synbiotic kefir on the neural control of cardiovascular function," *Journal of Food Microbiology*, vol. 2, Supplement 1, pp. 25–33, 2018.
- [29] A. G. F. Friques, C. M. Arpini, I. C. Kalil et al., "Chronic administration of the probiotic kefir improves the endothelial function in spontaneously hypertensive rats," *Journal of Translational Medicine*, vol. 13, no. 1, p. 390, 2015.
- [30] B. F. Klippel, L. B. Duemke, M. A. Leal et al., "Effects of kefir on the cardiac autonomic tones and baroreflex sensitivity in spontaneously hypertensive rats," *Frontiers in Physiology*, vol. 7, p. 211, 2016.
- [31] M. A. Silva-Cutini, S. A. Almeida, A. M. Nascimento et al., "Long-term treatment with kefir probiotics ameliorates cardiac function in spontaneously hypertensive rats," *The Journal of Nutritional Biochemistry*, vol. 66, pp. 79–85, 2019.
- [32] G. A. Brasil, M. d. A. Silva-Cutini, F. d. S. A. Moraes et al., "The benefits of soluble non-bacterial fraction of kefir on blood pressure and cardiac hypertrophy in hypertensive rats are mediated by an increase in baroreflex sensitivity and decrease in angiotensin-converting enzyme activity," *Nutrition*, vol. 51–52, pp. 66–72, 2018.
- [33] P. C. B. Lollo, P. N. Morato, C. S. Moura et al., "Hypertension parameters are attenuated by the continuous consumption of probiotic Minas cheese," *Food Research International*, vol. 76, no. 3, pp. 611–617, 2015.
- [34] M. Furushiro et al., "Blood pressure-lowering effect of extract from *Lactobacillus casei* in spontaneously hypertensive rats (SHR)," *Agricultural and Biological Chemistry*, vol. 54, no. 9, pp. 2193–2198, 1990.

- [35] K. Nakajima et al., "Antihypertensive effect of extracts of *Lactobacillus casei* in patients with hypertension," *Journal of Clinical Biochemistry and Nutrition*, vol. 18, no. 3, pp. 181–187, 1995.
- [36] M. Naruszewicz, M. L. Johansson, D. Zapolska-Downar, and H. Bukowska, "Effect of *Lactobacillus plantarum* 299v on cardiovascular disease risk factors in smokers," *The American Journal of Clinical Nutrition*, vol. 76, no. 6, pp. 1249–1255, 2002.
- [37] A. L. Brantsaeter, R. Myhre, M. Haugen et al., "Intake of probiotic food and risk of preeclampsia in primiparous women: the Norwegian Mother and Child Cohort Study," *American Journal of Epidemiology*, vol. 174, no. 7, pp. 807–815, 2011.
- [38] M. Hariri, R. Salehi, A. Feizi, M. Mirlohi, S. Kamali, and R. Ghiasvand, "The effect of probiotic soy milk and soy milk on anthropometric measures and blood pressure in patients with type II diabetes mellitus: a randomized double-blind clinical trial," *ARYA Atherosclerosis*, vol. 11, Supplement 1, pp. 74–80, 2015.
- [39] N. Kassaian, A. Aminorroaya, A. Feizi, P. Jafari, and M. Amini, "The effects of probiotic and synbiotic supplementation on metabolic syndrome indices in adults at risk of type 2 diabetes: study protocol for a randomized controlled trial," *Trials*, vol. 18, no. 1, p. 148, 2017.
- [40] S. Khalesi, J. Sun, N. Buys, and R. Jayasinghe, "Effect of probiotics on blood pressure: a systematic review and meta-analysis of randomized, controlled trials," *Hypertension*, vol. 64, no. 4, pp. 897–903, 2014.
- [41] J. Xu, I. L. Ahrén, O. Prykhodko, C. Olsson, S. Ahrné, and G. Molin, "Intake of blueberry fermented by *Lactobacillus plantarum* affects the gut microbiota of L-NAME treated rats," *Evidence-Based Complementary and Alternative Medicine*, vol. 2013, Article ID 809128, 9 pages, 2013.
- [42] K. L. Ivey, et al. J. M. Hodgson, D. A. Kerr, P. L. Thompson, B. Stojceski, and R. L. Prince, "The effect of yoghurt and its probiotics on blood pressure and serum lipid profile; a randomised controlled trial," *Nutrition, Metabolism and Cardiovascular Diseases*, vol. 25, no. 1, pp. 46–51, 2015.
- [43] F. M. Barreto, A. N. Colado Simão, H. K. Morimoto, M. A. Batisti Lozovoy, I. Dichi, and L. Helena da Silva Miglioranza, "Beneficial effects of *Lactobacillus plantarum* on glycemia and homocysteine levels in postmenopausal women with metabolic syndrome," *Nutrition*, vol. 30, no. 7-8, pp. 939–942, 2014.
- [44] T. Jauhiainen, M. Rönnback, H. Vapaatalo et al., "Long-term intervention with *Lactobacillus helveticus* fermented milk reduces augmentation index in hypertensive subjects," *European Journal of Clinical Nutrition*, vol. 64, no. 4, pp. 424–431, 2010.
- [45] M. Malik, T. M. Suboc, S. Tyagi et al., "Lactobacillus plantarum 299v supplementation improves vascular endothelial function and reduces inflammatory biomarkers in men with stable coronary artery disease," *Circulation Research*, vol. 123, no. 9, pp. 1091–1102, 2018.
- [46] D. Mehta, K. Ravindran, and W. M. Kuebler, "Novel regulators of endothelial barrier function," *American Journal of Physiology-Lung Cellular and Molecular Physiology*, vol. 307, no. 12, pp. L924–L935, 2014.
- [47] P. A. Cahill and E. M. Redmond, "Vascular endothelium - gatekeeper of vessel health," *Atherosclerosis*, vol. 248, pp. 97–109, 2016.
- [48] D. Konukoglu and H. Uzun, "Endothelial dysfunction and hypertension," in *Hypertension: from Basic Research to Clinical Practice*, M. S. Islam, Ed., vol. 956 of *Advances in Experimental Medicine and Biology*, pp. 511–540, Springer, Cham, 2016.
- [49] R. Khaddaj Mallat, C. Mathew John, D. J. Kendrick, and A. P. Braun, "The vascular endothelium: a regulator of arterial tone and interface for the immune system," *Critical Reviews in Clinical Laboratory Sciences*, vol. 54, no. 7-8, pp. 458–470, 2017.
- [50] A. O. Jackson, J. Zhang, Z. Jiang, and K. Yin, "Endothelial-to-mesenchymal transition: a novel therapeutic target for cardiovascular diseases," *Trends in Cardiovascular Medicine*, vol. 27, no. 6, pp. 383–393, 2017.
- [51] H. N. Zhang, Q. Q. Xu, A. Thakur et al., "Endothelial dysfunction in diabetes and hypertension: role of microRNAs and long non-coding RNAs," *Life Sciences*, vol. 213, pp. 258–268, 2018.
- [52] P. Rajendran, T. Rengarajan, J. Thangavel et al., "The vascular endothelium and human diseases," *International Journal of Biological Sciences*, vol. 9, no. 10, pp. 1057–1069, 2013.
- [53] Q. N. Dinh, G. R. Drummond, C. G. Sobey, and S. Chrissobolis, "Roles of inflammation, oxidative stress, and vascular dysfunction in hypertension," *BioMed Research International*, vol. 2014, Article ID 406960, 11 pages, 2014.
- [54] F. He and L. Zuo, "Redox roles of reactive oxygen species in cardiovascular diseases," *International Journal of Molecular Sciences*, vol. 16, no. 11, pp. 27770–27780, 2015.
- [55] T. Pereira, F. Pimenta, M. Porto et al., "Coadjuvants in the diabetic complications: nutraceuticals and drugs with pleiotropic effects," *International Journal of Molecular Sciences*, vol. 17, no. 8, p. 1273, 2016.
- [56] U. Forstermann, N. Xia, and H. Li, "Roles of vascular oxidative stress and nitric oxide in the pathogenesis of atherosclerosis," *Circulation Research*, vol. 120, no. 4, pp. 713–735, 2017.
- [57] F. Z. Marques, C. R. Mackay, and D. M. Kaye, "Beyond gut feelings: how the gut microbiota regulates blood pressure," *Nature Reviews Cardiology*, vol. 15, no. 1, pp. 20–32, 2017.
- [58] S. K. Rashid, N. I. Khodja, C. Auger et al., "Probiotics (VSL#3) prevent endothelial dysfunction in rats with portal hypertension: role of the angiotensin system," *PLoS One*, vol. 9, no. 5, p. e97458, 2014.
- [59] M. Toral, M. Gómez-Guzmán, R. Jiménez et al., "The probiotic *Lactobacillus coryniformis* CECT5711 reduces the vascular pro-oxidant and pro-inflammatory status in obese mice," *Clinical Science*, vol. 127, no. 1, pp. 33–45, 2014.
- [60] W. B. Yap et al., "Lactobacillus casei strain C1 attenuates vascular changes in spontaneously hypertensive rats," *The Korean Journal of Physiology & Pharmacology*, vol. 20, no. 6, pp. 621–628, 2016.
- [61] M. Gómez-Guzmán, M. Toral, M. Romero et al., "Antihypertensive effects of probiotics *Lactobacillus* strains in spontaneously hypertensive rats," *Molecular Nutrition & Food Research*, vol. 59, no. 11, pp. 2326–2336, 2015.
- [62] C. P. Cheng, S. W. Tsai, C. P. Chiu, T. M. Pan, and T. Y. Tsai, "The effect of probiotic-fermented soy milk on enhancing the NO-mediated vascular relaxation factors," *Journal of the Science of Food and Agriculture*, vol. 93, no. 5, pp. 1219–1225, 2013.
- [63] M. Szulińska, I. Łoniewski, K. Skrypnik et al., "Multispecies probiotic supplementation favorably affects vascular function and reduces arterial stiffness in obese postmenopausal



- women—a 12-week placebo-controlled and randomized clinical study,” *Nutrients*, vol. 10, no. 11, p. 1672, 2018.
- [64] N. J. Tripolt, et al. B. Leber, D. Blattl et al., “Short communication: Effect of supplementation with *Lactobacillus casei* Shirota on insulin sensitivity,  $\beta$ -cell function, and markers of endothelial function and inflammation in subjects with metabolic syndrome—A pilot study,” *Journal of Dairy Science*, vol. 96, no. 1, pp. 89–95, 2013.
- [65] N. Powell, M. M. Walker, and N. J. Talley, “The mucosal immune system: master regulator of bidirectional gut-brain communications,” *Nature Reviews Gastroenterology & Hepatology*, vol. 14, no. 3, pp. 143–159, 2017.
- [66] E. E. Noble, T. M. Hsu, and S. E. Kanoski, “Gut to brain dysbiosis: mechanisms linking Western diet consumption, the microbiome, and cognitive impairment,” *Frontiers in Behavioral Neuroscience*, vol. 11, p. 9, 2017.
- [67] B. Bonaz, T. Bazin, and S. Pellissier, “The vagus nerve at the interface of the microbiota-gut-brain axis,” *Frontiers in Neuroscience*, vol. 12, p. 49, 2018.
- [68] O. B. Neto et al., “Exercise training improves cardiovascular autonomic activity and attenuates renal damage in spontaneously hypertensive rats,” *Journal of Sports Science & Medicine*, vol. 12, no. 1, pp. 52–59, 2013.
- [69] M. Monteiro, M. França-Silva, N. Alves, S. Porpino, and V. Braga, “Quercetin improves baroreflex sensitivity in spontaneously hypertensive rats,” *Molecules*, vol. 17, no. 11, pp. 12997–13008, 2012.
- [70] W. H. W. Tang, D. Y. Li, and S. L. Hazen, “Dietary metabolism, the gut microbiome, and heart failure,” *Nature Reviews Cardiology*, vol. 16, no. 3, pp. 137–154, 2019.
- [71] Y. Nagatomo and W. H. W. Tang, “Intersections between microbiome and heart failure: revisiting the gut hypothesis,” *Journal of Cardiac Failure*, vol. 21, no. 12, pp. 973–980, 2015.
- [72] T. Kitai, J. Kirsop, and W. H. W. Tang, “Exploring the microbiome in heart failure,” *Current Heart Failure Reports*, vol. 13, no. 2, pp. 103–109, 2016.
- [73] A. Sandek, A. Swidsinski, W. Schroedl et al., “Intestinal blood flow in patients with chronic heart failure: a link with bacterial growth, gastrointestinal symptoms, and cachexia,” *Journal of the American College of Cardiology*, vol. 64, no. 11, pp. 1092–1102, 2014.
- [74] M. Kummen, C. C. K. Mayerhofer, B. Vestad et al., “Gut microbiota signature in heart failure defined from profiling of 2 independent cohorts,” *Journal of the American College of Cardiology*, vol. 71, no. 10, pp. 1184–1186, 2018.
- [75] V. M. Conraads, P. G. Jorens, L. S. de Clerck et al., “Selective intestinal decontamination in advanced chronic heart failure: a pilot trial,” *European Journal of Heart Failure*, vol. 6, no. 4, pp. 483–491, 2004.
- [76] E. Pasini, R. Aquilani, C. Testa et al., “Pathogenic gut flora in patients with chronic heart failure,” *JACC Heart Failure*, vol. 4, no. 3, pp. 220–227, 2016.
- [77] M. Al-Obaide, R. Singh, P. Datta et al., “Gut microbiota-dependent trimethylamine-N-oxide and serum biomarkers in patients with T2DM and advanced CKD,” *Journal of Clinical Medicine*, vol. 6, no. 9, p. 86, 2017.
- [78] J. R. Baker and S. Chaykin, “The biosynthesis of trimethylamine-N-oxide,” *The Journal of Biological Chemistry*, vol. 237, no. 4, pp. 1309–1313, 1962.
- [79] E. P. Rhee, C. B. Clish, A. Ghorbani et al., “A combined epidemiologic and metabolomic approach improves CKD prediction,” *Journal of the American Society of Nephrology : JASN*, vol. 24, no. 8, pp. 1330–1338, 2013.
- [80] T. Suzuki, et al. L. M. Heaney, S. S. Bhandari, D. J. L. Jones, and L. L. Ng, “Trimethylamine-N-oxide and prognosis in acute heart failure,” *Heart*, vol. 102, no. 11, pp. 841–848, 2016.
- [81] X. T. Gan, G. Ettinger, C. X. Huang et al., “Probiotic administration attenuates myocardial hypertrophy and heart failure after myocardial infarction in the rat,” *Circulation Heart Failure*, vol. 7, no. 3, pp. 491–499, 2014.
- [82] V. Lam, J. Su, S. Kopyrowski et al., “Intestinal microbiota determine severity of myocardial infarction in rats,” *The FASEB Journal*, vol. 26, no. 4, pp. 1727–1735, 2012.
- [83] P. P. Lin, Y. M. Hsieh, W. W. Kuo et al., “Probiotic-fermented purple sweet potato yogurt activates compensatory IGF-IR/PI3K/Akt survival pathways and attenuates cardiac apoptosis in the hearts of spontaneously hypertensive rats,” *International Journal of Molecular Medicine*, vol. 32, no. 6, pp. 1319–1328, 2013.
- [84] A. C. Costanza, S. D. Moscovitch, H. C. Faria Neto, and E. T. Mesquita, “Probiotic therapy with *Saccharomyces boulardii* for heart failure patients: a randomized, double-blind, placebo-controlled pilot trial,” *International Journal of Cardiology*, vol. 179, pp. 348–350, 2015.

## Research Article

# Protective Effect of Methane-Rich Saline on Acetic Acid-Induced Ulcerative Colitis via Blocking the TLR4/NF- $\kappa$ B/MAPK Pathway and Promoting IL-10/JAK1/STAT3-Mediated Anti-inflammatory Response

Guanghai Wang,<sup>1</sup> Bing Xu,<sup>2</sup> Feiyu Shi,<sup>1</sup> Mengfan Du,<sup>2</sup> Yaguang Li,<sup>1</sup> Tianyu Yu,<sup>1</sup> and Lihong Chen <sup>3</sup>

<sup>1</sup>Department of General Surgery, The First Affiliated Hospital of Xi'an Jiaotong University, Xi'an, 710061 Shaanxi Province, China

<sup>2</sup>Department of Immunology and Laboratory, Shaanxi University of Chinese Medicine, Xianyang, 712046 Shaanxi Province, China

<sup>3</sup>International Medical Center, The First Affiliated Hospital of Xi'an Jiaotong University, Xi'an, 710061 Shaanxi Province, China

Correspondence should be addressed to Lihong Chen; [clh1225@163.com](mailto:clh1225@163.com)

Received 2 February 2019; Revised 22 March 2019; Accepted 28 March 2019; Published 28 April 2019

Guest Editor: Marcelo P. Baldo

Copyright © 2019 Guanghai Wang et al. This is an open access article distributed under the Creative Commons Attribution License, which permits unrestricted use, distribution, and reproduction in any medium, provided the original work is properly cited.

Ulcerative colitis (UC) is an inflammation-related disease involved in uncontrolled inflammation and oxidative stress and is characterized by high recurrence and relapse risk. As a rising star in gas medicine, methane owns the properties of anti-inflammation, antioxidation, and antiapoptosis. Based on the possible mechanism, we aimed to investigate the effect of methane on UC. Methane-rich saline (MRS) was introduced here, and UC was induced by acetic acid. All the C57BL/6 mice were allocated into groups as follows: control group, colitis model group, colitis treated with salazosulfapyridine (SASP) group, and colitis treated with MRS (1 or 10 ml/kg) groups. Tissue damage, the degree of inflammation, oxidative stress, and apoptosis were evaluated in the study, as well as the TLR4/NF- $\kappa$ B/MAPK and IL-10/JAK1/STAT3 signaling pathways for further exploration of the potential mechanism. The results showed that MRS (1) alleviated tissue damage caused by acetic acid, (2) controlled acetic acid-induced inflammation, (3) inhibited acetic acid-caused oxidative stress, (4) reduced colonic cell apoptosis due to acetic acid, (5) suppressed the TLR-4/NF- $\kappa$ B/MAPK signaling pathway, and (6) activated IL-10/JAK1/STAT3 anti-inflammatory response to improve the injury induced by acetic acid. We conclude that MRS has a protective effect on acetic acid-induced ulcerative colitis in mice via blocking the TLR4/NF- $\kappa$ B/MAPK signaling pathway and promoting the IL-10/JAK1/STAT3-mediated anti-inflammatory response.

## 1. Introduction

Ulcerative colitis (UC), which belongs to the chronic nonspecific inflammatory bowel disease (IBD) family related to immunization, is inflammation in the mucosa and subserosa of the colon and rectum. The main manifestations of UC are diarrhea, mucopurulent bloody stools, abdominal pain, recurrence, and relapse. Additionally, severe UC will result in complications such as a toxic megacolon and an increased risk of colorectal cancer. It was indicated that the prevalence and incidence of UC have been increasing gradually in recent years [1, 2]. UC has been calling for increasing

concern because of its damage to individual lives and work capacity. However, the etiology of UC remains unclear, and multiple factors are considered, among which environmental factor, genetic factor, and microbial factor have gained wide acknowledgment.

Inflammation and oxidative stress are thought to play key roles in the pathophysiological process of UC. Stimulation from the outside or inside induced the activation of inflammation, leading to the oxidative stress and aggravation of inflammatory cells [3]. With proinflammatory peculiarity, the products of oxidative stress contribute to destroying cell structure by lipid peroxidation, eventually causing

cellapoptosis and necrosis [4]. Dead cells become new stimulation, and a vicious circle is started. Pivotal proinflammatory cytokines such as tumor necrosis factor- $\alpha$  (TNF- $\alpha$ ) and interleukin-6 (IL-6) have been applied to target UC [5]. However, an increased risk of infection and malignancies caused by immune suppression cannot be overlooked. Furthermore, it has been well demonstrated that nuclear factor  $\kappa$ B (NF- $\kappa$ B) and mitogen-activated protein kinase (MAPK) pathways are active in the inflammatory response by assisting the function of inflammatory cytokines. Targeting the TLR4/NF- $\kappa$ B/MAPK signaling pathway might be an alternative method to treat inflammatory diseases [6]. Meanwhile, IL-10, one of the best-studied anti-inflammatory cytokines, also contributed to the progress of colitis. The IL-10/JAK1/STAT3-mediated anti-inflammatory response is an essential negative regulator that controls the degree and duration of inflammation [7]. Efforts have been made to explore potential therapy for UC patients, and, herein, we would like to focus on a novel method, methane medicine.

As the simplest alkane, methane (CH<sub>4</sub>) has been thought to be useless to humans for decades until researchers have recently revealed its physiological actions. Previous reports have offered evidence of methane to improve ischemia reperfusion injury, sepsis, acute lung injury, and autoimmune hepatitis, and a positive outcome was even obtained in diabetic retinopathy [8–13]. Researchers found that the anti-inflammation, antiapoptosis, and antioxidation properties of methane make it a protector in those diseases [14]. Generally, methane is used by inhalation or injection of methane-rich saline (MRS). Considering the risk of methane gas explosion, some researchers prefer the latter route. Nevertheless, little attention has been paid to the biological function of methane in UC. Thus, we aimed to explore the curative effect of MRS on UC in this study.

## 2. Materials and Methods

**2.1. Animals and MRS Preparation.** Four- to five-week-old wild-type male C57BL/6 mice (21–25 g) were purchased from the Animal Feeding Center of Xi'an Jiaotong University Health Science Center. Right before the experiment, all the animals were kept in controlled circumstances where five mice shared a room at most with a 12 h light/dark cycle, stationary temperature of  $21 \pm 2^\circ\text{C}$ , and 50% humidity. Providing with standard food and tap water, the animal care principle was to minimize the discomfort to mice. All animal experiments obeyed the guidelines of the China Council on Animal Care and Use. All the procedures of animal feeding and handling in the study were reviewed, approved, and supervised by the Institutional Animal Care and Use Committee of the Ethics Committee of Xi'an Jiaotong University Health Science Center, China.

Methane was dissolved in sealed normal saline and underwent high pressure (0.4 MPa) for 8 hours to produce MRS. Prepared MRS was reserved using an aluminum bag at  $4^\circ\text{C}$  and sterilized by  $\gamma$ -radiation one day before utilization. The concentration of MRS was detected using gas chromatography, and the concentration of methane in the MRS was 1.2–1.5 mmol/l.

**2.2. Experimental Design.** The mice were separated into 5 groups at random with 6 animals in each group. Groups 1 (control group) and 2 (AA group) were pretreated with 0.9% saline at a dose of 50 ml/kg. In group 3 (AA+SASP group), the mice were given SASP at a dose of 500 mg/kg. Groups 4 (AA+MRS 1 group) and 5 (AA+MRS 10) received pretreatment with MRS at 1 or 10 ml/kg, respectively. All the drugs were administered by gastric gavage once a day. On the eighth day, the mice from groups 2 to 5 were subjected to colitis induction, while group 1 received a similar procedure with an equal volume of saline. The animals were sacrificed by isoflurane (5%) inhalation 24 h later. Subsequently, blood and tissue samples were collected.

**2.3. Colitis Induction.** The classical method was used here to induce colitis [15]. Mice were anesthetized by ether after fasting for 24 h. Next, a flexible catheter (3.5 F) was inserted into the colon with a depth of approximately 3 cm away from the anus. Acetic acid solution was responsible for inducing UC by being injected into the lumen of the colon intrarectally with a volume of 1 ml and dose of 5%. Next, the mice were kept in a supine Trendelenburg position for 30 s to prevent the leakage of the instilled solution. Mice from group 1 obtained the same treatment using 0.9% saline.

**2.4. Assessment of Tissue Damage Macroscopically.** The disease activity index (DAI) was calculated and consisted of three parameters, namely, weight loss, consistency of stool, and gross rectal bleeding. The assessment criteria were [16] weight loss (0, none; 1, reduced 1–5%; 2, reduced 5–10%; 3, reduced 11–15%; and 4, reduced over 15%), stool consistency (0, normal; 2, loose stool; and 4, watery diarrhea), and rectal bleeding (0, normal; 2, mild bleeding; and 4, severe bleeding). Herein, body weight on the particular day was compared with that on the initial day. The sum of all the grades was evaluated for each animal daily. Additionally, the ulcer area was recorded, and the ulcer index (UI) for each colon sample was calculated as follows:  $\text{UI} = [\text{ulcerated area}/\text{total colon area}] \times 100$  [17]. The length and weight of the colon between the ileocecal junction and rectum were measured, and the length/weight ratio was evaluated, as well as the spleen weight.

**2.5. Assessment of Microscopic Damage.** To evaluate the histological change, colon tissue was collected and fixed in 10% formalin solution. Next, the samples were embedded in paraffin, and consecutive 5  $\mu\text{m}$  thick sections were then stained with hematoxylin and eosin. The assessment of microscopic damage referred to the grading system as described previously [18]: (1) loss of mucosal structure (0–3), (2) infiltration of leukocyte (0–3), (3) muscle incrustation (0–3), (4) formation of crypt abscess (0–3), and (5) loss of goblet cells (0–3). The maximum score was 15. Each slide was examined under a microscope by investigators who were blind to the treatment.

### 2.6. Biochemical Assay

**2.6.1. Inflammation Parameter.** Blood samples were collected to measure the levels of TNF- $\alpha$  and IL-6 using enzyme-linked immunosorbent assay (ELISA) kits (Lianke, Hangzhou, China) according to the manufacturer's instructions.

Total RNA was isolated from colon specimens using the RNAfast200 kit (Fastagen Biotech, Shanghai, China). Reverse transcription was performed using the PrimeScript RT reagent kit (TaKaRa Biotechnology, Dalian, China). mRNA expression was assayed in triplicate and normalized to 18S mRNA expression. The relative levels were calculated using the comparative Ct method ( $\Delta\Delta\text{Ct}$  method). The primers used in the study were TNF- $\alpha$  (forward 5'-AAG CCT GTA GCC CAC GTC GTA-3' and reverse 5'-AGG TAC AAC CCA TCG GCT GG-3'), IL-6 (forward 5'-TCC ATC CAG TTG CCT TCT TG-3' and reverse 5'-TTC CAC GAT TTC CCA GAG AAC-3'), IL-1 $\beta$  (forward 5'-GGA GAC TTC ACA GAG GAT AC-3' and reverse 5'-CCA GTT TGG TAG CAT CCA TC-3'), IL-10 (forward 5'-GCT CTT ACT GAC TGG CAT GAG-3' and reverse 5'-CGC AGC TCT AGG AGC ATG TG-3'), and 18S (forward 5'-AAA CGG CTA CCA CAT CCA AG-3' and reverse 5'-CCT CCA ATG GAT CCT CGT TA-3').

**2.6.2. Oxidative Stress Parameter.** The colon sections were collected and homogenized. After centrifugation at 5,000 rpm at  $-4^{\circ}\text{C}$  for 30 min, the supernatant was separated to investigate common oxidative stress markers in it including malondialdehyde (MDA), myeloperoxidase (MPO), superoxide dismutase (SOD), and glutathione transferase (GSH) via activity assay kits (Nanjing Jiancheng Bioengineering Institute, Nanjing, China) following the manufacturer's protocols.

**2.7. Evaluation of Apoptosis.** The terminal deoxynucleotidyl transferase-mediated nick end labeling (TUNEL) apoptosis assay was performed on colon slides ( $4\ \mu\text{m}$  thickness) that were embedded by paraffin. Blue appeared when 4',6-diamidino-2-phenylindole (DAPI) marked the nucleus, and green stood for apoptotic cells. The results were observed by a fluorescence microscope with an emission wavelength of 530 nm and an excitation wavelength of 480 nm, after which ImageJ2x software was used to determine the fluorescence intensity.

**2.8. Western Blot Analysis.** Colon samples were harvested and homogenized in radioimmunoprecipitation assay (RIPA) lysis buffer. The BCA Protein Assay was performed to detect the protein content. Protein samples were separated by 10% sodium dodecyl sulfate polyacrylamide gel electrophoresis (SDS-PAGE) and were transferred onto polyvinylidene fluoride (PVDF) membranes, where they were blocked with 10% skim milk for 1 h and subsequently stained with specific primary antibodies of toll-like receptor 4 (TLR4), myeloid differentiation primary response protein 88 (MyD88), p38 and phosphorylated p38 (p-p38), extracellular signal-regulated kinase (ERK) and phosphorylated ERK (p-ERK), c-Jun N-terminal kinase (JNK) and phosphorylated JNK (p-JNK), nuclear factor  $\kappa\text{B}$  p65 subunit (NF- $\kappa\text{B}$  p65) and phosphorylated NF- $\kappa\text{B}$  p65 (p-NF- $\kappa\text{B}$  p65), IL-10, Janus kinase 1 (JAK1) and phosphorylated JAK1, and signal transduction and transcription activator 3 and phosphorylated STAT3 (Proteintech Group Inc., China; Beijing Biosynthesis Biotechnology Co. Ltd., China) overnight at  $4^{\circ}\text{C}$ . Next, the

membranes were washed three times with PBS. After staining with horseradish peroxidase- (HRP-) conjugated secondary antibodies, the blots were washed again and visualized by chemiluminescence (ECL). The statistical data of the protein levels were generated using ImageJ software with normalization to the level of the  $\beta$ -actin control.

**2.9. Statistical Analysis.** All data were recorded as mean  $\pm$  standard deviation. Statistical analysis was executed by SPSS 18.0 statistical software. Significant differences among groups were confirmed with one-way ANOVA, followed by Fisher's LSD test.  $P < 0.05$  was considered statistically significant.

### 3. Results

#### 3.1. Effect of MRS on Tissue Damage of Acetic Acid-Induced UC

**3.1.1. Spleen Weight.** As one of the common manifestations of acetic acid-induced UC, enlargement of the spleen was evaluated by the weight. We found that the spleen weight of mice with colitis showed an increase compared with that of the control group, while SASP and MRS significantly reduced the spleen weight of mice (Figure 1(a)).

**3.1.2. Disease Activity Index (DAI).** After the assessment of weight loss, consistency of stool, and gross rectal bleeding in each animal, we obtained a DAI score to judge the symptom severity of UC (Figure 1(b)). We found that the DAI score of group AA was significantly higher than that of any other group, showing that SASP or MRS treatment could relieve the symptoms of UC. Significant difference was shown between the variant dosages of MRS, and mice showed a better DAI score under MRS treatment at 10 ml/kg.

**3.1.3. Colon Weight/Length Ratio.** The colon weight/length ratio was calculated to assess the condition of colonic mucosal injury. The increased weight/length ratio appeared with a significant difference in animals from group AA compared with those from the naive group. Treatment with SASP and MRS-1 or MRS-10 showed a notable decrease in the colon weight/length ratio as shown in Figure 1(c). However, MRS at a dose of 10 ml/kg showed a significantly lower weight/length ratio than that of 1 ml/kg.

**3.1.4. Ulcer Area and Ulcer Index.** The ulcer area and ulcer index were calculated to evaluate the severity of ulceration in animals (Figures 1(d) and 1(e)). Mice treated with SASP showed smaller ulcer sites than did untreated colitis mice, as well as smaller ulcer indexes. Although a significant decrease in the ulcer area was shown with either 1 or 10 ml/kg of MRS, only the latter dose reduced the ulcer index with significant difference.

**3.1.5. Effect of MRS on Histology Damage of Acetic Acid-Induced UC.** H&E staining was utilized here to assess histology changes in animals. We observed colitis under the microscope with cellular infiltration, epithelium destruction, hyperemia, and necrosis compared with normal mice as shown in Figure 1(g). Treatment with SASP and MRS at 1 or 10 ml/kg alleviated the inflammatory microscopic

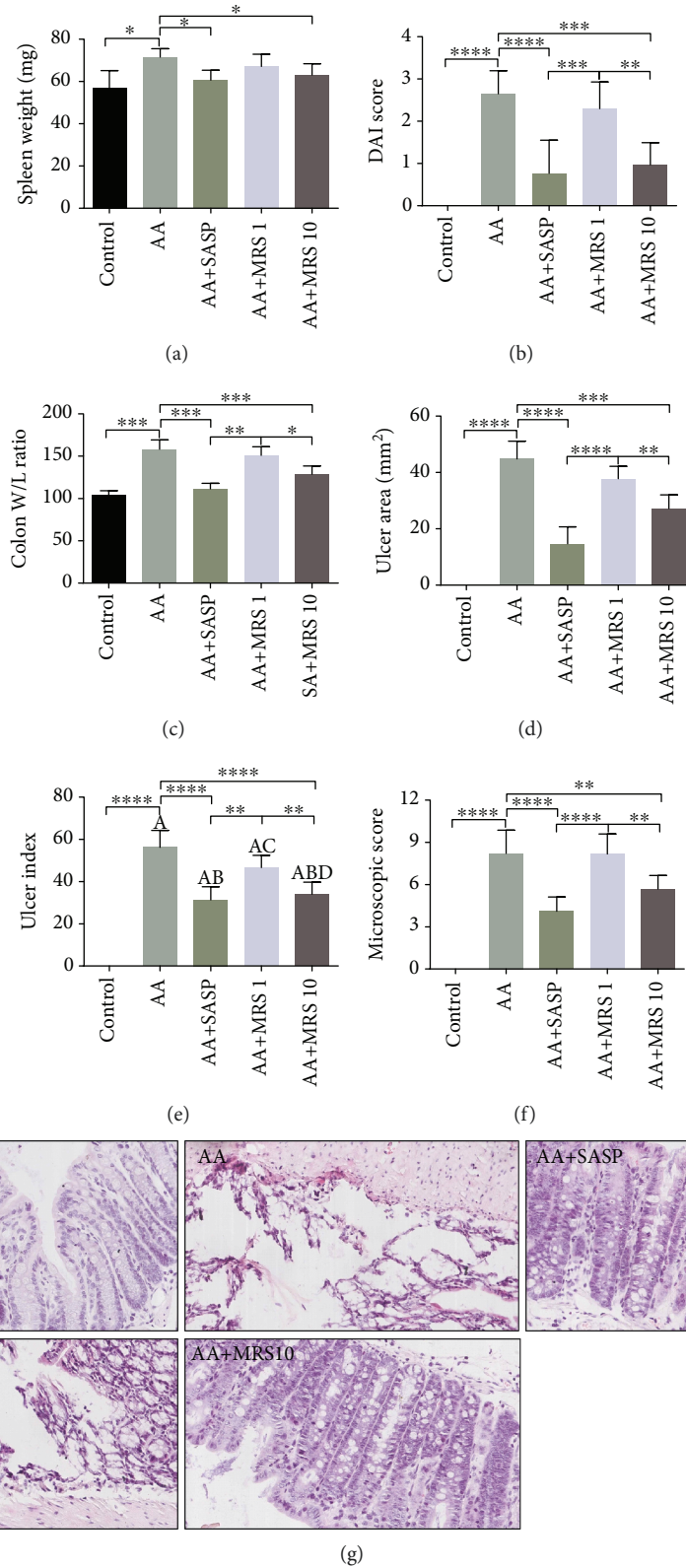


FIGURE 1: Treatment with MRS mitigated acetic acid-induced tissue damage. Mice were administered with MRS at a dose of 1 or 10 ml/kg by gastric gavage for a week before colitis establishment. SASP was used as a positive control at a dose of 500 mg/kg. Colitis was induced by acetic acid solution (*v/v*) injection into the lumen of the colon intrarectally with a volume of 1 ml and dose of 5% except for the sham group. The (a) spleen weight, (b) disease activity index (DAI), (c) colon weight/length ratio, (d) ulcer area, and (e) ulcer index were measured. Additionally, colon tissues were collected to evaluate the damage microscopically by (g) H&E staining (200x) and (f) microscopic scores were calculated. Data were expressed as means  $\pm$  SD. \* $P < 0.05$ , \*\* $P < 0.01$ , \*\*\* $P < 0.001$ , and \*\*\*\* $P < 0.0001$ .

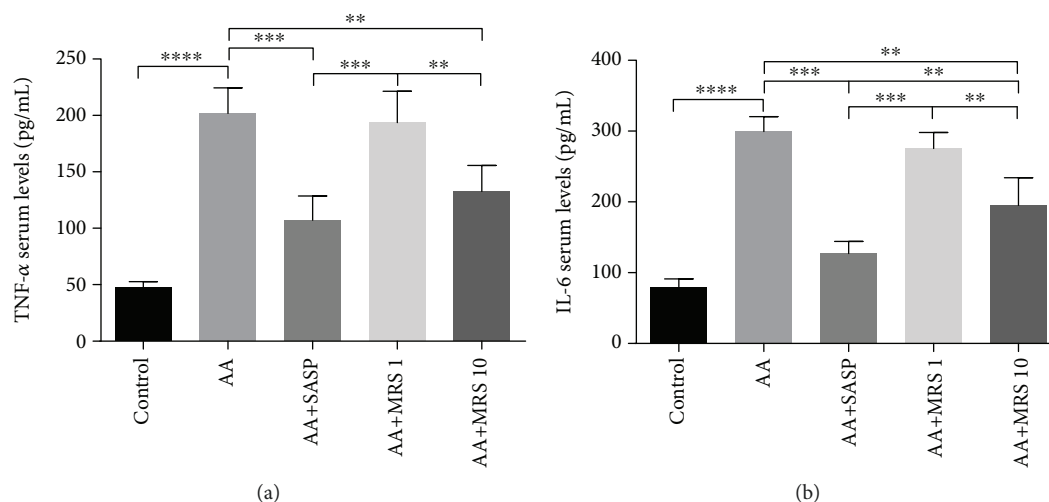


FIGURE 2: Treatment with MRS reduced the serum levels of inflammatory cytokines in acetic acid-induced UC. Mice were administered with MRS at a dose of 1 or 10 ml/kg by gastric gavage for a week before colitis establishment. SASP was used as a positive control at a dose of 500 mg/kg. Colitis was induced by acetic acid solution ( $v/v$ ) injection into the lumen of the colon intrarectally with a volume of 1 ml and dose of 5% except for the sham group. Blood samples were collected to determine the levels of (a) TNF- $\alpha$  and (b) IL-6 in the serum. Data were expressed as means  $\pm$  SD. \*\* $P < 0.01$ , \*\*\* $P < 0.001$ , and \*\*\*\* $P < 0.0001$ .

characteristics described above. Similarly, after assessing the microscopic score (Figure 1(f)), we found that the higher scores, which were shown in the AA group compared with those in the control group, were reduced markedly when colitis mice were treated with SASP and MRS (10 ml/kg), indicating that 10 ml/kg of MRS was more effective than the lower dose.

### 3.2. Effect of MRS on the Levels of Inflammatory Cytokines.

TNF- $\alpha$  and IL-6 serum levels were elevated significantly due to the stimulation of acetic acid compared with those in the sham group (Figure 2). Treatment with MRS (10 ml/kg), as well as SASP treatment, caused significant decreased levels of such proinflammatory cytokines compared with that in the colitis control group. Further investigation of the cytokine status at the mRNA level produced consistent results that MRS (10 ml/kg) reduced the mRNA level of TNF- $\alpha$  and IL-6 markedly (Figures 3(a) and 3(b)). Furthermore, the IL-1 $\beta$  mRNA fold change was recorded, showing an obvious increase caused by acetic acid as shown in Figure 3(c), while the level decreased with SASP and MRS treatment at 10 ml/kg. Additionally, as an anti-inflammatory cytokine, IL-10 was found to be decreased notably on the mRNA level when acetic acid is induced (Figure 3(d)). When colitis mice were treated with SASP and MRS (10 ml/kg), the anti-inflammation status was improved by increasing the mRNA level of IL-10 compared with that in the AA group.

**3.3. Effect of MRS on the Level of Oxidative Stress.** The MDA content revealed the level of lipid peroxidation caused by acetic acid. An elevated MDA content appeared in the AA group compared with that in the control group, which was reduced notably by treatments with SASP and MRS as shown

in Figure 4(a). MPO activity was also explored to assess the condition of neutrophil infiltration. Figure 4(b) shows that the MPO activity of colitis animals was markedly higher than that of the naïve group. SASP and MRS treatment all affected the inhibition of MPO activity. Additionally, the activities of endogenous antioxidants SOD and GSH were detected and found to be decreased in the AA group compared with those in the control group (Figure 4(c) and 4(d)). Additionally, SASP and MRS (10 ml/kg) improved the inhibition activities of SOD and GSH with a significant difference.

### 3.4. Effect of MRS on Apoptosis of Acetic Acid-Induced UC.

We explored the effect of MRS treatment on colonic cell apoptosis in acetic acid-induced UC through TUNEL staining. The AA group exhibited a stronger positive fluorescence signal than did the naïve group as shown in Figure 5. Additionally, the samples from the groups treated with SASP or MRS showed fewer positively stained cells. Quantitative measurement was taken, and the result revealed that the apoptotic rate in the colon was significantly reduced under treatment with SASP or MRS.

### 3.5. Effect of MRS on the TLR4/NF- $\kappa$ B/MAPK Signaling Pathway.

To elucidate the underlying mechanism of MRS in acetic acid-induced UC, Western blotting was performed to explore the TLR4/NF- $\kappa$ B/MAPKs signaling pathway that was in charge of the inflammatory reaction. As shown in Figure 6, acetic acid increased the expression level of TLR4 and MyD88 in colonic tissues compared with that in the control group, which was markedly reversed by MRS (10 ml/kg). Consistently, we found that the expression levels of p-NF- $\kappa$ B p65, p-JNK, p-ERK, and p-P38 were enhanced with acetic acid but were all significantly suppressed under treatment with MRS (10 ml/kg).

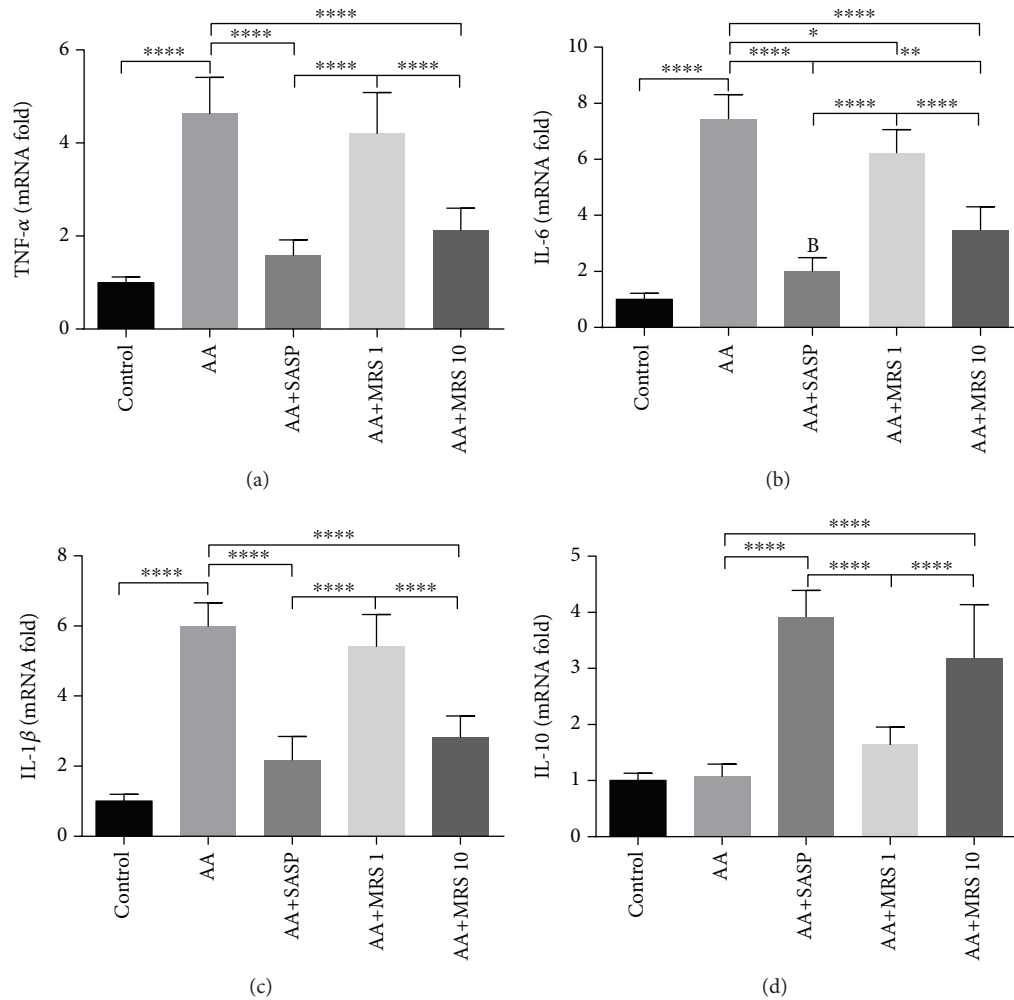


FIGURE 3: Treatment with MRS inhibited the expression of inflammatory cytokines at the mRNA level in acetic acid-induced UC. Mice were administered with MRS at a dose of 1 or 10 ml/kg by gastric gavage for a week before colitis establishment. SASP was used as a positive control at a dose of 500 mg/kg. Colitis was induced by acetic acid solution ( $v/v$ ) injection into the lumen of the colon intrarectally with a volume of 1 ml and dose of 5% except for the sham group. Total RNA was collected from colon specimens, and the expression levels of (a) TNF- $\alpha$ , (b) IL-6, (c) IL-1 $\beta$ , and (d) IL-10 were tested. Data were expressed as means  $\pm$  SD. \* $P$  < 0.05, \*\* $P$  < 0.01, and \*\*\*\* $P$  < 0.0001.

**3.6. Effect of MRS on IL-10/JAK1/STAT3-Mediated Anti-inflammatory Response.** On the basis of the effect of MRS on the transcriptional level of IL-10 which is a vital anti-inflammatory cytokine, we detect the protein expression of IL-10 and its downstream pathway molecules JAK1 and STAT3. The results showed that acetic acid did not significantly affect the expression levels of IL-10 and p-JAK1 but could increase the p-STAT3 expression that might be the initiation of endogenous protection. However, MRS (10 ml/kg) treatment could significantly increase the expression levels of IL-10/p-JAK1/p-STAT3 (Figure 7).

#### 4. Discussion

In our study, we investigated the effect of methane-rich saline (MRS) on colitis caused by acetic acid. The results were as follows: (1) MRS alleviated tissue damage in acetic acid-induced UC, (2) MRS controlled inflammation in acetic acid-induced UC, (3) MRS inhibited oxidative stress in acetic

acid-induced colon, (4) MRS reduced cell apoptosis in acetic acid-induced UC, (5) MRS protected acetic acid-induced colitis through the TLR-4/NF- $\kappa$ B/MAPKs signaling pathway, and (6) MRS improved anti-inflammatory response by promoting the IL-10/JAK1/STAT3 signaling pathway. Thus, for the first time, the prospect of MRS as a therapeutic method for ulcerative colitis is discussed.

Ulcerative colitis was established by acetic acid in the study and is a classical method that is widely used to imitate the pathophysiologic process of UC with high operability. When assessing the effect of MRS on colitis manifestation, we found a decrease in the spleen weight, DAI score, colonic weight/length ratio, ulcer area, and index. Together with positive microscopic results, MRS showed its ability to alleviate the tissue damage caused by acetic acid.

It was proven that colitis is closely related to inflammation [19]. The caspase cascade of inflammation is elicited during colitis and is characterized by the recruitment of inflammatory cells and release of cytokines to fight against

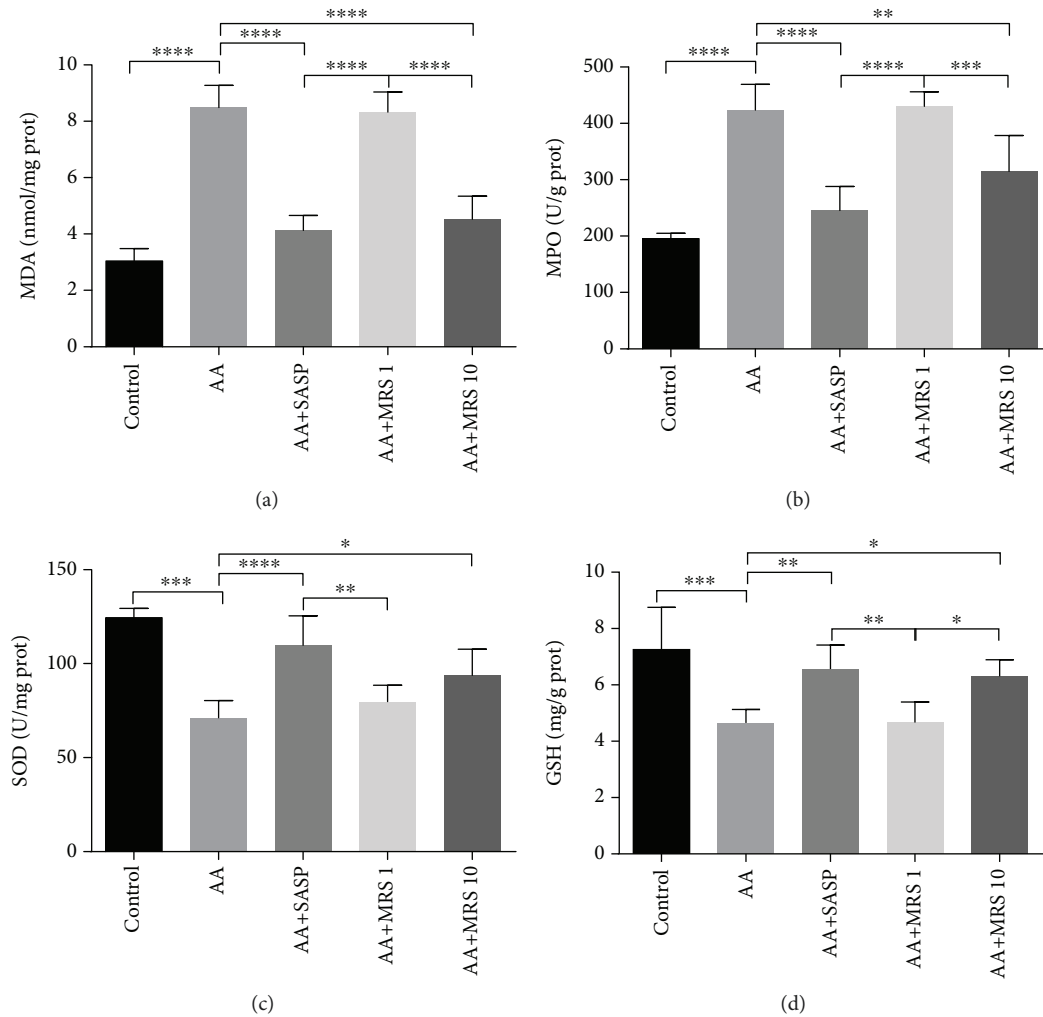


FIGURE 4: Treatment with MRS suppressed oxidative stress induced by acetic acid. Mice were administered with MRS at a dose of 1 or 10 ml/kg by gastric gavage for a week before colitis establishment. SASP was used as a positive control at a dose of 500 mg/kg. Colitis was induced by acetic acid solution ( $v/v$ ) injection into the lumen of the colon intrarectally with a volume of 1 ml and dose of 5% except for the sham group. Colon sections were isolated to investigate the markers of oxidative stress including (a) MDA, (b) MPO, (c) SOD, and (d) GSH. Data were expressed as means  $\pm$  SD. \*  $P < 0.05$ , \*\*  $P < 0.01$ , \*\*\*  $P < 0.001$ , and \*\*\*\*  $P < 0.0001$ .

stimulation and damage to the tissue simultaneously. Herein, TNF- $\alpha$  plays an essential role in triggering the production of a series of chemical mediators, leading to stronger inflammation [20]. Additionally, IL-6 is a key molecule contributing to neutrophil infiltration and cell apoptosis in colitis [21]. TNF- $\alpha$  and IL-6 serum levels were elevated in the colitis group as expected but were reduced by MRS. At the molecular to mRNA levels, the reduction of the TNF- $\alpha$  and IL-6 mRNA levels under MRS treatment suggested the anti-inflammatory effect of MRS again. The mRNA fold of IL-1 $\beta$  was also detected because of its important role in proinflammatory cytokines in colitis. Additionally, the mRNA fold of IL-1 $\beta$  was decreased with MRS. Furthermore, the expression level of IL-10, a well-known anti-inflammatory cytokine, was upregulated by MRS. It turned out that MRS could suppress the inflammation in acetic acid-induced colitis.

Oxidative stress is another prominent factor causing tissue destruction in UC [22]. Reactive oxygen and nitrogen

species (ROS and RNS), products of oxidative stress, are the culprits to promote lipid peroxidation, resulting in a negative influence on membrane organization and the structures of proteins and DNA bases [23]. MDA is an end-product from the oxidation of polyunsaturated fatty acids, which is a common marker of oxidative stress besides MPO. On the other hand, SOD and GSH act as inhibitors of oxygen radicals by scavenging oxygen radicals [24]. Thus, we detected the levels of oxidants and antioxidants to assess the degree of oxidative stress in colitis mice. The levels of SOD and GSH were found to be downregulated because of acetic acid, a finding that was consistent with an upregulated level of MDA and MPO. When the colitis mice were treated with MRS, their activities of SOD and GSH were improved and the levels of MDA and MPO were reduced. The result indicated that MRS demonstrated a protective effect when mice showed oxidative stress damage during colitis.



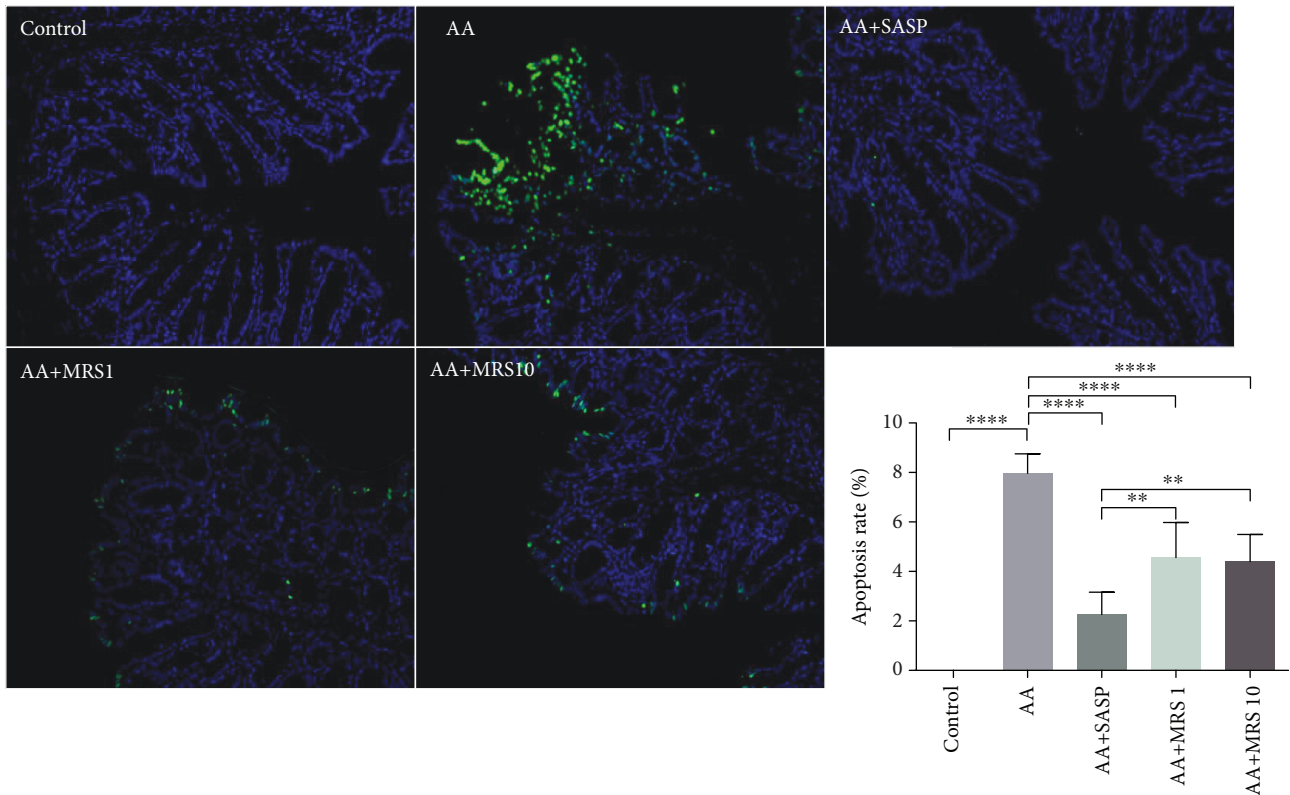


FIGURE 5: Treatment with MRS improved colonic cell apoptosis caused by acetic acid. Mice were administered with MRS at a dose of 1 or 10 ml/kg by gastric gavage for a week before colitis establishment. SASP was used as a positive control at a dose of 500 mg/kg. Colitis was induced by acetic acid solution (*v/v*) injection into the lumen of the colon intrarectally with a volume of 1 ml and dose of 5% except for the sham group. The collected colon slides were subjected to TUNEL staining to assess cell apoptosis, and green spots represented apoptotic cells (400x). And the apoptosis rate was calculated. Data were expressed as means  $\pm$  SD. \* $P < 0.05$ , \*\* $P < 0.01$ , \*\*\* $P < 0.001$ , and \*\*\*\* $P < 0.0001$ .

Colonic epithelial cell apoptosis was observed in acetic acid-induced colitis in line with a previous study [25]. Apoptosis has been regarded as a mechanism involving the homeostatic and pathogenic processes of colonic cells in IBD. When apoptosis occurs in epithelial cells, the surrounding histiocytes engulf the programmed death cells and attach to each other to fill the absence. Generally, the local defense is maintained if the quality and quantity of adjacent histiocytes are guaranteed, or inflammation will be activated once uncontrolled apoptosis results in mucosal integrity disruption and bacterial invasion. Additionally, excessive inflammation also leads to the damage of normal histiocytes [26]. It is controversial whether apoptosis or inflammation is the origin for the pathophysiological process of UC. However, apoptosis plays an eminent part in UC, and our TUNEL staining result revealed that MRS was helpful in reducing epithelial cell apoptosis.

To further investigate the mechanism of MRS in colitis, we focused on the TLR4-MyD88 signaling pathway, which is responsible for the expression of inflammatory cytokines and chemokine [27]. When the signals are transferred from TLR4 to MyD88, with the recruitment of IRAK4 and TRAF6 in succession, the IKK complex will be activated, leading to the destruction of  $I\kappa B$  by the proteasome. Next, the NF- $\kappa B$  p65 subunit is permitted to translocate into nuclei and

promote the production of proinflammatory cytokines such as TNF- $\alpha$ , IL-1 $\beta$ , and IL-6 [28]. Additionally, the other important TLR4 signaling pathway in charge of the immune response is mediated by MAP kinases such as JNK, ERK, and p38, which are closely correlated with inflammatory mediators such as inducible nitric oxide synthase and cyclooxygenase (COX-2). It was demonstrated that TLR4 recognizes bacterial LPS well and methods to inhibit NF- $\kappa B$  and that MAPK signaling pathways can improve inflammatory damages induced by LPS [29]. The present study showed that acetic acid stimulated the inflammation-related pathway showing upregulated expression levels of TLR4 and MyD88 and subsequent downstream molecules including NF- $\kappa B$ , JNK, ERK, and p38. Moreover, when we treated the colitis mice with MRS, components in the pathway were at lower expression levels. Thus, we speculated that MRS may exert a protective effect in acetic acid-induced colitis via the TLR-4/NF- $\kappa B$ /MAPK signaling pathway.

Moreover, we found that MRS could not only decrease the release of proinflammatory cytokines but also improve the anti-inflammatory ability through the increase in IL-10 production. In fact, several other studies showed that MRS could increase the IL-10 production in different diseases such as postoperative cognitive dysfunction, LPS-induced sepsis, carbon tetrachloride-induced liver injury, and chronic

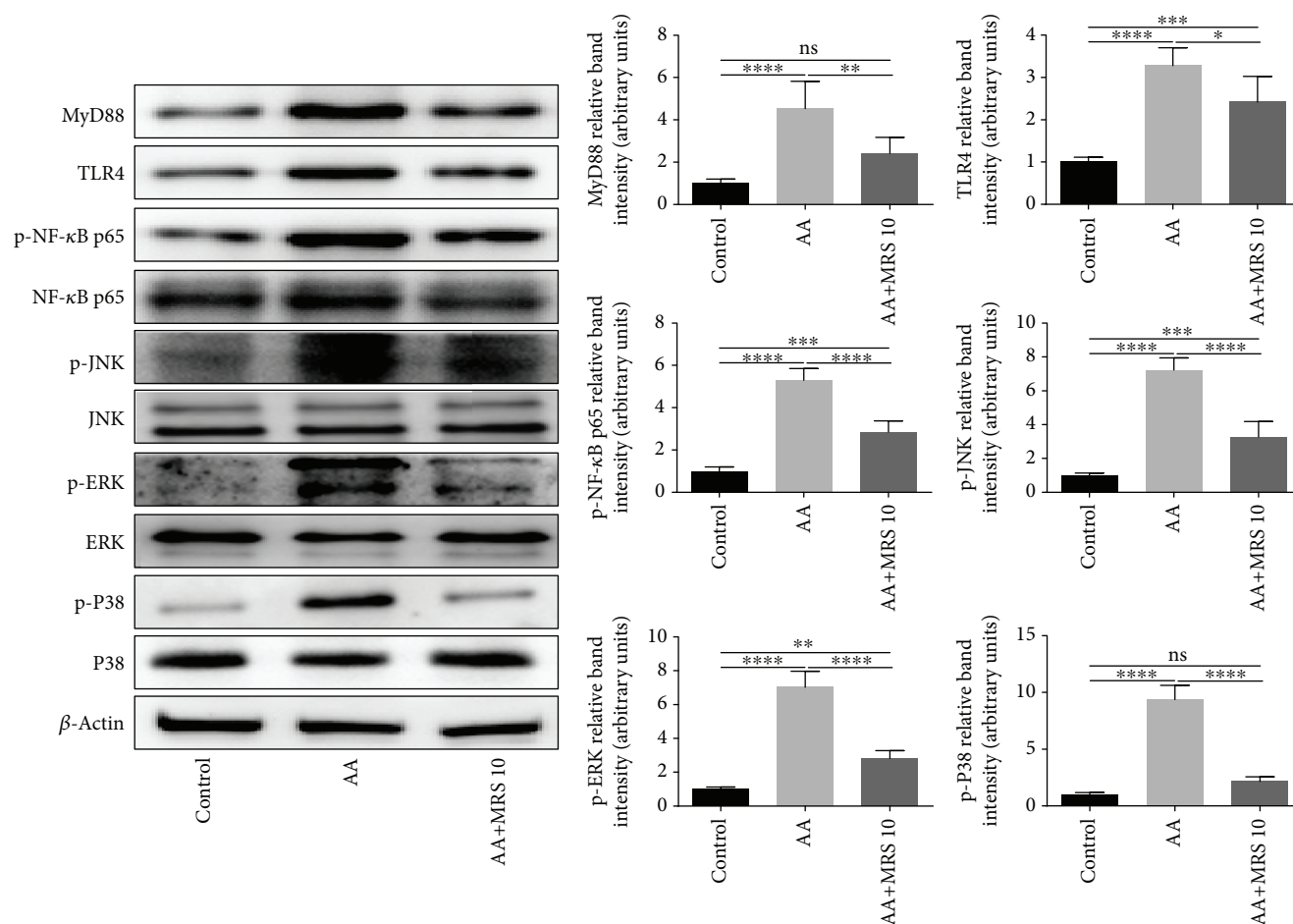


FIGURE 6: Treatment with MRS downregulated the inflammation-related TLR4/NF- $\kappa$ B/MAPK signaling pathway. Mice were administered with MRS at a dose of 10 ml/kg by gastric gavage for a week before colitis establishment. SASP was used as a positive control at a dose of 500 mg/kg. Colitis was induced by acetic acid solution ( $v/v$ ) injection into the lumen of the colon intrarectally with a volume of 1 ml and dose of 5% except for the sham group. Colon tissues were collected, and the protein levels of major pathway components, including TLR4, MyD88, ERK, p-JNK, p38, and NF- $\kappa$ B p65, were analyzed by Western blotting. Data were expressed as means  $\pm$  SD. \* $P < 0.05$ , \*\* $P < 0.01$ , \*\*\* $P < 0.001$ , and \*\*\*\* $P < 0.0001$ .

inflammatory pain [30–33]. IL-10/JAK1/STAT3 is a well-documented signaling pathway which can control the anti-inflammatory response. *Lactobacillus rhamnosus* GR-1 supernatant was able to increase IL-10 output and activated the JAK/STAT pathway to exert an anti-inflammatory property in lipopolysaccharide-stimulated placental trophoblast cells [34]. Carboxymethyl chitosan could attenuate inducible nitric oxide synthase and protect against osteoarthritis through the IL-10/JAK1/STAT3 pathway [35]. The expression of IL-10 could inhibit the expression of proinflammatory mediators such as cell surface receptors, chemokines, and cytokines. And the activation of STAT3 could stimulate the expression of anti-inflammatory properties of genes, which in turn suppress the expression of proinflammatory genes [7]. Previous studies showed that MRS may promote upstream PI3K/Akt/GSK-3 $\beta$ -mediated IL-10 expression [31, 32]. And our results first revealed that MRS may also promote the downstream IL-10/JAK1/STAT3 signaling pathway to elevate the anti-inflammatory response. In the future, more *in vivo* and *in vitro* studies can be launched to

detect and verify the novel effect of MRS on the IL-10/JAK1/STAT3 signaling pathway in different diseases. Because of its simple molecular structure, it is difficult to reveal the detailed mode of action between MRS and the corresponding receptor by traditional experimental methods. However, with the development of the structural biology methods, future work may be focused on the effect of MRS on the structure of influenced proteins such as TLR4, NF- $\kappa$ B, IL-10, JAK, and STAT3.

In summary, we found that methane-rich saline had a protective effect on acetic acid-induced ulcerative colitis, relying on the ability to alleviate oxidative stress and inflammation by inhibiting the TLR4/NF- $\kappa$ B/MAPK signaling pathway and promoting IL-10/JAK1/STAT3-mediated anti-inflammatory response. MRS showed anti-inflammation, antioxidation, and antiapoptosis properties once more in step with previous studies. However, the specific mechanism regarding how methane-rich saline is beneficial remains unclear. It was reported that methane could penetrate the cell membrane and exert its function. Thus, some researchers

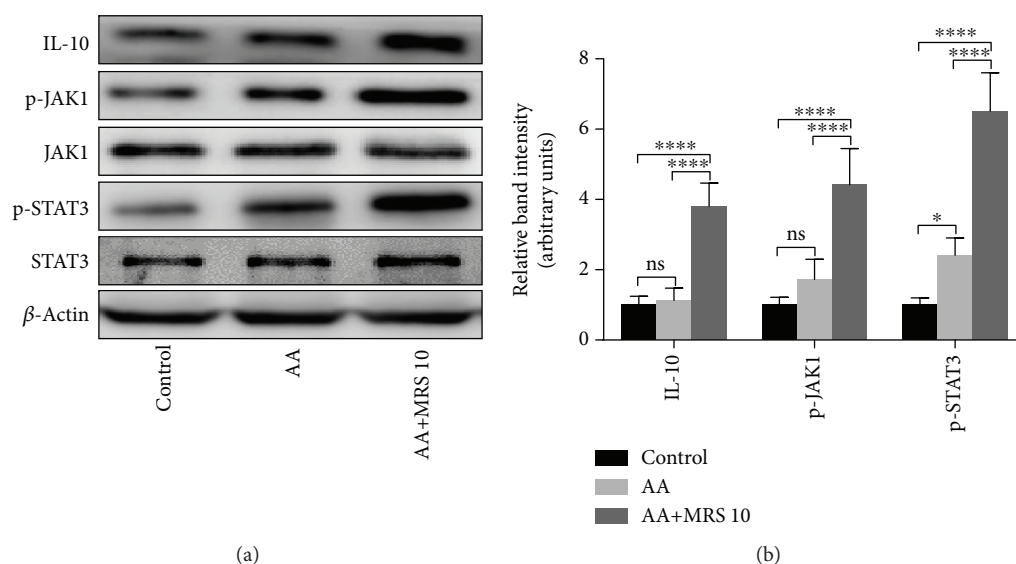


FIGURE 7: Treatment with MRS activated the anti-inflammatory response-related IL-10/JAK1/STAT3 signaling pathway. Mice were administered with MRS at a dose of 10 ml/kg by gastric gavage for a week before colitis establishment. SASP was used as a positive control at a dose of 500 mg/kg. Colitis was induced by acetic acid solution (v/v) injection into the lumen of the colon intrarectally with a volume of 1 ml and dose of 5% except for the sham group. Colon tissues were collected, and the protein levels of IL-10, p-JAK1, JAK1, p-STAT3, and STAT3 were analyzed by Western blotting. Data were expressed as means  $\pm$  SD. \* $P < 0.05$  and \*\*\*\* $P < 0.0001$ .

have predicted that methane acts through proteins embedded in the lipid bilayer of the membrane [36]. Speculation that methane was induced to form methanol or alcohol via a related receptor and then affected the oxidative environment in cells was also proposed to try to explain the biological mechanism. Besides, no appropriate dose of MRS was determined to apply according to previous studies. However, the setting of different doses in our experiment revealed that a high dose at 10 ml/kg performed better than the lower one at 1 ml/kg. However, further research concerning the appropriated dose is required. While ischemia-reperfusion damage was the earliest and most common investigation of methane, diseases like sepsis, hepatitis, and pancreatitis were explored recently. Our research could offer evidence to expand the application area of methane medicine in ulcerative colitis and a novel direction to solve the problem of colitis therapy. There are no certain instructions regarding the physicochemical properties, biological mechanisms, and usage of methane. However, the potential of methane medicine is of great prospect, and further study is warranted.

### Data Availability

The data related to mouse model data, serum cytokine levels, tissue cytokine mRNA levels, oxidative stress indicators, TUNEL staining, and Western blot images used to support the findings of this study are available from the corresponding author upon request.

### Conflicts of Interest

We declare that there is no conflict of interest regarding the publication of this article.

### Authors' Contributions

Wang GH participated in the research design, animal research, and writing of the paper. Xu B participated in animal research and writing of the paper. Wang GH and Xu B contributed equally to the paper. Shi FY participated in animal research. Du MF participated in the IHC performance. Li YG participated in the WB performance. Yu TY participated in data analysis; Chen LH provided substantial advice in designing the study and assisting in the division of labor and writing and revising the paper.

### Acknowledgments

This work was supported by the Scientific and Technological Development Research Project Foundation by Shaanxi Province (No. 2015SF057). We thank all individuals who participated in or helped with this research project.

### References

- [1] H. N. Iskandar, T. Dhere, and F. A. Farraye, "Ulcerative colitis: update on medical management," *Current Gastroenterology Reports*, vol. 17, no. 11, p. 44, 2015.
- [2] R. Ungaro, S. Mehandru, P. B. Allen, L. Peyrin-Biroulet, and J. F. Colombel, "Ulcerative colitis," *The Lancet*, vol. 389, no. 10080, pp. 1756–1770, 2017.
- [3] B. L. Xu, G. J. Zhang, and Y. B. Ji, "Active components alignment of Gegenqinlian decoction protects ulcerative colitis by attenuating inflammatory and oxidative stress," *Journal of Ethnopharmacology*, vol. 162, pp. 253–260, 2015.
- [4] Z. Wang, S. Li, Y. Cao et al., "Oxidative stress and carbonyl lesions in ulcerative colitis and associated colorectal cancer," *Oxidative Medicine and Cellular Longevity*, vol. 2016, Article ID 9875298, 15 pages, 2016.

- [5] R. A. Gupta, M. N. Motiwala, U. N. Mahajan, and S. G. Sabre, "Protective effect of *Sesbania grandiflora* on acetic acid induced ulcerative colitis in mice by inhibition of TNF- $\alpha$  and IL-6," *Journal of Ethnopharmacology*, vol. 219, pp. 222–232, 2018.
- [6] S. M. Lim, J. J. Jeong, G. D. Kang, K. A. Kim, H. S. Choi, and D. H. Kim, "Timosaponin AIII and its metabolite sarsasapogenin ameliorate colitis in mice by inhibiting NF- $\kappa$ B and MAPK activation and restoring Th17/Treg cell balance," *International Immunopharmacology*, vol. 25, no. 2, pp. 493–503, 2015.
- [7] A. P. Hutchins, D. Diez, and D. Miranda-Saavedra, "The IL-10/STAT3-mediated anti-inflammatory response: recent developments and future challenges," *Briefings in Functional Genomics*, vol. 12, no. 6, pp. 489–498, 2013.
- [8] Y. Meng, Z. Jiang, N. Li et al., "Protective effects of methane-rich saline on renal ischemic-reperfusion injury in a mouse model," *Medical Science Monitor*, vol. 24, pp. 7794–7801, 2018.
- [9] Z. Li, Y. Jia, Y. Feng et al., "Methane alleviates sepsis-induced injury by inhibiting pyroptosis and apoptosis in vivo and in vitro experiments," *Aging*, vol. 11, no. 4, pp. 1226–1239, 2019.
- [10] Z. Li, Y. Jia, Y. Feng et al., "Methane-rich saline protects against sepsis-induced liver damage by regulating the PPAR- $\gamma$ /NF- $\kappa$ B signaling pathway," *Shock*, p. 1, 2018.
- [11] Y. Jia, Z. Li, Y. Feng et al., "Methane-rich saline ameliorates sepsis-induced acute kidney injury through anti-inflammation, antioxidative, and antiapoptosis effects by regulating endoplasmic reticulum stress," *Oxidative Medicine and Cellular Longevity*, vol. 2018, Article ID 4756846, 10 pages, 2018.
- [12] A. Sun, W. Wang, X. Ye et al., "Protective effects of methane-rich saline on rats with lipopolysaccharide-induced acute lung injury," *Oxidative Medicine and Cellular Longevity*, vol. 2017, Article ID 7430193, 12 pages, 2017.
- [13] J. Wu, R. Wang, Z. Ye et al., "Protective effects of methane-rich saline on diabetic retinopathy via anti-inflammation in a streptozotocin-induced diabetic rat model," *Biochemical and Biophysical Research Communications*, vol. 466, no. 2, pp. 155–161, 2015.
- [14] Y. Jia, Z. Li, C. Liu, and J. Zhang, "Methane medicine: a rising star gas with powerful anti-inflammation, antioxidant, and antiapoptosis properties," *Oxidative Medicine and Cellular Longevity*, vol. 2018, Article ID 1912746, 10 pages, 2018.
- [15] M. T. de Santana Souza, D. F. Teixeira, J. P. de Oliveira et al., "Protective effect of carvacrol on acetic acid-induced colitis," *Biomedicine & Pharmacotherapy*, vol. 96, pp. 313–319, 2017.
- [16] X. Niu, H. Zhang, W. Li et al., "Protective effect of cavidine on acetic acid-induced murine colitis via regulating antioxidant, cytokine profile and NF- $\kappa$ B signal transduction pathways," *Chemico-Biological Interactions*, vol. 239, pp. 34–45, 2015.
- [17] G. Ozbakis Dengiz and N. Gursan, "Effects of *Momordica charantia* L. (*Cucurbitaceae*) on indomethacin-induced ulcer model in rats," *The Turkish Journal of Gastroenterology*, vol. 16, no. 2, pp. 85–88, 2005.
- [18] C. F. S. Guazelli, V. Fattori, B. B. Colombo et al., "Quercetin-loaded microcapsules ameliorate experimental colitis in mice by anti-inflammatory and antioxidant mechanisms," *Journal of Natural Products*, vol. 76, no. 2, pp. 200–208, 2013.
- [19] S. Banerjee, S. Ghosh, K. Sinha, S. Chowdhury, and P. C. Sil, "Sulphur dioxide ameliorates colitis related pathophysiology and inflammation," *Toxicology*, vol. 412, pp. 63–78, 2019.
- [20] Y. T. Xiao, W. H. Yan, Y. Cao, J. K. Yan, and W. Cai, "Neutralization of IL-6 and TNF- $\alpha$  ameliorates intestinal permeability in DSS-induced colitis," *Cytokine*, vol. 83, pp. 189–192, 2016.
- [21] J. Mudter and M. F. Neurath, "IL-6 signaling in inflammatory bowel disease: pathophysiological role and clinical relevance," *Inflammatory Bowel Diseases*, vol. 13, no. 8, pp. 1016–1023, 2007.
- [22] T. Mitani, Y. Yoshioka, T. Furuyashiki, Y. Yamashita, Y. Shirai, and H. Ashida, "Enzymatically synthesized glycogen inhibits colitis through decreasing oxidative stress," *Free Radical Biology & Medicine*, vol. 106, pp. 355–367, 2017.
- [23] L. Kruidenier, I. Kuiper, W. van Duijn et al., "Imbalanced secondary mucosal antioxidant response in inflammatory bowel disease," *The Journal of Pathology*, vol. 201, no. 1, pp. 17–27, 2003.
- [24] N. V. Margaritelis, A. S. Veskokoukis, V. Paschalis et al., "Blood reflects tissue oxidative stress: a systematic review," *Biomarkers*, vol. 20, no. 2, pp. 97–108, 2015.
- [25] S. Zeissig, C. Bojarski, N. Buergele et al., "Downregulation of epithelial apoptosis and barrier repair in active Crohn's disease by tumour necrosis factor alpha antibody treatment," *Gut*, vol. 53, no. 9, pp. 1295–1302, 2004.
- [26] W. Qiu, B. Wu, X. Wang et al., "PUMA-mediated intestinal epithelial apoptosis contributes to ulcerative colitis in humans and mice," *The Journal of Clinical Investigation*, vol. 121, no. 5, pp. 1722–1732, 2011.
- [27] T. Kawai and S. Akira, "The role of pattern-recognition receptors in innate immunity: update on Toll-like receptors," *Nature Immunology*, vol. 11, no. 5, pp. 373–384, 2010.
- [28] M. Tsubaki, T. Takeda, T. Kino et al., "Mangiferin suppresses CIA by suppressing the expression of TNF- $\alpha$ , IL-6, IL-1 $\beta$ , and RANKL through inhibiting the activation of NF- $\kappa$ B and ERK1/2," *American Journal of Translational Research*, vol. 7, no. 8, pp. 1371–1381, 2015.
- [29] Y. Gao, W. Jiang, C. Dong et al., "Anti-inflammatory effects of sophocarpine in LPS-induced RAW 264.7 cells via NF- $\kappa$ B and MAPKs signaling pathways," *Toxicology In Vitro*, vol. 26, no. 1, pp. 1–6, 2012.
- [30] D. Zhang, N. Li, Y. Wang et al., "Methane ameliorates post-operative cognitive dysfunction by inhibiting microglia NF- $\kappa$ B/MAPKs pathway and promoting IL-10 expression in aged mice," *International Immunopharmacology*, vol. 71, pp. 52–60, 2019.
- [31] X. Zhang, N. Li, H. Shao et al., "Methane limit LPS-induced NF- $\kappa$ B/MAPKs signal in macrophages and suppress immune response in mice by enhancing PI3K/AKT/GSK-3 $\beta$ -mediated IL-10 expression," *Scientific Reports*, vol. 6, no. 1, article 29359, 2016.
- [32] Y. Yao, L. Wang, P. Jin et al., "Methane alleviates carbon tetrachloride induced liver injury in mice: anti-inflammatory action demonstrated by increased PI3K/Akt/GSK-3 $\beta$ -mediated IL-10 expression," *Journal of Molecular Histology*, vol. 48, no. 4, pp. 301–310, 2017.
- [33] S. Z. Zhou, Y. L. Zhou, F. Ji et al., "Analgesic effect of methane rich saline in a rat model of chronic inflammatory pain," *Neurochemical Research*, vol. 43, no. 4, pp. 869–877, 2018.
- [34] M. Yeganegi, C. G. Leung, A. Martins et al., "Lactobacillus rhamnosus GR-1-induced IL-10 production in human placental trophoblast cells involves activation of JAK/STAT and MAPK pathways," *Reproductive Sciences*, vol. 17, no. 11, pp. 1043–1051, 2010.

- [35] Y. Kong, Y. Zhang, X. Zhao, G. Wang, and Q. Liu, "Carboxymethyl-chitosan attenuates inducible nitric oxide synthase and promotes interleukin-10 production in rat chondrocytes," *Experimental and Therapeutic Medicine*, vol. 14, no. 6, pp. 5641–5646, 2017.
- [36] M. P. Fink, "Pharmacological effects of inhaled methane: plausible or not?," *Critical Care Medicine*, vol. 40, no. 4, pp. 1379–1380, 2012.